Identifying the Influences on Network Formation in Structural Isomers of Multifunctional Epoxies

Matthew Benedict Whittaker

A thesis submitted in partial fulfilment of the requirements for the degree of Doctor of Philosophy

The University of Sheffield
Faculty of Engineering
School of Chemical, Materials and Biological Engineering

June 2025

ACKNOWLEDGEMENTS

Firstly, I would like to thank the person who made this all possible, Dr Joel Foreman. I always looked forward to a Tuesday supervisor meeting discussing the ins and outs of my work and usually trying to get me out of whichever rabbit hole I'd gone down that week. I could not have got here without your support and guidance.

Secondly, I'd like to thank Joel's research group, who have had to put up with me. Everyone has been a great help, whether that's to bounce ideas off one another or just go for a coffee and try to forget about work. To name a few, Dr Euan Gray, whom, without, I probably wouldn't have even found my desk. He was invaluable in the beginning despite having his own PhD to finish, and he remains a great friend. Somthida Likhitlert (Mook), my office neighbour, sorry for the overflowing papers on your desk. She is someone whom I talked at for three and a half years, I deeply value those conversations and I will miss your amazing cooking. Anıl Marmara, a great guy and a good friend. Thanks for all the coffee, football discussions and teaching me about Turkish culture (they don't have a Pasam on the Island).

Thirdly, I'd like to thank the members of the K Floor office. I liked to hide away in my corner, but when I needed a chat or a bit of help, there was always someone there. Stephanie, Shaun, Gaone and Cassandra, thanks for all the lunchtimes getting away from work. James Nohl, thanks for all the cycling chat. Watching the Tour in the office will be greatly missed.

I'd also like to thank Dr Oday Hussein, who always had the time for me when I was using the DSC and making a mess of the TGA. Dr Matteo Di Benedetti and Dr Harry Day for making my time in the structures lab really enjoyable, and I appreciate the time they took to help me with my FHEA application.

Finally, the two guys who I couldn't have finished the PhD without. Sam Latimer and Tom Wilkinson. Sam, the most motivated man in the world. An office mate turned housemate turned friend forever. Leaving the bags in the office and heading straight to a gig after work was probably the thing that got me through the middle of the PhD. Tom, genuinely one of the most thoughtful people I've ever met, ending up living ten doors down from you was a godsend. Both of you were a massive support and were always up for much needed pints. I'll be forever grateful for that.

Thanks to my parents, without their ongoing support, I couldn't have got to the end of my PhD. Hopefully this explains what I've been doing for the past three and a half years.

ABSTRACT

The network formation of the structural isomers of triglycidyl aminophenol cured with the structural isomers of diaminodiphenyl sulphone was monitored using three different cure monitoring techniques. Four different epoxy-rich formulations were made: TG*p*AP/44'DDS, TG*p*AP/33'DDS, TG*m*AP/44'DDS and TG*m*AP/33'DDS.

Near-infrared spectroscopy (NIR) was used to monitor the functional group concentration change throughout network formation. From this, the type of reactions occurring were identified. Differential scanning calorimetry (DSC) was used to measure the thermal response of the curing reactions, allowing for the calculation of kinetic parameters. Dielectric analysis (DEA) monitored the ion viscosity or the change in the mobility of the reactive species during the cure.

Each cure monitoring technique identified that the 33'DDS hardener was initially more reactive. During the second dwell of the cure cycle, the 44'DDS hardener formulations were found to be more reactive.

NIR identified that TG*p*AP formulations underwent more etherification reactions at lower temperatures as the glycidyl amine in TG*p*AP behaves as a more effective tertiary amine catalyst than TG*m*AP. TG*m*AP formulations consumed secondary amines earlier than the TG*p*AP formulations, suggesting that more internal cyclisation reactions took place in the TG*m*AP formulations. From this, it was found that TG*p*AP/44'DDS had the most homogenous network, resulting in the highest glass transition temperature and the least dense network.

DSC suggested etherification took place during network formation due to the under performance of the autocatalytic model compared to experimental data at higher degrees of cure. The multi-dwell cure was modelled using a combined isothermal and dynamic measurement technique, showing good agreement with standalone isothermal and dynamic DSC measurements.

DEA showed evidence of annealing occurring during the final parts of the cure in TG*m*AP/33'DDS due to its T_g falling within the cure temperature. The cure state was calculated for each technique, and good agreement was shown despite them measuring different phenomena.

DECLARATION

I, Matthew Benedict Whittaker, confirm that the Thesis is my own work. I am aware of the University's Guidance on the Use of Unfair Means (www.sheffield.ac.uk/ssid/unfair-means). This work has not been previously been presented for an award at this, or any other, university.

Chapter 4. Investigation of the Network Development in Structural Isomers of TGAP/DDS using Near-Infrared Spectroscopy consists of work previously published.

> **M.B. Whittaker**, J.P. Foreman, Identifying the Influences on Network Formation in Structural Isomers of Multifunctional Epoxies Using Near-Infrared Spectroscopy, Macromolecules (2024) 3438–3450. https://doi.org/10.1021/acs.macromol.4c00274.

In the publication I, Matthew Benedict Whittaker, designed and performed the experiments, analysed the data and planned and wrote the manuscript, the co-author, Dr Joel P. Foreman, reviewed and provided comments on the manuscript. This work has been rewritten into traditional thesis format.

TABLE OF CONTENTS

TABLE OF FIGURES

TABLE OF TABLES

1. INTRODUCTION

The demand for lightweight, high-performance structure materials is great given the current environmental and economic circumstances. Composite materials fit these requirements due to the combination of two distinctly different materials: a fibre phase and a matrix phase. The matrix phase is commonly epoxy resin, a thermosetting polymer that forms a highly crosslinked 3D network upon curing. Understanding how a resin cures is of great importance, as network development influences resultant cured material properties. What these material properties are determines the resin's suitability for particular applications.

Bifunctional resin systems have been widely studied, as will be made apparent in Chapter 2. Literature Review, but with this comes lower crosslink density and a more flexible backbone. Utilising higher functionality resins such as the triglycidyl aminophenol (TGAP), which will be the subject of this thesis, increases the crosslink density, resulting in a higher performance resin. TGAP has two different structural isomers, and curing them with the two structural isomers of diaminodiphenyl sulphone (3,3'DDS and 4,4'DDS) gives four different formulations. With these four different materials, different material properties are made possible. How these material properties arise through differences in network development is important to understand.

It is possible to monitor the cure of epoxy resins using different techniques that measure different properties. The different properties give different insights into the network development of the different resins. Understanding the cause of the differences will enable the tailoring of the resin properties to fit the desired application.

1.1. AIMS AND OBJECTIVES

The main aim of this thesis is to identify the influences on network formation in the four structural isomers of triglycidyl aminophenol and diaminodiphenyl sulphone.

1. The main objective was to monitor the cure of the four structural isomers of TGAP/DDS using three different techniques:
    a. near-infrared spectroscopy
    b. differential scanning calorimetry
    c. dielectric cure monitoring.

2. Identify the differences in network development and use previous studies and knowledge of the chemical behaviour to identify the reasoning behind the cure behaviour.

3. Understand how different temperatures in the cure cycle impact the different isomers' curing behaviour.

4. Compare the cure state indication given by the three different curing techniques.

5. Correlating these differences to the resultant cured material properties to confirm the findings of the cure monitoring techniques.

2. LITERATURE REVIEW

2.1. INTRODUCTION

Polymers are a class of long-chain molecules comprising of multiple repeating units connected by covalent bonds. The classification of a polymer is broad. For example, DNA and RNA, the building blocks of life, are made up of natural polymers. In the 1800s, modifying natural polymers, such as the vulcanization of natural rubber, was a common technique, increasing their suitability for structural materials such as tyres by introducing sulphur crosslinks [1]. This type of modification gave semi-synthetic polymers. Fully synthetic polymers, such as the phenolic resin Bakelite, were first synthesised in the early 1900s, and from then on, the synthesis and production of new polymers for different applications have been endless [2]. As a result, synthetic polymers have a broad range of applications such as plastics, synthetic fibres, rubbers, coatings, sealants, and adhesives [3].

Polymers are hydrocarbon-containing molecules, often obtained from crude oil derivatives. For example, polyethylene (PE), shown in Figure 2.1, is a product of the polymerisation of *n* units of ethylene, where ethylene is obtained from steam cracking of petroleum or natural gas [4]. Despite ethylene's apparent molecular simplicity, the resultant polymer in Figure 2.1 is not often that linear, branching can occur depending on the reaction conditions. PE has multiple classifications, including ultra-high molecular weight, high density, low density, and linear low density. High-density PE is used for chemical containers, low-density PE for plastic bags, and ultra-high molecular weight can be used as fibres (Dyneema) in impact resistance applications [5].

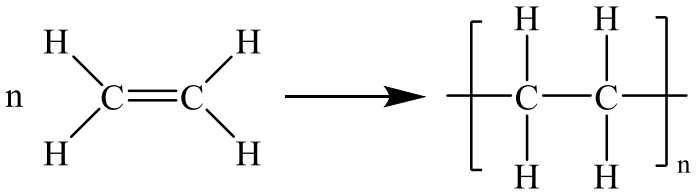

Figure 2.1 – Polymerisation of ethylene to polyethylene.

PE consists of either linear or branched chains. In the macromolecular structure, polymer chains are not bonded together. They are held together by intermolecular forces such as van der Waals, hydrogen bonding or permanent dipole-dipole forces depending on the chemical groups

[6]. At low temperatures, the intermolecular forces hold the polymer chains together. However, the forces are overcome upon heating, allowing the chains to move, resulting in a phase transition from solid to liquid, melting. The temperature at which these polymers melt depends on many factors. In the case of PE, when there is less linearity, there are lower amounts of crystallinity, reducing the effectiveness of the secondary forces holding the chains together, resulting in a lower melting temperature. Approximately 20 ^{o}C lower melting temperature for LDPE compared to UHMWPE [2].

Polymers without chemical crosslinks are known as thermoplastics. Polymers where there are chemical crosslinks between chains are known as thermosets. An irreversible state change occurs upon forming the crosslinks, usually from liquid to solid. The resultant material cannot be further melted and reformed like thermoplastics. It's like baking a cake. You can't 'unbake' it afterwards (in most cases). The classification of thermosets is not specific. There are different types. One such is Bakelite, a phenolic resin first commercialised by Leo Baekeland in the first decade of the 1900s and is a product of a polymerisation reaction between phenol and formaldehyde widely used in adhesives and binders [7]. Another is crosslinked polyurethane, formed from polymerising polyols and diisocyanates [8]. One final example is epoxy; these are (in my opinion) the best thermoset and what the topic of the thesis will be.

2.2. EPOXY RESIN

When discussing epoxy resin, the cured final product is often referred to rather than the actual epoxy molecule. If the epoxy resin is cured correctly, no epoxy should remain, only hydroxyls and perhaps ethers. It is, in fact, a misnomer [9].

Epoxy resin refers to the epoxide or oxirane ring functional group in the molecule shown in Figure 2.2. The optimised bond angle in a sp^3 hybridised molecule is 109.5°, whereas in epoxide rings, the bond angle is around 60°. The small bond angle results in significant ring strain, making it more reactive than other linear or cyclic ethers. The strained cyclic structure favours opening to reduce the strain and is therefore susceptible to ring-opening reactions.

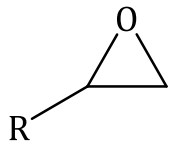

Figure 2.2 – Chemical structure of an epoxide ring.

The structure in Figure 2.2 shows one reactive group, a monofunctional epoxy. If a ring-opening reaction took place with an amine, this would result in a very short molecule, which is neither a polymer nor crosslinked. Thus, the epoxy resins used to make thermosetting resins are often multifunctional, with more than one epoxy functional group. The opening of an epoxide ring occurs during a reaction with molecules known as hardeners, which are also multifunctional. In the case of diamine hardeners, there are at least four reactive sites [9]. This multifunctionality allows for long chains and crosslinking, resulting in materials that don't melt and have excellent mechanical properties and high-temperature resistance.

There are numerous different epoxy resins available on the market from different suppliers. Figure 2.3 shows three different resins with different functionalities: (a) diglycidyl ether of bisphenol-A (DGEBA), (b) triglycidyl-*para*-aminophenol (TG*p*AP) and (c) *N,N'*-tetraglycidyl-4,4'-diaminodiphenylmethane (TGDMM).

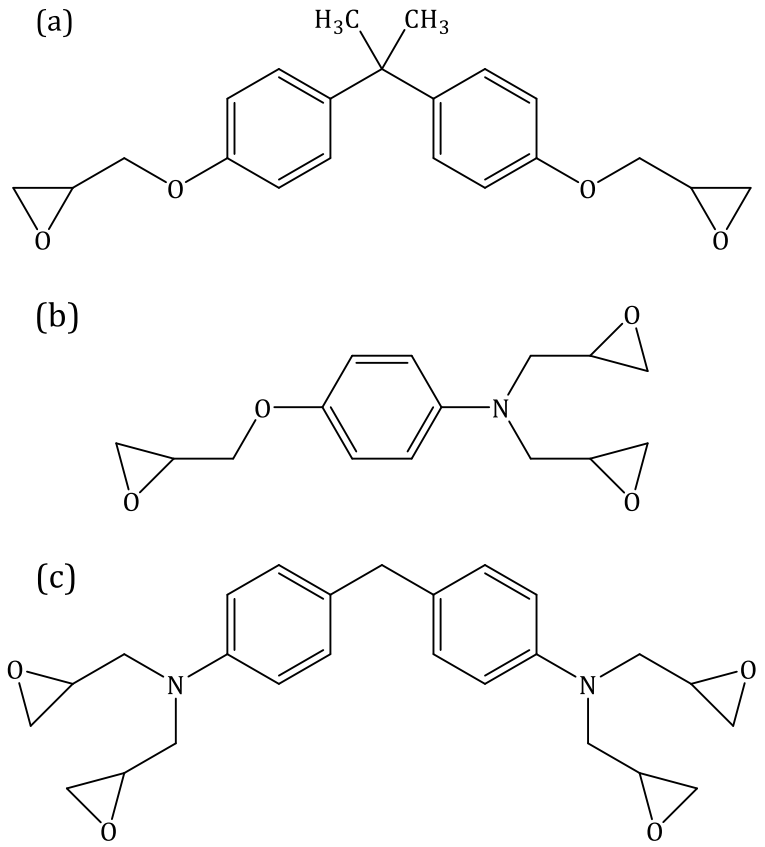

Figure 2.3 – Chemical structures of three widely available epoxy resins: (a) diglycidyl ether of bisphenol-A, (b) triglycidyl-*para*-aminophenol and (c) *N, N*'-tetraglycidyl-4,4'-diaminodiphenylmethane.

DGEBA is bifunctional and is the most common epoxy resin used, with 80 – 85 % of the global epoxy consumption being DGEBA [10]. TG*p*AP and TGDDM are multifunctional resins with a functionality of three and four, respectively. Higher functionality corresponds to more crosslinking sites, leading to potentially better performance.

The synthesis route for these three resins is very similar. It consists of reacting epichlorohydrin with the corresponding hydroxyl compound using a catalyst in alkali conditions [9,11]. Figure 2.4 shows the synthesis of DGEBA using bisphenol-A and epichlorohydrin. Specific reaction conditions are needed to obtain the pure DGEBA monomer. There must be at least two molecules of epichlorohydrin for every molecule of bisphenol-A, and an excess is often used [9].

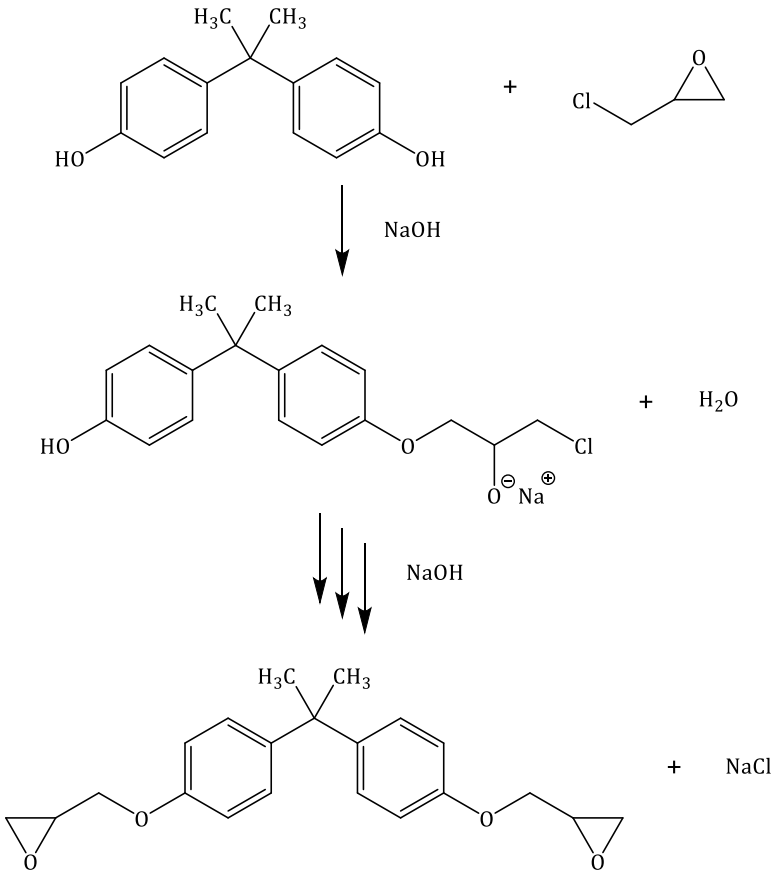

Figure 2.4 – Reaction pathway for the synthesis of diglycidyl ether of bisphenol-A from bisphenol-A and epichlorohydrin in alkali conditions.

Even if the ratio of epichlorohydrin to bisphenol-A is 2:1, other side reactions often prevent the formation of pure DGEBA. A different DGEBA product is formed if the ratio of epichlorohydrin to bisphenol-A is lower than 2:1. It has a repeat unit between the two epoxy groups, increasing the molecular weight and chain length, as shown in Figure 2.5. The *n* value refers to the number of repeat units; the higher the number, the greater the molecular weight. Increasing the distance between crosslinks results in different cured properties, a reduction in glass transition temperature (T_g) is often seen [12,13].

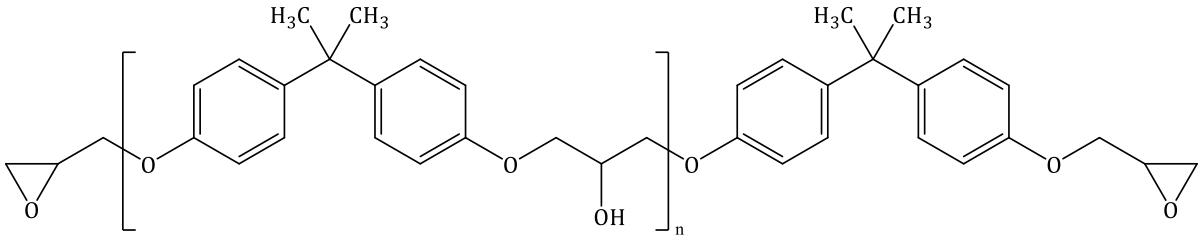

Figure 2.5 – General formula for diglycidyl ether of bisphenol-A.

Manufacturers provide the resin in different forms and purity levels. For example, in the Foreman group lab, there are four different grades of DGEBA: monomer DGEBA, Epikote 828, Epikote 834 and Epon 1001F. Each grade has a different molecular weight per epoxide group, known as the epoxy equivalent weight (EEW). The EEW of DGEBA is 170 g mol^{-1}, Epikote 828 187 g mol^{-1}, Epikote 834 249 g mol^{-1} and Epon 1001F 537.5 g mol^{-1}. The higher the EEW, the higher the number of repeat units between the epoxy groups. The same is true for TGAP and TGDDM. A study by St John *et al*. analysed different grades of TGDDM, MY721, MY720 and purified TGDDM [14]. Higher levels of dimers, trimers, and oligomers were present in MY720, and higher levels of impurities from synthesis were also present in the resin in the form of hydroxyl groups.

2.2.1. NETWORK FORMATION

Epoxy resin is often known as two-part epoxy, suggesting that there is a second component. The epoxide ring wants to open; they can open on their own through homopolymerisation, but for effective crosslinking, they need a reactant to open them. Therefore, curing agents or hardeners are widely used to cure epoxy resins. There are different types such as anhydrides, polyamides, thiols and amines. This study focuses on the use of amines as curing agents.

An amine hardener is a molecule with a functional group that consists of nitrogen and two hydrogens. Each hydrogen can react with an epoxide ring, suggesting a functionality of two. The amine hardeners commonly used are diamines, Figure 2.6 shows three examples: (a) 4,4'-diaminodiphenyl sulphone (44'DDS) and (b) *para*-phenylenediamine and (c) ethylenediamine. (a) and (b) are examples of aromatic diamine hardeners, whereas (c) is an example of an aliphatic diamine. Curing using aliphatic diamines results in significantly lower T_g values when compared to aromatic diamines [15]. Lv *et al.* saw a 40 °C difference between aromatic and aliphatic hardeners when using resorcinol glycidyl ether, diethylenetriamine, and benzidine [16]. An aromatic ring is stiff and inflexible, whereas aliphatic chains are flexible.

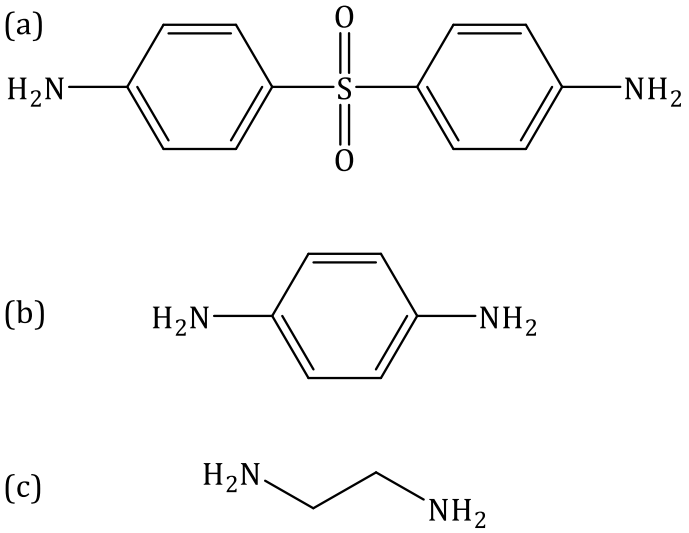

Figure 2.6 – Chemical structures of three different diamine hardeners: (a) 4,4'-diaminodiphenyl sulphone, (b) *para*-phenylenediamine and (c) ethylenediamine.

The T_g is often talked about being higher or lower for different epoxies cured with different amine resins, but what is T_g and what does it tell us about the crosslinked network? T_g is the temperature at which there is an onset of significant chain mobility, and the network transitions from a glassy to a rubbery state [17]. Many parameters affect the temperature at which the transition occurs, such as the crosslink density, chemical structure of chains and branches (aromatic vs. aliphatic) and intermolecular interactions. In the case of epoxy amine resins, T_g is thought to be primarily affected by two things: one, the stiffness of the linear backbone and secondly, the crosslinking density. Lesser and Crawford found that the case was slightly more complex than just two components [18]. If the simple view is taken, chemical structure influences the stiffness of a linear chain, aromatic rings will make a stiffer chain thus higher T_g, whereas flexible aliphatic chains will reduce the T_g. The effect of crosslinking on the T_g will be determined by how many crosslinks there are and the molecular weight between crosslinks, the crosslink density. A higher crosslink density will result in a network with a greater T_g, how these crosslinks form is dependent on the reactions taking place during the cure. There are also other factors that influence T_g, such as intermolecular forces between chains like hydrogen bonding between polar groups which in turn increase T_g and then also the size of side groups, bulky side groups can restrict the flexibility of the network increasing T_g.

Figure 2 .7 shows the reactions that occur in an epoxy amine curing process: (a) shows the epoxide ring opening reaction with a primary amine, which forms the linear backbone, (b)

shows the epoxide ring-opening reaction with a secondary amine, this forms crosslinks between the linear chains and (c) shows the epoxide ring-opening reaction with a hydroxyl group known as etherification. The extent to which these reactions occur depends on the starting reagents' chemistry [19–22]. In an epoxy amine system, the main reactions are primary and secondary amine reactions, but in high-temperature environments where there is sufficient tertiary amine concentration, etherification will occur [19], and in some cases, it will also occur at lower temperatures and earlier in the reaction [22].

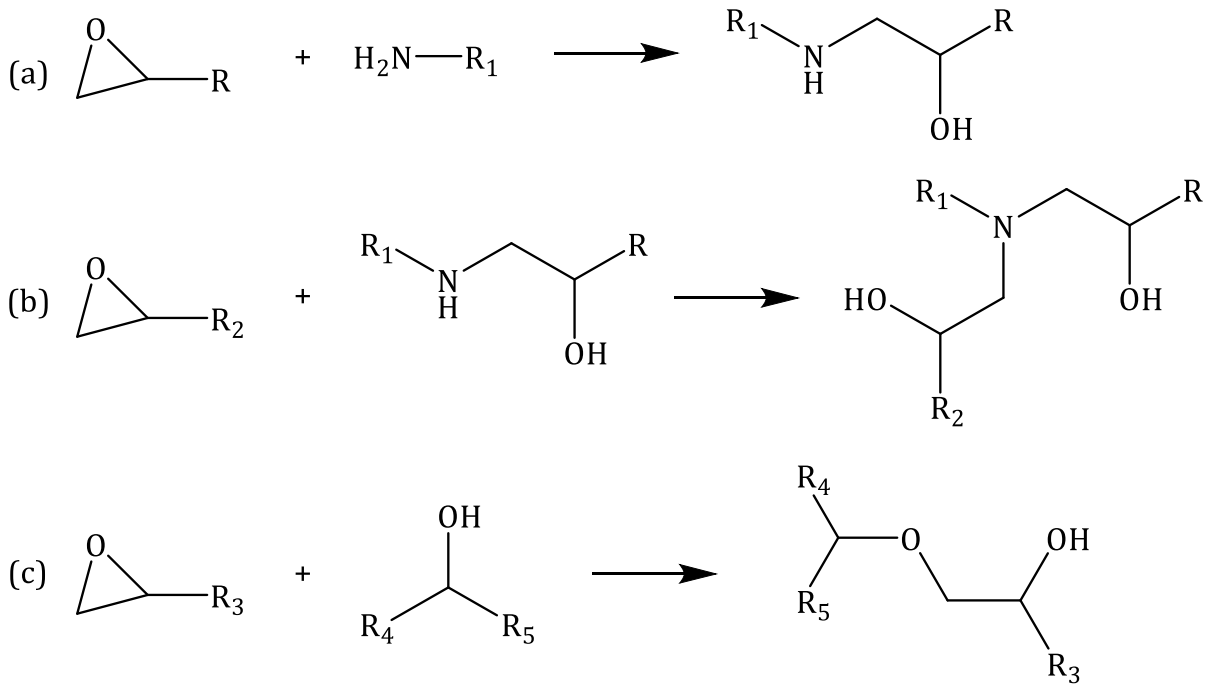

Figure 2 .7 – Chemical reactions that occur in the epoxy amine curing process: (a) epoxy/primary amine, (b) epoxy/secondary amine and (c) etherification.

The extent to which the reactions occur partially dictates the T_g. As suggested earlier, the greater the crosslink density, the higher the T_g but there has to be a sufficient linear backbone in the network; without this, the network will be inhomogeneous [23]. When designing the cure protocol, epoxide ring primary amine reactions must occur initially to form adequate linear portions that go onto crosslink [24]. Otherwise, regions of high and low crosslink density form when linear and crosslinking reactions compete, resulting in a broad T_g range of which is lower than a more homogeneously crosslinked network. Sahagun and Morgan depicted the difference between a homogeneously and non-homogeneously crosslinked network using the a similar

diagram to the one shown in Figure 2.8. (a) shows a homogeneous crosslinked network, whereas (b) shows areas of high crosslinking density connected by linear and branched regions [23].

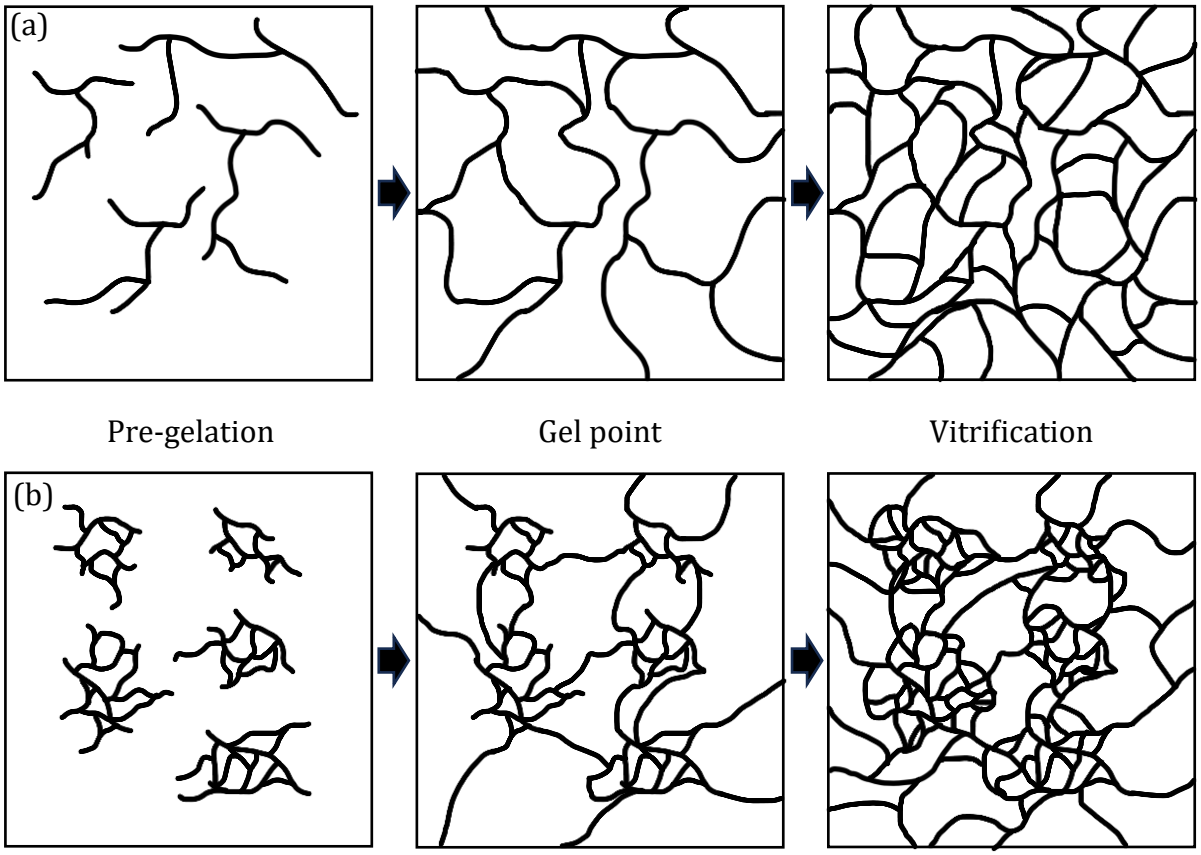

Figure 2.8 – Network growth where different curing reactions dominate at different points: (a) where the linear and crosslinking reactions occur consecutively and (b) where linear and crosslinking reactions compete. Adapted from Sahagun and Morgan under copyright licence 6156571362522 [23].

The curing reactions of epoxy amines must be monitored and optimised. Using cure monitoring techniques to understand the difference in the network formation is vital. Knowing the effects on network formation allows control of the thermal, mechanical and chemical properties, making the production of optimal materials possible. This results in waste and cost reduction and ensures the efficient use of raw materials to reduce the environmental impact of thermosetting resins – something of great importance given the current global predicament.

2.2.2. STRUCTURAL ISOMERISM

As mentioned above, many different epoxy resins and hardeners are available. The hardeners shown in Figure 2.6 are all different molecules; they have different molecular structures and weights but the same number of reactive sites. Consequently, they have different reactivities, which results in cured resins with different properties. Instead of using completely different molecules, different structural isomers with the same molecular weight as starting reagents can be used to change the curing process and optimise resin properties. A structural isomer is a set of molecules with the same chemical formula but different arrangements of atoms. For example, Figure 2.9 shows the three isomers of pentane. Despite having the same chemical formula (C_5H_{12}), these three molecules have different properties: *n*-pentane has a boiling point of 36 °C [25], 2-methyl butane 28 °C [26] and 2,2-dimethyl propane 9.5 °C [27]. Decreasing the length-to-width ratio makes the attraction (van der Waals forces) between the molecules weaker due to increased branching, resulting in different boiling temperatures.

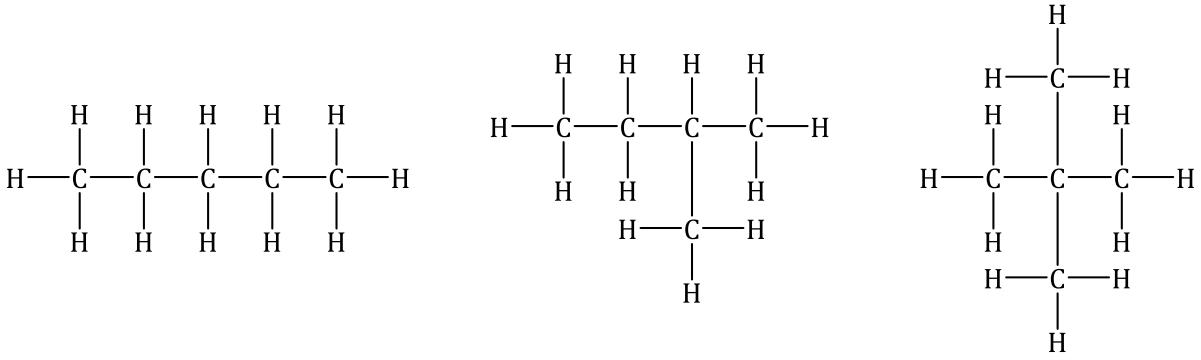

(a) *n*-pentane (b) 2-methyl butane (c) 2,2-dimethyl propane

Figure 2.9 – Chemical structures of the three structural isomers of pentane: (a) *n*-pentane, (b) 2-methyl butane and (c) 2,2-dimethyl propane.

Many studies have compared the difference between using structural isomers of epoxies and hardeners [28–34]. A good example is a study by Riad *et al*. where they used three different structural isomers of the diamine hardener, phenylene diamine, cured with resorcinol diglycidyl ether, which are shown in Figure 2.10 [29]. The hardener is based on a single phenylene ring, a disubstituted benzene ring. There are three different isomers possible: (a) is the *ortho* isomer with the two amines at positions 1 and 2, (b) is the *meta* isomer with amines at positions 1 and 3 and (c) the *para* isomer with amines at position 1 and 4. In this study, Riad *et al.* found the

T_g of cured *ortho*, *meta* and *para* were 129 °C, 131 °C and 148 °C respectively and their maximum rate of reaction of 0.0010 mol g^{-1} min^{-1}, 0.0022 mol g^{-1} min^{-1} and 0.0070 mol g^{-1} min^{-1} respectively [29].

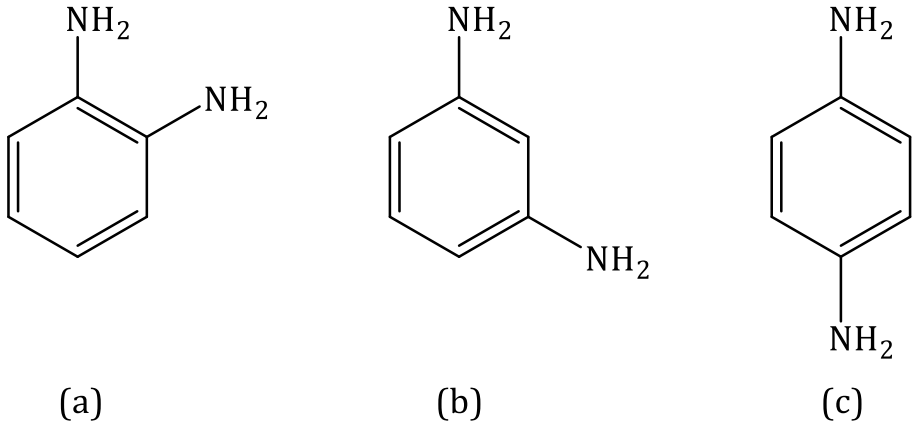

Figure 2.10 – Chemical structures of the three structural isomers of phenylene diamine: (a) *ortho*-phenylene diamine, (b) *meta*-phenylene diamine and (c) *para*-phenylene diamine.

Riad *et al.* found the greater the angle of separation, the faster the rate of reaction and the higher the final T_g value. The *ortho* position decreases the packing efficiency due to the less linear shape compared to *para* isomers, resulting in a lower a T_g and a less mobile hardener, reducing the rate of reaction [29]. Suggesting that network formation in PDA systems is dictated by steric hindrance.

Varley *et al.* used isomers of another diamine hardener, bis(aminophenoxy)benzene, cured with diglycidyl of bisphenol-F (DGEBF) [28]. Due to the extended length and incorporation of three phenylene rings, four different isomers are possible by varying the *ortho*, *meta*, and *para* positions, shown in Figure 2.11. These different isomers incorporate many different effects, one being the difference in T_g values. The T_g values obtained when cured isothermally at 140 °C for (a) 1,3-bis(3-aminophenoxy)benzene (133 APB), (b) 1,2-bis(4-aminophenoxy)benzene (124 APB), (c) 1,3-bis(4-aminophenoxy)benzene (134 APB) and (d) 1,4-bis(4-aminophenoxy)benzene (144 APB) were 119.5 °C, 121.5 °C, 129.5 °C and 136.2 °C respectively. Varley *et al*. found that when there was greater *para* substitution in the diamine hardener, the linearity and rigidity of the chain was increased and T_g increased. It is important to stress that T_g is not the only property that is of interest in when characterising materials, but it is a good

indication of the network structure. T_g can be obtained by using a dynamic mechanical analysis (DMA) tan δ plot, a large peak at high temperature indicates T_g.

DMA can also give information regarding the sub-ambient transitions. One main transition will be referred to as the β transition as done so by Ramsdale-Capper and Foreman [32], different studies use different terminology. For example, Varley *et al.* use γ nomenclature for this transition [28].

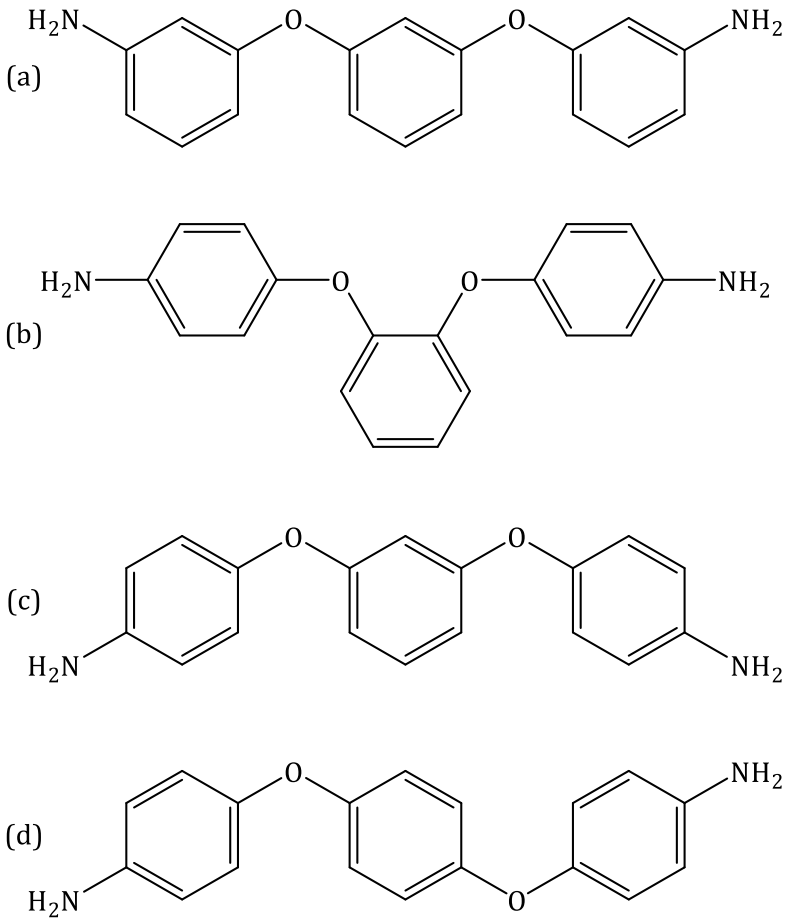

Figure 2.11 – Chemical structures of the four structural isomers of the diamine hardener bis(aminophenoxy)benzene: (a) 1,3-bis(3-aminophenoxy)benzene, (b) 1,2-bis(4-aminophenoxy)benzene, (c) 1,3-bis(4-aminophenoxy)benzene and (d) 1,4-bis(4-aminophenoxy)benzene.

The β transition refers to the short-range molecular motions [28,32,35], particularly what the phenylene rings do at sub-ambient temperatures. Depending on the chemical structures, the phenylene rings can rotate if their bonding is symmetrical, 1,3 position on the aromatic ring. In the case of Varley *et al.*, 144 APB had a broader β transition due to the ability of all three phenylene rings to rotate, whereas 133 APB had the sharpest β peak as the phenylene rings in

the hardener could not rotate [28]. These findings were also similar in Ramsdale-Capper and Foreman, where they used the *para* and *meta* isomers of diaminodiphenyl sulphone (33'DDS and 44'DDS) and triglycidyl aminophenol (TG*p*AP and TG*m*AP), the broadest β transition was observed for the most *para* containing formulations and the sharpest for the most *meta* containing formulations [32]. Tu *et al*. also found similar results when comparing 44'DDS and 33'DDS [35]. If the phenylene rings can rotate, a decrease in modulus is often seen, or vice versa, which is speculated to be related to the amount of molecular space that ring rotation takes up [28,32].

Staying with Varley *et al*., another effect on the crosslinked network was related to the reactivity of the functional groups depending on their position on the ring. Consideration of two principles is needed when comparing the chemistry of the starting materials, the resonance and the inductive effects. The inductive effect refers to the ability of a functional group to either withdraw or donate electron density. At *ortho* or *para* positions, the ether in APB will activate the amine group. Resonance refers to the delocalisation of lone pairs of electrons from the reactive functional group through the aromatic ring to another functional group. Depending on whether it is an electron-withdrawing or donating group will depend on how this affects the reactivity. In the case of APB, there is an electron-donating ether group; thus, the amine group is activated at *para* and *ortho* positions. This is a rather complicated case, but the more *para* positions in APB, the more activated the amine groups are [28]. Leading to differences in network formation due to the different activation energy required between the different structural isomers.

The resonance effect for comparing 44'DDS and 33'DDS has been commented on in past literature and has a more straightforward explanation. Varma and Bhama stated that due to an electron-withdrawing sulphone group in DDS, the delocalisation of the nitrogen's lone pair of electrons is possible when in the *para* position. This is not possible in 33'DDS as the amine is in the *meta* position [36]. This results in 33'DDS being more reactive than 44'DDS. As mentioned above, a more reactive hardener will affect the network growth, the reactions that occur at points in the cure, and the crosslink density; thus, the thermal and mechanical properties will be affected. Kim and Nutt found that the T_g values for TGAP:TGDDM blends cured with 44'DDS and 33'DDS were 236.8 °C and 216.4 °C respectively.

2.2.3. FUNCTIONAL GROUP SUBSTITUTION

It is also possible to change the resultant properties of epoxy resin by substituting functional groups in the starting reagent, resulting in multiple effects. One example is DGEBA vs DGEBF (diglycidyl ether of bisphenol F). Figure 2.12 shows the comparisons of the chemical structures. The chemical structure difference between these two resins is the substitution of two hydrogens in DGEBF for two methyl groups in DGEBA. There should be little effect on the reactivity of the epoxide group by replacing a methyl with hydrogen. Still, Frank and Wiggins found by near-infrared spectroscopy that when curing with 44'DDS, DGEBF had a lower final epoxide concentration than DGEBA, 0.39 mol kg $^{-1}$ and 1.03 mol kg$^{-1,}$ respectively [37]. The reasoning for this finding could be related to the flexibility of the epoxy chain; the methyl groups restrict movement, reducing the mobility compared to the hydrogens.

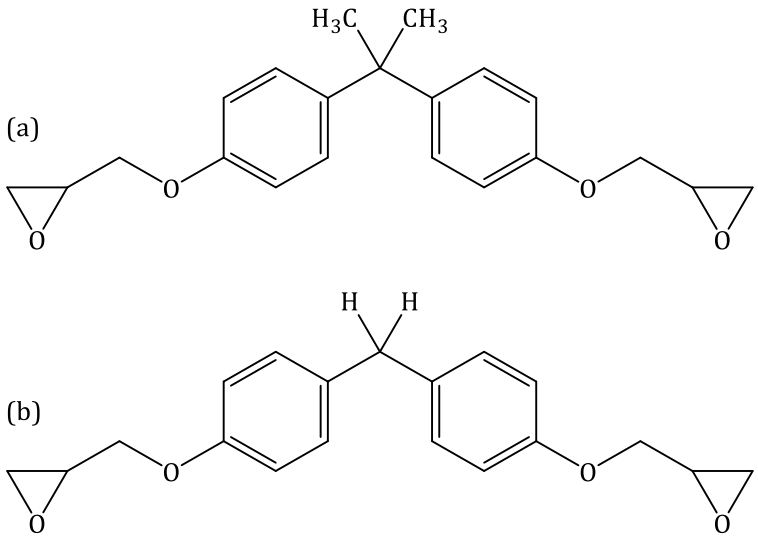

Figure 2.12 – Chemical structures of (a) diglycidyl ether of bisphenol A (DGEBA) and (b) diglycidyl ether of bisphenol F (DGEBF).

Another study by Knox *et al*. studied the chemical performance of DGEBA and DGEBF and found that DGEBF showed better chemical resistance which they related to density, despite a mix of *para-para*, *para-ortho* and *ortho-ortho* isomers [12]. These results align with Frank and Wiggins's findings: DGEBF/44'DDS had smaller pore sizes than DGEBA/44'DDS, 64 Å^3 and 76 Å^3 respectively [37]. The smaller pore sizes as determined by positron annihilation lifetime spectroscopy resulted in less methyl ethyl ketone and water uptake for the DGEBF resins, as

confirmed by Jackson *et al.* [30]. Small changes in chemical composition can significantly impact resin properties despite no apparent change in the reactivity of the epoxide group.

Another example of functional group substitution is in aromatic diamine hardeners. As mentioned, 44'DDS is a widely used hardener, but other hardeners are available based on the diaminodiphenyl structure. A study by Patel *et al*. used three different 4,4'-diaminodiphenyl hardeners to investigate how chemical structure influences the properties of the cured material [38]. Figure 2.13 shows three different diaminodiphenyl hardener structures used where the group at the phenylene bridge differs: (a) 4,4'-diaminodiphenyl sulphone (DDS), (b) 4,4'-diaminodiphenyl methane (DDM) and (c) 4,4'-diaminodiphenyl ether. Unlike DGEBA vs DGEBF, it would be expected to see a change in the reactivity of the amines due to the different chemical groups being next to an aromatic ring.

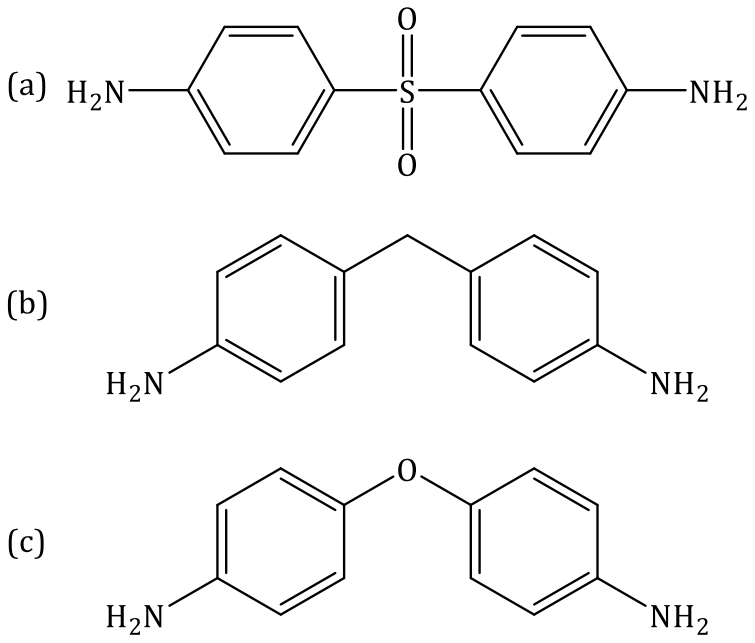

Figure 2.13 – Chemical structures of the three 4,4'-diaminodiphenyl hardeners: (a) 4,4'-diaminodiphenyl sulphone (DDS), (b) 4,4'diaminodiphenyl methane (DDM) and (c) 4,4'-diaminodiphenyl ether (DDE).

Patel *et al*. found that when cured with TG*p*AP, the reactivities of diaminodiphenyl hardeners differed, with DDM being the most reactive, followed by DDE and then DDS [38]. The maximum rate of reaction temperature using dynamic DSC measurements with a heating rate of 5 °C min^{-1} for DDM, DDE and DDS were 138 °C, 149 °C and 186 °C, respectively. The cause of this was the *para* position of the amines on the phenylene rings, which allowed for the delocalisation of

electrons through the phenylene ring. The sulphone group is considered an electron-withdrawing group, which allows for delocalisation of the lone pair of electrons from the nitrogen, thus reducing its nucleophilicity. The ether and methane groups are not; they are electron-donating groups. Instead, they increase the reactivity of the amine group. The *para* position relates to the ethers in APB from Varley *et al*.; the more *para* components, the greater the amine reactivity [28]. Costa *et al.* also found that DDM was more reactive than DDS when cured with DGEBA, as the maximum rate of reaction temperature was 157 °C and 226 °C, respectively [39]. Mustafa *et al*. corroborated this by comparing the cures of DDM and DDS with TGDDM. They found that the amine of DDM was more basic than DDS using nuclear magnetic resonance, proving it is a more effective nucleophile [40]. Siddaramaiah and Jagadeesh investigated the cure properties and thermal stability of TGDDM cured with DDS, DDM and DDE [41]. The T_g for TGDDM DDS, DDM and DDE were 233 °C, 227 °C and 226 °C, respectively.

2.2.3.1. GLYCIDYL ETHER VS. GLYCIDYL AMINE

Epoxide groups are bonded to the epoxy backbone in two different ways. One by an ether link shown in Figure 2.14 (a) and the other by tertiary amine as shown in Figure 2.14 (b). A clear difference between these two is the number of epoxide groups present; glycidyl ethers have one epoxide, and glycidyl amines have two epoxide groups present. Consider DGEBF and TGDDM in Figure 2.12 (b) and Figure 2.3 (c); the chemical structure between the glycidyl links is the same, two aromatic rings with a methyl bridge, but DGEBF contains two glycidyl ethers, whereas TGDDM contains two glycidyl amines. The functionality of DGEBF is two, and TGDDM is four, the EEW is lower for TGDDM. For pure monomers of DGEBF and TGDDM, the EEW are 156 g mol^{-1} and 105.5 g $mol^{-1,}$ respectively. Using the same hardener, it would be expected that the thermomechanical properties of the cured resin to be higher in TGDDM. The T_g as determined by DMA for DGEBF/44'DDS was 175 ^oC [42] and TGDDM/44'DDS was 263 ^oC [43].

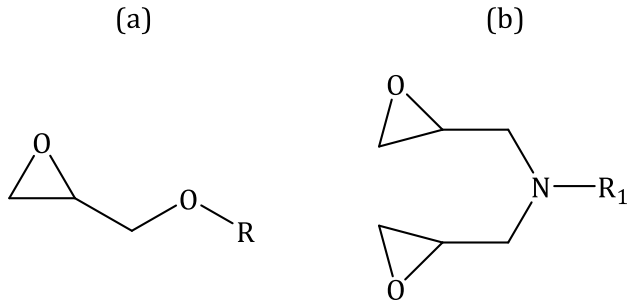

Figure 2.14 – Chemical structures of (a) glycidyl ether and (b) glycidyl amine.

It is well documented that unwanted side reactions occur in glycidyl amines [14,44–48]. These side reactions are not reactions with different types of atoms but with atoms on the same glycidyl amine, causing a cyclic structure. These structures are not directly detectable using techniques such as infrared spectroscopy or differential scanning calorimetry [49]; instead, Matějka *et al.* used high-performance liquid chromatography (HPLC) [45], and Attias *et al*. used HPLC and ^{13}C nuclear magnetic resonance (NMR) [46]. Cyclisation occurs due to the proximity of reactive groups in the glycidyl amine. This does not occur in glycidyl ether-based resins as there is only one epoxide group. Internal cyclisation can occur through two reactions, a secondary amine epoxy addition and etherification, as shown in Figure 2.15 (a) and (b), respectively. Internal cyclisation has been found to proceed through the etherification reaction more prevalently than the secondary amine epoxy reaction [50,51].

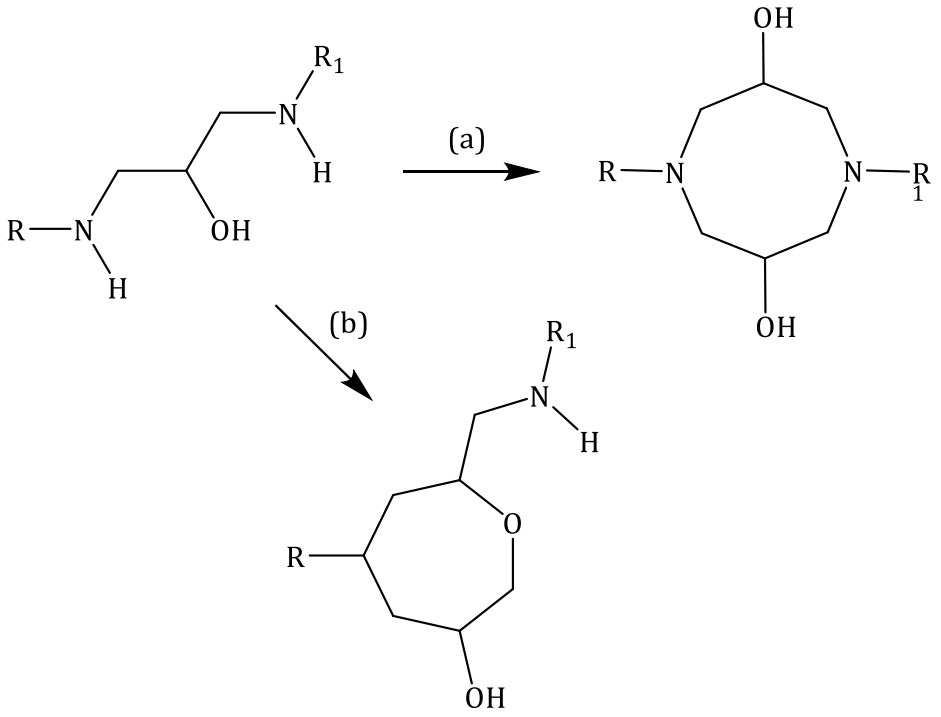

Figure 2.15 – Internal cyclisation of glycidyl amine through two different reactions: (a) secondary amine epoxy addition and (b) etherification.

Forming cyclic structures reduces the crosslink density as instead of linking chains, the chain is extended. This is seen in the degree of cure at which gelation occurs [14,48,52]. The Flory equation shown in equation (2-1) indicates the conversion at which the network will gel [53]:

$$\alpha_{gel}^2 = \frac{1}{(f-1)(g-1)} \qquad (2\text{-}1)$$

Where f is the functionality of the epoxy monomer, and g is the functionality of the amine monomer. For a stoichiometric ratio of TGDDM and 44'DDS, the predicted gel point would be 33 % conversion, whereas St John found the gel point to be 59 %, which is significantly higher than the theoretical [14]. One reason is that they did not use a stoichiometric ratio, and the Flory equation does not support excess epoxy calculations, but even then, the theoretical gel point would be approximately 48 %. This discrepancy was attributed to high levels of etherification, which caused cyclic structures to form.

Liu *et al.* and Swan *et al*. studied the effect of using tetra-glycidyl ether epoxies compared to tetra-glycidyl amine epoxies [43,52]. Liu *et al*. used a resin based on 1,4-Bis(4-

formylphenoxy)butane given the nomenclature TFTE, using a blend of TFTE and DGEBA cured with 44'DDS, similar T_g values were obtained when 40 wt % was used in the blend (260 °C vs. 263 °C), the viscosity of the neat resin was lower enabling better processing and there was 30 % less water absorption. These improved properties were associated with the lack of internal cyclisation reactions [43]. Swan *et al*. saw a similar trend using bis(2,7-glycidyl ether naphthalenediol) methane (NNE) cured with 44'DDS, where a higher T_g was obtained in comparison to TGDDM/44'DDS and better fracture toughness, whereas higher fluid uptake was observed as attributed to the poorer packing of the rigid naphthalene backbone [52]; the lack of internal cyclisation allowed for higher crosslink density.

Another point Swan *et al.* raised was TGDDM glycidyl amine's ability to promote homopolymerisation as nitrogen can behave as a tertiary amine catalyst [52]. St John and George stated that the tertiary amine can form a 'quaternary amine-alcoholate' with an epoxide group and then react with another epoxy group [54]. No nitrogen is present in glycidyl ether; therefore, homopolymerisation and etherification reactions are less likely at low degrees of cure than glycidyl amine-containing resins.

2.2.4. TOUGHENING

As suggested from the discussion above, increased crosslink density results in an increase in T_g. Nielsen gave an equation which relates the shift in T_g to M_c, the average molecular weight between crosslink junctions as shown in equation (2-2) [55]:

$$T_g - T_{g_0} = \frac{3.9 \times 10^4}{M_c} \qquad (2\text{-}2)$$

Where T_{g_0} is the glass transition temperature of uncured resin. As M_c decreases, the shift in T_g increases. Using multifunctional epoxies such as TGAP, TGDDM, TFTE and NNE results in lower mass between crosslinks and, thus, a higher T_g. While high service temperatures are desirable for high-performance applications in sectors such as aerospace [56], there comes an inherent brittleness [43,48,57]. Toughening is critical to increasing the suitability of these high-temperature epoxies for wider applications where impact and fracture events are likely to occur.

There have been many different approaches to toughening, such as the addition of thermoplastics, most notably polyetherimide [47], polyethersulphone [58,59] and phenolic terminated polysulphone [60,61]. Shang *et al.* commented on this approach's increased viscosity and the elevated processing temperature needed; instead, they focused on modifying the epoxy backbone to increase toughness [62]. The study compared the effect of adding a flexible oxyphenylene ring to TG*p*AP to give triglycidyl of 4-(4-aminophenoxy) phenol) (TGAPP) as shown in Figure 2.16. Processability was similar to TG*p*AP, and tensile strength and impact strength improved but with an 8 °C decrease in T_g. A decrease in T_g is often seen when toughening as crosslink density decreases but the improvement in toughness outweighs this decrease.

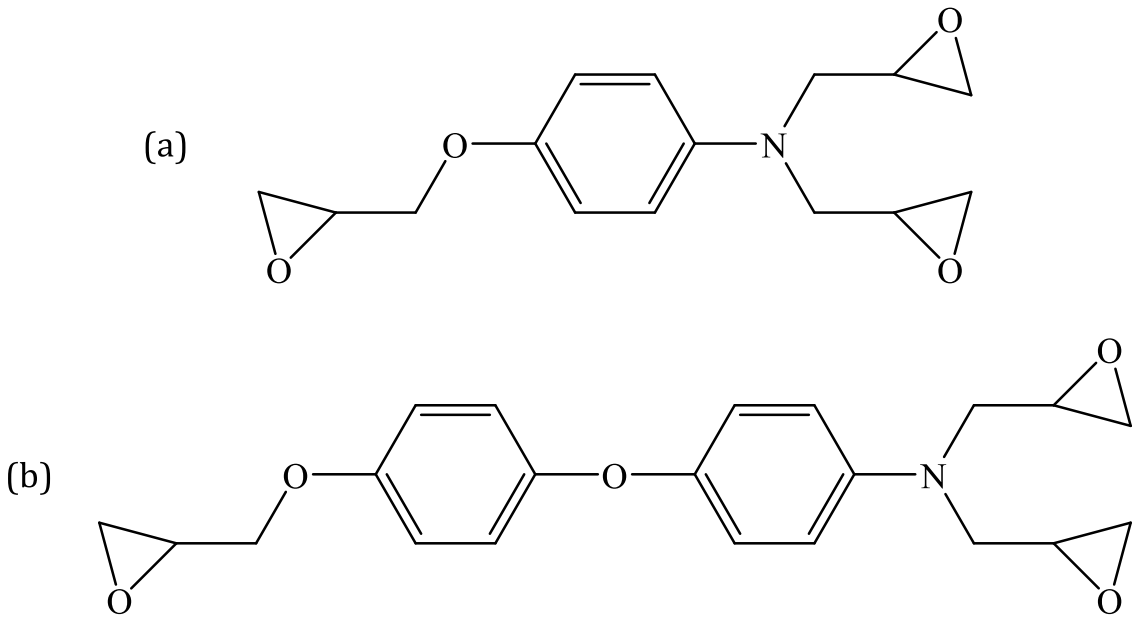

Figure 2.16 – Chemical structures of (a) triglycidyl-para-aminophenol (TG*p*AP) and (b) triglycidyl of 4-(4-aminophenoxy) phenol) (TGAPP).

Ramsdale-Capper and Foreman investigated the resultant properties of cured structural isomers of TGAP/DDS. They found that the *meta* formulations of TGAP/DDS resulted in internal antiplasticisation, an increase in glassy modulus, yield stress, density, strain to failure and fracture toughness [32]. Unlike toughening using thermoplastic fillers, they observed increased strain to failure as the crosslink density decreased, allowing for greater plastic flow. This study will follow this work and study the network formation of the structural isomers of TGAP/DDS,

investigating the causes of this toughening effect through changes in chemical structure rather than the addition of different phases.

2.3. CURE MONITORING

The factors that affect network formation can be found by analysis of the resultant properties outlined in 2.2 and by the knowledge of the chemistry of the reactants. The point at which these reactions occur is important, and by using cure monitoring techniques, the real-time changes in the curing process can be tracked [63]. Various techniques can be used to track the numerous properties that change in the cure. Such properties are thermal, mechanical, electrical and optical. The following section will discuss the uses of techniques that have monitored these properties.

2.3.1. OPTICAL

Optical cure monitoring techniques utilise the nature of a chemical bond's ability to vibrate when exposed to light. In this case, the wavelength of light is in the infrared region (10 cm^{-1} to 12500 cm^{-1}). Within this range, there are three regions: far-infrared (10 cm^{-1} to 400 cm^{-1}), mid-infrared (400 cm^{-1} to 4000 cm^{-1}) and near-infrared (4000 cm^{-1} to 12500 cm^{-1}) [64]. Far infrared is not a well-used technique when monitoring the cure of epoxy resins due to the high energy light source required and its overlap with the microwave region. It is more suited to analysing metals and the rotational energies of gases [65], whereas mid- and near-infrared are much more useful for cure monitoring, as made apparent by the number of studies utilising either of the two techniques. Both have pros and cons and are generally dependent on the epoxies in question due to the type of bonds broken and formed in the curing process.

2.3.1.1. MID-IINFRARED SPECTROSCOPY

Mid-infrared spectroscopy (MIR) is often called Fourier transform infrared spectroscopy (FTIR). However, most FTIR equipment can take measurements in the mid- and near- region [66]. In the MIR region, fundamental vibrational transitions are observed upon energy absorption. Fundamental transitions are transitions from one vibrational energy state to the next, resulting in high-intensity spectral peaks. The strength (or in fact, the stiffness) of the bond

determines the frequency at which the vibration occurs, and the vibration either comes from the stretching or bending of the bond [67].

The functional groups of interest for epoxy amine-cured resins are the epoxide rings, primary amines, secondary amines, and hydroxyl groups. These functional groups show numerous peaks in the MIR spectra, and it is possible to track the intensity of these peaks as the cure progresses [68]. This technique has been used as early as 1956 when Dannenberg and Harp utilised the epoxide ring peak at 916 cm^{-1} to monitor the formation of crosslinks and determine the softening point in DGEBA systems [69]. Yamasaki and Morita used two regions in the MIR to monitor the cure, 2400 cm^{-1} to 3700 cm^{-1} and 700 cm^{-1} to 1700 cm^{-1}. Within these regions, the functional groups shown in Table 2.1 could be observed [22].

Table 2.1 – Band assignments for the functional groups of diglycidyl ether of bisphenol A and 4,4'-diaminodicyclohexane methane resins using mid-infrared spectroscopy. Adapted from Yamasaki and Morita [22]

Functional Group	Wavenumber / cm^{-1}
Epoxide Ring	912
Ether C–O stretching	1012
Ether C–O stretching	1054
Alcohol C–O stretching	1097
N–H stretching	3300 – 3365
O–H stretching	3456

While there are peaks available to monitor the cure, how these peaks present themselves is often a problem. Amine and hydroxyl peaks occur at very similar positions, 3300 cm^{-1} to 3365 cm^{-1} and 3456 $cm^{-1,}$ respectively, producing broad overlapping peaks, which presents a problem, as seen in Figure 2.17. The overlapping in both regions for the amine and hydroxyl groups and ether and alcohols means quantitatively analysing the spectra is difficult [70]. Overlapping of peaks is common in MIR due to the measurement of fundamental transitions as

they occur in a similar position. A common feature of MIR spectra is the fingerprint region. There is significant overlap in this area, which tells us more about the bulk material than the complex functional group makeup [67]. Despite this, studies have managed to quantitatively analyse MIR spectra using a technique known as perturbation-correlation moving-window two-dimensional correlation spectroscopy (PCMW2D) alongside modulated DSC (MDSC) [22,70,71].

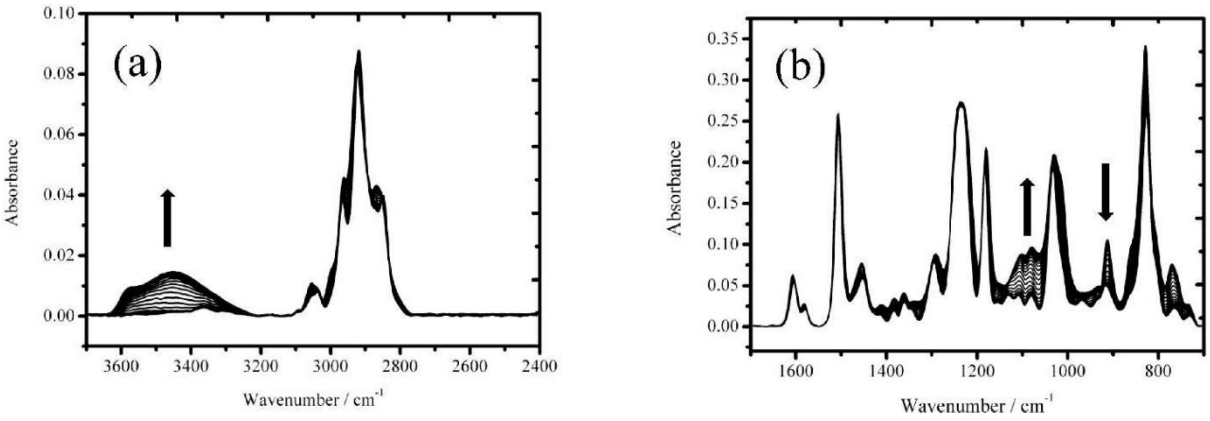

Figure 2.17 – FTIR spectra of diglycidyl ether of bisphenol A and 4,4'-diaminodicyclohexane methane resin in two regions: (a) 3700 cm^{-1} to 2400 cm^{-1} and (b) 1700 cm^{-1} to 700 cm^{-1}. Taken from Yamasaki and Morita under copyright licence 5890210960032 [22].

Poisson *et al.* found that monitoring the epoxide ring peak at roughly 915 cm^{-1} resulted in higher conversion values when compared to near-infrared spectroscopy (NIR), which they attributed to unknown non-reactive group overlap [72]. Mijović and Andjelić found a similar result when comparing MIR and NIR, with their epoxide conversion being 80 % and 90 %, respectively [73]. They also concluded that the epoxy ring peak at 915 cm^{-1} was not a unique measurement as previously thought. They gave two possible causes: an unreactive group suggested by Poisson *et al.* or a new form of hydrogen bonding occurring in the system [72,73]. Poisson *et al.* stated that MIR is unsuitable for quantifying the cure of their epoxy resin system unless this consideration was applied to the analysis. Cholake *et al.* encountered a similar overlap problem for quantifying the epoxide peak at 3050 cm^{-1} but instead with a known species, aromatic C–H. Despite the concentration not changing throughout the cure [74], care was taken to deconvolute the overlapped peak to determine the area, and they still encountered errors and instead relied on the epoxide ring peak at 915 cm^{-1} despite the known issues.

One unique motivation behind using MIR as a cure monitoring technique is the ability to observe the ether links formed during the process. Ethers are formed as a result of the etherification process [75]. Another study by Yamasaki and Morita used MIR to monitor the ether peak at 1107 cm^{-1}, whereas the other functional groups were monitored using NIR [71]. This study confirmed the difference in reactivity between amine and etherification reactions, highlighting the effect of temperature on the crosslinking formation in epoxy resins. MIR can also be used to identify tertiary amine species, which is not possible in NIR. Strehmel and Scherzer were able to analyse the content of primary, secondary and tertiary amines when epoxy:amine ratio and tertiary amine catalyst (imidazole) content were varied to investigate the importance of etherification during DGEBA/DDM cure [75]. While MIR is a useful technique, especially for identification of the ether group, NIR has particular advantages related to sample preparation and functional group band identification.

2.3.1.2. NEAR-INFRARED SPECTROSCOPY

Near-infrared spectroscopy (NIR) utilises the same theory behind MIR, but instead of fundamental vibrational transitions, non-fundamental transitions are observed. These are known as overtone and combination modes. Instead of a vibrational transition of one energy level, overtones occur when the transition is greater than one upon energy absorption and the quantum number is greater than one. Combination modes occur when two or more fundamental vibrational transitions occur. These are both forbidden transitions, which occur due to the anharmonic oscillator model and are not 'forbidden' in the sense that they don't occur. They appear as low-intensity bands at higher wavenumber values [64].

These transitions do not occur in all the functional groups that display peaks in the mid-infrared region due to the anharmonic constant, χ_e. A group with a small anharmonic constant will require more energy for a non-fundamental vibrational transition, as shown in equation (2-3).

$$\Delta\tilde{E}_{(0\rightarrow\upsilon)} = \tilde{\upsilon}_e\upsilon[1-\chi_e(\upsilon+1)] \qquad (2\text{-}3)$$

Where $\Delta\tilde{E}_{(0\rightarrow\upsilon)}$ is the observed energy required for the vibrational transition to occur, υ is the vibrational quantum number, and $\tilde{\upsilon}_e$ is the absorption wavenumber. Hydrogen-containing

molecules generally have the largest anharmonic constants; for example, the anharmonic constant of H_2 is 0.02685, whereas NO is 0.007337 [64]. Therefore, peaks are only observed from hydrogen-containing functional groups in the NIR spectra. This is also a benefit, as the functional groups that react in the epoxy amine cure are hydrogen-containing functional groups, CH and CH_2 on the epoxide ring, the N–H for both primary and secondary amines and the O–H hydroxyl group [77]. As a result, NIR produces spectra with clearly separated peaks that can be quantitatively analysed. NIR sample preparation is simple due to the low intensity compared to MIR, and the absorption is less affected by sample length, meaning thicker samples can be used [78,79].

Quantitative analysis of both NIR and MIR is possible due to the behaviour of light when absorbed through a material. Its behaviour has been well studied, and relationships have been found between the initial and emitted light intensity as early as 1854 [80]. As a result, a law for optical spectroscopy was determined through much collaboration and was first published in the modern-day form by Luther and Nikolopulos in 1913 [81]. It is known as the Bouguer-Beer-Lambert law and is shown in equation (2-4). There is a particularly extensive review by Mayerhöfer *et al.* on the development of the Bouguer-Beer-Lambert law, which is very useful [82].

$$\log\frac{I_0}{I} = A = \varepsilon\, c\, l \qquad (2\text{-}4)$$

Where I_0 is the initial intensity of light, I is the intensity of light after travelling through the material, A is absorbance, ε is the molar absorption coefficient, c is concentration and l is the path length. The first part of the expression is the Bouguer-Lambert derived section, and although necessary, NIR utilises the last section, known as the Beer law, where there is a proportional dependence between absorbance and concentration. Previous studies have found the area of the relevant peak and used the path length of the material under test and the predetermined molar absorption coefficient to determine the concentration of the functional group in question during the cure [48,49].

A wide range of epoxy resin systems have been studied using NIR, but depending on the hardener choice determines how extensively the functional groups can be analysed. Duemichen *et al.* analysed two different classes of hardener cured with DGEBA resin: an anhydride,

methyltetrahydropthalic anhydride and an aliphatic amine mixture of isophorodiamine and alkyletheramine [83]. Due to the lack of hydrogen-containing reactive groups in anhydrides, different information is obtained, as shown in Figure 2.18. Three more peaks are shown in the epoxy amine-cured system allowing for further analysis and information about the curing process.

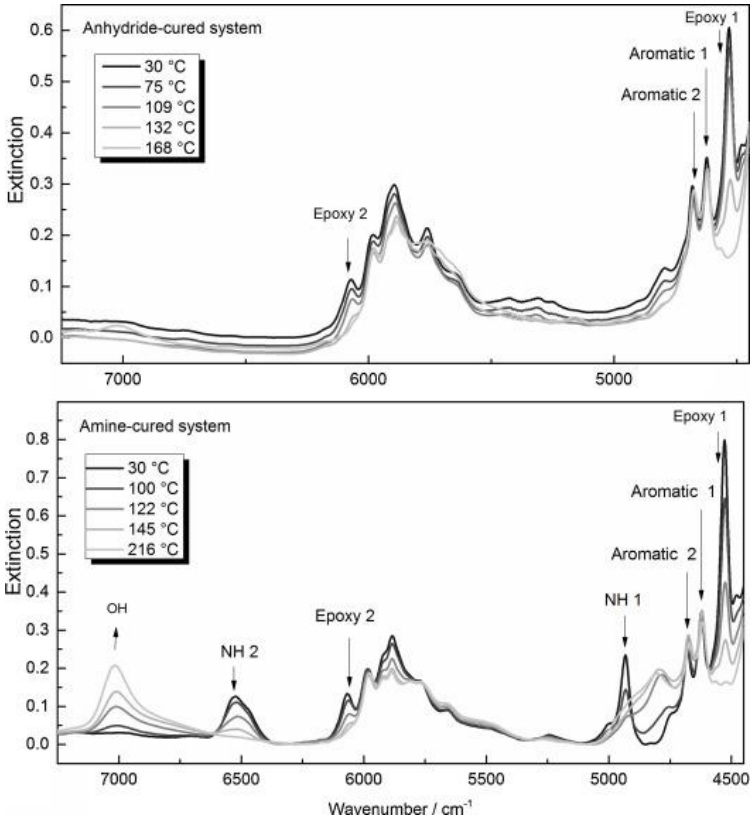

Figure 2.18 – Near-infrared spectra of two different epoxy hardener cured systems: epoxy/anhydride cured system (top) and epoxy/amine cured system (bottom). Taken from Duemichen *et al.* under copyright licence 5890860193095 [83].

With this, it is no surprise that NIR has been used to monitor the cure in many resin systems. Min *et al*. quantitively analysed DGEBA/44'DDS systems with a polysulphone modifier [61], Varley *et al.* used NIR for a study investigating TG*p*AP/44'DDS systems [48], Billaud *et al.* studied DGEBF/TG*p*AP blends cured with 4,4'-methylene-*bis*-(2,6,-diethylaniline) [84], St John and George with TGDDM/44'DDS resins [49] and Mijović and Andjelić used NIR to model a model epoxy system of phenyl glycidyl ether and aniline [85]. These are a few excellent studies; there are many more [30,37,70,72,75,86–93].

Figure 2.18 shows peaks that are well separated and of suitable intensity to analyse. That said, the analysis is still not simple as suggested by Varley *et al.* [48]. Identification is not as simple as reading from a characterisation table. Analysis of starting reagents is required to assign as many peaks as possible. A study by Mijović and Andjelić used the epoxide ring peak at 4530 cm^{-1} to monitor epoxide concentration [85], whereas in Varley *et al.,* a peak at 4530 cm^{-1} occurred in the NIR spectra of both TG*p*AP and 44'DDS suggesting 4530 cm^{-1} is a combination of epoxide rings and primary amines [48]. The same was found in Min *et al.* [61]. This could be a feature of the DDS hardener that the NH_2 peak overlaps with the epoxide ring in the 4530 cm^{-1} region, whereas in other hardeners such *meta*-xylylenediamine as used by Knox *et al.* [87] or aniline as used by Mijović and Andjelić [85] the bands are treated as not overlapping. The benefit of NIR is that if there is overlap in the same region, the next overtone or combination band of the functional group can be used as Varley *et al.* and St John and George did when studying TGpAP and TGDDM, respectively. They used the epoxide peak at 5880 cm^{-1} and 6060 cm^{-1}, where there was less overlap, and the peak could be more accurately measured [48,49].

As mentioned in 2.2.2, isomerism effects have also been studied using NIR. Jackson *et al.* studied the difference in the glassy epoxy network in DGEBA, DGEBF and TGDDM cured with the structural isomers DDS [30]. NIR was able to identify the difference in reactivity between 44' and 33'DDS. In DGEBA/33'DDS, primary amines were 99 % consumed in 2 hours; in DGEBA/44'DDS, only 50 % of primary amines were consumed in 2 hours. This reactivity difference was shown in their average pore size free volume, 33'DDS formulations resulted in smaller average hole-size than 44'DDS [30].

Using different isomers or reactants, it would be expected to see a difference in morphology and mechanical properties [24]. NIR allows us to attribute the reactions responsible for the change in properties. Etherification has been accounted for using NIR by either measuring the hydroxyl concentration change or calculating the concentration of ethers using the concentration of epoxide groups that have reacted without amines [20]. Thus, determining the effect structural isomerism has on network formation.

2.3.2. THERMAL

When reactions take place, energy changes occur. These can be either endothermic and exothermic reactions. An endothermic reaction absorbs energy from the surroundings, whereas

exothermic reactions release energy into the surroundings. The total change in enthalpy is positive for endothermic reactions as the reactants have a lower energy level than the reactants and negative for exothermic reactions as the reactants have a higher energy level than the products, as shown in the potential energy diagrams in Figure 2.19. In endothermic reactions, the products are less stable than the reactants and vice versa for an exothermic reaction.

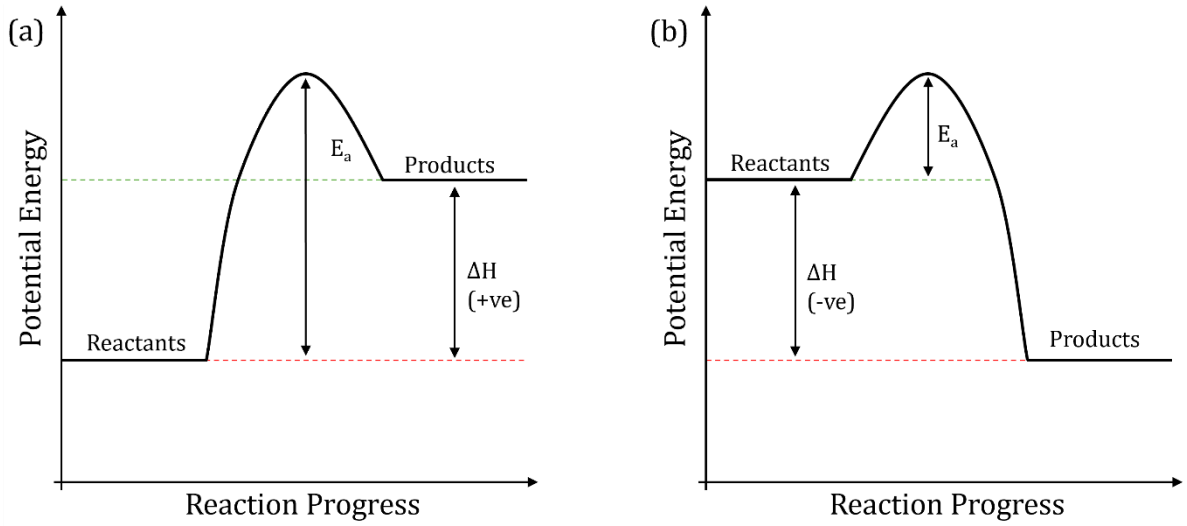

Figure 2.19 – Potential energy diagram that shows the potential energy of a reacting system: (a) shows an endothermic diagram where the potential energy of the products is greater than the reactants, energy is absorbed from the surroundings, the enthalpy of reaction is positive and (b) shows an exothermic reaction where the potential energy of the reactants is greater than the products, energy is released to its surroundings, the enthalpy of reaction is negative.

Epoxide ring opening reactions are exothermic as the reactants are less stable than the products [94]. An epoxide ring is constrained and does not require much energy to open from an attack by a chemical species such as a nucleophile. The 'hump' shown in Figure 2.19 is the activation energy, the energy required for the reaction to occur. The size of this depends on the reactivity of the hardeners and if any catalysts are present. Reactions at room temperatures will have a smaller activation energy than those that can only occur at high temperatures. With this behaviour of epoxide ring reactions, the cure can be observed by monitoring either the temperature of the resin or the enthalpy changes during the cure.

2.3.2.1. RESIN TEMPERATURE MEASUREMENTS

From the exothermic nature of the curing reactions, it is possible to track the network formation using resin temperature with respect to the applied oven temperature. It is a straightforward technique and, surprisingly, something that has not been widely commented on in previous studies. According to Lodeiro and Mulligan, four different temperature measurement methods are available: thermal imaging using infrared radiation, resistance temperature detectors, thermochromic devices and thermocouples [63].

The simplest of these techniques are thermocouples. They consist of two dissimilar wires connected at a junction where a voltage is generated that corresponds to a particular temperature [95]. This occurs because of the Seebeck effect, where an electromagnetic field is generated as the free electrons in one wire have a higher temperature than that of the other wire with fewer electrons, which then diffuse, causing a negative charge resulting in charge separation and thus a measurable net voltage between the two wires [96]. Due to the Seebeck effect, no power is needed to measure temperature. There are many different types of thermocouples available depending on the temperature range. For measuring epoxy curing oven temperatures, K types, which consist of nickel-chromium and nickel-aluminium wires, are usually used [97]. These are connected to a data logger, and the temperature readings are taken as a function of the cure. The flexibility of the wires mean that thermocouples can be placed in various places, they are perfect for embedding in uncured resin of different moulds and composite moulds and can monitor the cure on-line without impacting the manufacturing process other than sacrificing a small section of resin for thermocouple insertion.

Surprisingly, little literature has commented on the behaviour of epoxy resin using thermocouples, possibly due to the lack of sensitivity that comes with the measurement. Despite the cure of epoxy resin being an exothermic reaction, if small amounts of resin are used, a significant temperature overshoot may not occur. Similar studies from both Duemichen *et al.* and Erdmann *et al.* used thermocouples to track the resin temperature during the cure of epoxy amine systems while taking near infrared measurements [83,88]. Figure 2.20 is taken from Erdmann *et al.* and shows a modest temperature overshoot at the start of the 120 °C dwell in both systems, which coincides with the point at which the rate of change of degree of cure is the greatest. This slight overshoot is obtained from a sample of 3 – 4 grams. If the sample was bigger, the overshoot may be more significant, and it could be possible that temperature overshoots

would be seen at other places during the cure. No comment was made by Erdmann *et al.* on this finding, perhaps because the cure could be explained more accurately by their results from DSC and NIR [88].

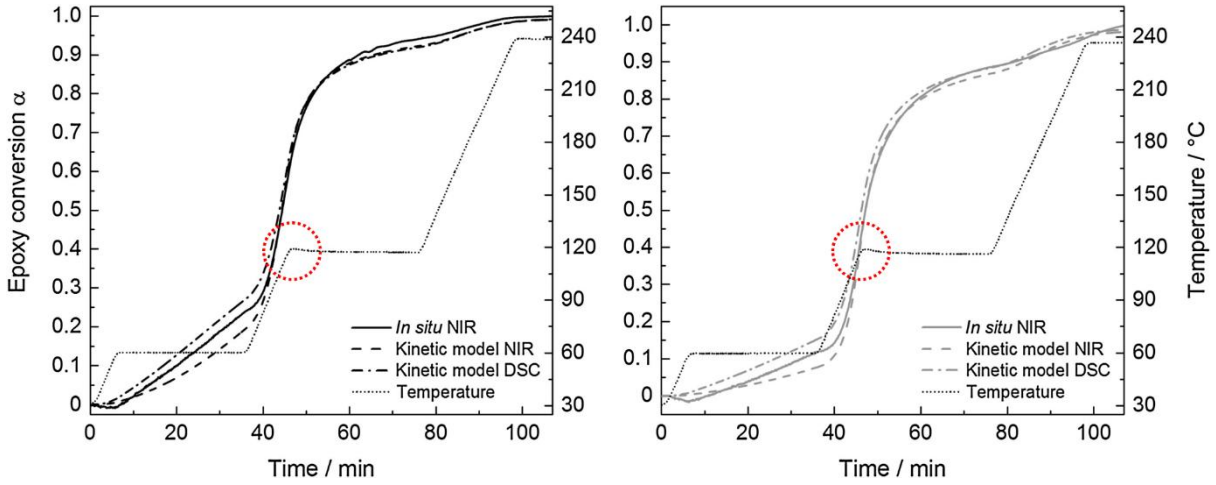

Figure 2.20 – Resin temperature measurements taken using thermocouples in two different epoxy amine systems. Temperature overshoots are identified by a red dotted circle. Modified from Erdmann *et al.* [88] under copyright licence 5902020318683.

Shigue *et al*. and Wu *et al.* also used thermocouples to monitor the temperature of the resin while curing but did not comment on the results [98,99]. While it would have been insightful to see the results, the technique was perhaps more to validate that the required temperature was reached rather than investigate the thermal response of the resin while curing. This study used isothermal heating, a constant curing temperature, and a temperature overshoot would only be seen where the maximum rate of reaction occurred.

Ran *et al.* measured the exotherm in two different DGEBA diethylene triamine systems. The two systems can cure at room temperature as the hardeners, Versamid diethylene triamine and butyl ether modified diethylene triamine (BDETA), generate a significant exotherm that drives the curing reaction. BDETA undergoes an extreme temperature increase up to 175 ^{o}C from a cure temperature of 25 ^{o}C as measured by thermocouples in the centre of the sample. Temperature measurements were used to determine the causes of this exothermic behaviour and to determine a method to control it so that it can be utilised in the curing process [100]. Zhang *et al*. also found a significant temperature overshoot (25 ^{o}C) when curing DGEBA and phenolic aldehyde resin using a photoinitiator and electron beam radiation. They found that a temperature overshoot occurred when the energy supply was increased, which then decreased as the cure progressed [101]. They determined that the overshoot did not affect the gel fraction.

The information gained from temperature measurements is limited, as high-temperature overshoots can lead to thermal degradation and premature cure, resulting in poor resin properties. An alternative method is needed to accurately measure the resin system's exothermic response as it cures.

2.3.2.2. DIFFERENTIAL SCANNING CALORIMETRY

Differential scanning calorimetry is another technique that utilises the exothermic nature of the epoxide ring opening nature. Instead of measuring the temperature of the resin while it cures in a standard convection oven, it is possible to accurately monitor the exothermic (or endothermic) response during the cure using a differential scanning calorimeter. DSC can measure epoxy samples as small as 5 – 20 mg taken from a larger sample, an example of an offline cure monitoring technique.

There are two types of DSC available: heat flux and power compensated. Heat flux measures the difference between the temperature of the sample and a reference pan. In contrast, power compensation measures the difference in power required to heat the sample and reference pan to a particular temperature. Both have their benefits and can be used interchangeably for epoxy resins. There have been extensive studies into the cure of epoxy resins, all focusing on different kinetic analyses of the crosslinking network [29,41,58,102–136].

Degree of cure is a measurement of great interest. It tells us how cured the resin is; a high degree of cure would suggest that the resin is nearly fully reacted and highly crosslinked. Degree of cure can be related to T_g by the Di Benedetto equation given in equation (2-5) [55,137].

$$\frac{T_g - T_{g0}}{T_{g\infty} - T_{g0}} = \frac{\lambda\alpha}{1 - (1 - \lambda)\alpha} \qquad (2\text{-}5)$$

Where T_{g0} is the glass transition temperature of the uncured resin, $T_{g\infty}$ is the glass transition temperature of a fully cured resin, α is the degree of cure, and λ is a parameter related to the difference in heat capacity between the uncured and fully cured resin.

Degree of cure measurements are used to understand how many unreacted groups remain in the system, which may relate to water and chemical resistance but also indicates how much the thermomechanical properties can be improved. Ramsdale-Capper and Foreman used DSC to determine the residual enthalpy of cured samples of structural isomers of TGAP/DDS [32].

First, dynamic heating (constant heating rate) of uncured samples was used to determine the total enthalpy of cure, ΔH_0, from where the degree of cure could be determined by finding the residual enthalpy from the cured samples, ΔH_{res}, the calculation is shown in equation (2-6).

$$\alpha = \left(1 - \left(\frac{\Delta H_{res}}{\Delta H_0}\right)\right) \times 100 \qquad (2\text{-}6)$$

Where α is degree of cure. A similar method was used to determine the degree of cure when taking isothermal measurements. The sample was held at a constant temperature for a set time, cooled and then dynamically heated, and the residual exotherm was found [102,118,138]. When dynamically heating uncured resin using different heating rates, the samples are heated to a temperature where no further curing occurs. The difference in network formation can be observed using the degree of cure. An example from Wu *et al.* is shown in Figure 2.21 (a), where TGDDM was cured with dicyanodiamide at different heating rates [134]. The overall behaviour was the same but shifted to higher temperatures when a faster heating rate was used. The derivative of degree of cure is the rate of reaction, and this tells us how fast the reaction is occurring. When comparing dynamic measurements, it is expected that the rate of reaction will be higher when using faster heating rates. It is important to note that in Figure 2.21 (b), the *x*-axis is degree of cure. In dynamic scans, these values are obtained at different temperatures, which indicates that the reaction mechanism is the same irrespective of temperature. Karkanas undertook similar measurements and validated that the reaction mechanism was the same at different heating rates by normalising the reaction rates and found that the curves overlapped [139].

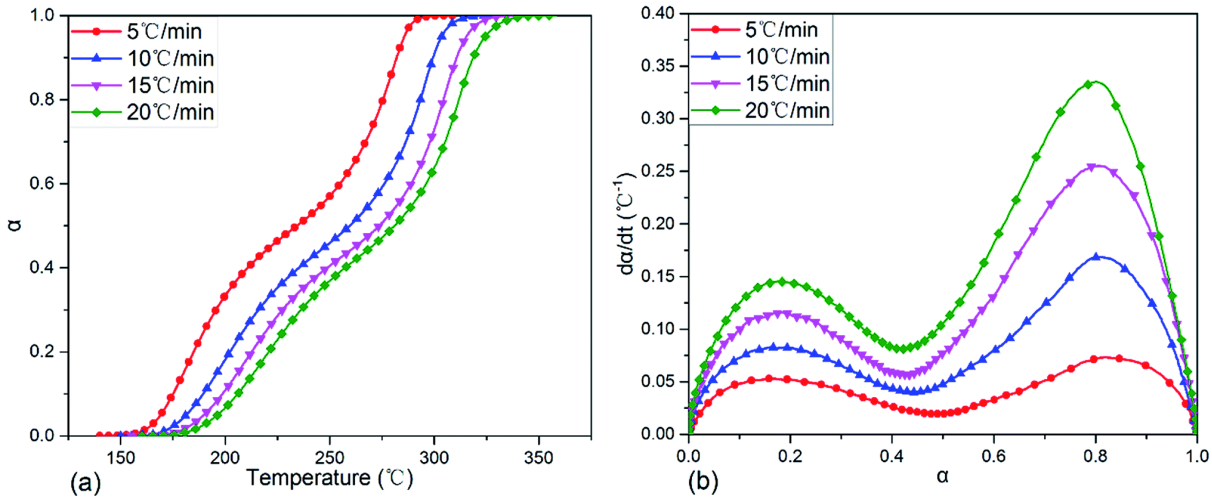

Figure 2.21 – (a) Degree of conversion and (b) rate of reaction plot from DSC dynamic heating measurements of TGDDM/DICY using different heating rates. Taken from Wu *et al.* [134] licenced under CC BY 3.0.

DSC can apply heat in two different ways: dynamically and isothermally. Gerami *et al.* stated that dynamic heating provided more reliable information than isothermal measurements [118]. This statement might not be entirely accurate. Dynamic measurements heat over a range of temperatures, and the resin is expected to achieve a cure degree of 100 %, whereas isothermal heating doesn't often completely cure the resin. Dynamic heating gives information about the temperatures at which the resins cure most effectively, whereas isothermal heating gives information about the time required to cure at that temperature. Activation energies as a function of cure using dynamic measurements are calculated using methods such as Friedman or Flynn-Wall-Ozawa [140,141], where insight into the mechanism is gained. Still, the information is limited as these methods assume a single-step curing process [83]. The problem with dynamic measurements is that the epoxy resin cures over a temperature range. Epoxy resins are not solely cured like this, and the temperature change adds complexity to the kinetic analysis, as suggested by Varley *et al.* [102]. Therefore, a lot of the kinetic modelling is undertaken using isothermal measurements. However, success has been seen using either heating method, enabling significant predictions into the crosslinking process in different epoxy networks.

As discussed in earlier sections, different epoxy hardener combinations undergo network formation through different processes. There is a need for different phenomenological or semi-empirical kinetic approaches [111]. The most straightforward approach assumes that there is only one step in the curing process, therefore one rate constant, which is related to the rate of

reaction *via* a function related to the degree of cure such as the n^{th} order model given in equation (2-7).

$$\frac{d\alpha}{dt} = k(1-\alpha)^n \qquad (2\text{-}7)$$

Where $\frac{d\alpha}{dt}$ is the rate of reaction, k is the temperature-dependent rate constant, and n is a constant representing the reaction order. Gerami *et al.* suggest n^{th} order kinetics are suitable for simple reactions where the reactants only interact when reacting and thus suitable for dynamic and isothermal measurements. It often fails to accurately model the epoxy amine curing reaction as impurities and reaction products interact with reactants self-catalysing the reaction; Varley *et al.* found this to be the case when applying *nth* order kinetics to TG*p*AP/44'DDS [102]. Instead, they used the autocatalytic method given in equation (2-8) [105,142,143]. Autocatalytic behaviour is observed under dynamic heating [83,88,106,111], but often, isothermal heating is used for implementing the autocatalytic method [134].

$$\frac{d\alpha}{dt} = (k_1 + k_2\alpha^m)(1-\alpha)^n \qquad (2\text{-}8)$$

Where k_1 is the non-catalysed temperature-dependent rate constant, k_2 is the catalysed temperature-dependent rate constant, and m and n are constants that represent the reaction order. Bifunctional resins have been extensively studied using this model, with some focus on multifunctional epoxies such as TGAP and TGDDM [102,127,144].

Even with this modified method, difficulties are encountered when predicting the cure kinetics. Most notably, the change in control of the reaction. In the early stages of the cure, there are mainly monomers and oligomers present in the system, and the reaction is kinetically controlled, whereas, at some point between gelation and vitrification, the reaction becomes diffusion-controlled due to the formation of crosslinks [145,146]. When the system is diffusion controlled, there is a slowing down in reaction rate, which is not accounted for by the autocatalytic method; therefore, studies have developed a kinetic model that accounts for diffusion control, such as one developed by Barton, which assumed a linear decrease in reaction

rate with conversion [126]. Other diffusion control methods developed by Chern and Poehlein utilised the Williams-Landel-Ferry equation to relate the diffusion control process to changes in free volume [147]. Both Cole *et al.* and Fournier *et al.* used this method to successfully improve the description of cure in this region [104,148]. Interestingly, Varley *et al.* implemented both the Barton and the Chern and Poehlein diffusion control methods and found improvements in both methods [102].

Prediction of cure properties using DSC is a valuable tool for manufacturing composites as it allows industry to predict the properties of resins and determine the cure temperatures necessary to achieve a complete cure [83,138,149]. Cure cycles are often a combination of dynamic and isothermal heating regimes. Very few studies have employed DSC to monitor multiple dwell cure cycles [83,88], perhaps something that is overlooked due to its complexity. Even without applying kinetic models, valuable insights can be achieved, such as the rate of reaction and degree of cure, using this method.

2.3.3. DIELECTRIC

A dielectric material has negligible conductivity but can store charge due to its crosslinked chemical structure [150]. Epoxy resin is a dielectric material by definition. Dielectric analysis (DEA) is a technique that monitors the change in the dielectric properties of the epoxy resin during the cure. It is a sensitive technique that can provide insight into the curing process of epoxy resins, but as Skordos and Partridge state, "the information can be useful when interpreted by a specialist" [151]. The definition of specialist varies, but this statement suggests that correct assumptions and data treatments must be made to the data for it to become insightful. A significant amount of research has been undertaken into DEA as like NIR, DEA measurements can be taken while the resin is curing, either as neat resin or in a composite part, making it a perfect technique for use in industrial applications. In the early years of composite manufacturing, industry was limited to simple sensors such as the thermocouples mentioned above or pressure transducers. DEA allows for a similar process with much-improved information, allowing for a more efficient and cost-effective manufacturing process [152]. DEA can provide information regarding the cure state, mechanical viscosity prior to gelation, ion viscosity after gelation. Its simplicity of setup allows for effective cure monitoring of a wide

variety of different materials such as neat resins, adhesives and composite structures in different manufacturing settings.

DEA is implemented by applying an alternating voltage between two electrodes, generating a response current [153]. The magnitude and phase difference of the response current corresponds to dielectric constant and loss values, which are related to the material properties [139]. Three different phenomena may occur: dipole polarisation, migrating charge conduction and electrode polarisation [151]. During the early stages of the cure, when monomers and oligomers are present, the resin behaves more like an ionic liquid rather than a dielectric material. The conductivity and dielectric constant of the material is the greatest. As the resin cures, the mobility of the species decreases, reducing dipole polarisation and migrating charge conduction therefore, conductivity decreases. Conductivity will reach a minimum upon vitrification as the system is crosslinked and dipole polarisation and charge migration will be difficult. Full cure is identified as conductivity remaining constant, no more bonds are formed, therefore, the restriction to the flow of species or dipole polarisation will not change.

Many studies have used DEA to study the properties of resin [98,99,138,151,152,154–177]. As with many of the techniques previously mentioned, DGEBA has been extensively studied [98,138,155,157–160,174], whereas few studies have been published on the dielectric behaviour of TGAP, most notably Jdidi *et al.* investigated the frequency dependency of conductivity on cured TGAP/DETA resin [164]. Currently, none have monitored the curing properties of TGAP cured with DDS using DEA.

This study will focus on monitoring the ion viscosity during cure, which is a measurement related to the material's frequency-independent conductivity to identify the differences in network formation [138,170,171,171,177]. Ion viscosity is especially useful as the measurement can be validated with other cure monitoring techniques such as DSC [138]. The Di Benedetto equation shown in equation (2-5) relates T_g of the uncured resin to the fully cured resin to determine the degree of cure, α. The same relationship can be applied to ion viscosity, IV, as shown in equation (2-9).

$$\text{cure index} = \frac{\log(IV)_x - \log(IV)_0}{\log(IV)_\infty - \log(IV)_0} = \frac{T_g - T_{g0}}{T_{g\infty} - T_{g0}} \qquad (2\text{-}9)$$

Where $\log(IV)_x$ is the ion viscosity at $\alpha = x$, $\log(IV)_0$ is the ion viscosity at $\alpha = 0$ and $\log(IV)_\infty$ is the ion viscosity at $\alpha = \infty$, or 100 %. Note that the value obtained is given the name cure index, as it does not describe the same phenomena as degree of cure obtained from DSC [153]. Skordos and Partridge, Hardis et al., and Wu et al. use this method of calculating the cure index to compare the DEA cure index to the DSC degree of cure [99,138,151]. In all three studies, good agreement was seen between the two methods. Both Skordos and Partridge and Hardis *et al.* highlighted that isothermal cures are best suited for dielectric measurements as temperature changes affect the values. In the case of ion viscosity, an increase in temperature will cause a decrease in ion viscosity. This will have an adverse effect on the cure index calculation. Wu *et al.* solved this issue by removing the data in the temperature ramp and using degree of cure data from DSC in the ramp to account for the change; therefore, they could use DEA to calculate the cure index in multi-dwell cure cycles [99].

Other than cure index, Hussain *et al.* used the change in conductivity to identify different critical points of the cure, such as onset of cure, minimum viscosity point, gelation, end of cure and T_g [163]. Critical points such as gelation are challenging to observe in DEA, as suggested by both Lee and Clôpet *et al.,* as the network structure is not restricted enough at this point to show this in the conductivity or ion viscosity data, an alternative technique such as rheology is better suited to this. This is similar to minimum viscosity; a dielectric minimum viscosity value can be obtained and compared between resin formulations. However, it is not directly comparable with rheological data, as shown by Simpson and Bidstrup [174]. Despite the dielectric measurements giving information about ion viscosity, the term viscosity is slightly different from mechanical viscosity as other factors affect it, such as temperature and free volume, which will be discussed later in Chapter 5. Despite this, DEA will be useful for investigating the difference in network formation for the structural isomers of TGAP/DDS and can give insight that other cure monitoring techniques may not be able to.

2.4. SUMMARY OF LITERATURE

Extensive literature surrounds the cure monitoring of epoxy resins, but very few studies have taken a multi-faceted approach to understand network formation further. The effect of structural isomerism in TGAP/DDS on the cured properties has been previously investigated.

However, there is a lack of research into understanding what occurs during network formation that results in these properties.

This work sets out to understand how structural isomerism affects network formation using different cure monitoring properties:

a) Optical properties using near-infrared spectroscopy
b) Thermal properties using differential scanning calorimetry and resin temperature measurements
c) Dielectric properties using dielectric cure monitoring

The different techniques will be overlayed, and the reliability of the different measurements will be compared.

The differences in network formation will be used to understand their effect on the cured properties of the different networks. By doing so, fine-tuning of the mechanical and thermomechanical properties using resin properties such as chemical structure and epoxy:amine ratios rather than additives will be possible.

3. MATERIALS AND METHODS

3.1. INTRODUCTION

The methods and materials used in the following chapters are outlined in this section. Any deviation from this will be made clear in the chapters as it occurs.

3.2. MATERIALS

The epoxy resins and hardeners used in this study are triglycidyl-*para*-aminophenol (TG*p*AP), triglycidyl-*meta*-aminophenol (TG*m*AP), 4,4'-diaminodiphenyl sulphone (44'DDS) and 3,3'-diaminophenyl sulphone (33'DDS) are shown in Figure 3.1. The two epoxies, TG*p*AP and TG*m*AP, were supplied by Huntsman Advanced Materials as Araldite MY0510 and Araldite MY0610, respectively. The two hardeners, 44'DDS and 33'DDS, were supplied by Thermo Scientific and Huntsman Advanced Materials as 4-aminophenyl sulfone and Aradur 9719-1 NL, respectively. Four different formulations were produced and will be referred to as TG*p*AP/44'DDS, TG*p*AP/33'DDS, TG*m*AP/44'DDS and TG*m*AP/33'DDS.

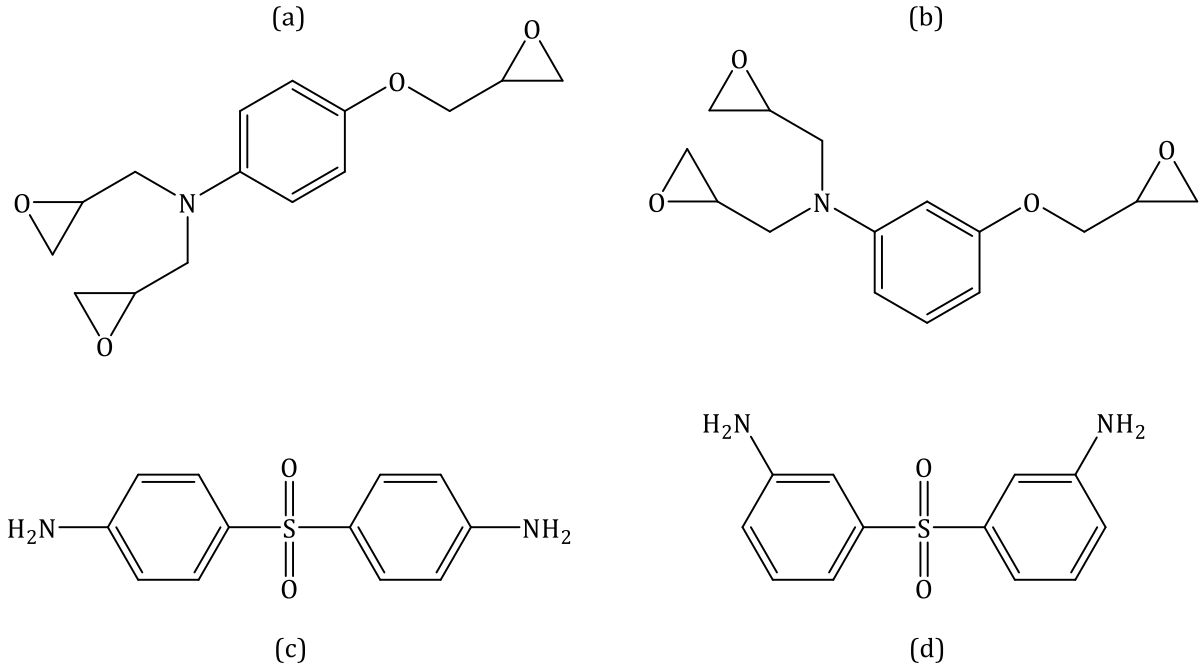

Figure 3.1 – Chemical structures of the resins and hardeners: (a) triglycidyl-*para*-aminophenol (TG*p*AP), (b) triglycidyl-*meta*-aminophenol (TG*m*AP), (c) 4,4'-diaminodiphenyl sulphone (44'DDS) and (d) 3,3'-diaminodiphenyl sulphone (33'DDS).

The epoxy to amine mass ratio is 100:36 (molar ratio 1:0.58), a significant epoxy excess to ensure that all amine groups fully react to prevent moisture ingress and to account for differences between theoretical and actual functionality, a commonly used technique in industry [32,48]. The ratios are based on the functional group equivalent weight, shown in Table 3.1. A stoichiometric mass ratio would be 100:62. The epoxy equivalent weight (EEW) for pure TGAP is 100 g mol^{-1}, whereas the EEW for MY0510 and MY0610 is 92.3 g mol^{-1}, indicating that both TG*p*AP and TG*m*AP have small amounts of oligomers present. This indicates that hydroxyl groups are present in the starting material.

Table 3.1 – Epoxies and hardeners used

Material	Abbreviation	Chemical Name	EEW / g mol^{-1}	Supplier
Epoxy Monomer	TG*p*AP	triglycidyl-*para*-aminophenol	100	Huntsman Advanced Materials
Epoxy Monomer	TG*m*AP	triglycidyl-*meta*-aminophenol	100	Huntsman Advanced Materials
Amine Hardener	44'DDS	4,4'-diaminodiphenyl sulphone	62	Thermo Scientific
Amine Hardener	33'DDS	3,3'-diaminodiphenyl sulphone	62	Huntsman Advanced Materials

3.2.1. PREPARATION OF EPOXY RESINS

Firstly, epoxy was weighed out using a two-point balance (around 30-50 g), and the necessary amount of hardener (according to the epoxy amine ratio) was weighed. An oil bath on a hot plate heated the epoxy to around 60 °C, at which point the hardener was added, and the temperature was increased to 120 °C. The epoxy hardener mixture was mechanically stirred for 10 minutes until the hardener was completely dissolved (a clear solution). The mixed liquid resin was then degassed at 100 °C using a vacuum oven until no more bubbles were present. The resin was then poured into the appropriate preheated mould and cured in a convection oven. The moulds differed depending on the technique: a glass panel was used for flat cast samples (approximately 2 mm thick), and a 100 mm by 100 mm glass dish was used for thicker

samples (approximately 4 mm thick). Frekote 770-NC was applied to the mould surface as a release agent.

3.2.2. CURE OF EPOXY RESINS

Unless otherwise stated, all TGAP/DDS resins were cured using the same cure cycle as follows: 100 to 130 °C at 2 °C min^{-1} (15 min), 130 °C for 2 hr, 130 to 160 °C at 2 °C min^{-1} (15 min), 160 °C for 1 hr, 160 to 200 °C at 1 °C min^{-1} (40 min) and 200 °C for 2 hr: 6 hr 10 min total curing time. This is shown graphically in Figure 3.2. This cure cycle was previously used by Ramsdale-Capper and Foreman and achieved nearly 100 % cure for all formulations [32].

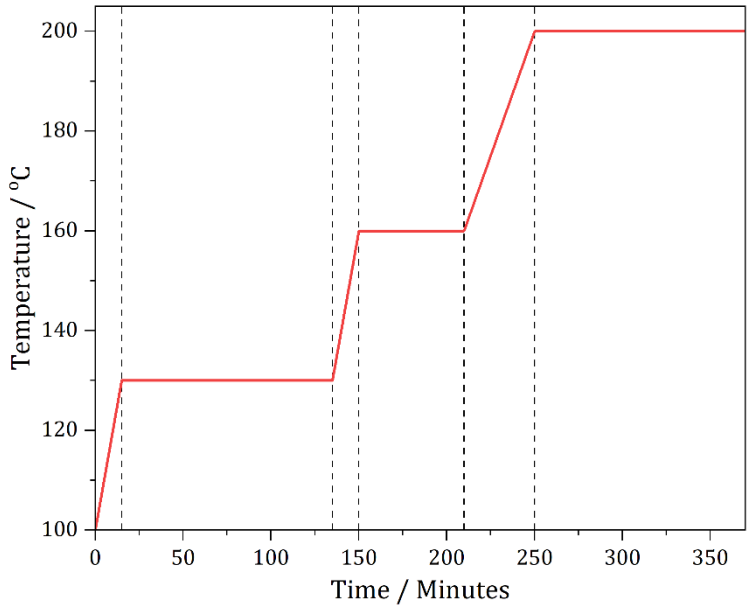

Figure 3.2 – Standard multi-dwell cure cycle of TGAP/DDS. Note that the temperature axis starts at 100 °C. Dashed lines indicate the start and end of dwells.

3.3. CURE MONITORING

The cure of the TGAP/DDS formulations was monitored throughout the following studies using multiple techniques that monitor different properties associated with the epoxy resin cure. The methods are outlined below.

3.3.1. NEAR-INFRARED SPECTROSCOPY

Near-infrared spectroscopy is a Fourier transform infrared spectroscopy (FTIR) technique in the near-infrared region (4000 cm^{-1} to 12500 cm^{-1}). Light is passed through the sample, and the resultant transmitted light differs depending on the material's absorbance at different wavelengths. The near-infrared region is used as the reactive groups involved in the epoxy curing process have good separation and intensity in NIR spectra.

NIR was performed using an Ocean Optics NIRQuest 2500 in transmission mode between 4000 cm^{-1} and 11000 cm^{-1} using an integration time of 16ms, 16 scans to average and 4 cm^{-1} resolution. A light source was connected to a fibre optic cable which was mounted to a bespoke stand, fixing the position and ensuring alignment with the receiving fibre optic cable connected to the spectrometer. A heating stage was placed on the stand in between the fibre optic cables allowing light to transmit through the epoxy sample. Sample holders were prepared using a PTFE spacer of approximately 0.4 mm thickness attached to a square cut glass microscope slide using flashbreaker tape. The glass slides were preheated to 100 °C and the elevated temperature mixed TGAP/DDS was placed in the PTFE spacer, and another glass slide was placed on top, to ensure the path length stayed constant and the epoxy surface was flat. The glass slides were then placed onto a preheated (100 °C) Linkam THMS600 heating stage. The spectrometer was connected to a PC where the spectra were visualised and exported using OceanView and then smoothed and analysed using OriginPro and Fityk [178,179]. An example of the setup is shown in Figure 3.3.

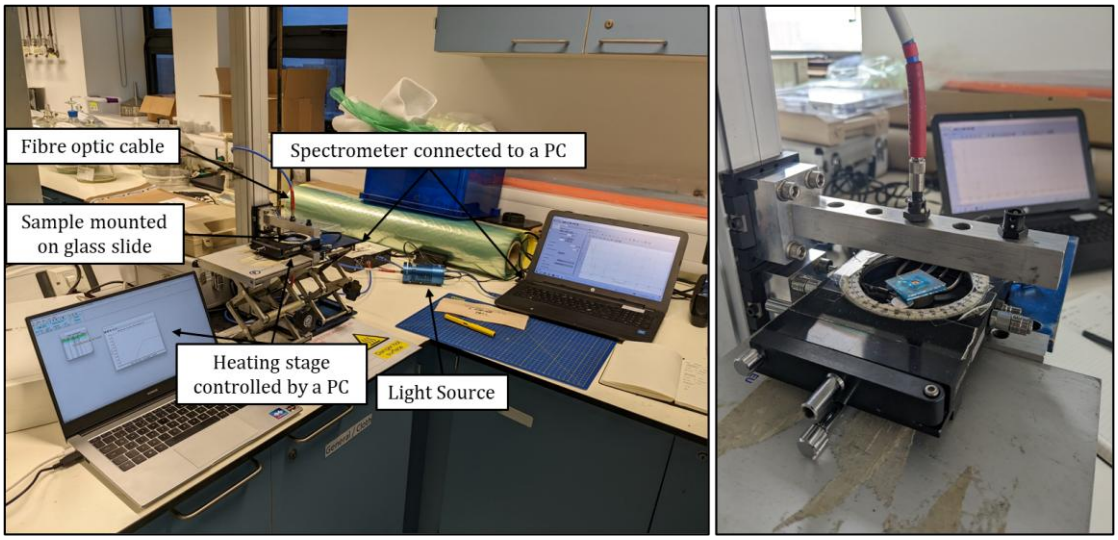

Figure 3.3 – An example of the setup of near infrared cure monitoring

The resultant absorbance spectra allow quantitative analysis of the functional groups present during the epoxy resin cure due to the relationship between absorbance and concentration given by Bouguer-Beer-Lambert law in equation (3-1):

$$\log \frac{I_0}{I} = A = \varepsilon\, c\, l \qquad (3\text{-}1)$$

Where I_0 is the initial intensity of light, I is the intensity of light after travelling through the material, A is absorbance, ε is the molar absorption coefficient, c is concentration and l is the path length. $A = \varepsilon\, c\, l$ is the section of interest for NIR, known as Beer's law. The molar absorption efficient is different for each functional group as it is a measure of how the chemical species interacts with light. The path length should stay constant throughout the cure, but it can change by very small amounts as DDS resins can expand and contract during the cure, so a standard peak which doesn't change concentration throughout the cure is used to normalise the signal and account for any path length changes.

The following procedure will closely follow the methods used in St John and George and Varley *et al*. [48,49].

3.3.1.1. BAND IDENTIFICATION

Firstly, the chemical functional groups must be identified. The reaction mechanism outlined in Figure 2 .7 shows that the groups of interest are the epoxide ring, primary amines, secondary amines, tertiary amines and ether groups. The tertiary amines and ether groups cannot be monitored using NIR as the lack of a hydrogen bond means the overtone or combination band is not intense enough to monitor; therefore, the concentration must be determined indirectly, as will be shown later. The bands associated with epoxide groups and primary and secondary amines must be identified. Mid-infrared spectroscopy can be used to determine the possible overtone and combination bands, but this has already been undertaken in previous literature [48,61,85]. Using literature and NIR measurements of the individual reagents, band assignments for the epoxide, primary and secondary amines, aromatic and hydroxyl groups for the structural isomers of TGAP and DDS are shown in Table 3.2. It is worth noting that with this technique, the light source needs to transmit through the material. Both TGAPs are liquid,

allowing measurements to be taken at low temperatures (100 °C). Both 44'DDS and 33'DDS are powdered solids at room temperature, and they need to be melted at 200 °C to take reliable NIR measurements [180,181].

Table 3.2 – Functional group band assignments for the structural isomers of TGAP and DDS

Functional Group Assignment	Wavenumber / cm^{-1}
Epoxide C–H	6038 (TG*p*AP)
	6034 (TG*m*AP)
	5850 (TG*p*AP and TG*m*AP)
	4517 (TG*p*AP and TG*m*AP)
NH_2 (primary amine)	4522 (44'DDS and 33'DDS)
	5059 (44'DDS)
	5047 (33'DDS)
NH (primary and secondary amine)	6657 (44'DDS)
	6642 (33'DDS)
Aromatic C–H	5962 (TG*p*AP and TG*m*AP)
	5970 (44'DDS and 33'DDS)
	4616 (TG*p*AP)
	4683 (TG*p*AP)
	4602 (TG*m*AP)
	4675 (TG*m*AP)
Hydroxyl O–H	7000 (broad)

As mentioned in the literature review, studies have used the epoxide ring band at 4500 cm^{-1}, such as Poisson *et al.* [72], but there is overlap here with the primary amine group at 4522 cm^{-1} in both 44' and 33'DDS. The epoxide bands around 6000 cm^{-1} are more suitable, as used by St John and George and Varley *et al.* [48,49]. This region has three peaks: epoxide C–H at 5850 cm^{-1}, aromatic C–H at 5960 and epoxide CH_2 at 6035 cm^{-1}. These are an isolated group of peaks that can be deconvoluted and reliably tracked throughout the cure. It is possible to track the 4522

cm^{-1} peak, but its overlap with the primary amine possibly introduces greater error in the results, and the baseline is more challenging to determine. The NIR spectra of the four different starting reagents are shown in Figure 3.4.

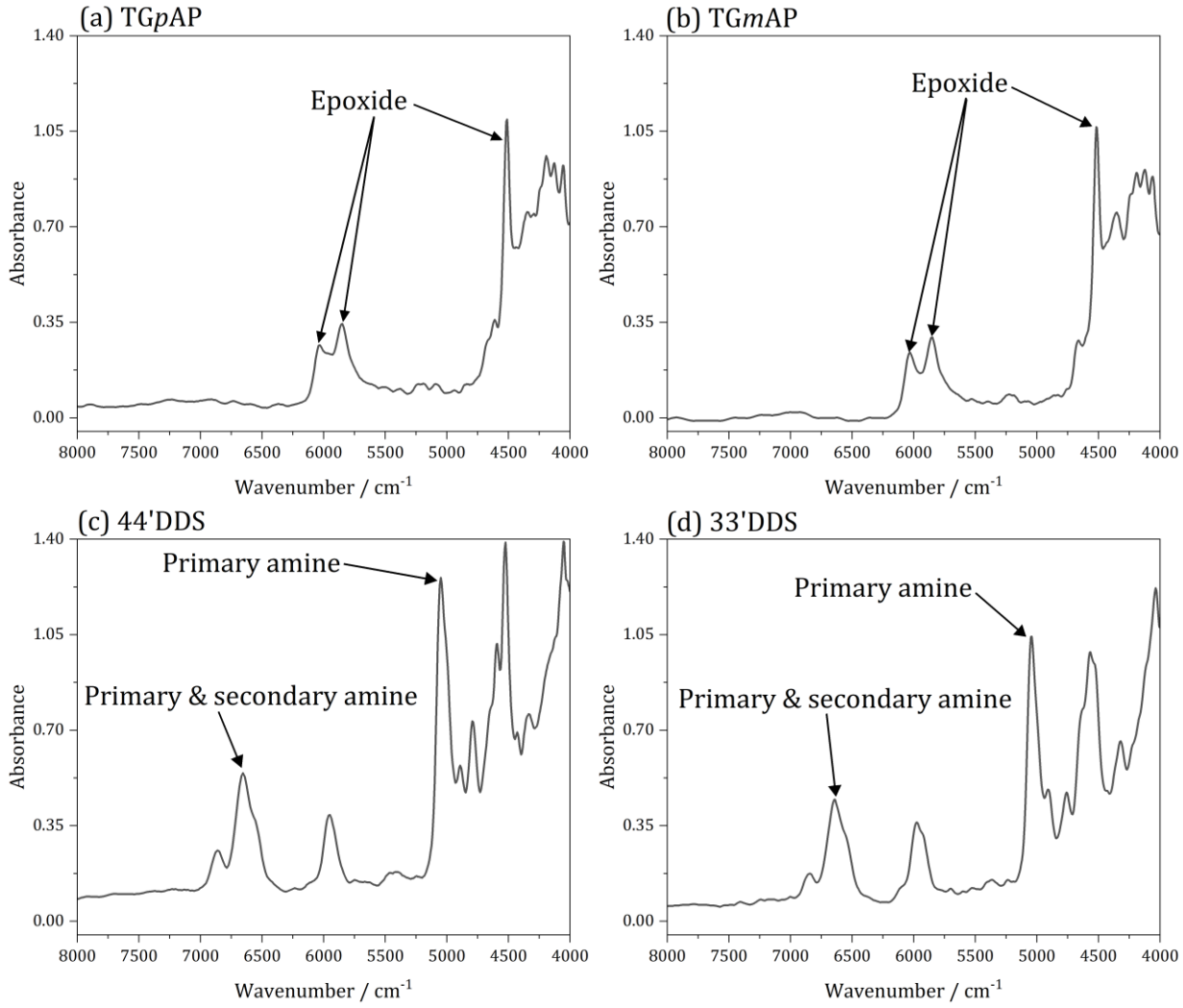

Figure 3.4 – Near-infrared spectra of the starting reagents: (a) triglycidyl-*para*-aminophenol (TG*p*AP), (b) triglycidyl-*meta*-aminophenol (TG*m*AP), (c) 4,4'-diaminodiphenyl sulphone (44'DDS) and (d) 3,3'-diaminodiphenyl sulphone (33'DDS) (smoothed).

A baseline was applied using fityk to the spectra to allow for deconvoluting the assigned peaks and determining the peak area [179]. An example of the baseline applied to the epoxide and aromatic region around 6000 cm^{-1} is shown in Figure 3.5.

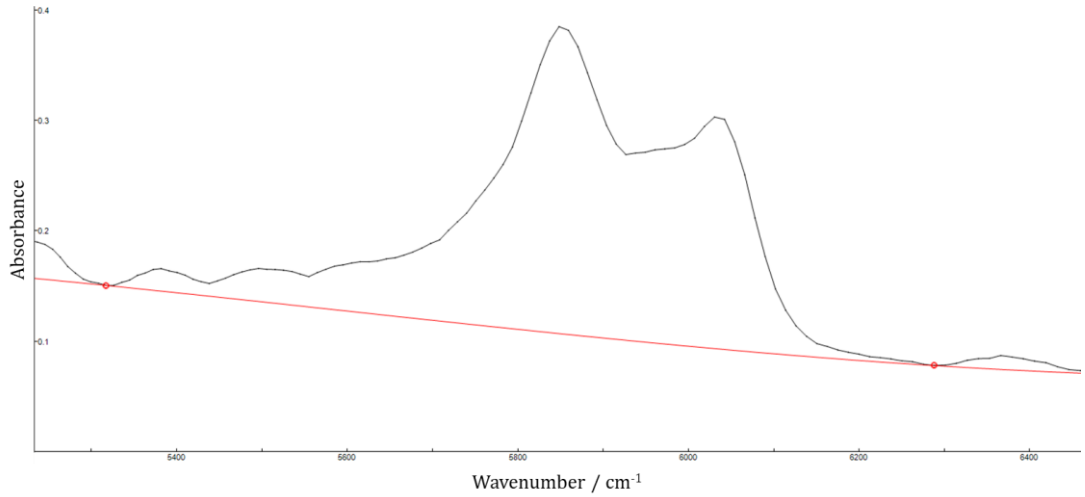

Figure 3.5 – An example of the baseline applied the NIR spectra in the epoxide and aromatic group region around 6000 cm^{-1} for pure TG*p*AP using Fityk software.

An example of the deconvolution of the epoxide bands in TG*p*AP that occur around 6000 cm^{-1} is shown in Figure 3.6. An unassigned band at approximately 6130 cm^{-1} can be seen, this was also seen in pure TG*m*AP and the four different TGAP:DDS formulations throughout the cure. As it was constant feature of the spectra throughout the cure, it was included in the deconvolution method to determine both the epoxide C-H band and aromatic C-H band area.

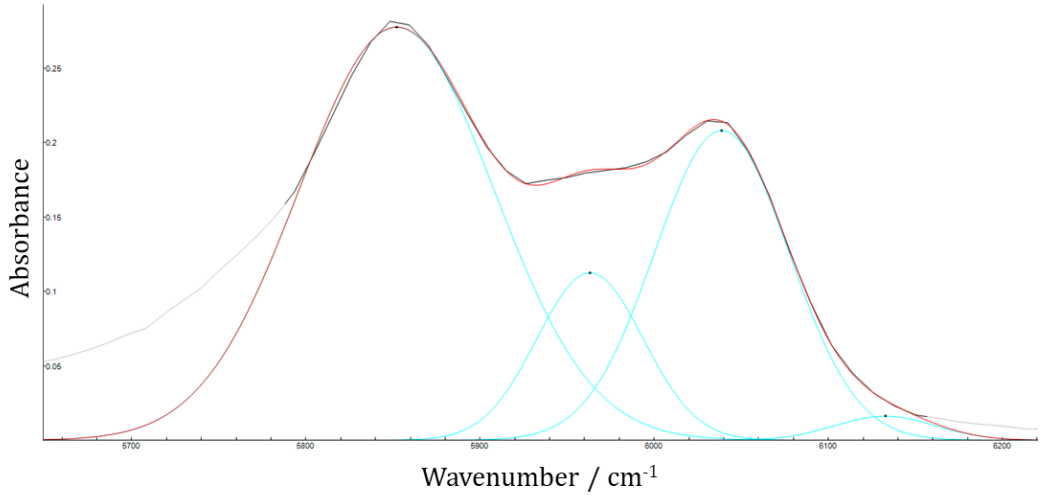

Figure 3.6 – An example of deconvolution of the epoxide C-H bands (6038 cm^{-1} and 5850 cm^{-1}) and the aromatic C-H band (5962 cm^{-1}) in pure TG*p*AP using Fityk software.

The deconvolution of the primary and secondary amine peak at 6657 cm^{-1} in 44'DDS is shown in Figure 3.7. As this is pure 44'DDS, the band should only arise from primary amines, however,

during the cure, it represents the absorbance of primary and secondary amines. Like with the epoxy region above, there are other bands present during deconvolution, however, literature has assigned the two bands at approximately 6550 cm^{-1} and 6860 cm^{-1} to primary amine symmetric stretching and asymmetric stretching respectively [85]. These will also decrease during the cure. There is no alternative peak for determining secondary amine concentration therefore care must be taken when deconvoluting these peaks in order to reduce potential error.

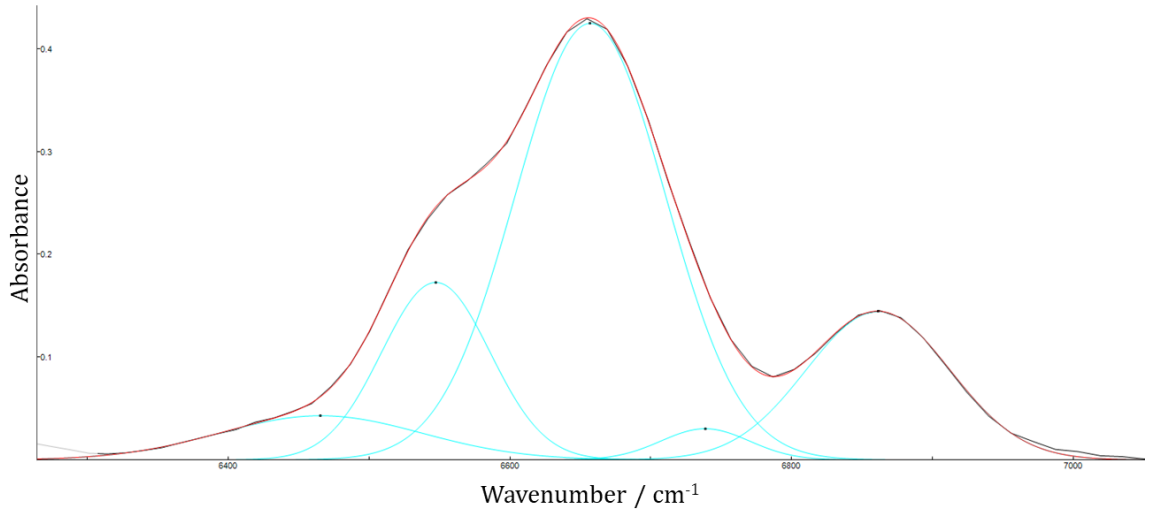

Figure 3.7 – An example of deconvolution of the primary and secondary amine band at 6657 cm^{-1} in pure 44''DDS using Fityk software.

3.3.1.2. MOLAR ABSORPTION COEFFICIENT

Now the bands of interest have been identified, the molar absorption coefficient can be calculated. Each band and functional group will have a unique value as the interaction with light differs, which can be calculated using Beer's law from equation (3-1). The absorbance is the area under the peak. The path length is measured, and the concentration is determined from the equivalent weights and ratio of TGAP:DDS. The initial concentrations of the epoxide and primary amine groups are given in Table 3.3.

It is assumed that only epoxide groups are present in TGAP, and only primary amines are in DDS. To calculate the concentration, the molecular weight per mole of reactive group is needed. This is known as the epoxy equivalent weight or primary amine equivalent weight and is given in Table 3.3. The functional group concentration is the number of moles of the functional group per kilogram, therefore it would 1 divided by the equivalent weight (in kg mol^{-1}). This gives the values for pure TGAP and pure DDS in Table 3.3. To calculate the functional group concentration

in the mixture, the epoxy:amine mass ratio is taken into account. In this case, it is a 100:36 mass ratio of TGAP:DDS. The epoxide group concentration is multiplied by $\frac{100}{136}$ and the primary amine group concentration is multiplied by $\frac{36}{136}$, giving the initial functional group concentrations for TGAP/DDS mixture in Table 3.3. As the chemical composition does not change between structural isomers, the values are only given for TGAP and DDS.

Table 3.3 – Initial functional group concentration values for pure TGAP and DDS and TGAP/DDS with epoxy amine mass ratio of 100:36

	Initial functional group concentration / mol kg^{-1}	
Formulation	Epoxide	Primary amine
TGAP (EEW = 0.100 kg mol^{-1})	10.00	-
DDS (pAEW = 0.124 kg mol^{-1})	-	8.06
TGAP/DDS (100:36)	7.35	2.14

Using these values and equation (3-1), the molar absorption coefficient, ε, can be calculated for the epoxide group at 6035 cm^{-1} and the primary amine at 5059 cm^{-1} and 6650 cm^{-1}. Knox *et al.* used a calibration curve method to validate the value at different path lengths [87]. A calibration curve method was not used in this thesis as a significant temperature gradient occurred at thicker path lengths due to using a single-sided heating stage. Instead, they were validated using different temperatures like Varley *et al.* [48]. It was found that the molar absorption coefficient did change depending on temperature. Therefore, a similar approach to Janisse was used, where a scaling factor accounted for this change. It was found that molar absorption values vary by 0.3 % for each °C. This was applied to the values depending on the measurement temperature [182], resulting in values similar to those in the literature. The 44'DDS values were very similar to that of Jackson *et al.* [30].

Calculating the secondary amine molar absorption values is a more complicated method. The band at roughly 6650 cm^{-1} contains both primary and secondary amines. Initially, there are only primary amines present, but shortly after the start of the reaction (around 20 minutes), it is assumed that any consumption of primary amines has produced only secondary amines, and

there has been no formation of tertiary amines. The secondary amine concentration at short-time values can be calculated using equation (3-2).

$$[SA]_t = [PA]_0 - [PA]_t \quad (3\text{-}2)$$

Where $[PA]_0$ is the initial primary amine concentration, $[PA]_t$ is the primary amine concentration at time, t, and $[SA]_t$ is the secondary amine concentration at time, t. When bands overlap, a superposition assumption can be used given in equation (3-3).

$$A = A_1 + A_2 + \cdots + A_n = l(\varepsilon_1 c_1 + \varepsilon_2 c_2 + \cdots + \varepsilon_n c_n) \quad (3\text{-}3)$$

Giving equation (3-4) for the overlapping band of primary and secondary amines at 6650 cm^{-1}.

$$A_{NH_2+NH} = A_{NH_2} + A_{NH} = l\left(\varepsilon_{NH_2}[PA]_t + \varepsilon_{NH}([PA]_0 - [PA]_t)\right) \quad (3\text{-}4)$$

Rearranging this gives equation (3-5), which can be used to calculate the molar absorption coefficient for the secondary amine at 6650 cm^{-1}.

$$\varepsilon_{NH_{6650\ cm^{-1}}} = \frac{A_{NH_2+NH} - \left(\varepsilon_{NH_2}[PA]_t l\right)}{l([PA]_0 - [PA]_t)} \quad (3\text{-}5)$$

As several assumptions are involved in the calculation, the values are different for each formulation. All values are given in Table 3.4.

Table 3.4 – Molar absorption coefficients for the different functional groups of the structural isomers of TGAP and DDS as varying wavenumbers

Functional group (band position)	Molar absorption coefficient / kg mol^{-1} cm^{-1}
TG*p*AP epoxide CH_2 (6038 cm^{-1})	33.0
TG*m*AP epoxide CH_2 (6034 cm^{-1})	38.6
44'DDS primary amine NH_2 (5059 cm^{-1})	125.9
33'DDS primary amine NH_2 (5059 cm^{-1})	147.5
44'DDS primary amine NH_2 (6657cm^{-1})	81.5
33'DDS primary amine NH_2 (6642cm^{-1})	82.3
TG*p*AP/44'DDS secondary amine NH (6657 cm^{-1})	140.0
TG*p*AP/33'DDS secondary amine NH (6642 cm^{-1})	157.0
TG*m*AP/44'DDS secondary amine NH (6657 cm^{-1})	140.0
TG*m*AP/33'DDS secondary amine NH (6642 cm^{-1})	127.0

3.3.1.3. FUNCTION GROUP CONCENTRATION CALCULATIONS

Epoxide and primary amine concentrations are determined using the rearranged Beer law given in equation (3-6).

$$[X]_t = \frac{A_t}{\varepsilon_X l} \tag{3-6}$$

Where $[X]_t$ is the functional group concentration at time, t, when X is epoxide (EP) or primary amine (PA) and A_t is the area of the absorbance band at time, t.

Secondary amine concentration, $[SA]$, is determined using the calculated primary amine concentration value from the band 5059 cm^{-1} using equation (3-7).

$$[SA]_t = \frac{A_{6650\ cm^{-1}} - \left(\varepsilon_{NH_2}{}_{6650\ cm^{-1}} [PA]_t l\right)}{\varepsilon_{NH}{}_{6650\ cm^{-1}} l} \quad (3\text{-}7)$$

These equations give all the directly obtainable functional group concentrations from the NIR spectra. It is possible to obtain the concentration of species not present in the NIR. The tertiary amine concentration, $[TA]_t$, can be determined using the primary and secondary amine concentrations, as shown in equation (3-8).

$$[TA]_t = [PA]_0 - [PA]_t - [SA]_t \quad (3\text{-}8)$$

The other functional group concentration that can be determined is the ether group concentration, assuming that any epoxide reaction that does not involve an amine forms an ether, as suggested by St John and George [49]. In these TGAP/DDS formulations, there is significant epoxy excess, which suggests that epoxide will react with hydroxyl groups through etherification or with other epoxide groups through homopolymerisation. The epoxide amine only concentration, $[EP^a]_t$, and therefore the ether concentration, $[ether]_t$, is given by equation (3-9) and (3-10) respectively.

$$[EP^a]_t = [EP]_0 - ([PA]_0 - [PA]_t + [TA]_t) \quad (3\text{-}9)$$

$$[ether]_t = [EP]_t - [EP^a]_t \quad (3\text{-}10)$$

3.3.2. RESIN TEMPERATURE MEASUREMENTS

An exposed junction K-type thermocouple connected to a Pico Technology TC-08 USB data logger was used to measure the temperature of the resins during the cure as a comparison to oven temperature. Uncured resin was cast into a 100 mm by 100 mm glass dish, a thermocouple was placed into the centre of the resin, and temperature measurements were taken as the resin cured. A different K-type thermocouple measured the temperature of the oven during the cure.

3.3.3. DIFFERENTIAL SCANNING CALORIMETRY

Differential scanning calorimetry (DSC) was performed using a Perkin Elmer DSC 6 calibrated to an indium standard in a constant flow of dry nitrogen gas at 50 mL min^{-1}. The measurement method was heat flux, where the difference between the sample and reference pan temperature was measured. When thermal events occur, the sample will heat differently to the reference pan, and the difference is shown in the differential heat flow output, which is either an exothermic or endothermic response.

Cured and uncured samples were measured using DSC. For uncured samples, the process outlined in section 3.2.1 was followed, and approximately 5 – 10 mg of uncured resin was placed in an aluminium sample pan sealed with an aluminium lid and heated accordingly. For cured samples, a small piece of cured resin obtained from a flat cast sample, 5 – 10 mg, was placed in an aluminium pan so that the maximum surface area was in contact with the base of the pan.

Two different methods of heating were used. One is dynamic heating, where a constant heating rate is used between a temperature range. This study heated samples from 30 to 300 °C at five different heating rates (2.5, 5, 10, 15 and 20 °C min^{-1}). The other is isothermal heating, where a sample is heated quickly up to a temperature where it is held until no more curing takes place. This study used five different isotherms (130, 160, 200, 210 and 220 °C) with differing lengths of time. After each test, the resin is cooled to 30 °C and dynamically heated to 300 °C to determine the residual cure and T_g (if possible). For dynamic and isothermal measurements, a baseline run of an empty sample pan has been measured to account for any changes in the heating procedures for the aluminium pan. Isothermal and dynamic heating have been used for uncured resin, whereas dynamic heating has been used for cured resin to determine the degree of cure and T_g.

3.3.3.1. DSC ANALYSIS

The thermal response in DSC tests is shown in terms of the heat flow. From this, the enthalpy of reaction can be found by integrating heat flow with respect to either time or temperature. The heat flow measurements are outputted as mW, and the heat flow is normalised using the sample mass to give $W\,g^{-1}$. The baseline for dynamic measurements is determined using a user defined cubic spline baseline, an example is shown in Figure 3.8.

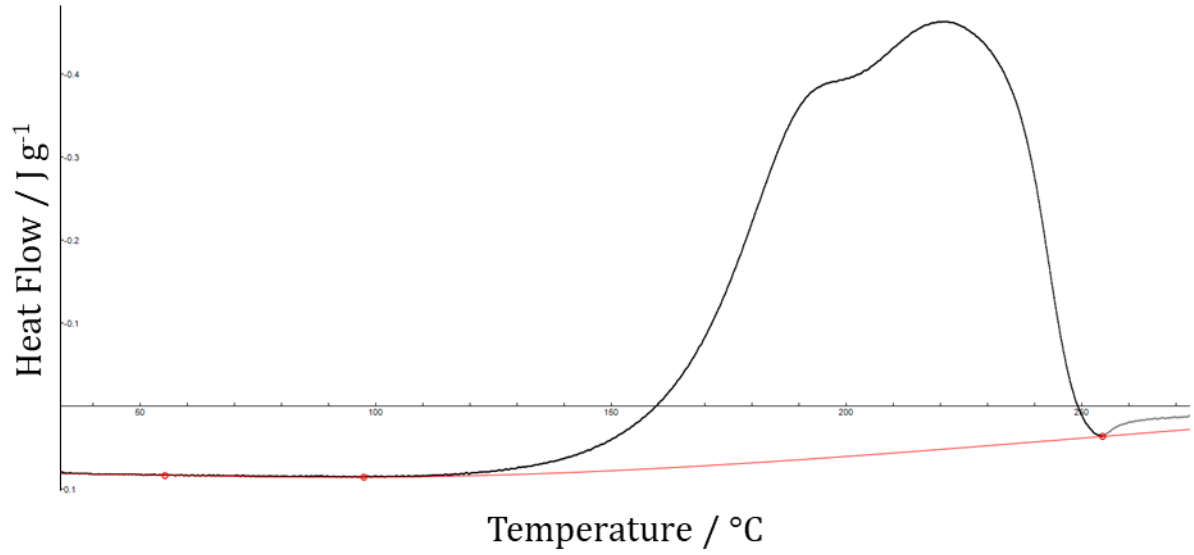

Figure 3.8 – An example of baseline determination for a dynamic DSC measurement of TG*p*AP/44'DDS heating at a rate of 2.5 °C min^{-1}. Red line indicates baseline.

The baseline for isothermal measurements are determined as the straight line from when rate of reaction is zero, an example is shown in Figure 3.9.

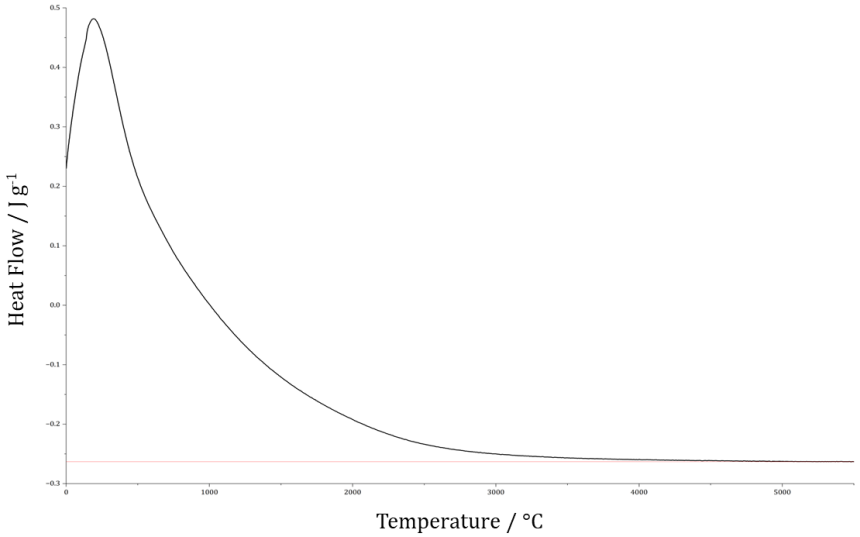

Figure 3.9 - An example of baseline determination for an isothermal DSC measurement of TG*p*AP/44'DDS heating at a rate of 200 °C. Red line indicates baseline.

Equation (3-11) shows the method for calculating the enthalpy of reaction for isothermal heating procedures.

$$\Delta H(t) = \int_0^t \frac{dq}{dt} dt \tag{3-11}$$

Where $\Delta H(t)$ is the enthalpy of reaction at time, t and $\frac{dq}{dt}$ is heat flow. Equation (3-12) shows the method for calculating the enthalpy of reaction for dynamic heating procedures.

$$\Delta H(T) = \frac{1}{\beta} \int_0^T \frac{dq}{dt} dT \tag{3-12}$$

Where $\Delta H(T)$ is the enthalpy of reaction at temperature, T and β is heating rate ($\frac{dT}{dt}$). The total enthalpy of cure, ΔH_0, is defined as the point at which the rate of change in heat flow is zero. The degree of cure is calculated by comparing the enthalpy of reaction to the total enthalpy of cure. Equation (3-13) shows the method for calculating degree of cure for isothermal measurements, and equation (3-14) shows the calculation for degree of cure in dynamic measurements.

$$\alpha(t) = \frac{\Delta H(t)}{\Delta H_0} \tag{3-13}$$

$$\alpha(T) = \frac{\Delta H(T)}{\Delta H_0} \tag{3-14}$$

Where α is degree of cure. The rate of reaction can be calculated by the heat flow with the total enthalpy of cure as shown in equation (3-15) with respect to time and in equation (3-16) with respect to temperature.

$$\frac{d\alpha}{dt} = \frac{\frac{dq}{dt}}{\Delta H_0} = \frac{\beta \frac{dq}{dT}}{\Delta H_0} \tag{3-15}$$

$$\frac{d\alpha}{dT} = \frac{\frac{dq}{dT}}{\Delta H_0} \tag{3-16}$$

Where $\frac{d\alpha}{dt}$ is rate of reaction with respect to time and $\frac{d\alpha}{dT}$ is rate of reaction with respect to temperature.

Different methods will be used to calculate activation energies and rate constants for the curing reactions, but they will not be given here as each method comes with significant discussion. These will be presented and explained in Chapter 5.

3.3.4. DIELECTRIC ANALYSIS

Dielectric analysis (DEA) measures the response of a material when an alternating voltage is applied [177]. Monitoring the change in conductivity throughout the cure indicates how the curing process is progressing and allows for the identification of critical points.

DEA was performed on all four formulations of TGAP/DDS using a Lambient Technologies LT-451 dielectric cure monitor (single channel) with single-use Mini-Varicon sensors. Measurements are taken at six different frequencies (1, 10, 100, 1000, 10,000 and 100,000 Hz)

at thirty-second intervals during the cure and the cooling period. An image of the dielectric cure monitor equipment and resin covering the Mini-Varicon sensor is shown in Figure 3.10.

Figure 3.10 – An image of the Lambient LT-451 Dielectric Cure Monitor equipment and resin cast onto a Mini-Variscon sensor with a K-type thermocouple.

The Mini-Varicon sensors are shown in Figure 3.11 and consist of a polyimide substrate and copper electrodes. The B line indicates the position at which the sensor can be cut and form a smaller electrode should it be needed; in this study, the entire sensor is used as it allows for the highest sensitivity, which is imperative for low-conductivity materials such as epoxy resin. The dimensions are 40 mm by 19 mm by 0.1 mm with a ratio of electrode area to electrode separation (A/D) of 80 cm. The procedure for preparing resins in 3.2.1 was followed and the mixed resin was cast into a 100 mm by 100 mm glass dish to ensure complete sensor coverage. The sensor was attached the glass dish using flashbreaker tape to prevent any unnecessary movement during the cure.

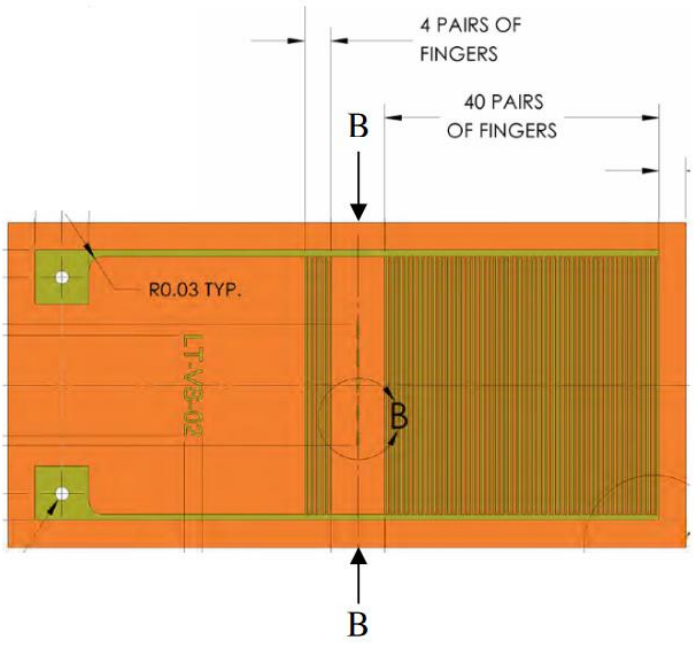

Figure 3.11 – Schematic of Mini-Varicon sensor where B is the cut line for making the sensor smaller. Taken from Lambient Technologies [183].

The resin is cured in a convection oven with the wires attached from the sensor to the cure monitoring equipment outside the oven. Lambient Technologies provides the CureView data acquisition and analysis software [184]. There are multiple parameters outputted from the measurements. For this study, a measurement known as ion viscosity is of interest.

To obtain the ion viscosity values, the relationship between the response current and the alternating exciting voltage is used. When a voltage of the form of equation (3-17).

$$V(t) = V_0 \exp(i\omega t) \tag{3-17}$$

Where V is voltage and ω is angular frequency. A corresponding time-dependent current will lag by a phase angle, δ, in the form of equation (3-18) [152].

$$I(t) = I_0 \exp[i(\omega t - \delta)] \tag{3-18}$$

Where I is current. Using this relationship, the cure can be described in a phenomenological approach using a parallel circuit known as the dielectric Maxwell model, as shown in Figure 3.12.

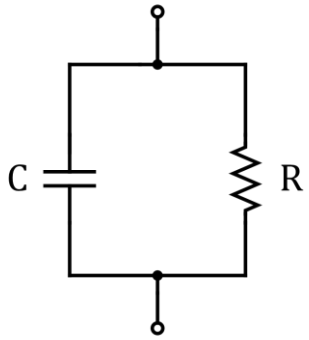

Figure 3.12 – Electric model of a dielectric material under test where C is capacitance and R is resistance.

Using the relationship between voltage and current and the model in Figure 3.12, the equation (3-19) is obtained, which relates the admittance of the circuit to the resistance and capacitance of the material under test.

$$Y = \frac{1}{R} + i\omega C = \frac{I(t)}{V(t)} \tag{3-19}$$

Where Y is admittance, R is resistance, C is capacitance, and ω is angular frequency. A similar expression can be obtained for complex permittivity in equation (3-20).

$$\varepsilon^* = \varepsilon' - i\varepsilon'' \tag{3-20}$$

Where ε^* is complex permittivity, ε' is relative permittivity and ε'' is dielectric loss factor. Relative permittivity accounts for the dipole orientation, whereas the dielectric loss factor accounts for the energy loss in the material attributed to dipole motion and ionic flow [156]. From that, relative permittivity, $\varepsilon' = \frac{C}{C_0}$, is obtained and dielectric loss factor, $\varepsilon'' = \frac{1}{R\omega C_0}$. The model in Figure 3.12 can be improved upon by incorporating the same circuit but in series as

shown in Figure 3.13. Mijović *et al.* named this the four-parameter dielectric model [152]. This allows us to determine both the frequency-independent and frequency-dependent responses of the dielectric loss factor [152,185].

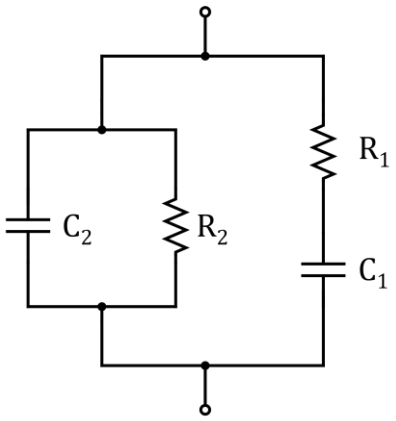

Figure 3.13 – Four-parameter electric model of a dielectric material under test where C_x is capacitance and R_x is resistance.

Therefore, the dielectric loss factor component is shown in equation (3-21) and accounts for frequency-dependent dipole motion and frequency-independent conductivity.

$$\varepsilon'' = \frac{1}{R_1 \omega C_0} + \frac{1}{R_2 \omega C_0} = \frac{(\varepsilon_r - \varepsilon_u)\omega\tau}{1 + \omega^2\tau^2} + \frac{\sigma}{\omega\varepsilon_0} \tag{3-21}$$

Where ε_r is the relaxed permittivity, the highest amount of dipole orientation possible in the sample, ε_u is the unrelaxed permittivity, the baseline value of dielectric permittivity [152], τ is the relaxation time, ε_0 is the permittivity of free space and σ is conductivity. To obtain ion viscosity data, the frequency independent component is of interest and it is often found that at low frequencies, equation (3-22) is satisfied [156].

$$\frac{(\varepsilon_r - \varepsilon_u)\omega\tau}{1 + \omega^2\tau^2} \ll \frac{\sigma}{\omega\varepsilon_0} \tag{3-22}$$

The contribution from dipole orientation is negligible, and ion flow is equal to the dielectric loss factor giving equation (3-23). Ionic flow arises from the flow of mobile ions. In the case of epoxy resin, it is the flow of the reactive groups which experience induced dipoles from the applied alternating voltage and the flow of ionic impurities generated in the synthesis process. The ionic impurity content has not been studied, but it is expected that sodium and chloride ions will be present from the synthesis process [165,186].

$$\varepsilon'' = \frac{\sigma}{\omega \varepsilon_0} \tag{3-23}$$

The dielectric cure monitoring equipment provided by Lambient Technologies outputs a measurement known as ion viscosity, which this study will use. It directly relates to resistivity, as shown in (3-24).

$$\log(IV) = \log\left(\frac{1}{\sigma}\right) = \log(\rho) \tag{3-24}$$

Where ρ is resistivity, and IV is ion viscosity. This study will analyse the changes in IV to identify the differences in network formation between the four structural isomer combinations of TGAP/DDS.

3.4. CURED RESIN

The properties of the cured resins were investigated using multiple techniques. These properties were used to justify the findings of the cure monitoring techniques, many of which have already been undertaken in a previous study by Ramsdale-Capper and Foreman [32].

3.4.1. DYNAMIC MECHANICAL ANALYSIS

Dynamic mechanical analysis (DMA) was used to determine the viscoelastic behaviour of a polymer. A Perkin Elmer DMA8000, in single cantilever mode at 1 Hz with a strain amplitude of 0.05 mm between -180 ^{o}C and 300 ^{o}C using a heating rate of 3 ^{o}C min^{-1} was used to determine

the glass, beta and omega transition temperatures. The samples were obtained from flat cast samples and cut using a tile saw to dimensions of 30 mm by 10 mm by 1.6 mm. The glass transition temperatures were taken as the peak temperature, whereas the beta and omega transitions were analysed using the peak areas.

In DMA, an oscillating force is applied to a sample, and the material's response is measured [187]. Applying a constant load at sinusoidal oscillation will result in a stress that changes sinusoidally, as given in equation (3-25).

$$\sigma(t) = \sigma_0 \sin(\omega t) \tag{3-25}$$

Where $\sigma(t)$ is the stress at time, t, σ_0 is the maximum stress, and ω is the angular frequency. When the material behaves viscoelastically, the resultant strain is given by equation (3-26).

$$\varepsilon(t) = \varepsilon_0 \sin(\omega t + \delta) \tag{3-26}$$

Where $\varepsilon(t)$ is the strain at time, t, ε_0 is the strain at the maximum stress, and δ is the phase lag between the applied stress and resultant strain. From this, complex strain can be obtained in equation (3-27) (a very similar equation to one seen in section 3.3.4; note that ε refers to strain in this case, not permittivity).

$$\varepsilon^* = \varepsilon' + i\varepsilon'' \tag{3-27}$$

From this, the storage modulus can be calculated where, E' is related to the elastic response and loss modulus, E'' related energy dissipation due to viscous behaviour in equation (3-28) and (3-29).

$$E' = \frac{\sigma_0}{\varepsilon_0} \cos \delta \tag{3-28}$$

$$E'' = \frac{\sigma_0}{\varepsilon_0} \sin \delta \tag{3-29}$$

The ratio between loss modulus and storage modulus indicates the damping in the material and how efficiently the material loses energy due to molecular rearrangements and internal friction [187]. This is shown in equation (3-30).

$$\tan \delta = \frac{E''}{E'} \tag{3-30}$$

When molecular mobility changes occur in the material, such as glass transition temperature, T_g, there is a significant change in storage modulus, and this results in a significant peak in the $\tan \delta$. The same can be said for sub-T_g transitions, such as the *beta* transition, but these will be less pronounced as the change in molecular mobility is less significant.

3.4.2. FLEXURAL MECHANICAL TESTING

Flexural testing was used to determine the material's bending properties. A Lloyd TA500 tensometer was used to apply a load to a sample mounted on a three-point bending jig. The sample was deformed until it broke or reached the maximum load of the load cell (400 N). The three-point bending jig had a span of 25 mm, and the samples were obtained from a flat cast sample and cut using a tile cutter to dimensions of 60 mm by 12.7 mm by 1.6 mm. A compliance test was conducted on a stiff steel block to account for any compliance (deformation) in the testing rig, which was applied to the sample data. A load-displacement graph was obtained, and the flexural modulus, strength and strain at break could be calculated. Flexural modulus, E_{flex}, is given in equation (3-31).

$$E_{flex} = \frac{L^3 m}{4bd} \tag{3-31}$$

Where L is the support span, m is the gradient of the linear portion of the load-displacement graph, b is the width of the sample, and d is the thickness of the sample. Flexural stress, σ_{flex}, is given in equation (3-32).

$$\sigma_{flex} = \frac{3FL}{2bd^2} \tag{3-32}$$

Where F is the applied load. Flexural strain is calculated using equation (3-33).

$$\varepsilon_{flex} = \frac{6Dd}{L^2} \tag{3-33}$$

Where D is the deflection. A stress-strain graph can then be plotted. The flexural strength is the maximum stress value, and the strain at break is the strain value at failure. The number of samples in each batch was 17.

3.4.3. GAS PYCNOMETRY

The volume of cured epoxy samples was obtained using a Micrometrics AccuPyc 1340 in a 1 cm^3 sample cell. Samples were weighed and placed in the cell, where helium gas was pumped into the sample cell at a pressure of 19 PSI and purged five times. Samples were obtained from resin cast in cylindrical test tubes of 10 mm diameter and then cut to 4 mm length. Consistent sample sizes were used to ensure that the surface area was consistent, as this could potentially affect the volume measurements. From this, the volume was obtained, and the sample's density was calculated using equation (3-34).

$$\rho = \frac{m}{V} \tag{3-34}$$

Where ρ is density, m is mass and V is volume.

3.4.4. THERMOGRAVIMETRIC ANALYSIS

Thermogravimetric analysis was performed on cured samples to investigate the thermal stability. A Perkin Elmer Pyris 1 TGA was used under a dry nitrogen gas flow of 20 mL min^{-1} between 30 °C and 700 °C at a heating rate of 10 °C min^{-1}. 10 – 20 mg samples were obtained from flat-cast cured samples. The equipment weighed the initial mass of the sample and monitored the mass as a function of temperature. From this, the onset of thermal degradation, the temperature at maximum rate of degradation and char yield were found.

3.4.5. POSITRON ANNIHILATION LIFETIME SPECTROSCOPY

Postitron annihilation lifetime spectroscopy was performed to investigate the free-volume voids of cured resin samples using the Tao-Eldrup bubble model. Tests were performed at room temperature on samples obtained from flat cast samples cut using a tile saw to 25 mm by 25 mm by 2 mm using the Sheffield positron annihilation lifetime spectrometer (SPALS). Technical information regarding SPALS follows as taken from a thesis by Alec Shackleford who developed the equipment [188]. Positron source information is shown in Table 3.5.

Table 3.5 – SPALS Source information taken from [188].

Source Information	
Source Identifier	^{22}Na Positron Source
Half life	2.6 years
Activity	1.85 MBq ± 15 %
Active diameter	5.08 mm
Overall dimensions	12.7 mm

EJ232Q quenched with 0.5 % benzophenone was used as the scintillator and the information is summarised in Table 3.6.

Table 3.6 – SPALS Scintillator information taken from Eljen Technology [189].

Scintillator Information	
Type	EJ232Q 0.5 % benzophenone
Shape	Cylinder
Diameter	51 mm
Length	51 mm
Scintillation efficiency (photons/KeV)	2.9
Light output (% anthracene)	19
Decay time (ps)	700
Wavelength maximum emission (nm)	370

A H1919-X photomultiplier tube (PMT) is used to convert the photons produced by the scintillator to detectable electrical current [188], the information is summarised in Table 3.7.

Table 3.7 – SPALS H1919-X photomultiplier tube information taken from Shackleford [188].

PMT Information	
Spectral range (nm)	300 - 650
Wavelength maximum emission (nm)	420
Rise time (ns)	1.3
Gain	2×10^7

A fourfold coincidence unit was used to discriminate noise and scatter. A DRS4 evaluation board was used to digitally measure the electrical signal.

These tests and analysis were undertaken by Joseph Orgill in the physics department at the University of Sheffield.

4. INVESTIGATION OF THE NETWORK DEVELOPMENT IN STRUCTURAL ISOMERS OF TGAP/DDS USING NEAR-INFRARED SPECTROSCOPY

4.1. INTRODUCTION

The network formation of epoxy resins can be monitored using near-infrared spectroscopy (NIR) by tracking the changes in the concentration of functional groups involved in the network formation reactions. NIR gives information regarding what bonds make up the network and how these affect the resultant properties of the resin in question.

NIR is widely used due to its versatility for different applications such as medical imaging, food science, and, in this case, online cure monitoring of thermosetting resins [64]. It can be performed in two different modes: transmission and reflectance. Transmission mode makes it suitable for materials that will transmit light through them, colourless or a weak colour. In contrast, reflectance allows NIR to be used for dark materials such as carbon fibre thermoset composites where light cannot transmit through. The spectra should show the same results between the two different techniques.

Due to the use of overtones and combination bands that result in relatively low-intensity bands compared to mid-infrared spectroscopy, the samples can be thick, meaning that very little sample preparation is needed to start taking measurements, making it an attractive technique for industrial applications for monitoring the cure. Generally, industry is interested in knowing whether their part is completely cured. This can be done by tracking the epoxide group band as the ratio of the epoxide group concentration at a given time, $[EP]_t$, to the initial epoxide group concentration, $[EP]_0$. Equation (4-1) gives a measure of how cured the resin is, known as epoxide degree of cure, α_{EP}.

$$\alpha_{EP} = \frac{[EP]_0 - [EP]_t}{[EP]_0} \tag{4-1}$$

This is a suitable measure for industry, but NIR can tell us more about network formation. Knowing when specific reactions occur can allow us to identify what reactions affect the cured resin properties. This is especially important in high-functionality resins such as triglycidyl aminophenol (TGAP), where the network formation is considerably more complex than a

bifunctional resin such as diglycidyl ether of bisphenol A (DGEBA). TGAP has three epoxide groups, whereas DGEBA has two. The crosslink density should be higher. When the crosslinking reactions occur will have more effect on the properties such as glass transition temperature, compressive, tensile and flexural properties and free volume space. Therefore, it is crucial to understand and quantitatively analyse the network formation in high-functionality epoxy resins.

4.2. CHAPTER OVERVIEW

This chapter of the study will monitor the network formation of the structural isomers of TGAP (triglycidyl-*para*-aminophenol and triglycidyl-*meta*-aminophenol) and DDS (4,4'diaminodiphenyl sulphone and 3,3'-diaminodiphenyl sulphone) using near-infrared spectroscopy. The formation of these networks (TG*p*AP/44'DDS, TG*p*AP/33'DDS, TG*m*AP/44'DDS and TG*m*AP/33'DDS) will be analysed and compared between each formulation and how these differences influence the resultant cured resin properties. A multistep cure cycle outlined in Chapter 1. Materials and Methods will be used, which is not often done due to the complexity of taking measurements at different dwells and the effect of temperature change on the molar absorptivity coefficient [182]. Understanding how particular reactions influence the resultant resin properties, such internal antiplasticisation [32], will allow us to fine-tune the properties of resins using chemical structure. The method used and the equations used have been outlined in Chapter 1. Materials and Methods.

4.3. NETWORK FORMATION

The network formation of epoxy amine resins involves three key reactions that are quantifiable using NIR. The ring-opening reactions are shown in Figure 4.1: (a) is the reaction between epoxide groups and primary amines, (b) is the reaction between epoxide groups and secondary amines and (c) is the reaction between epoxide groups and hydroxyl groups. Where these reactions occur can vary; the position on which part of the epoxide group or hardener cannot be determined *via* NIR. Assumptions have to made based on previous literature and chemical structures.

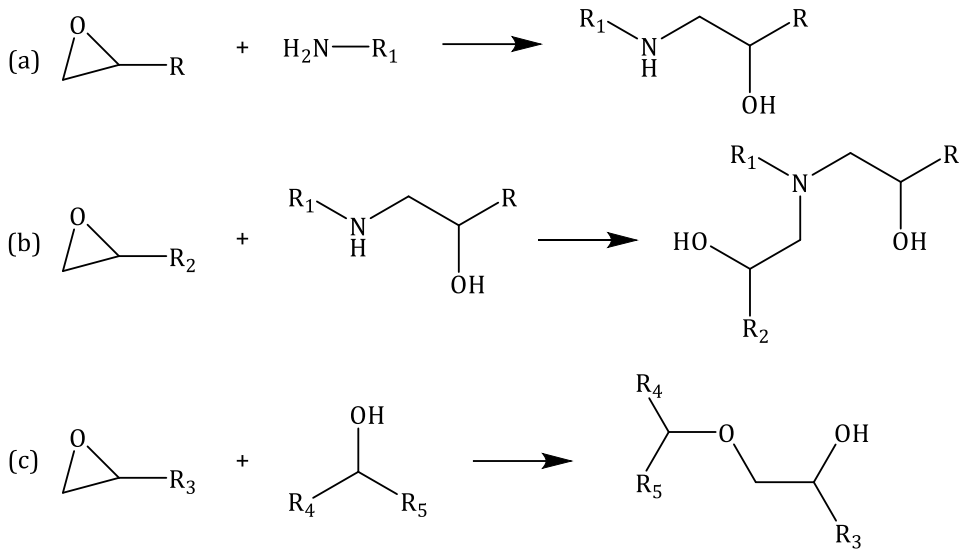

Figure 4.1 – Chemical reactions that occur during the network formation of an epoxy amine resin: (a) epoxide ring and primary amine, (b) epoxide ring and secondary amine and (c) epoxide ring and hydroxyl group (etherification).

The NIR spectra of the four formulations during the cure are presented in Figure 4.2. The reactions in Figure 4.1 can be identified by the change in the absorbance of the epoxide, primary and secondary amines and hydroxyl group bands. Figure 4.2 shows the evolution of these bands. Reaction (a) is shown by an epoxide group and primary amine decrease and a secondary amine increase, (b) by a decrease in the epoxide and secondary amine groups and (c) by a decrease in the epoxide group and no change in either amine group. The spectra are given at 60-minute intervals. In the analysis, spectra were analysed at 10-minute intervals, but not all were successfully analysed due to interference. The epoxide band at 4530 cm^{-1} is a prominent band but is not used in this study as there is overlap with a primary amine band and also baseline shift due to light scatter at these wavenumbers. The proximity of other peaks also makes analysis difficult and unreliable; therefore, the epoxide peak identified in Figure 4.2 at 6035 cm^{-1} will be used for all formulations.

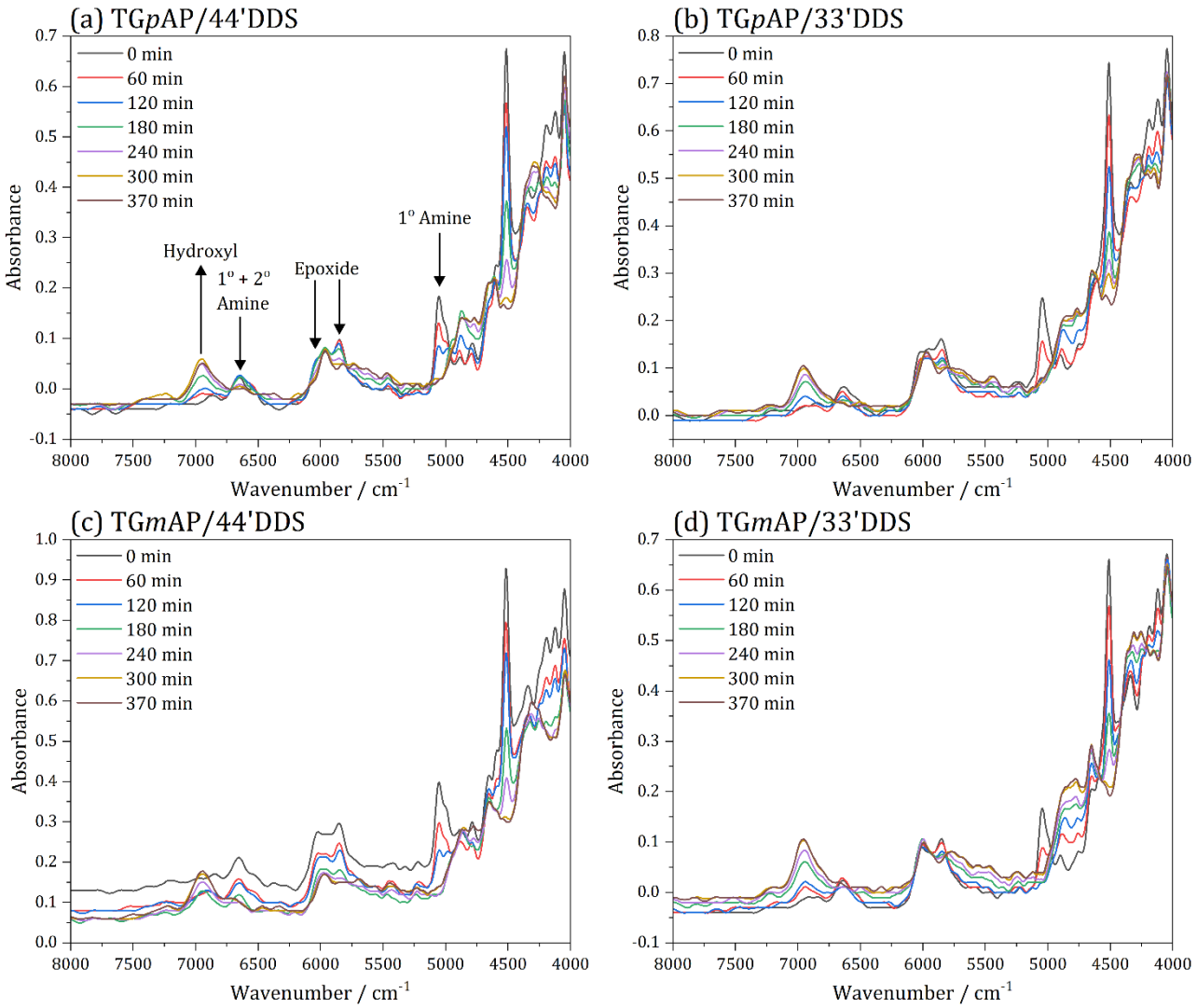

Figure 4.2 – Near-infrared spectra of the network formation of the four structural isomer formulations of TGAP/DDS over a temperature range of 100 °C to 200 °C at 60-minute intervals: (a) TG*p*AP/44'DDS, (b) TG*p*AP/33'DDS, (c) TG*m*AP/44'DDS and (d) TG*m*AP/33'DDS (smoothed).

Figure 4.2 also identifies the hydroxyl group in the spectra. This band is challenging to analyse quantitatively due to hydrogen bonding, which causes the band to be broad. Previous studies have analysed this band, but it will not be done here as etherification cannot be identified using this band as there is no net change in $[OH]$ [70,90].

The equations based upon Beer's law outlined in Chapter 3. Materials and Methods were used to calculate the concentration of epoxide, primary amine and secondary amines for the four formulations of TGAP/DDS, as shown in Figure 4.3. It is worth noting that the time axis does not start at 0 minutes. 0 minutes is the point at which the mixed TGAP:DDS sample is placed on the preheated glass slide and then placed on the preheated heating stage. To

completely mix the powdered DDS hardener into TGAP and obtain a clear mixture, the two must be mixed at approximately 120 °C for ten minutes, and then degassed in a vacuum oven at approximately 100 °C for five minutes. This process takes approximately 15 minutes. The concentration at -15 minutes (or pre 0 minutes) is not a concentration determined by NIR but rather the theoretical conctrations determined using their functional group equivalent weight and TGAP:DDS mass ratio. These calculations and values are shown in section 3.3.1.2. During mixing at elevated temperatures, it is expected that some reactions will take place and the first NIR measurement will not equal the theoretical maximum concentration. Showing the initial theoretical concentration at -15 minutes highlights that reactions take place during the period from mixing to the initial NIR measurement. The first measurements are taken just after 0 minutes, and the concentration values are lower than the theoretical as reactions have occurred during the mixing stage.

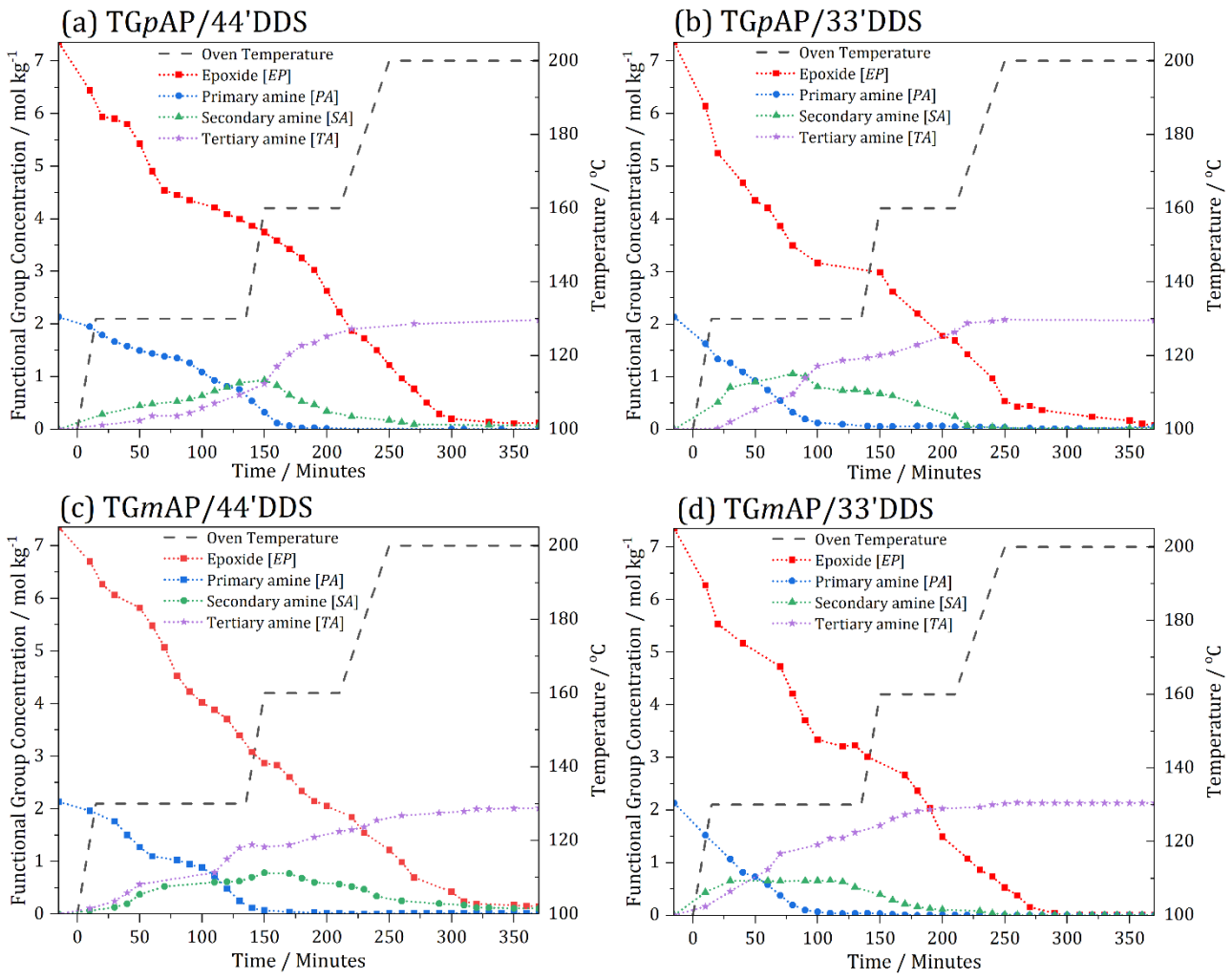

Figure 4.3 – Functional group concentration profiles for the four structural isomer formulations of TGAP/DDS as a function of time as determined by near-infrared spectroscopy: (a) TG*p*AP/44'DDS, (b) TG*p*AP/33'DDS, (c) TG*m*AP/44'DDS and (d) TG*m*AP/33'DDS (smoothed). Temperature axis starts at 100 °C - the temperature of the preheated stage and approximately the resin mixing temperature. Time axis starts before zero indicating reactions during mixing.

The network formation of TG*m*AP/33'DDS will be discussed regarding functional group concentrations in the following section. Each functional group will be discussed separately, and the different TGAP/DDS formulations will be compared. In Figure 4.3, the data sampling rate is not consistent throughout all formulations. This is more apparent in the tertiary amine functional group concentration values. There are occasions where there are spectral features that interfere with accurate deconvolution of the functional group bands, so rather than potentially introduce error into the calculations, data at some time intervals are missing. To calculate tertiary amine concentrations it is the sum of the primary amine concentration and

the secondary amine concentration at the time interval, if these do not line up there will be a lack of data. This is more apparent towards the end of the cure in Figure 4.3 (a) and (b) where the functional group bands are low intensity due to low concentrations of primary and secondary amines and overlap makes deconvolution and integration of the bands difficult. Figure 4.4 shows the NIR cure monitor of TG*m*AP/33'DDS expanded from Figure 4.3.

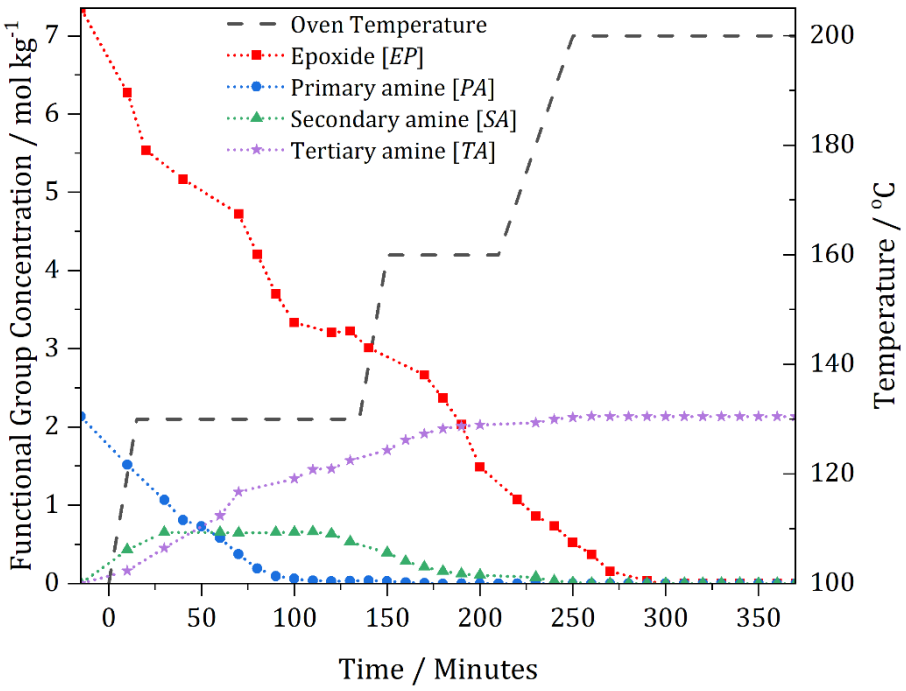

Figure 4.4 – Functional group concentration profile of TG*m*AP/33'DDS as a function of time as determined by near-infrared spectroscopy (smoothed). Temperature axis starts at 100 °C - the temperature of the preheated stage and approximately the resin mixing temperature. Time axis starts before zero indicating reactions during mixing.

Between, the mixing and the first temperature ramp up to 130 °C, there is a sharp decrease in the epoxide concentration, $[EP]$, and a decrease in the primary amine concentration, $[PA]$. With this, there is an increase in secondary amine concentration, $[SA]$, the product of an epoxide ring opening reaction with primary amine. Once the first dwell temperature is reached, the rate of epoxide consumption reduces. Initially, when there have been few reactions, there are many free TGAP and DDS molecules. The reactions that occur between -15 minutes and 15 minutes reduce the mobility of the molecules, resulting in a reduction in the rate of epoxide consumption.

At 30 minutes, the [SA] value stabilises and remains approximately 0.7 mol kg^{-1} until 130 minutes. This suggests that secondary amines react with epoxide groups as soon as they are formed after an epoxy primary amine reaction. If secondary amines were not consumed until the total consumption of primary amines, the maximum [SA] value would be 2.1 mol kg^{-1}. This shows that in TG*m*AP/33'DDS formulations, epoxy secondary amine reactions can occur as low as 130 °C. However, this is only true when considering the [PA] and [TA] values. Primary amines are nearly all consumed within 100 minutes, and from 30 minutes to 100 minutes, secondary amines are consumed as soon as they are produced, as shown by an increase in [TA]. Between 100 minutes and 130 minutes, very few reactions occur, as shown in the [EP] and [TA] values. There is little consumption of epoxide groups and little formation of tertiary amines. This period coincides with the end of the 130 °C dwell, indicating insufficient energy for significant reactions at this temperature.

At 135 minutes, the cure temperature increases from 130 °C to 160 °C. During this ramp and dwell, there is significant consumption of secondary amine groups. At the start of the 160 °C dwell, [EP] falls by a similar amount to [SA], suggesting that the main reaction occurring at this point is epoxy secondary amine crosslinking. [EP] starts to fall significantly at 180 minutes, substantially more than the amount of epoxide reacting with primary and secondary amines. This is assumed to be etherification, which is plausible as there is a significant amount of epoxide and hydroxyl groups in the system [20]. It is not possible to measure etherification directly using NIR as there is no band for an ether group in the near-infrared range, and there is also no net change in hydroxyl groups during the etherification reaction as a hydroxyl group is consumed but also produced.

The chemical structure of TGAP allows for side reactions known as internal cyclisation [45,46,52,190]. In TGAP epoxide rings are bonded the phenyl ring by two different groups, glycidyl ethers and glycidyl amines. Glycidyl amines place two epoxy groups close to each other, increasing the chance of them reacting and forming a cyclic structure in the polymer chain. There is little evidence of these internal cyclic structures forming in glycidyl ether only containing resins, as suggested by Reyes *et al.* [13]. Etherification reactions that internally cyclise occur slowly, so they will only form once all amines have reacted and if spare glycidyl amine portions are free. The reaction mechanism to form a seven-membered ring is shown in Figure 4.5. Matějka *et al.* found that the seven-membered ring product was favoured over a six-membered ring [45].

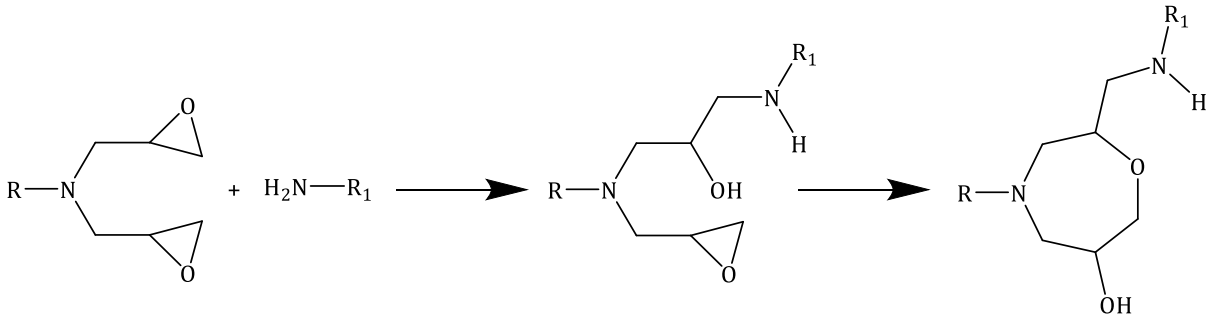

Figure 4.5 – Internal cyclisation through etherification in TGAP to form a seven-membered ring

Attias *et al.* found that when the cyclic structure shown in Figure 4.5 were formed, the resins were less crosslinked due to the secondary amine not being able to react, although the hardener used was 44'DDS which is less reactive than 33'DDS. Therefore, this may not be the case in TG*m*AP/33'DDS [191], especially as Figure 4.4 shows that secondary amines are completely consumed in the curing reaction. However, it is difficult to confirm this phenomenon using NIR. Attias *et al.* and Matějka *et al.* used both high performance liquid chromatography and nuclear magnetic resonance to confirm the presence of these adducts [45,46,190,191].

The final temperature ramp from 160 °C to 200 °C consumes the remaining secondary amines, as shown by stabilisation in $[TA]$. Once the dwell is reached, $[EP]$ decreases to 0.00 mol kg^{-1} by approximately 300 minutes. An additional 70 minutes remain in the cure cycle, and no more reactions occur as the resin is 100 % cured. There may be a small amount of error when the concentration values become small; the bands may be obscured by noise, making it difficult to say they are completely 100 % cured.

The functional group profiles for TG*p*AP/44'DDS, TG*p*AP/33'DDS and TG*m*AP/44'DDS show a similar set of events to the ones discussed here for TG*m*AP/33'DDS, and they will not be individually commented on. The following section will discuss and compare the individual functional groups for all formulations of the structural isomers of TGAP/DDS. Comparing the different behaviours will enable meaningful comments to be made on how the crosslink network forms differently and how this affects material properties.

4.3.1. EPOXIDE

The four different epoxide concentration profiles for the four formulations of TGAP/DDS while curing are presented in Figure 4.6. Upon mixing at -15 minutes, epoxide consumption separates based on the hardener. There is greater consumption in the 33'DDS formulations for the first 30 minutes than in the 44'DDS formulations. This suggests that the 33'DDS hardener is more reactive than the 44'DDS hardener. This is expected as the sulphone group between the two phenylene rings in DDS has an electron-withdrawing effect, allowing for electron lone pair delocalisation and reducing the nucleophilicity of the amine. Delocalisation can occur in 44'DDS due to the *para* position of the two amine groups, whereas in 33'DDS, the amine groups are in the *meta* position, and the lone pair of electrons cannot delocalise.

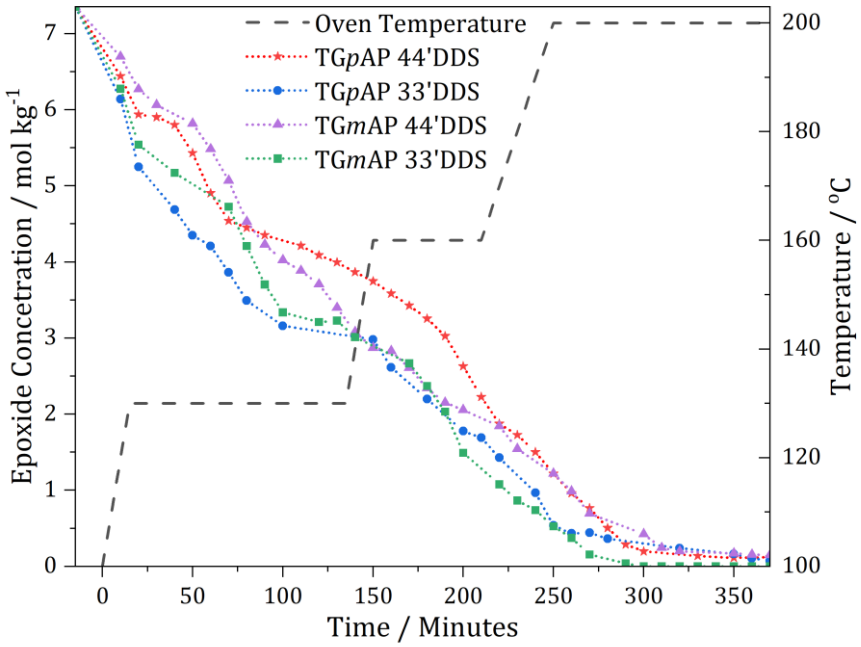

Figure 4.6 – Epoxide concentration profiles for the four structural isomer formulations of TGAP/DDS as a function of time as determined by near-infrared spectroscopy (smoothed). Temperature axis starts at 100 °C - the temperature of the preheated stage and approximately the resin mixing temperature. Time axis starts before zero indicating reactions during mixing.

The delocalisation of electrons through the aromatic rings in 44'DDS is shown in Figure 4.7. 44'DDS is a less effective nucleophile as the effective charge on the amine group can be delocalised throughout the aromatic structure, thus reducing the charge and making 44'DDS less reactive than 33'DDS.

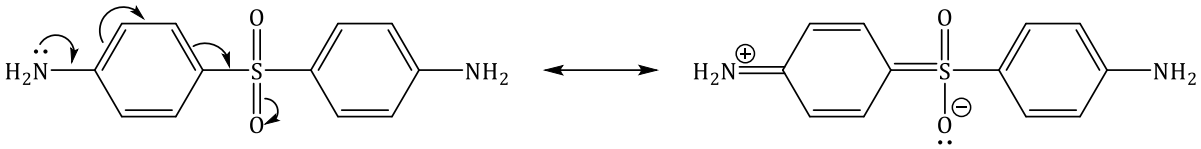

Figure 4.7 – Delocalisation of a lone pair of electrons through the aromatic structure of 44'DDS

Epoxide group consumption is quick upon mixing and during the first temperature ramp up to the 130 °C dwell, after which there is a slowdown in the rate of consumption for all TGAP/DDS formulations. In both 44'DDS and 33'DDS, more epoxide groups were consumed in the TGpAP formulations than in the TGmAP formulations. This is contrary to what has previously been thought about the relative reactivities of TG*p*AP and TG*m*AP, where the *meta* epoxies have been found to be less stable than the *para* epoxies [32]. As TG*p*AP consumes more epoxide groups initially, this suggests that there are not only epoxy amine reactions occurring at this point but also etherification reactions.

The 33'DDS formulations continue to consume epoxide groups quicker than the 44'DDS formulations until 110 minutes when the rate of consumption slows. As seen in Figure 4.4, this is roughly the point at which primary amines are nearly completely consumed. The 44'DDS formulations follow a similar trend up to 80 minutes, where the trend differs, with TG*m*AP/44'DDS consuming more epoxide than TG*p*AP/44'DDS. The trend for TG*p*AP/33'DDS, TG*m*AP/44'DDS and TG*m*AP/33'DDS is similar between 150 minutes and 230 minutes when TG*p*AP/44'DDS starts to follow the same trend till the end of the curing process as the other formulations.

For each formulation, the initial $[EP]$ value was 7.35 mol kg^{-1} and the final $[EP]$ values are shown in Table 4.1. The 33'DDS formulations have a lower final $[EP]$ value than the 44'DDS formulations, although the differences are small. During the cure, when significant crosslinking has taken place, the reaction becomes diffusion controlled and this can result in the trapping of unreacted functional groups [48]. It is not surprising that there are remaining epoxide groups in the cured network. As these are epoxy-rich formulations, an excess of 3.07 mol kg^{-1} when all epoxy amine reactions are accounted for, it would be anticipated that the final $[EP]$ values are related to the structure of the epoxy monomer rather than the hardener alone. The data in Table 4.1 shows this for the 33'DDS formulations. The shape of the hardener must also influence the final $[EP]$ value. The difference between the structural isomer formulations is the position of the reactive groups on the phenyl rings in both the epoxy and hardener.

Table 4.1 – Final epoxide concentration values for the four structural isomer formulations of TGAP/DDS

	TG*p*AP/44'DDS	TG*p*AP/33'DDS	TG*m*AP/44'DDS	TG*m*AP/33'DDS
Final $[EP]$ / mol kg^{-1}	0.12	0.07	0.15	0.00

Considering TG*p*AP/44'DDS, the combination results in a more linear shape than the bent shape TG*m*AP/33'DDS. The *meta* isomers (TG*m*AP and 33'DDS) have higher conformational freedom, rotation around a bond in the molecule results in different arrangement of atoms. The number of conformation states relates to the configurational entropy of the molecule. 33'DDS has been found to have a higher configurational entropy than 44'DDS in previous studies [34,192,193]. Without conformational analysis and only considering the planar chemical structure, the different possible conformations of the four different starting reagents through bond rotation are shown in Figure 4.8. The two *para* starting reagents, TG*p*AP (a) and 44'DDS (c), have only one conformation possible, as rotation around a bond results in the same arrangement (or 'location') of atoms whereas in the *meta*-starting reagents, TG*m*AP and 33'DDS, multiple conformations are possible. TG*m*AP has two different conformational arrangements whereas, 33'DDS has three different conformational arrangements as rotation can occur in two different bonds.

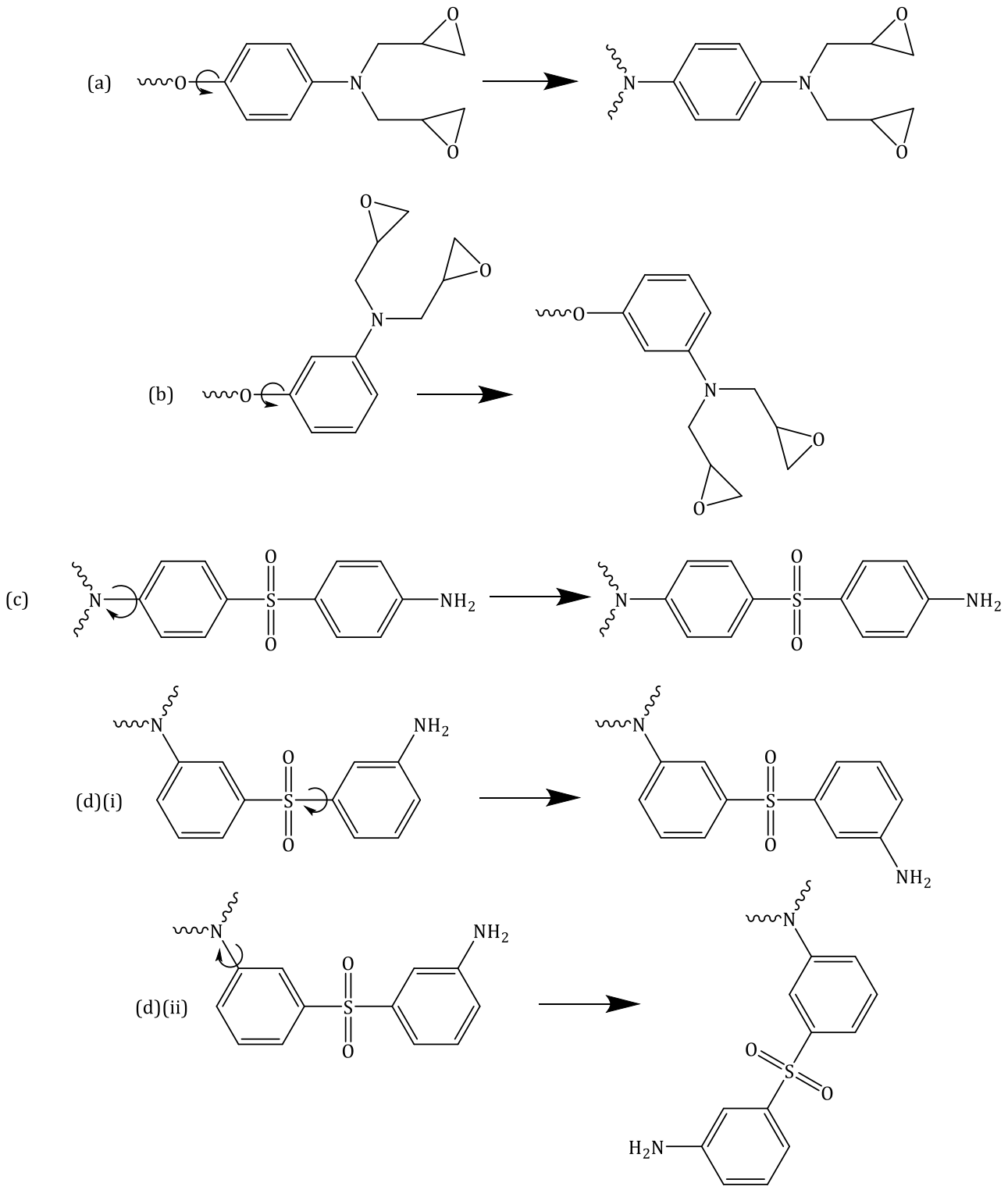

Figure 4.8 – The different conformations possible in the starting reagents of TGAP/DDS: (a) one in triglycidyl-*para*-aminophenol (TG*p*AP), (b) two in triglycidyl-*meta*-aminophenol (TG*m*AP), (c) one in 4,4'-diaminodiphenyl sulphone (44'DDS) and (d)(i) and (d)(ii) three in 3,3'-diaminodiphenyl sulphone (33'DDS).

This lower configurational entropy in TG*p*AP/44'DDS may explain the slowing of epoxide consumption at 80 minutes compared to other less linear formulations. Varley *et al.* used the Flory equation to determine the gel point of TG*p*AP/44'DDS as 41 %, which is approximately the point (4.3 mol kg^{-1}) at which epoxide consumption slows down in TG*p*AP/44'DDS for this study [48,53]. Gelation is when mobility starts to be restricted as the oligomers begin to crosslink, and their movement is limited to short-range motions. TG*p*AP/44'DDS will leave unfilled volume in the network due to its linear shape. The distance between reactive groups will be greater than the other formulations, meaning that the reaction may slow down prematurely when there is insufficient energy for the reactions to occur. TG*m*AP/33'DDS will not have as much unfilled volume due to its conformational states, resulting in a less significant slow-down in epoxide consumption and a lower final $[EP]$.

The argument of greater conformational freedom fails when comparing the final $[EP]$ value of TG*p*AP/44'DDS and TG*m*AP/44'DDS. It is slightly higher for TG*m*AP/44'DDS. This suggests that the dominating geometry effect is the hardener. 33'DDS has three different conformations compared to the one in 44'DDS, but it is also two phenyl rings long, twice the length of TGAP, and the reactive are one bond from the phenyl ring. When linear 44'DDS is paired with a non-linear TG*m*AP, the linearity of 44'DDS may be the limiting factor. The reactive epoxide group in the TGAP is four bonds away from the phenyl ring and flexible, the effect of *para* vs. *meta* may be limited. Therefore, it is not surprising that the final $[EP]$ of TG*p*AP/44'DDS and TG*m*AP/44'DDS is similar.

It is important to note that monitoring $[EP]$ does not tell us what specific reactions are occurring, as shown in Figure 4.1, where epoxide groups are involved in every reaction. When considering $[EP]$ alone, it gives us more of an indication of how cured the network is and at what points significant curing reactions take place.

4.3.2. PRIMARY AMINE

The four different primary amine concentration profiles for the four formulations of TGAP/DDS while curing are presented in Figure 4.9. There is a clear difference in behaviour when comparing the 44'DDS and 33'DDS formulations; the 33'DDS formulations consume primary amines more quickly than the 44'DDS formulations.

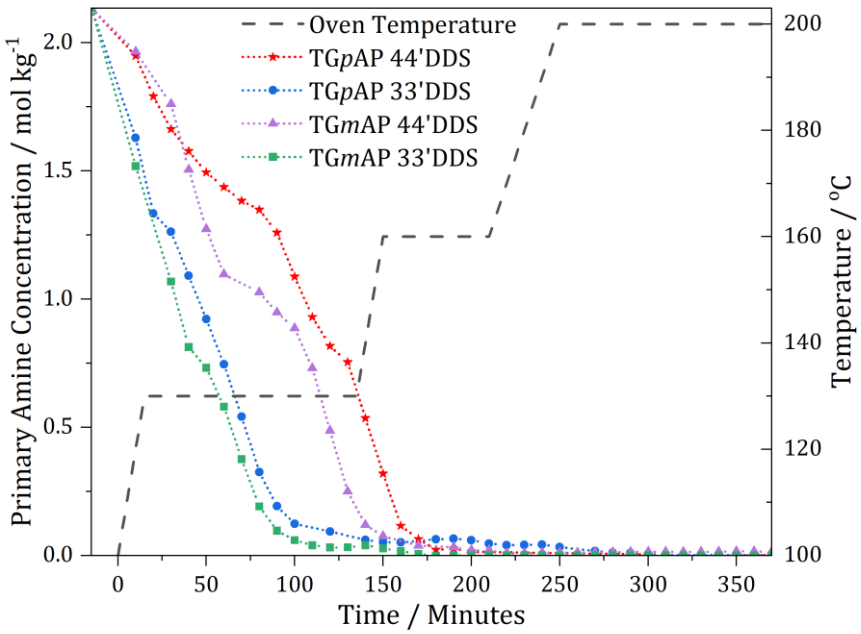

Figure 4.9 – Primary amine concentration profiles for the four structural isomer formulations of TGAP/DDS as a function of time as determined by near-infrared spectroscopy (smoothed). Temperature axis starts at 100 °C - the temperature of the preheated stage and approximately the resin mixing temperature. Time axis starts before zero indicating reactions during mixing.

[*PA*] gives information about the epoxide primary amine reaction shown in Figure 4.10. This reaction forms the linear backbone of the network, although as TGAP is trifunctional, the backbone will not be as linear as that of a bifunctional epoxy such as DGEBA. Ideally, this reaction would occur at the beginning of the cure before any secondary amine crosslinking occurs to obtain a stiff, homogenous network. It cannot be determined what other reactions are occurring by only monitoring the [*PA*] but it can give us vital information about the reactivities of the hardener and if and when primary amines are completely consumed.

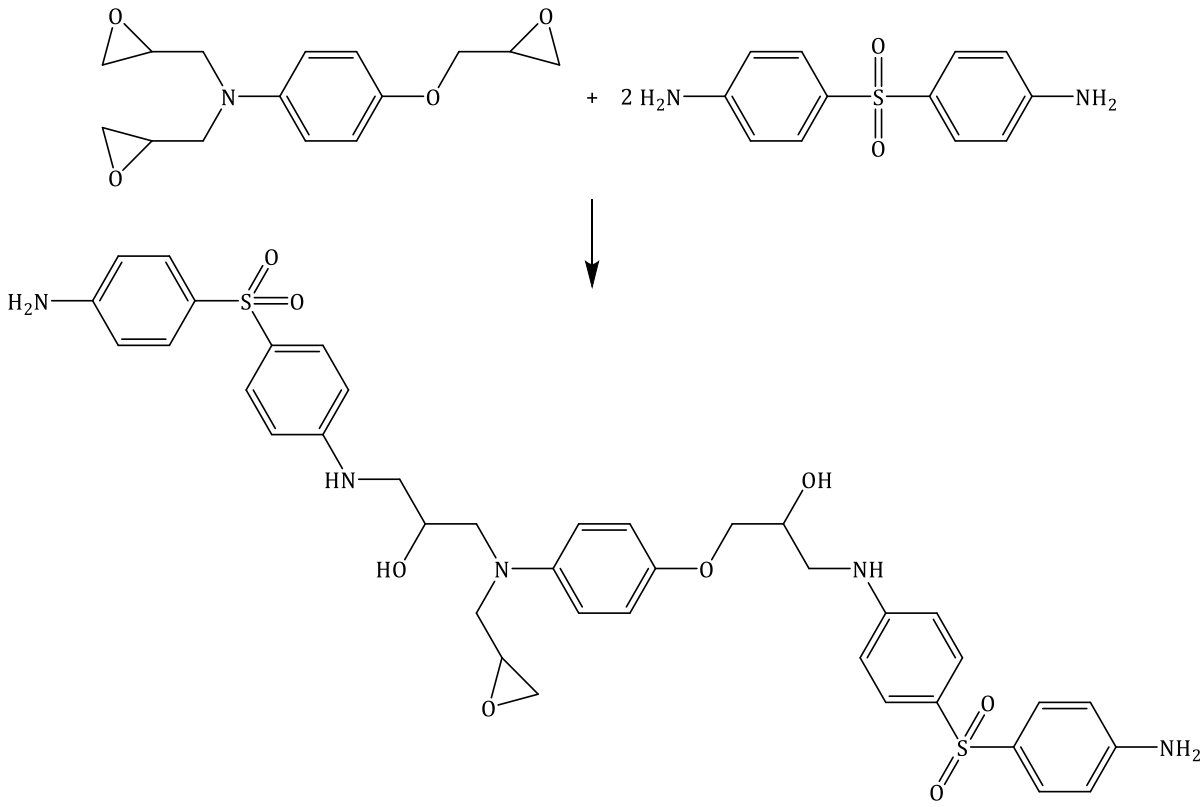

Figure 4.10 – An example of an epoxy primary amine reaction which forms the 'linear' backbone of the network structure in TG*p*AP/44'DDS.

Initially, it is seen that before approximately 40 minutes, TG*p*AP/44'DDS consumes more primary amines than TG*m*AP/44'DDS, but then the rate of consumption of primary amine increases in TG*m*AP/44'DDS. For the 33'DDS formulations, both TG*m*AP and TG*p*AP have a similar rate of consumption until 30 minutes, where TG*p*AP/33'DDS slows slightly. Overall, the TG*m*AP formulations consume primary amines quicker than the TG*p*AP formulations. The same justification for why 33'DDS is more reactive than 44'DDS cannot be applied here as it would be expected that the reactivity of the epoxide ring to be unaffected by whether it is *para* or *meta* substituted on the phenylene ring. The epoxide ring is too far from the phenyl ring to be affected by resonance or inductive effects.

Interestingly, each formulation has a point where the consumption of primary amines slows. This point is less significant in the 33'DDS formulations than in the 44'DDS formulations. The reason for this is unclear. One reason may be steric hindrance and a reduction in mobility that is overcome at a particular point where the primary amines can go on to react. The rate of consumption increases in the same temperature dwell, so it is not something that is overcome by an increase in oven temperature. All formulations apart from TG*p*AP/44'DDS consume

nearly all primary amines before the 130 °C temperature dwell ends. It could also be related to a competing reaction such as etherification or gelation. Resin temperature measurements have been made and will be discussed in Chapter 5. Thermal, where one potential reason may become more apparent.

For all formulations, the near-total consumption of primary amines occurs between 100 and 180 minutes. From there [PA], remains stable for the remainder of the cure apart from one formulation, TG*p*AP/33'DDS, where there is an increase in [PA] at approximately 180 minutes. The increase is small and not representative of what is happening in the curing reaction. Primary amines are not known to be formed during the cure; it is most probably a feature of NIR spectra. The primary amine band in the NIR spectra is situated at 5050 cm^{-1}, directly in the middle of two hydroxyl group bands at 4900 cm^{-1} and 5200 cm^{-1}. Mijović and Andjelić commented on the band at 4900 cm^{-1} causing an "abrupt baseline shift due to hydrogen bonding" of the hydroxyl groups, which could introduce inaccuracy into the determination of absorbance for the primary amine band, resulting in an unexpected increase in [PA] [85].

All formulations, except TG*m*AP/44'DDS, have no primary amines remaining in the final cured system. There is 0.01 mol kg^{-1} primary amine remaining in TG*m*AP/44'DDS. The validity of this value is hard to confirm, given the reasons related to the position of the primary amine band mentioned above.

4.3.3. SECONDARY AMINE

The four different secondary amine concentration profiles for the four formulations of TGAP/DDS while curing are presented in Figure 4.11. Initially, 0 mol kg^{-1} of secondary amines are present in the starting mixture. It is not until epoxy primary amine reactions have occurred that secondary amines will become present. What is interesting about monitoring secondary amines is that they are a species that are both produced and consumed. The concentration value of secondary amines does not indicate precisely what the crosslinked network looks like. Limited information regarding network structure can be gained from monitoring secondary amines.

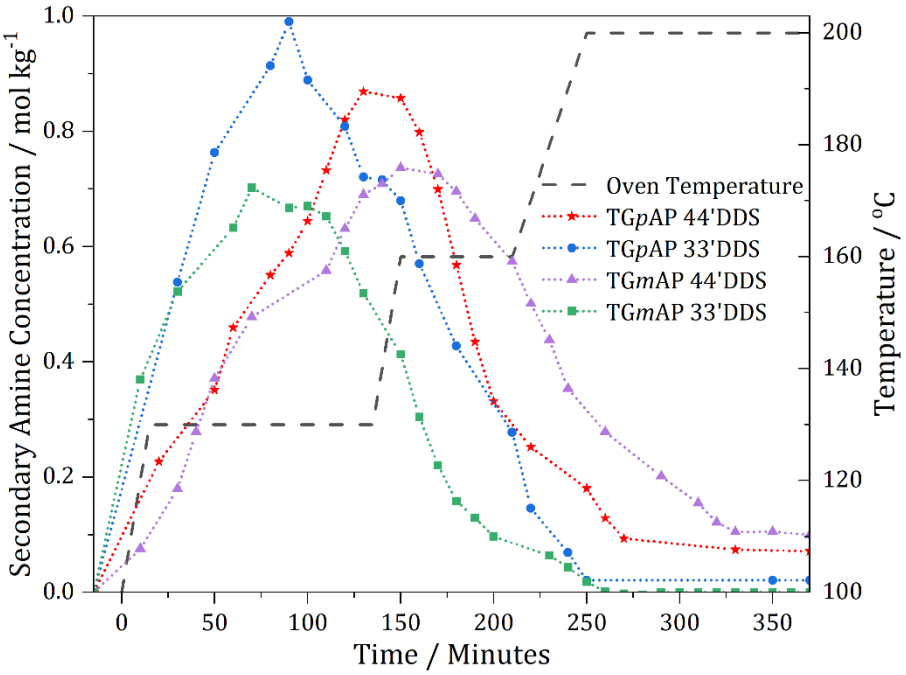

Figure 4.11 – Secondary amine concentration profiles for the four structural isomer formulations of TGAP/DDS as a function of time as determined by near-infrared spectroscopy (smoothed). Temperature axis starts at 100 °C - the temperature of the preheated stage and approximately the resin mixing temperature. Time axis starts before zero indicating reactions during mixing.

Once again, similar trends between hardeners are seen in the first section, as this is the product of the epoxy primary amine reaction discussed in section 4.3.2. The peak and consumption trend of [*SA*] is also similar suggesting that greater reactivity of 33'DDS has a similar effect when considering the epoxy secondary amine reaction. However, the trend observed for TG*m*AP displaying greater reactivity than TG*p*AP, as seen in PA consumption, is not shown.

As Figure 4.11 shows a combination of the formation and consumption of secondary amines, the peak of the [*SA*] value is important. The maximum possible [*SA*] value is 2.14 mol kg^{-1}, the number of primary hydrogens in the starting reagents. There should be equal amounts of primary amine hydrogens to secondary amine hydrogens, but it is apparent from Figure 4.11 that no formulation achieves a concentration value anywhere near 2.14 mol kg^{-1}. The highest [*SA*] value is approximately 1.0 mol kg^{-1} obtained by the TG*p*AP/33'DDS formulation. This is significant as the peak values indicates the amount of secondary amines that have gone on to react with epoxide groups to form tertiary amines before complete consumption of primary amine groups. If secondary amines did not react before the complete consumption of primary amines, then a peak of 2.14 mol kg^{-1} would be reached. It is well-documented that primary and

secondary amine reactions have different reactivities. However, these results show that epoxy secondary amine reactions are possible at temperatures of 130 °C and will compete with epoxy primary amine reactions. Estridge undertook computational modelling on the epoxy amine curing process, modelling the amine reactions as different reactivities and found that network architecture varied greatly depending on how reactivities of primary and secondary amines differed [194].

NIR studies on DGEBA cured with 44'DDS and 33'DDS by Jackson *et al*. found that the peak value of [*SA*] was nearly the theoretical peak value, suggesting that few secondary amines took place before the total consumption of primary amines [195]. Janisse and Wiggins compared TGDDM to DGEBF cured with 33'DDS and found that TGDDM underwent epoxy secondary amine reactions before complete consumption of primary amines, whereas DGEBF consumed all primary amines and then secondary amines went on to react with epoxy at various heating rates, therefore, reaching its peak [*SA*] value [24].

Liu *et al*. undertook NIR kinetic analysis of various epoxy and hardener combinations to investigate the relative reactivities of primary and secondary amines [196]. The relative reaction rate coefficient of secondary to primary amines (k_2/k_1) in 44'DDS, was found to be approximately 0.2 across all three epoxies (DGEBA, TG*p*AP and TGDDM), irrespective of temperature. This suggests that the primary amine of 44'DDS is more reactive than the secondary amine but can undergo simultaneous reactions, this supports trends seen above They also found that the primary amine is primarily affected by the substituent effects, in this case the electron withdrawing sulphone group, justifying why 33'DDS is initially more reactive than 44'DDS formulations. However, if substituent effects influenced the secondary amine reactivity, the maximum [*SA*] value would not be similar, the 44'DDS formulations would be higher. When the primary amine hydrogen is replaced by an epoxide branch, Liu *et al.* found that the aromaticity is broken, these substituent effects have less influence and can be affected by the steric influence of the bonded epoxide branch [196]. This relates to the maximum [*SA*], TG*p*AP containing formulations achieve a higher [*SA*], suggesting that more linear structure of TG*p*AP has increased steric influence on the reactivity of the secondary amine compared to TG*m*AP.

Once the peak [*SA*] value has been reached; all formulations decrease at a similar rate of consumption but to different final values. The final [*SA*] values are shown in Table 4.2. Only

TG*m*AP/33'DDS completely consumes all secondary amines, a similar trend to the [EP] values. Less linear starting reagents allow for more reactions.

Table 4.2 – Final secondary amine concentration values for the four structural isomer formulations of TGAP/DDS

	TG*p*AP/44'DDS	TG*p*AP/33'DDS	TG*m*AP/44'DDS	TG*m*AP/33'DDS
Final [SA] / mol kg^{-1}	0.08	0.02	0.10	0.00

4.3.4. TERTIARY AMINE

The four different tertiary amine concentration profiles for the four formulations of TGAP/DDS while curing are presented in Figure 4.12. Unlike secondary amines, tertiary amines are the product of one reaction. Direct assumptions can be made based on the [TA] value.

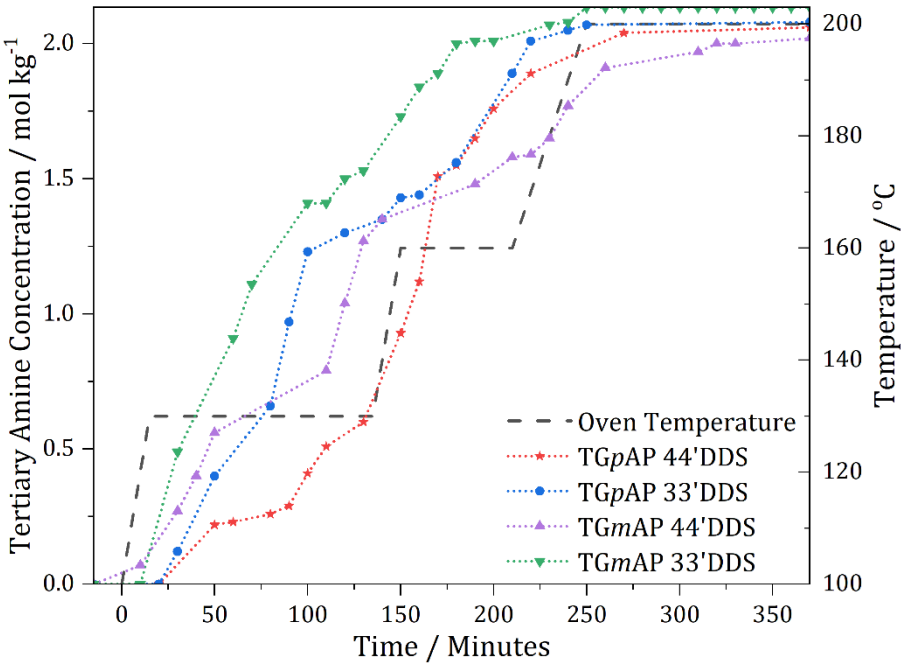

Figure 4.12 – Tertiary amine concentration profiles for the four structural isomer formulations of TGAP/DDS as a function of time as determined by near-infrared spectroscopy (not smoothed). Temperature axis starts at 100 °C - the temperature of the preheated stage and approximately the resin mixing temperature. Time axis starts before zero indicating reactions during mixing.

Tertiary amines are produced as a result of the reaction between epoxy and secondary amine groups, shown in Figure 4.13. As discussed in section 4.3.3, secondary amines are consumed before the total consumption of primary amines in TGAP/DDS systems. The reaction is, therefore, not only the crosslinking of long chains but also the crosslinking of smaller chains. The point at which crosslinking occurs heavily affects the network structure and the resultant properties.

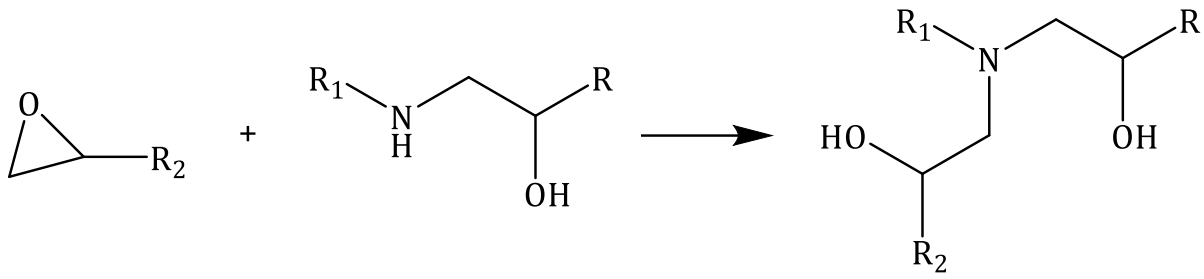

Figure 4.13 – Epoxy secondary amine crosslinking reaction to produce tertiary amines where the R groups are long chains.

In the first temperature dwell, TG*m*AP/33'DDS forms the most tertiary amines. TG*p*AP/33'DDS and TG*m*AP/44'DDS follow a similar trend with similar concentrations of tertiary amines forming in the first temperature dwell, whereas TG*p*AP/44'DDS produces significantly fewer tertiary amines in the first part of the cure. During the temperature ramp to the second temperature dwell, the $[TA]$ in TG*p*AP/44'DDS increases dramatically until reaching a similar value to both TG*p*AP/33'DDS and TG*m*AP/44'DDS at approximately 170 minutes.

Crosslinking occurs between relatively short chains when significant formation of tertiary amines occurs early in the cure. This occurs in TG*m*AP/33'DDS and to an extent in TG*p*AP/33'DDS and TG*m*AP/44'DDS, which is related to the reactivity of the secondary amine compared to the primary amine. When the reactivity of the secondary amine is comparable to that of the primary amine, secondary amines will react with epoxy groups as soon as they are formed, leading to areas of localised crosslinking.

The reasoning behind the similarity can be one of two things: the nucleophilicity of the amine and steric hindrance. The primary amine in 33'DDS is more reactive than 44'DDS, which would explain why tertiary amines are formed earlier in TG*p*AP/33'DDS and TG*m*AP/33'DDS. For TG*m*AP/44'DDS, there must be an alternate reason which could be related to the mobility and proximity of the reactive groups. In a more linear epoxy amine such as TG*p*AP/44'DDS, the

reactivity of the secondary amine will be limited by the steric influences, essentially the non-bonding parts of the molecules preventing reactions on either the epoxy or the secondary amine. In more non-linear starting structures, TG*m*AP/33'DDS, TG*m*AP/44'DDS and TG*p*AP/33'DDS, there is less steric restriction on the secondary amine due to the conformational freedom of the bent structures, see Figure 4.8 which relates the secondary amine reactivity discussed in 4.3.3.

When tertiary amines are formed early in the cure, areas of high crosslink density are formed, joined together by areas of lower crosslink density, resulting in a less homogeneously crosslinked network. As tertiary amines form more slowly in the curing process in TG*p*AP/44'DDS, the network is thought to be more homogenous as linear bonds form initially, which are then connected by crosslinks. Similar findings were found by Sahagun and Morgan when comparing the effect of cure temperature on network formation [23]. A higher cure temperature resulted in areas of high crosslink density connected by areas of low crosslinking density, whereas lower cure temperatures resulted in a more homogenously crosslinked network. This can be related to the four formulations of TGAP/DDS, where some formulations form tertiary amines (crosslinks) early in the reaction, creating a less homogenous network and where other formulations form crosslinks more slowly, creating a more homogenous network. This is represented by the schematic shown in Figure 4.14.

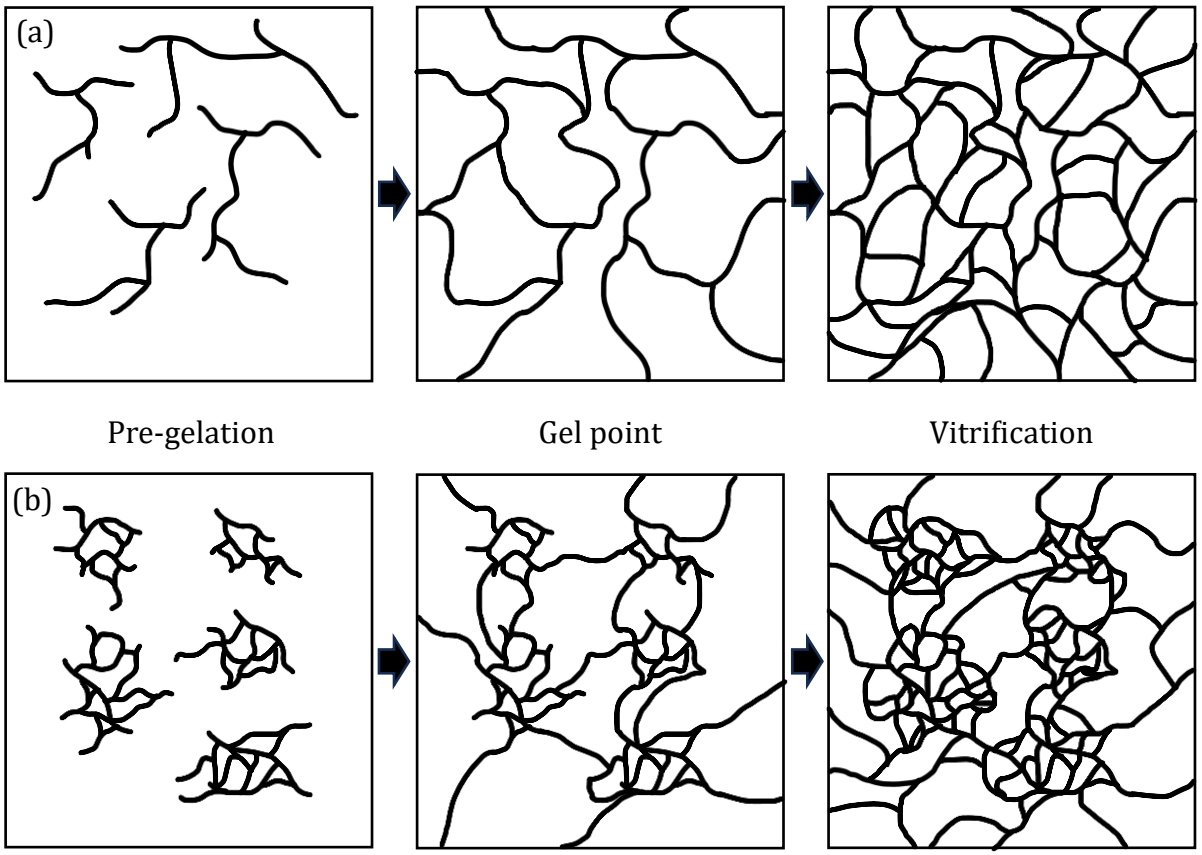

Figure 4.14 – Network growth where different curing reactions dominate at different points: (a) where the linear and crosslinking reactions occur consecutively and (b) where linear and crosslinking reactions compete. Adapted from Sahagun and Morgan under copyright licence 6156571362522 [23].

Schindler and Morosoff suggested that microgels are formed when crosslinking occurs early in the cure, as shown in Figure 4.14 [197]. This inhomogeneity will result in different properties compared to homogenously crosslinked networks. Table 4.3 shows the T_g and density values for the four formulations of TGAP/DDS obtained from dynamic mechanical analysis and gas pycnometry of the cured products. It has previously been reported that networks with a mixture of high and low crosslink density areas will result in a lower T_g [23,197]. TG*p*AP/44'DDS forms tertiary amines slowest, suggesting that crosslinking occurs homogeneously. This correlates with the T_g values as TG*p*AP/44'DDS has the highest values suggesting the highest crosslink density. TG*m*AP/33'DDS has the lowest T_g and the fastest formation of tertiary amines. Previous literature has accounted the decrease in T_g in 33'DDS formulations to the greater configurational entropy allowing for a less stiff network [34], but it is clear that the distribution of crosslink density also has a significant contribution to the T_g values.

Table 4.3 – Glass transition temperatures (T_g) and density measurements for the four structural isomer formulations of TGAP/DDS.

	TG*p*AP/44'DDS	TG*p*AP/33'DDS	TG*m*AP/44'DDS	TG*m*AP/33'DDS
T_g / °C	253.7 ± 0.3	216.2 ± 0.8	226.2 ± 0.1	198.6 ± 0.5
Density / g cm^{-3}	1.3112 ± 0.0007	1.3164 ± 0.0014	1.3211 ± 0.0005	1.3212 ± 0.0024

Table 4.3 also shows the density of the cured samples. The lowest density is the TG*p*AP/44'DDS, suggesting that it has the highest free volume space, which is expected as it is the most homogenously crosslinked and the formulation with the most linear starting reagents. The least homogenously crosslinked, TG*m*AP/33'DDS has the highest density therefore, the most efficient packing, which is related to the non-linearity of the starting reagents and the regions of high and low crosslink density. As the areas of high crosslink density form early in the cure, the density of these sections will be high [197]. The areas of low crosslink density will initially have low density. However, during the entire cure, relaxation will occur. As they are not highly crosslinked, the chains can rearrange themselves in the most efficient packing arrangement, resulting in a higher density.

The final [TA] values vary for each formulation and are shown in Table 4.4. Only TG*m*AP/33'DDS reaches the maximum [TA] possible, confirming there are no primary and secondary amines remaining in the crosslinked network. In addition, TG*p*AP/33'DDS has the second highest amount of tertiary amine present in the network, as it would be expected due to the increased reactivity of the 33'DDS hardener compared to 44'DDS. Interestingly, TG*m*AP/44'DDS has the lowest tertiary amine content present in the network. This coincides with the highest final secondary amine content.

Table 4.4 – Final tertiary amine concentration values for the four structural isomer formulations of TGAP/DDS

	TG*p*AP/44'DDS	TG*p*AP/33'DDS	TG*m*AP/44'DDS	TG*m*AP/33'DDS
Final $[TA]$ / mol kg^{-1}	2.06	2.08	2.02	2.14

It is important to note that even with excess epoxy used in the systems, secondary amines are still present in the cured network. This means that etherification plays a role in the epoxy cure of all the structural isomer formulations.

4.3.5. NON-AMINE REACTIONS

As suggested throughout the previous sections, epoxy amine reactions are not the only reaction that occurs during the curing process. Etherification and homopolymerisation reactions are also possible. An etherification reaction occurs between an epoxide and a hydroxyl group as shown in Figure 4.15 (a). An epoxy homopolymerisation reaction occurs between two epoxide groups when catalysed by an initiator such as a tertiary amine, as shown in Figure 4.15 (b).

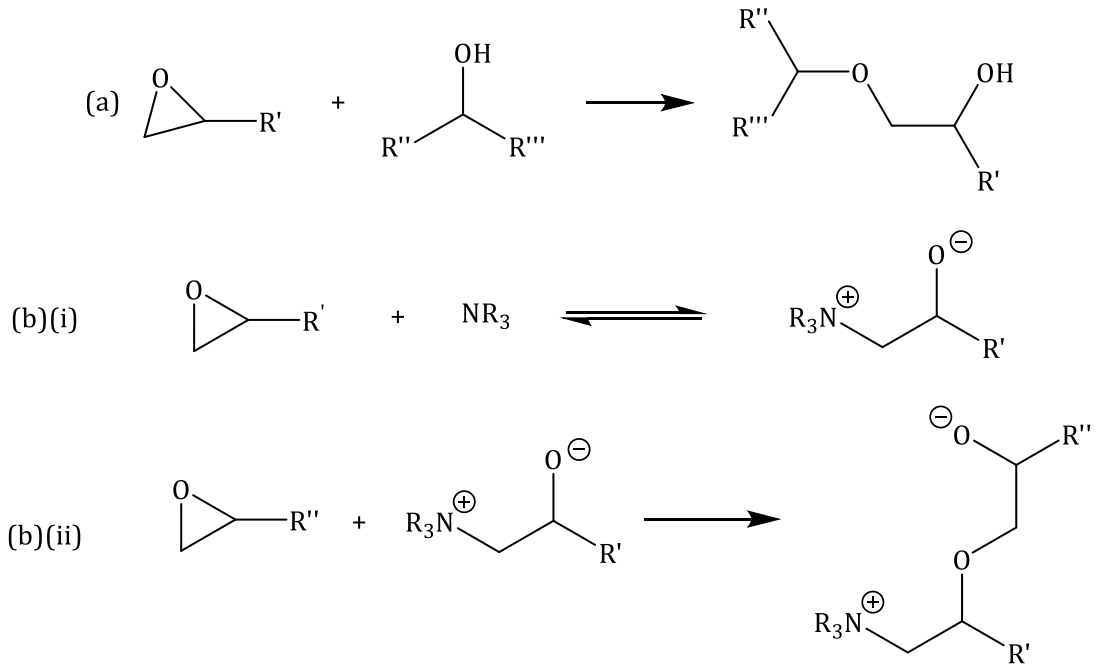

Figure 4.15 – Two non-amine epoxide reactions: (a) etherification reaction between an epoxide group and a hydroxyl group and (b) homopolymerisation reaction between multiple epoxide groups catalysed by an initiator.

The product of these reactions is an ether group, which is difficult to observe in the near-infrared spectra due to the lack of a flexible hydrogen bond, so the intensity of the overtone or combination band is too low. There is also no net increase in hydroxyl groups in both etherification and homopolymerisation, therefore it is a difficult to directly monitor these reactions using NIR. However, no amine groups are involved in either of these reactions, therefore, it is assumed that if the epoxide concentration decreases without a change in the amine concentration, then a non-amine reaction (etherification or homopolymerisation) has taken place. Whether etherification or homopolymerisation is occurring is difficult to say Generally, homopolymerisation reactions will terminate through a reaction with a hydroxyl group like that of etherification, therefore, for simplicity, these non-amine reactions will be referred to as etherification throughout this section. St John and George used the hydroxyl peak at 7000 cm^{-1} to analyse the consumption of epoxide groups when there was no increase in hydroxyl groups [49]. This band is broad and is affected by hydrogen bonding, which makes accurate analysis of the peak difficult.

This assumption can be used to determine the concentration of epoxide groups that react with only amines throughout the cure. This will be referred to as amine-only epoxide concentration, $[EP^a]$, by considering the measured $[EP]$ and the amount of primary and tertiary amines present in the network - the concentration of hydroxyl groups produced from the reaction of epoxy and amines. Any other decrease in $[EP]$ can be assumed to be a non-amine reaction. The calculation is shown in equation (4-2).

$$[EP^a] = [EP]_0 - ([PA]_0 - [PA]_t + [TA]_t) = [EP]_0 - [OH]_t \qquad (4\text{-}2)$$

The comparison of amine-only epoxide concentration and the measured epoxide concentration as a function of the curing process is shown in Figure 4.16. The greater the separation between $[EP^a]$ and $[EP]$ indicates that non-amine epoxy reactions are taking place. A similar trend of $[EP^a]$ and $[EP]$ indicates that reactions are generally epoxy amine reactions. As an epoxy excess is used, etherification should take place during cure, however, it would be expected that it would take place at high temperature and when amine concentration is low. It is worth noting that the calculation of $[EP^a]$ is not a direct measurement, and there is evidence of inaccuracies present in (a) TG*p*AP/44'DDS, (c) TG*m*AP/44'DDS and (d) TG*m*AP/33'DDS where the two lines cross

over or converge, this indicates that ethers are consumed during in the cure which is unlikely. This is potentially an error caused by deconvolution inconsistency in the analysis process. In this instance, it is evidence that MIR is a better candidate for monitoring non-amine reactions during network formation, as the ether functional group concentration could be directly measured. MIR equipment capable of cure monitoring was not available during the time of this study.

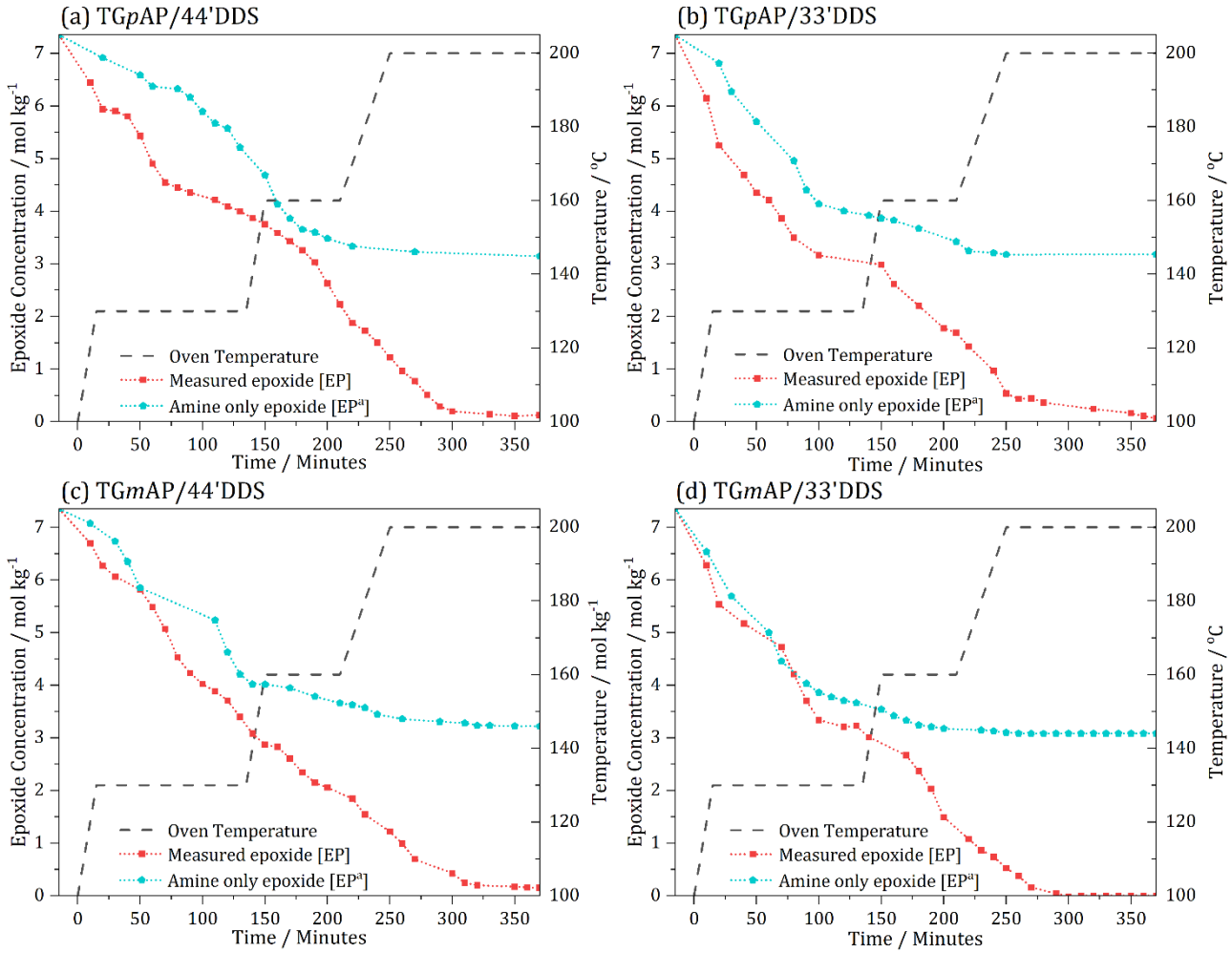

Figure 4.16 – Amine-only epoxide concentration compared to measured epoxide concentration as a function of time as determined by near-infrared spectroscopy: (a) TG*p*AP/44'DDS, (b) TG*p*AP/33'DDS, (c) TG*m*AP/44'DDS and (d) TG*m*AP/33'DDS (smoothed). Temperature axis starts at 100 °C - the temperature of the preheated stage and approximately the resin mixing temperature. Time axis starts before zero indicating reactions during mixing.

The measured [*EP*] values have already been discussed in 4.3.1 and show similar behaviour between the different formulations apart from an instance discussed above where

TG*p*AP/44'DDS epoxide consumption slows between 110 and 230 minutes. Unlike the previous sections, similar behaviour is observed between the same epoxy formulations.

Initially, there is a significant difference between the measured $[EP]$ and $[EP^a]$ in both TG*p*AP/44'DDS and TG*p*AP/33'DDS, suggesting that epoxy groups are consumed through a reaction other than epoxy amine reactions in the initial part of the cure, etherification. In both, TG*m*AP/44'DDS and TG*m*AP/33'DDS, there is little difference between $[EP]$ and $[EP^a]$ suggesting that the main consumption of epoxy groups at the start of the cure is through epoxy amine reactions.

This is different from what is seen in DGEBA amine systems, where etherification, if it occurs at all, occurs at high temperatures towards the end of the cure when few reactive amine groups remain. The start of the TGAP/DDS cure is under relatively low-temperature conditions (130 °C), and significant amounts of reactive primary and secondary amine groups are present in the system. This means that there must be a property of TG*p*AP that encourages competition between epoxy amine and etherification reactions that is not also present in TG*m*AP.

As mentioned in Chapter 2. Literature Review, glycidyl amines behave differently to glycidyl ether. Internal cyclisation reactions are possible [45,190] due to the proximity of epoxy groups. A nitrogen group also links glycidyl amines, whereas glycidyl ethers are linked to the phenylene ring by ether groups. It is known that in glycidyl ether systems, etherification reactions occur at high temperatures and are catalysed by the high concentration of tertiary amines [198]. The tertiary amine in the glycidyl amine of TGAP can also do this. St John and George found that in TGDDM (two glycidyl amine groups), etherification was catalysed by TGDDM [49]. Although in TGDDM, the glycidyl amines only accounted for 10 % catalytic activity of the etherification reaction, which is relatively low compared to what has been found here, this is related to size. In TGDDM, MY721 specifically, the resin has undergone side reactions in the synthesis process, and there are fewer monomer units than those present in TG*p*AP (MY0510) and TG*m*AP (MY0610), which would reduce the mobility of TGDDM [44] and its ability to form a catalytic intermediate. Their mobility in the starting mixture is also greater than that of TGDDM as there is only one phenylene ring between the epoxy groups in TGAP compared to a phenylene-methyl-phenylene structure between the epoxy groups in TGDDM. It is important to note that St John and George used different epoxy-amine ratios, and the excess epoxy used will impact the effectiveness of the tertiary amine behaviour.

Anhydride hardeners react differently to amine hardeners. They require a tertiary amine catalyst to produce hydroxyl groups through epoxy homopolymerisation to initiate the reaction with anhydrides, which can then form a crosslinked network through a reaction known as esterification. Rocks *et al.* investigated curing glycidyl amine-containing epoxies with anhydride hardeners without the traditional tertiary amine catalysts at ambient temperatures (imidazole and dimethylbenzylamine) [199]. They found that anhydride curing reactions could occur with TGDDM and TG*p*AP. Contrary to what was said above, TGDDM was more reactive than TG*p*AP and, therefore, a more effective tertiary amine catalyst. Jagadeesh found that in a TGDDM/TG*p*AP/DDS system, when the TG*p*AP content increased, the activation energy increased, suggesting that when a glycidyl amine is replaced with glycidyl ether, the catalytic effect decreases. This finding was only in reference to the activation energy calculated using an empirical method rather than spectroscopic findings, so how reliable this is questionable as many methods do not account for etherification [115]. However, Varley *et al.* found that TG*p*AP underwent more etherification at low temperatures than TGDDM when cured with a phosphorus-based hardener [200]. This could be related to the size of TGDDM, which prevents the formation of the intermediate and results in lower amounts of etherification. Whereas in TGAP, the intermediate is more readily formed due to it being less sterically hindered, therefore the etherification and epoxy-amine reactions compete.

Additionally, Morgan and Mones found that pure TGDDM could not undergo homopolymerisation under 200 °C without the presence of a hardener, suggesting that the reactions that occur are more likely to be etherification produced from an epoxy primary amine reaction than homopolymerisation of the epoxy monomers [44]. A dynamic DSC scan was undertaken to see if 100 % TG*p*AP homopolymerised, no notable reactions occurred at temperatures similar to the cure cycle.

Given that the tertiary amine of TGAP behaves as a catalyst, there is clearly a difference in the effectiveness of the catalytic effect between the TG*p*AP and TG*m*AP. The position of the glycidyl amine on TG*p*AP allows the tertiary amine to interact with a free epoxide group more effectively due to its *para* position. The reaction pathway for tertiary amine catalysed etherification of TG*p*AP is shown in Figure 4.17.

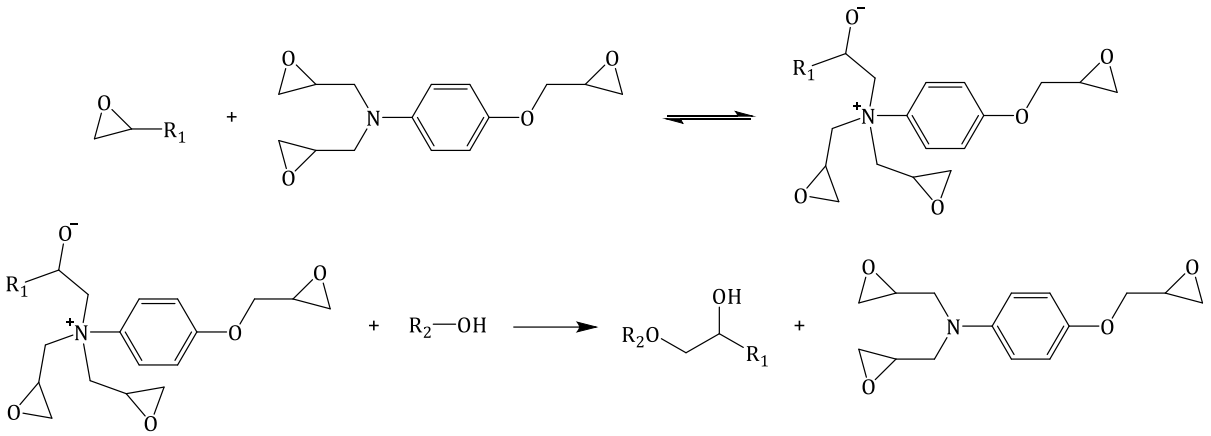

Figure 4.17 – Reaction pathway for the tertiary amine catalysed etherification of triglycidyl-*para*-aminophenol

The *para* position is significant as the ether group behaves as an electron-donating group when in a *para* position. As seen with 44'DDS, the nitrogen is activated through delocalisation in the aromatic ring. This is not possible in *meta* positions, like in 33'DDS, so TG*m*AP is a less effective tertiary amine than TG*p*AP. This reasoning justifies the results shown in Figure 4.16, where TG*p*AP undergoes etherification earlier in the reaction than TG*m*AP. Some assumptions can be made about whether glycidyl amines or glycidyl ethers are involved in these reactions.

As shown in Figure 4.17, when the catalytic intermediate structure is formed, the glycidyl amine groups become sterically hindered, and the probability of an epoxide ring opening on this section is reduced. Therefore, the free glycidyl ether is more susceptible to attack from amines in TG*p*AP. Stutz and Mertes commented on the lower activation of glycidyl ether in DGEBA compared to the glycidyl amine in TGDDM due to it being less stiff [201]. As seen in 4.3.2, the TG*m*AP formulations react with primary amines slightly quicker than TG*p*AP. Before, this may have been attributed to TG*m*AP being more reactive than TG*p*AP. Instead, TG*m*AP is initially more reactive with respect to amines as TG*p*AP reacts with both primary amines and hydroxyl groups. Another thing to consider is that from Figure 4.16, TG*p*AP/44'DDS undergoes more non-amine reactions than TG*p*AP/33'DDS. This can be related to the increased reactivity of 33'DDS compared to 44'DDS.

Due to the reduced catalytic efficiency of the tertiary amine in TG*m*AP, the glycidyl amines are freer to react with primary amines. This opens up the increased possibility of internal cyclisation in the epoxy secondary amine reaction due to the proximity of the epoxide rings [45]. The reaction is shown in Figure 4.18.

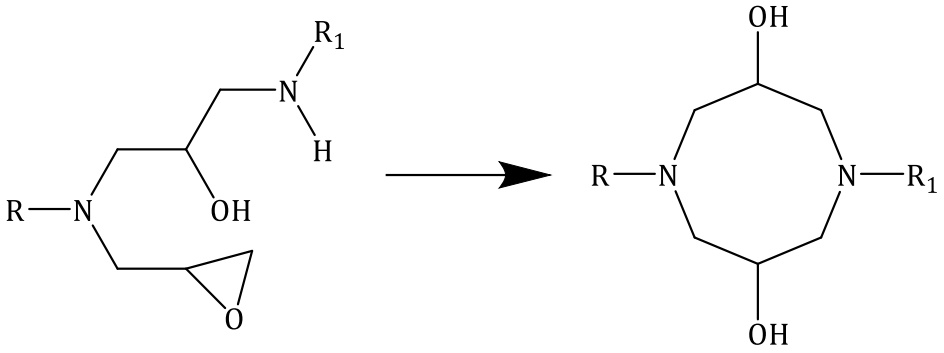

Figure 4.18 – Internal cyclisation via an epoxide and secondary amine to form an eight-membered ring.

This reaction will lead to a network where the T_g and the crosslink density is lower than one that doesn't internally cyclise. This is because instead of forming a crosslink as the secondary amine reaction does, it forms a cyclic structure. Cyclic structures are less stiff than aromatic rings due to freedom from the lack of planar aromaticity. This is seen in the T_g values shown in Table 4.3, TG*m*AP/33'DDS has a significantly lower T_g compared to TG*p*AP/44'DDS, 253 °C compared to 199 °C. This has been seen experimentally in a study characterising the cured properties of the structural isomers of TGAP/DDS by Ramsdale-Capper and Foreman [32].

When etherification occurs early in the reaction in the TG*p*AP formulations, this aids the formation of the linear backbone structure and should result in a more homogeneously crosslinked structure as it effectively prevents the formation of the perhaps unwanted internal cyclised structures. Etherification at the later stages of the cure is desirable as these are crosslinking reactions which make the network stiffer and should increase the crosslink density of the overall network. Tangthana-unrung *et al.* studied the use of excess epoxy formulations and how homopolymerisation and etherification reactions could be tailored to fine-tune the mechanical and toughness properties of vitrimers; etherification resulted in the improvement of these properties [202].

During the second dwell, when most primary and secondary amines were consumed, etherification became the dominant reaction in all formulations as there were relatively high concentrations of epoxide groups compared to amine groups. Lesser and Crawford suggested that tertiary amine-catalysed etherification can only occur at high temperatures [203]. This was not the case in this study; etherification occurred as low as 130 °C and was a dominant reaction at 160 °C. This finding has also been confirmed by Gupta *et al.* when studying the cure of

TGDDM/44'DDS [204]. The tertiary amines in TG*m*AP and TG*p*AP were sufficient for low-temperature etherification reactions. In DGEBA, etherification is impossible at these low temperatures due to the lack of tertiary amines; therefore, it only occurs at high temperatures due to the presence of tertiary amines from the epoxy secondary amine reaction. However, it is also possible in DGEBA through the use of tertiary amine catalysts such as imidazole [75].

4.4. CONCLUSIONS

The results from this study confirm that structural isomerism strongly influences network formation in TGAP/DDS isomers, as Ramsdale-Capper and Foreman previously suggested [32]. NIR has determined that two main contributing factors determine network formation.

The first is the amine hardener structure, with 33'DDS (*meta* position) being more reactive than 44'DDS (*para* position). In 33'DDS formulations, the primary and secondary amines are consumed more quickly than in 44'DDS formulations. The fast formation of tertiary amines results in areas of high and low crosslink density, whereas the relatively slower formation of tertiary amines leads to more uniformly distributed crosslink density in the network.

The second factor is the structure of the epoxy monomer, where TG*m*AP behaved differently from TG*p*AP. The evidence suggested that TG*p*AP underwent etherification at lower temperatures due to the increased catalytic behaviour of the tertiary amine in the glycidyl amine at the *para* position. In contrast, TG*m*AP epoxy amine reactions on the glycidyl amine dominated at low temperatures, potentially forming eight-membered cyclic structures due to internal cyclisation. It is important to note that this has not been experimentally determined. It is only assumed from NIR and thermomechanical properties.

This resulted in two different types of networks despite comprising the same functional groups. The results suggest that TG*p*AP/44'DDS forms the most homogenous network with the least likelihood of internal cyclisation, whereas TG*m*AP/33'DDS forms a less homogenous network. This behaviour is influenced by the epoxy:amine ratio and the particular cure cycle used. In stoichiometric ratios, non-amine reactions may not be seen at such low temperatures due to the lack of excess epoxide groups present in the system. Excess epoxy formulations are more relevant due to their use in industry to ensure that complete consumption of amines occurs.

The results found here will be related to the later sections and discussed in Chapter 6. Cured Properties with a complete comparison to the characterisation of the cured properties of TGAP/DDS.

5. INVESTIGATING THE NETWORK DEVELOPMENT IN THE STRUCTURAL ISOMERS OF TGAP/DDS BY THEIR THERMAL RESPONSE

5.1. INTRODUCTION

The cure of an epoxy resin can be monitored using thermal techniques. This is done differently from how the curing reactions were monitored in Chapter 4. NIR using near-infrared spectroscopy. Instead of identifying the specific bonds being broken and formed, the thermal response of these reactions is monitored. The curing process is exothermic. Exothermic reactions release energy into the surroundings, resulting in a difference between the applied and resultant temperature, which can be measured using differential scanning calorimetry or more simply, thermocouples. The extent of the thermal response indicates how cured the epoxy resin is.

Thermocouples are widely used in composite manufacturing to monitor the curing response of large parts, ensuring that the part is evenly cured [205,206]. Few studies have directly used thermocouples to monitor the cure in neat resin studies, and where they have, few comments have been made [83,88,98,99]. The lack of studies is partly due to the undesirability of large temperature overshoots, which may lead to thermal degradation. In some low-temperature cures, a temperature overshoot is desirable as this drives the reaction without additional temperature input, saving energy and money [100]. Understanding where there are temperature overshoots provides information about where significant reactions are occurring and where the temperature is perhaps lower than the input temperature, which provides insight into when the curing reaction has finished. Despite the lack of precise information this method provides, thermocouples are cheap. K-type thermocouples retail at approximately £5 a metre. They intrude very little on the manufacturing process. Samples can be any size as long as the thermocouple junction is covered, making them a key candidate for understanding the exothermic response of an epoxy-amine curing reaction quickly and cheaply.

A more precise method, differential scanning calorimetry (DSC), can provide more detailed information about the thermal response of the epoxy-amine curing reaction. Where there may be no temperature overshoot using thermocouples, DSC may measure an exothermic response, making it a candidate for in-depth kinetic analysis of the cure. While thermocouples could take measurements online, while the resin or composite part cures in the oven, DSC cannot. A small

sample of uncured resin must be removed and placed in the DSC, which may have a negative impact on the manufacturing process and require an additional testing lab to house the equipment. However, the information gained from DSC often outweighs this drawback. DSC can provide information on how cured the resin is, at what temperature reactions occur, or how long it takes to cure, and it allows for further kinetic modelling of the curing process. It is no surprise that many studies have been undertaken using DSC to investigate the cure of different epoxy resins as outlined in Chapter 2. Literature Review.

5.2. CHAPTER OVERVIEW

This chapter of the thesis will monitor the thermal response of the structural isomers of TGAP (triglycidyl-*para*-aminophenol and triglycidyl-*meta*-aminophenol) and DDS (4,4'-diaminodiphenyl sulphone and 3,3'-diaminodiphenyl sulphone) during network formation using thermocouples and differential scanning calorimetry. In Chapter 4. NIR, specific reactions occurred at different points in the cure dependent on the TGAP/DDS formulations (TG*p*AP/44'DDS, TG*p*AP/33'DDS, TG*m*AP/44'DDS and TG*m*AP/33'DDS). The thermal response will validate these differences through analysis of dynamic, isothermal and multi-step heating. Thermocouples will measure the resin temperature during the cure, and qualitative analysis will be made, whereas DSC will measure the exothermic response while curing and quantitative analysis will be made. Resin temperature analysis is not widely used to understand the network formation in neat resins. In contrast, DSC is widely used, but as far as can be seen, no studies have used DSC to compare the network formation of the structural isomers of TGAP/DDS using a multi-step cure cycle. Using these two techniques will allow for understanding the thermal response of the epoxies during the curing process and aid in fine-tuning the resultant properties.

5.3. RESIN TEMPERATURE MEASUREMENTS

5.3.1. CURE SCHEDULE

Resin temperature measurements were taken during the cure of the four structural isomers of TGAP/DDS using the standard cure cycle, as shown in Figure 5.1. The black dashed line shows the oven temperature, whereas the four different coloured lines (red, blue, purple and green)

show the resultant resin temperatures. Temperature overshoots are seen among all four formulations, suggesting that significant exothermic curing reactions occur at these temperatures. The temperatures at which the overshoots occur differ and depend on several factors relating to resin and hardener structure. This section will discuss these differences qualitatively. It is important to note that specimen dimensions will influence the exotherm. The resin monitored here was cured in a walled glass dish and the specimens were 100 mm by 100 mm by 4 mm. The heat dissipation will be less than that of a specimen cured on a flat glass plate. This in turn may have exaggerated the exothermic nature, however for qualitative analysis, the method has demonstrated the most reactive points during the cure.

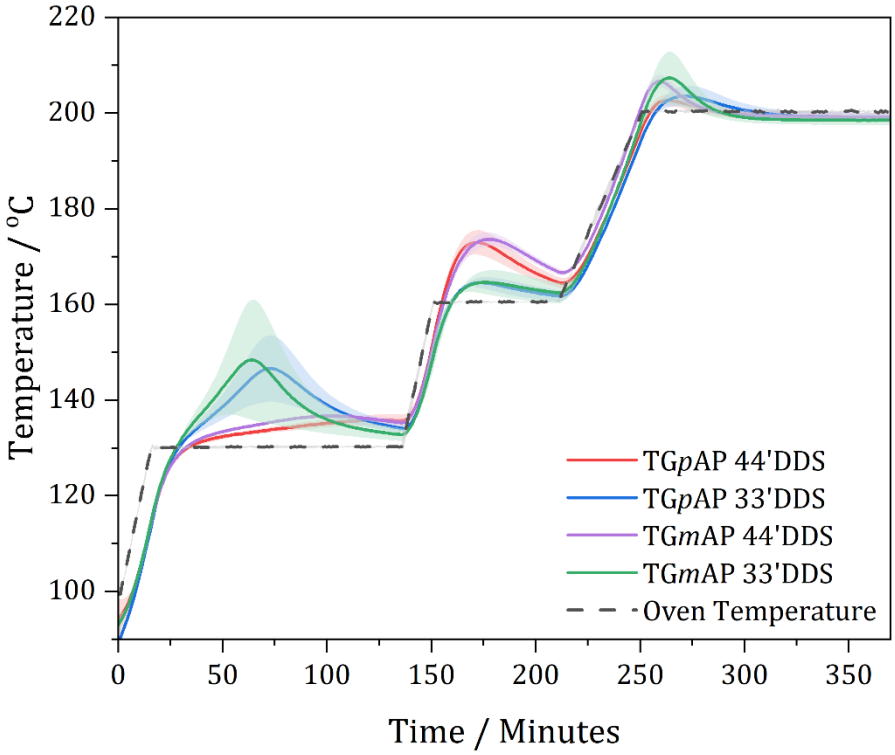

Figure 5.1 – Temperature profiles for the four structural isomers of TGAP DDS during the standard cure cycle as measured by thermocouples for resin and oven temperatures, where the shaded region is the standard deviation. 100 mm by 100 mm by 4 mm sample dimensions.

The first thing of note is the oven temperature. Although not completely clear in Figure 5.1, the oven's actual temperature is not precisely the temperature programmed into the oven controller. This is a feature of how the temperature is controlled. A proportional integral derivative (PID) controls the oven's heat by calculating the difference between the desired and

actual temperatures. There is often a small delay in this calculation, resulting in small temperature overshoots during and after a temperature ramp, as seen in Figure 5.2. They are also designed to save energy. Therefore, when a constant temperature is wanted in the temperature dwell, the temperature may fluctuate by a very small amount (under 0.1 ^{o}C), as seen by the slightly noisy flat line in Figure 5.2. The temperature differences are not so significant that they would significantly affect the curing reaction. However, it is worth noting that the temperature and heating rate programmed into the oven are not consistently replicated in practice.

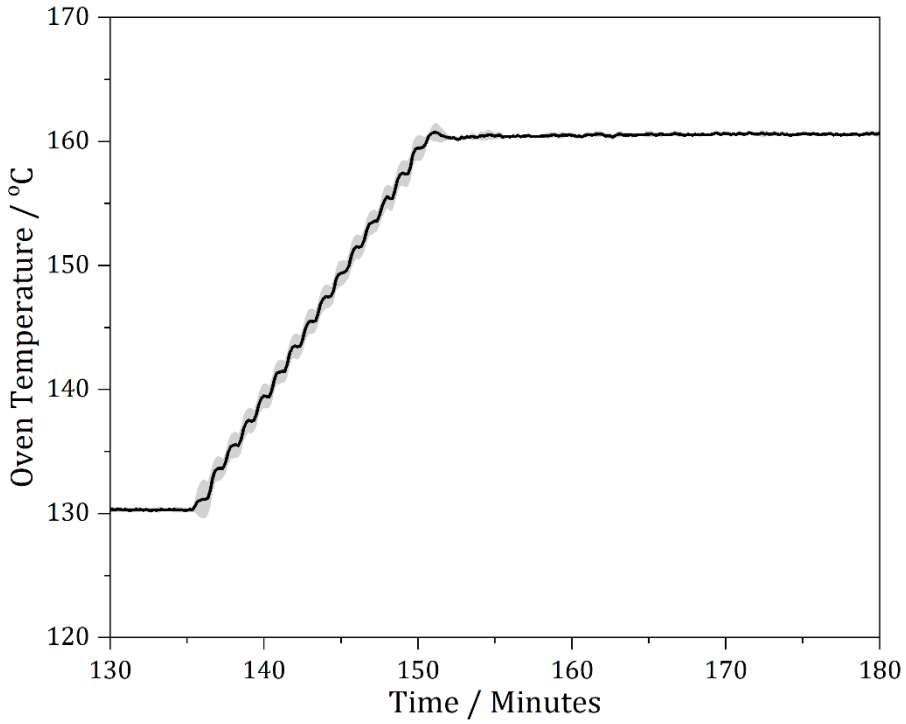

Figure 5.2 – The fluctuation of oven temperature measurements using thermocouples during the second ramp and dwell of the TGAP/DDS cure, where the shaded region is the standard deviation.

Figure 5.1 helps see the difference in temperature as a function of the cure. Still, for easy analysis, it is best normalised so that the difference between oven and resin temperature is shown in Figure 5.3. As the cure cycle cannot be seen graphically, the figure has been sectioned up and labelled to show the heating regimes in the cycle. The standard deviation is not shown in Figure 5.3, as it can make the graph difficult to interpret. When it is significant, Figure 5.1 will be referred to.

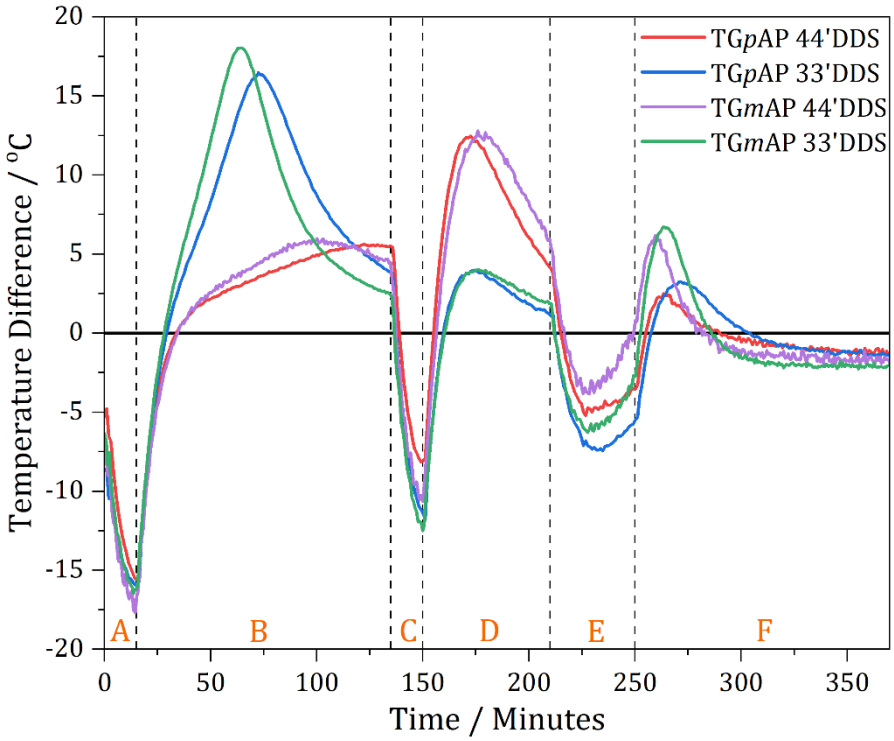

Figure 5.3 – Normalised temperature difference between the oven and resin temperature measurements for the four structural isomers of TGAP DDS during the standard cure where: A is the temperature from 100 °C to 130 °C at 2 °C min^{-1}, B is the temperature dwell at 130 °C for 120 minutes, C is the temperature ramp from 130 °C to 160 °C at 2 °C min^{-1}, D is the temperature dwell at 160 °C for 60 minutes, E is the temperature ramp from 160 °C to 200 °C at 1 °C min^{-1}, and F is the temperature dwell at 200 °C for 120 minutes. 100 mm by 100 mm by 4 mm sample dimensions.

The first ramp from 100 °C to 130 °C, A, shows similar behaviour between the four formulations. The resin temperature lags behind the oven temperature as it takes time for the heat to transfer entirely through the liquid resin due to its thermal mass, indicating that few curing reactions are occurring at this point. By approximately 30 minutes, all four resins have reached the set oven temperature of 130 °C. After this point in the first temperature dwell, B, the formulations behave differently depending on their starting materials.

The formulations separate based on the hardener. The 33'DDS formulations' temperature rises quickly to + 17 °C for TG*m*AP and + 15 °C for TG*p*AP over the oven temperature at 65 and 75 minutes, respectively. As there was little reduction in the rate of temperature change once the oven temperature was reached, the 33'DDS were most likely undergoing curing reactions in

the first temperature ramp. Once the maximum temperature has been reached, the temperature overshoot decreases, suggesting that the curing reactions reach a maximum rate of reaction, and then the rate slows down. The temperature overshoot is still present at the end of the first temperature dwell, indicating that curing reactions still occur at the end but not as fast as they do at the start of the dwell. The 44'DDS are not as exothermic as the 33'DDS formulations during B. There is still a temperature overshoot, but not as significant. TG*m*AP/44'DDS reaches a maximum temperature overshoot at approximately 105 minutes and TG*p*AP/44'DDS at approximately 125 minutes. The temperature overshoot is roughly 5 °C compared to the oven temperature, lower than the 33'DDS formulations, indicating fewer curing reactions occur in this dwell. 33'DDS showed a significant slowing of reaction rate towards the end of the dwell. The TG*m*AP/44'DDS does show a slight slowing down after reaching a maximum, whereas TG*p*AP/44'DDS reaches the maximum rate just before the end of the dwell.

As seen in A, there is thermal lag in the second temperature ramp up to 160 °C for all formulations. TG*p*AP/44'DDS shows a smaller temperature difference than the other three formulations, indicating more curing reactions taking place during the ramp. This doesn't mean that TG*p*AP/44'DDS is more reactive than the 33'DDS formulations at this point. It is important to remember that TG*p*AP/33'DDS and TG*m*AP/33'DDS initially showed a more significant temperature overshoot. Suggesting that the 33'DDS formulations are more reactive at lower temperatures, and as fewer reactions have occurred at 130 °C for TG*p*AP/44'DDS, it is unsurprising that TG*p*AP/44'DDS shows a greater temperature overshoot when the oven temperature is increased to 160 °C as the initial reactions that occurred in 33'DDS have not taken place to the same extent.

TG*p*AP/44'DDS and TG*m*AP/44'DDS show a significant temperature overshoot in the 160 °C temperature dwell, D, a maximum overshoot of roughly 12 °C at 170 minutes and 180 minutes, respectively. TG*p*AP/33'DDS and TG*m*AP/33'DDS show a maximum 3 °C temperature overshoot at 175 minutes. For all four formulations, there is a slowing down in the rate of reaction towards the end of the dwell, but there is still a higher resin temperature than oven temperature at the end of the dwell.

The final temperature ramp up to 200 °C, E, shows resin temperature again lagging behind oven temperature, although not as large a difference as seen in both A and C.

This behaviour is based on the starting hardener, 44'DDS vs 33'DDS, which results from the idea discussed in Chapter 4. NIR. 44'DDS is a less effective nucleophile due to the *para* position

of the amine groups on the phenylene ring, enabling the delocalisation of nitrogen's lone pair of electrons through the phenylene ring onto the electron-withdrawing sulphone group. The activation energy for epoxy-amine reactions to occur in 33'DDS formulations will be lower than that of the 44'DDS formulations, resulting in greater activity at lower temperatures.

The behaviour changes in the remainder of the cure. Instead of similar behaviour based on the starting hardener, the similarity is based on the starting epoxy. The TG*m*AP formulations display a greater temperature difference than the TG*p*AP formulations in the final dwell at 200 °C (section F). It is known from NIR in Chapter 4. that nearly no epoxy primary amine reactions occur at this point, only a small amount of epoxy secondary amine and etherification reactions. NIR also shows fewer reactions occur in the 44'DDS formulations than in the 33'DDS formulations, so, interestingly, the temperature difference is based on the epoxy rather than the hardener. This highlights the downside of measuring the temperature response using thermocouples. It might not represent what is happening on the macromolecular scale.

When the resin cures, the heat capacity of the material changes. As seen in Chapter 4. NIR, the network of each TGAP/DDS formulation forms differently; therefore, the point of vitrification and heat capacity of the vitrified material will be different [207]. Heat capacity is the energy required to change the temperature by one degree. Suppose the heat capacity of the TG*m*AP formulations is lower than the TG*p*AP formulations at the start of F. The same exothermic response will show a more significant temperature difference, as seen here. It is important to note that the change in heat capacity has not been measured in this study.

If only Figure 5.3 is considered, the temperature difference can be accounted for by the non-linear shape of TG*m*AP, allowing for quicker etherification reactions in the final 200 °C dwell compared to the linear shape of TG*p*AP. The difference in shape is shown in Figure 5.4. At this point in the cure, it is expected that vitrification will occur, and due to its high amount of crosslinking, the reaction will be diffusion-controlled. TG*m*AP has greater conformational freedom; therefore, the speed at which etherification can occur is greater, resulting in a more significant exothermic temperature difference than TG*p*AP.

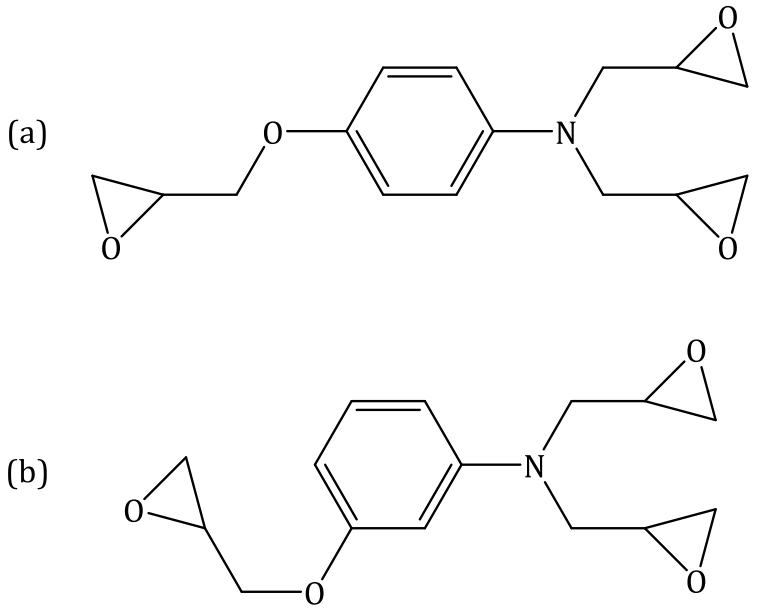

Figure 5.4 – Chemical structures of the two structural isomers of TGAP: (a) triglycidyl-*para*-aminophenol (TG*p*AP) and (b) triglycidyl-*meta*-aminophenol (TG*m*AP).

After the peak temperature difference in F, the resin temperature drops below the oven temperature, as shown by a negative temperature difference at approximately 300 minutes. These thermocouples have not been calibrated to obtain their correction factors at high temperature so to suggest that epoxy is insulating the thermocouple to obtain a negative temperature difference would be wrong. However, as the difference is constant, it suggests that no additional heat is being generated by any curing reactions, indicating that the curing process is finished.

Referring back to Figure 5.1, the standard deviation of the different formulations is high when there is a significant temperature difference. Although the sample dimensions were the same, this can be accounted for because the curing reaction does not occur the same way every time. Therefore, there is a significant difference in B for the 33'DDS formulations.

As said, the material's heat capacity has to be considered towards the end of the cure to understand the accurate thermal response of the material. Still, as stressed at the beginning, this is a straightforward technique to monitor the thermal response of an epoxy resin during cure. The most exothermic points of the reaction can visualised, and the differences between the four different TGAP/DDS formulations can be clearly identified.

5.3.2. ISOTHERMAL HEATING

Multi-step cure schedules are not the only method of curing epoxy resins. Isothermal heating (holding at a single temperature) is a common heating method to cure resins. A post-cure is often undertaken for multifunctional epoxies as it does not always result in 100 % cure, which is, in fact, a multi-step cure schedule. Either way, it is helpful to investigate what happens when epoxy resin is cured at one temperature.

Differential scanning calorimetry, as will be seen, is more suited to this type of heating as it utilises very small samples and controlled heating. Hence, the risk of a runaway reaction, often called 'exotherm', is minimal. Instead of a slight temperature overshoot, a significant temperature overshoot occurs, and the reaction runs away, resulting in thermal degradation and, in some cases, combustion. A slow heating rate is important to avoid this when using isothermal heating in the oven. Frank and Wiggins cured diglycidyl ether of bisphenol A (DGEBA) and diglycidyl ether of bisphenol F (DGEBF) with 44'DDS at a 180 °C isotherm for three hours but did not state a heating rate [37]. Whereas, Janisse and Wiggins used a 180 °C isotherm to cure DGEBF and tetraglycidyl-4,4'diaminodiphenylmethane (TGDDM) with 33'DDS but with different heating rates (1, 5, 10 and 20 °C min^{-1}) [24]. Surprisingly, they did not suggest they experienced any exotherms at the fast heating rates, perhaps because they used very small samples, but this was not stated.

For these measurements, the same procedure was used as outlined in section 0 but with two different heating procedures. The four TGAP/DDS resins were ramped from 100 °C to 130 °C at 1 °C min^{-1} and held for 12 hours and from 100 °C to 160 °C at 0.5 °C min^{-1} and held for 12 hours. Ideally, a fast heating rate is used where minimal curing would occur, but this is not possible in larger quantities (50 g). Therefore, instead of using the term 'isotherm', it will be called a dwell. Initially, the same heating rate for the 130 °C dwell (1 °C min^{-1}) was used for the 160 °C dwell to help with comparability, but this resulted in a significant temperature overshoot to 200 °C for TG*p*AP/44'DDS (see Appendix) which is thought to have induced thermal degradation as indicated by the image in Figure 5.5. A darker colour suggests that the sample has thermally degraded or at least oxidised more than when a slower heating rate of 0.5 °C min^{-1} was used.

Figure 5.5 – TG*p*AP/44'DDS cured using a 160 °C dwell where the top resin underwent a ramp at 1 °C min^{-1}, whereas the bottom resin underwent a ramp at 0.5 °C min^{-1}.

5.3.2.1. 130 °C DWELL

The resin temperature measurements for the four TGAP/DDS formulations during the 130 °C dwell are shown in Figure 5.6. The temperature overshoots are similar to the ones observed in Figure 5.1, as they are the same as the first part of the cure cycle but with a slower ramp. The 33'DDS formulations overshoot earlier and higher than the 44'DDS formulations. The measurements are an average of two tests where the shaded region is the standard deviation. There is a significant deviation in all formulations except TG*m*AP/44'DDS.

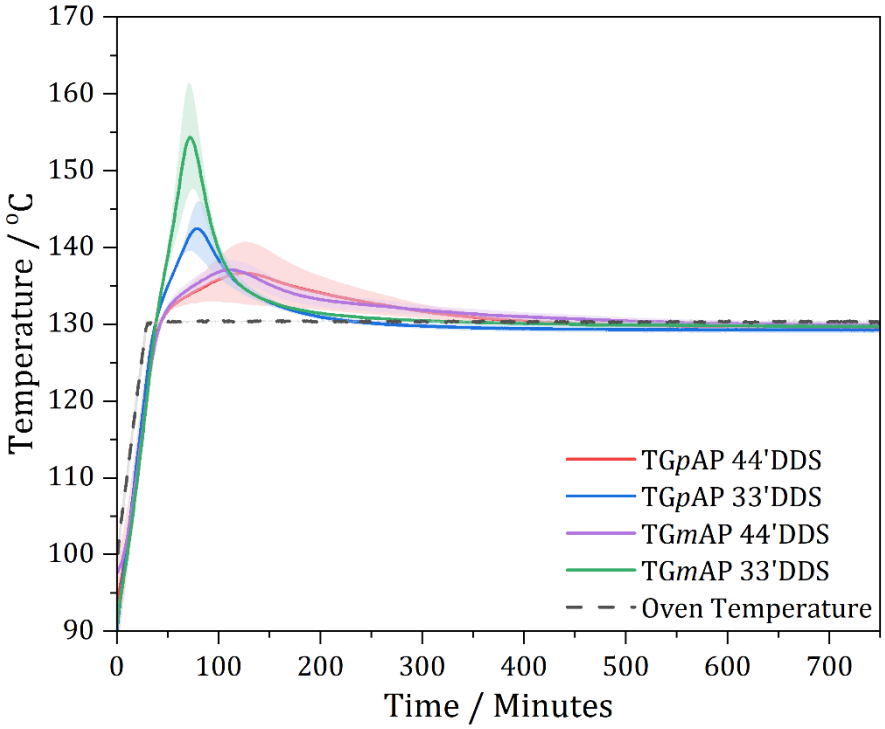

Figure 5.6 – Temperature profiles for the four structural isomers of TGAP/DDS during the 130 °C dwell as function time as measured by thermocouples for resin and oven temperatures, where the shaded region is the standard deviation. 100 mm by 100 mm by 4 mm sample dimensions.

The difference between Figure 5.6 and Figure 5.1 is that the overshoot in TG*p*AP/33'DDS is less than TG*m*AP/33'DDS when using the slower ramp. This suggests that the reactions are less exothermic in TG*p*AP/33'DDS. By considering temperature measurements alone, this is difficult to interpret. Considering the findings in Chapter 4. NIR, it was suggested that TG*p*AP undergoes more etherification at lower temperatures. It could be the case that the slow ramp allows for more competition between etherification and epoxy primary amines reactions, resulting in a lower temperature overshot, as previous literature has suggested that the etherification reaction is less exothermic than epoxy primary amine reactions [208]. Like in the standard cure cycle, TG*p*AP/44'DDS and TG*m*AP/44'DDS behave very similarly, with TG*p*AP/44'DDS reaching a maximum temperature overshoot slightly later than TG*m*AP/44'DDS.

The final observation from these measurements is the point at which the resin temperature drops below the oven temperature. These differ greatly for all formulations. TG*p*AP/33'DDS falls below oven temperature at approximately 230 minutes, TG*m*AP/33'DDS at 350 minutes, TG*p*AP/44'DDS at 450 minutes and TG*m*AP/44'DDS at 550 minutes. This indicates the point at which few reactions occur, and the material effectively insulates the thermocouple from the

oven. It wouldn't be expected that these samples are 100 % cured although the degree of cure of these samples has not been tested, but DSC has been undertaken at 130 °C and will be discussed later in this chapter.

5.3.2.2. 160 °C DWELL

The resin temperature measurements for the four TGAP/DDS formulations during the 160 °C dwell are shown in Figure 5.7. The results observed here are very different from those in Figure 5.1 as there is no dwell at 130 °C in these measurements. They once again pair up based on the hardener used. The 33'DDS formulations show a double peak, whereas the 44'DDS formulations show a single peak, which overshoots more significantly than the 33'DDS formulations.

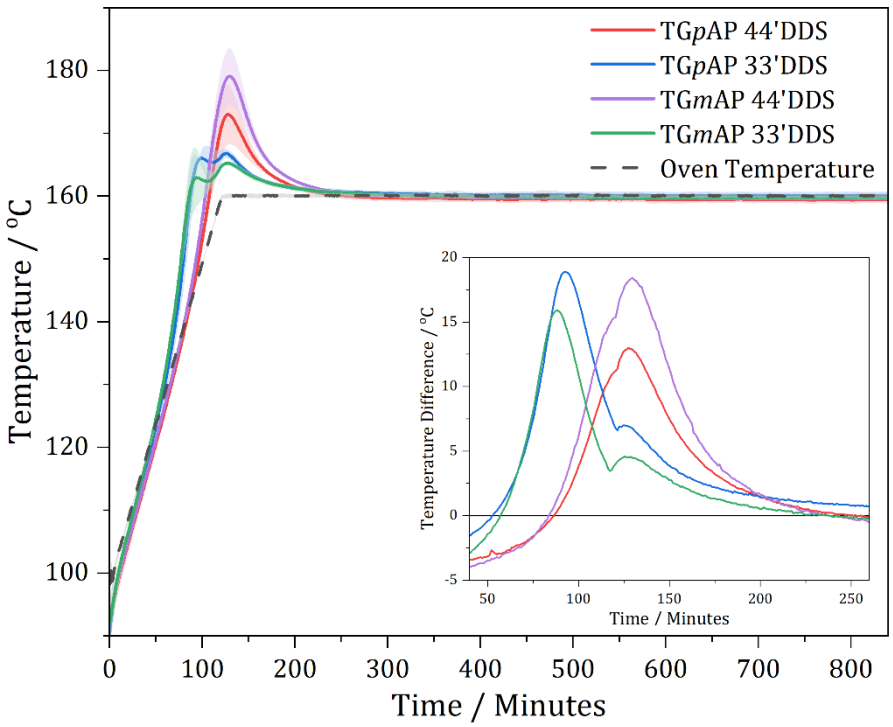

Figure 5.7 – Temperature profiles for the four structural isomers of TGAP/DDS during the 160 °C dwell as a function of time as measured by thermocouples for resin and oven temperatures, where the shaded region is the standard deviation. The inset graph shows the difference between the resin and oven temperature between 40 and 260 minutes. 100 mm by 100 mm by 4 mm sample dimensions.

In Figure 5.6, the temperature overshoot began once the dwell temperature had been reached, indicating that significant curing reactions only occurred after the ramp. In contrast, in Figure

5.7, the temperature overshoot occurred during the ramp for all formulations, indicating that curing reactions occurred during the ramp. This can be considered the cure onset temperature, a critical point often discussed in DSC dynamic scans. For 33'DDS, the cure onset temperature is approximately 125 °C and for 44'DDS, approximately 140 °C. As the cure onset for 33'DDS is lower than 130 °C, it would be expected that a temperature overshoot would be seen in the 130 °C dwell. This is not the case, as the heating rates are different. The ramp-up to 160 °C is half that of 130 °C; therefore, the onset will occur earlier due to reduced thermal gradients within the sample [209].

The 33'DDS formulations show a double peak. This suggests that it is a combination of the peaks seen in the 130 and 160 °C dwell in the standard cure schedule shown in Figure 5.1. The 44'DDS formulations show only one peak. The same superposition of the two temperature overshoots occurs in the 44'DDS formulations. Still, as the temperature overshoot in the 130 °C dwell is small and delayed, it can be predicted that when no low-temperature dwell occurs, a significant overshoot will be observed at higher temperatures, possibly around the point at which the temperature overshoots in the ramp (140 °C). The reasoning behind this is the lower reactivity of 44'DDS compared to 33'DDS.

In the 33'DDS peak, the TG*p*AP resin peaks higher than TG*m*AP. This was not seen in the standard cure schedule and 130 °C measurements. It is unclear why this occurs, but it could be related to the higher temperature the heating regime goes to. A greater proportion of reactions can occur at this temperature for TG*p*AP/33'DDS compared to TG*m*AP/33'DDS. However, in the 44'DDS peak, TG*m*AP shows a higher temperature overshoot than TG*p*AP. In the previous heating regimes, the two formulations have achieved similar overshoots. The reasoning behind this can be thought to be similar to one for TG*p*AP/33'DDS compared to TG*m*AP/33'DDS.

Unlike the 130 °C dwell, the point at which the resin temperature drops below the oven temperature is not as clear and occurs at similar points for TG*p*AP/44'DDS, TG*m*AP/33'DDS and TGmAP/44'DDS. This is related to the dwell being at a higher temperature, 160 °C. More curing reactions occur in a shorter period, and the three formulations vitrify and insulate the resin thermocouple at similar times. The resin temperature of TG*p*AP/33'DDS does not drop below the oven temperature for the entirety of the cure, suggesting it is not as cured as the other three formulations.

5.3.3. DYNAMIC HEATING

The final heating regime is a dynamic cure. This applies a constant heating rate of 0.25 °C min^{-1} between 100 °C and 200 °C. The heating rate is slow enough that temperature overshoots should be seen during the heating ramp rather than when the heating ramp finishes. The temperature measurements for the dynamic heating regime of 0.25 °C min^{-1} for the four formulations of TGAP/DDS are shown in Figure 5.8. No temperature overshoot occurs once the dynamic heating stage has finished, indicating that most of the cure has occurred during the temperature ramp.

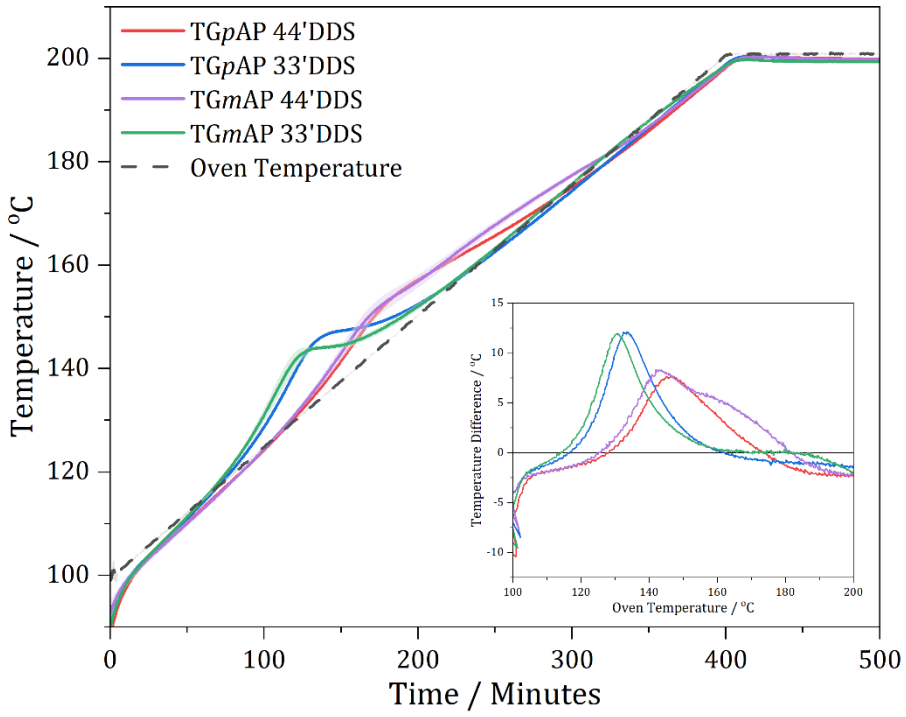

Figure 5.8 – Temperature profiles for the four structural isomers of TGAP/DDS during the 0.25 °C min^{-1} dynamic heat as a function of time measured by thermocouples for resin and oven temperatures, where the shaded region is the standard deviation. The temperature difference between resin and oven temperature is shown on the inset graph as a function of oven temperature. 100 mm by 100 mm by 4 mm sample dimensions.

In previous heating regimes, resin temperature often lags behind oven temperature during the heating ramp, but this is not the case here. When significant curing reactions occur, the resin temperature is higher than the oven temperature. The resin temperature overshoot is shown as a function of oven temperature on the inset graph of Figure 5.8, similar to dynamic DSC

measurements shown in 5.4. The recurring theme of 33'DDS formulations overshooting earlier than 44'DDS occurs. A significant temperature overshoot occurs at approximately 130 °C for the 33'DDS and approximately 145 °C for the 44'DDS formulations. The TG*p*AP formulations peak around 5 °C after the TG*m*AP formulations.

From the standard cure schedule measurements in Figure 5.1, three different temperature overshoots are seen at each dwell. This is not the case. Each formulation shows one distinct peak. This suggests that there is one point where the reaction is most exothermic and where many curing reactions occur. Despite a lack of overshoot at higher temperatures, reactions do occur here; they are just not significant enough to show an overshoot. If larger quantities were used, this may result in a runaway reaction, the same with isothermal heating. Multi-dwell cure cycles help prevent this by allowing the reactions to occur in steps rather than all at once.

Limited information can be gained from this measurement as the phenomena are not sensitive enough. Curing reactions could occur at higher temperatures, but this cannot be seen using thermocouples. A more sensitive technique is needed to measure the thermal response of the epoxy resin cure. This is where DSC comes in.

5.4. DIFFERENTIAL SCANNING CALORIMETRY

As evidenced in section 5.3, the curing reactions of TGAP/DDS are exothermic. Points at which curing reactions occur can be identified by exothermic behaviour. Using thermocouples to measure the resin temperature compared to oven temperature has provided initial insight into how the different TGAP/DDS formulations behave. Still, it has only been helpful when there is a significant overshoot. Differential scanning calorimetry can measure very small samples and measure the thermal behaviour of the epoxy amine cure. This section will discuss similar measurements to section 5.3 but in reverse. Dynamic measurements will be discussed first, followed by isothermal measurements and finally, the overall cure schedule.

5.4.1. DYNAMIC DSC MEASUREMENTS

The cure of the four formulations of TGAP/DDS has been investigated using dynamic heating between 30 °C and 300 °C at five different heating rates (2.5, 5, 10, 15 and 20 °C min^{-1}). The heat flow plots are shown in Figure 5.9. No significant thermal activity was observed between 30 °C

and 100 °C. Therefore, the plots are shown between 100 °C and 300 °C. In each formulation and for every heating rate, an exothermic peak is seen.

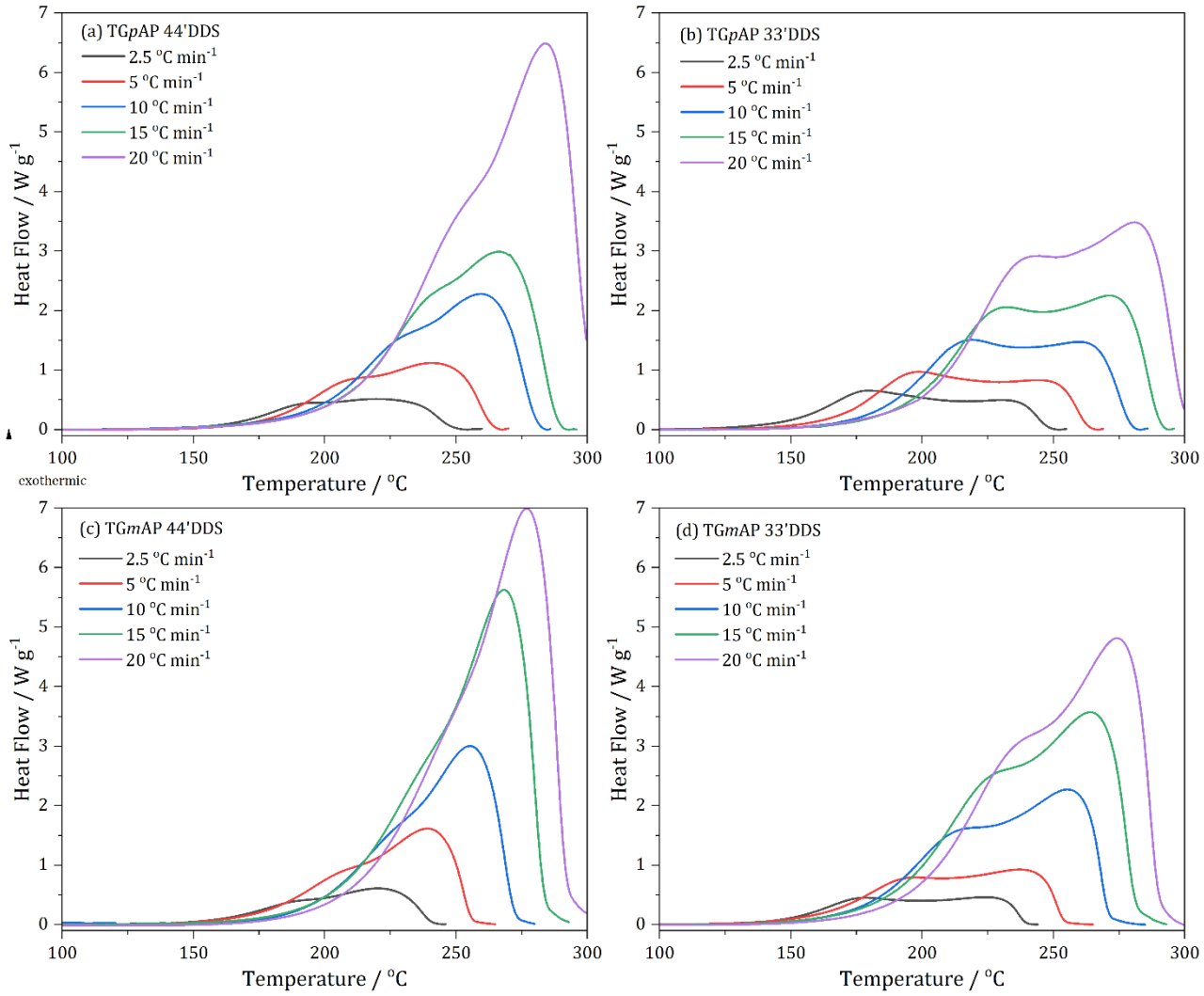

Figure 5.9 – DSC heat flow plots for the four structural isomers of TGAP/DDS under dynamic heating conditions (2.5, 5, 10, 15 and 20 °C min^{-1}): (a) TG*p*AP/44'DDS, (b) TG*p*AP/33'DDS, (c) TG*m*AP/44'DDS and (d) TG*m*AP/33'DDS. Exothermic is up.

The exothermic peak can be likened to the temperature overshoot seen in 5.3. Still, instead of comparing temperatures, DSC compares the energy required to heat the sample to a specific temperature compared to the energy required to heat the reference pan to a specific temperature. If less energy is required to heat the sample to a specific temperature, then an exothermic process occurs, and vice versa for an endothermic process.

When dynamically heating TGAP/DDS and comparing the resin and oven temperatures in Figure 5.8, only one peak was shown in the temperature overshoot. When using the DSC to measure the response, Figure 5.9 shows a double peak for nearly all formulations and heating rates. This is something that hasn't been explicitly commented on before. The double peak formation was seen in Ramsdale-Capper and Foreman's study on the four structural isomer formulations of TGAP/DDS when undertaking DSC at 10 °C min^{-1} but was not extensively commented on [32]. Varley *et al.* also investigated TG*p*AP/44'DDS under dynamic heating, but no comment was made on the shape of the heat flow plot, suggesting this double peak occurrence was not seen [102]. Padama *et al*. undertook dynamic measurements using DSC on TG*p*AP with three different hardeners: 44'DDS, pyridenediamine (PDA) and toluenediamine (TDA) [210]. They found that at different heating rates (10, 15 and 20 °C min^{-1}), TG*p*AP/44'DDS and TG*p*AP/PDA produced a single exothermal peak, whereas TG*p*AP/TDA produced two exothermal peaks. Although the single exothermal peaks were true single Gaussian peaks, there was a broad initial shoulder. Padma *et al.* accounted the two peaks to the greater reactivity of TDA compared to 44'DDS and PDA [210]. TDA had a lower cure onset temperature where the primary amines reacted initially, the first peak, and due to this, the reactivity of the secondary amine is much reduced, and therefore, a second exothermic peak is seen at higher temperature.

Figure 5.9 shows that none of the formulations are true single exothermic peaks. In the slower heating rates, a double peak is more evident than in the faster heating rates. This can be related to thermal lag. There is less thermal lag in the slower heating rates, allowing for greater separation between the different exothermic events in the faster heating rates. These different exothermic events are difficult to assign to specific reactions as DSC does not tell you what those reactions are. Knowledge of the reactivities of the starting reagents must be used to make a suitable assignment. It is sensible to analyse the heat flow plots and assign the following critical features: reaction kick-off (T_i), cure onset (T_o), peak temperature (T_{p_n}), cure end (T_f), cure range (ΔT_{cure}) and total enthalpy of cure (ΔH) as done so in previous studies such as Padma *et al.* and Varma and Bhama [36,210]. Table 5.1 shows these values.

Table 5.1 – Cure critical points of dynamic DSC measurements of the four structural isomers of TGAP/DDS at different heating rates (2.5, 5, 10, 15 and 20 °C min^{-1}). Where *p*/44' is TG*p*AP/44'DDS, *p*/33' is TG*p*AP/33'DDS, *m*/44' is TG*m*AP/44'DDS, *m*/33' is TG*m*AP/33'DDS, T_i is reaction kick-off temperature, T_o is the cure onset temperature, T_{p_1} is the first peak temperature, T_{p_2} is the second peak temperature, T_f is the cure end, ΔT_{cure} is the cure temperature range, and ΔH is the total enthalpy of cure. Italicised values note that DSC stopped before a plateau was reached. Underlined peak temperatures note that this peak was the maximum heat flow value.

	Heating Rate / °C min^{-1}	T_i / °C	T_o / °C	T_{p_1} / °C	T_{p_2} / °C	T_f / °C	ΔT_{cure} / °C	ΔH / J g^{-1}
p/44'	2.5	112	161	197	<u>220</u>	254	144	791
p/33'		85	146	<u>179</u>	230	252	167	1157
m/44'		96	157	193	<u>220</u>	251	155	784
m/33'		87	145	178	<u>223</u>	248	161	825
p/44'	5	122	174	212	<u>240</u>	267	145	799
p/33'		105	163	<u>199</u>	245	267	162	872
m/44'		109	171	210	<u>239</u>	267	158	947
m/33'		97	158	197	<u>237</u>	248	169	791
p/44'	10	113	192	232	<u>260</u>	284	171	772
p/33'		122	180	<u>219</u>	260	283	161	702
m/44'		129	192	227	<u>255</u>	281	152	807
m/33'		111	175	218	<u>255</u>	285	174	852
p/44'	15	124	203	243	<u>266</u>	293	169	678
p/33'		129	190	232	<u>271</u>	294	165	668
m/44'		130	202	244	<u>268</u>	298	168	989
m/33'		117	186	230	<u>264</u>	293	176	887
p/44'	20	139	211	252	<u>284</u>	*300*	161	993
p/33'		137	198	244	<u>281</u>	*300*	163	748
m/44'		150	211	253	<u>277</u>	*300*	150	911
m/33'		130	194	239	<u>275</u>	*300*	170	836

Generally, the faster the heating rate, the higher the temperatures at which the critical points occur. One important distinction to make is the difference between T_i and T_o. T_i is the temperature at which exothermic reactions begin, whereas T_o is the temperature at which

significant curing reactions begin. The two differences are shown in Figure 5.10 for TG*p*AP/44'DDS heated at 2.5 °C min^{-1}. The difference is 48 °C, which is quite large, but before 160 °C, the exotherm is insignificant and only accounts for a small amount of curing reactions. A similar technique was employed by Padma *et al.* and Xia *et al.* [210,211]. The reactions that occur between T_i and T_o are difficult to assign whereas at T_o, this can be thought of as the point at which epoxy primary amine reactions begin. Using T_i from Table 5.1 makes for a complex analysis as there are points at which the reactivities of the epoxy and hardener make sense. 33'DDS begin reactions at a lower temperature 44'DDS, but this isn't the case for all formulations and heating rates. However, if T_o is used, the behaviour is explicit. The reason behind this unclear behaviour when using T_i values could be related to the preparation method before undertaking DSC measurements. There is significant time between mixing the starting reagents at elevated temperatures and starting the measurements in the DSC. Initial reactions will have taken place in mixing and sample transfer, as shown in Chapter 4. NIR which may affect the T_i. Therefore, it is better practice to use T_o values.

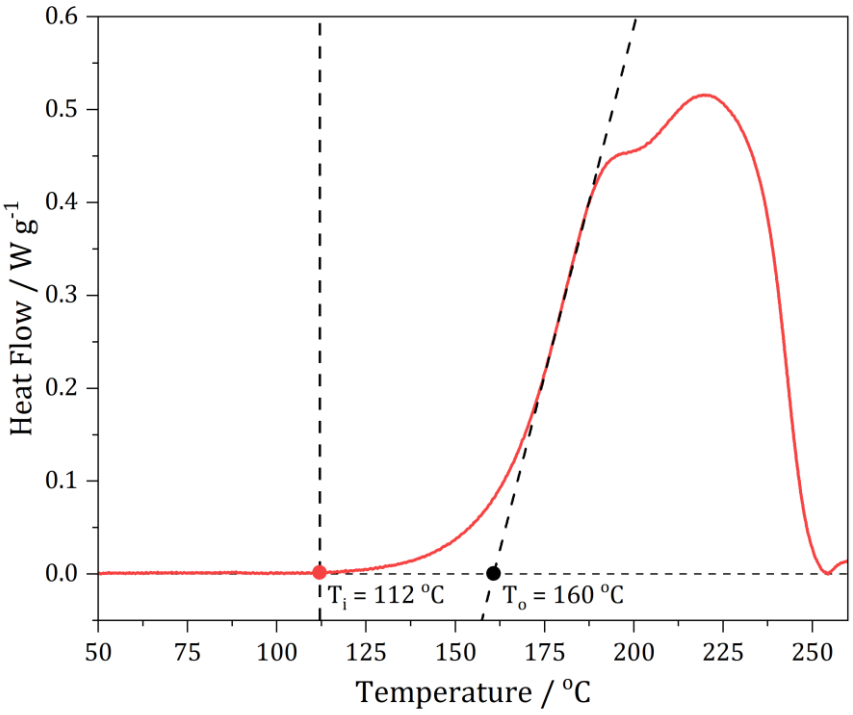

Figure 5.10 – Reaction kick-off temperature (T_i) vs cure onset temperature (T_o) for DSC heat flow plot of TG*p*AP/44'DDS under dynamic heating at 2.5 °C min^{-1}.

Considering the T_o values in Table 5.1, there is a clear trend in reactivity. The onset of reaction occurs at lower temperatures for the 33'DDS formulations compared to the 44'DDS formulations. Considering all formulations, the following trend in onset temperatures is seen:

TG*p*AP/44'DDS > TG*m*AP/44'DDS >> TG*p*AP/33'DDS > TG*m*AP/33'DDS

The difference between TG*p*AP/44'DDS and TG*m*AP/44'DDS is very small in 2.5, 5 and 15 °C min^{-1} heating rates, and the 10 and 20 °C min^{-1} heating rates, the onset temperature is the same to the nearest °C. However, in the 33'DDS formulations, TG*m*AP/33'DDS has a lower onset temperature than TG*p*AP/33'DDS. There is a 5 °C difference for 2.5 and 5 °C min^{-1} and a 2 °C difference for 10, 15 and 20 °C min^{-1}. This would suggest that TG*m*AP is more reactive than TG*p*AP despite some onset temperatures being the same in the 44'DDS formulations. The reactivity is increased, but it is not related to the chemistry of the epoxide ring. It is related to the position of it. TG*m*AP is non-linear compared to the TG*p*AP, and configurational entropy is greater; thus, the chance of collisions with primary amines is greater. Therefore, the onset temperature of the TG*m*AP formulations is often lower than the respective TG*p*AP formulations.

The T_o values define the point at which substantial curing reactions begin but not which reaction. The three common reactions that occur during an epoxy amine cure are epoxy-primary amine, epoxy-secondary amine and etherification (epoxy-hydroxyl). On its own, DSC cannot distinguish between these. In the case of dynamic heating, it is more of a challenge to assign the reactions as the temperature is constantly increasing. A constant increase in heat increases the energy provided to the system; therefore, the traditional progression of reactions seen in a multi-dwell cure schedule used in section 5.3.1 does not necessarily occur. Instead, reactions compete. Primary amines may not all be consumed before the minimum energy required for epoxy-secondary amine or etherification is reached. Therefore, the reactions compete and, in some formulations, may occur at similar times. In summary, if temperature increases, reactive groups will react with any reactant in proximity rather than the type of reaction. This behaviour increases as the heating rate increases.

Figure 5.11 shows the different exotherms of the four structural isomers of TGAP/DDS obtained using 2.5 °C min^{-1} dynamic DSC measurements. TG*p*AP/33'DDS and TG*m*AP/33'DDS have two clear maxima, whereas TG*m*AP/44'DDS and somewhat TG*p*AP/44'DDS have one clear maximum and a shoulder. If these exotherms were deconvoluted, they would not result in two

peaks. There would be multiple peaks, of which none would be assignable. Shiravand *et al.* deconvoluted the dynamic heat flow scan into three assigned peaks, and the resultant superposition plot was not an exact fit [133]. Treating them as two peaks is more suitable, as Wu *et al*. did in their dynamic DSC study on TGDDM cured with dicyanodiamide [134]. However, they attributed the two different peaks to the reaction being a two-step cure – one reaction has to occur before the second reaction can. This is not the case in TGAP/DDS, as discussed in Chapter 4. NIR, the different curing reactions compete. The fact that the 33'DDS formulations reach a maximum and heat flow decreases and then increases to another maximum is interesting. This could indicate autocatalysis in the system – products from one reaction allow another reaction to occur more quickly.

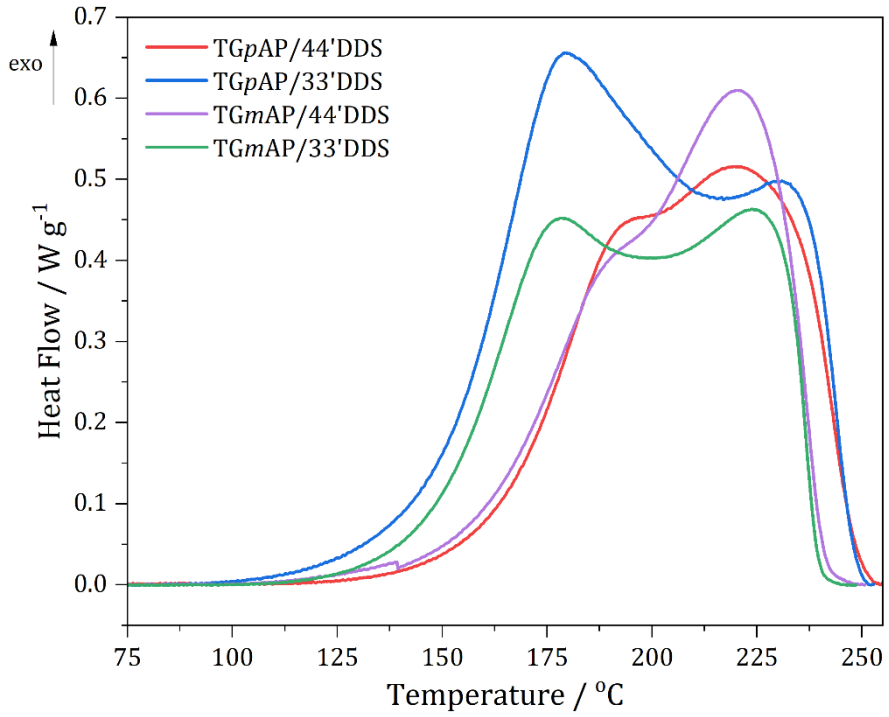

Figure 5.11 - DSC heat flow plots for the four structural isomers of TGAP/DDS under dynamic heating 2.5 °C min^{-1}. Exothermic is up.

In Figure 5.11, the 33'DDS formulations curing reactions occur in two distinct phases. Due to the increased reactivity of 33'DDS compared to 44'DDS, curing reactions can begin at lower temperatures and as a mix of primary and secondary amine reactions. Two clear peaks may occur because of this increased reactivity. TG*m*AP/33'DDS is a good example, as it has two

nearly equal height peaks. The first peak accounts for a combination of all reactions, with the majority most likely being epoxy-primary amine and epoxy-secondary amine reactions. The general rate of reaction slows, but as temperature increases, effective free volume space increases, and the mobility of reactants and concentration of potential catalysts increases; therefore, the rate of reaction then increases. A second peak is reached, and the reactions accounting for this exotherm are once again a combination, with the majority most likely being epoxy-secondary amine and etherification. TG*p*AP/33'DDS looks slightly different with a greater initial maximum; this can be accounted for by the tertiary amine catalyst behaviour seen in Chapter 4. NIR, where TG*p*AP can promote etherification reactions at lower temperatures than TG*m*AP, causing the lower temperature peak to be more significant. The 44'DDS formulations show a shoulder, which is the initial epoxy-primary amine reaction. Still, due to the lower reactivity of 44'DDS, this exotherm overlaps with the prominent peak, a combination of all curing reactions.

Not all heating rates will be discussed as they follow similar trends. Figure 5.12 shows the different exotherms of the four structural isomers of TGAP/DDS obtained using 20 °C min^{-1} dynamic DSC measurements.

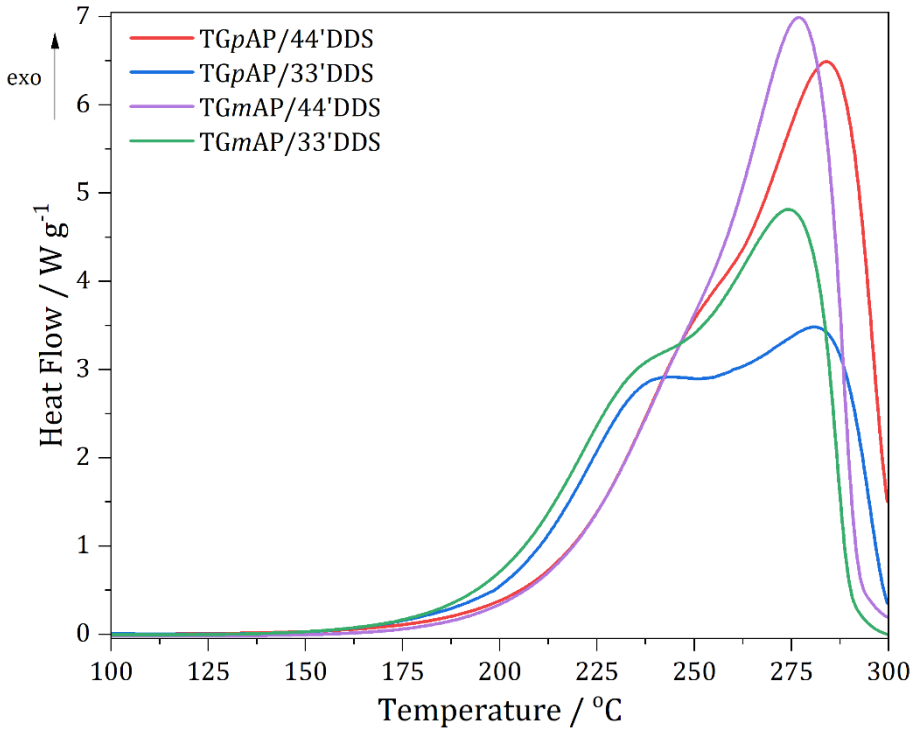

Figure 5.12 – DSC heat flow plots for the four structural isomers of TGAP/DDS under dynamic heating 20 °C min^{-1}. Exothermic is up.

Rather than two clear maxima in the 33'DDS formulations, the higher temperature peak dominates. The heating rate is so fast that there is little time for reactions to occur in two stages, like in the 2.5 °C min^{-1} measurements. The 44'DDS exotherms appear more single peak-like with only a small discernible shoulder.

These heat flow plots indicate that the four structural isomers of TGAP/DDS cure under dynamic heating through different mechanisms. By using equation (5-1), the enthalpy of reaction as a function of temperature, $\Delta H(T)$, can be calculated.

$$\Delta H(T) = \frac{1}{\beta}\int_0^T \frac{dq}{dt}dT \qquad (5\text{-}1)$$

Where β is heating rate, and $\frac{dq}{dt}$ is heat flow. By integrating the heat flow plot to the point where the rate of change in heat flow is zero, the total enthalpy of cure, ΔH_0, can be calculated. These values are shown in Table 5.2 and are an average of the values obtained for the five different heating rates. The total enthalpy of cure values should be the same irrespective of the mechanism, as the same number of reactive groups are present. It is important to note that each dynamic scan cured each formulation completely, as validated by the fact that no exotherm was observed during the repeated heating procedure.

Table 5.2 – Average total enthalpy of cure (ΔH_0) values for the four structural isomers of TGAP/DDS obtained from dynamic DSC measurements using five different heating rates (2.5, 5, 10, 15, and 20 °C min^{-1}).

	TG*p*AP/44'DDS	TG*p*AP/33'DDS	TG*m*AP/44'DDS	TG*m*AP/33'DDS
ΔH_0 / J g^{-1}	806.8	829.7	887.7	838.4
ΔH_0 / kJ mol^{-1}	109.7	112.8	120.7	114.0

The value obtained for TG*p*AP/44'DDS agrees very well with the literature. Varley *et al.* reported a value of 110.5 kJ mol^{-1} for TG*p*AP/44'DDS [102]. It is worth noting that these values agreed despite different epoxy:amine ratios used, indicating that the same epoxide ring-opening reactions occur between different ratios. TG*p*AP/33'DDS and TG*m*AP/33'DDS have similar values and lie close to literature values, whereas TG*m*AP/44'DDS is slightly higher. This

shouldn't be the case, as the value refers to the energy release of an epoxy ring opening reaction. The higher value doesn't indicate a different mechanism or a more reactive type of reaction but rather an error with the technique.

To prepare the sample for testing in the DSC, the epoxy and amine hardener must be mixed at elevated temperatures. During this stage, reactions take place. In the case of TG*m*AP/44'DDS, fewer reactions occur in the mixing stage, as shown in Chapter 4. NIR. This results in more reactants remaining in the DSC sample that haven't reacted, resulting in a greater exothermic response when tested. It cannot be corrected, but it is worth considering when querying the higher value for TG*m*AP/44'DDS.

Knowing the total enthalpy of cure allows for calculating the degree of cure shown in equation (5-2).

$$\alpha(T) = \frac{\Delta H(T)}{\Delta H_0} \tag{5-2}$$

The degree of cure as a function of temperature for the four structural isomers of TGAP/DDS is shown in Figure 5.13. As the heating rate increases, the degree of cure curve is shifted to a higher temperature. Small variations in the degree of cure between the different formulations are observed and are difficult to comment on in this format.

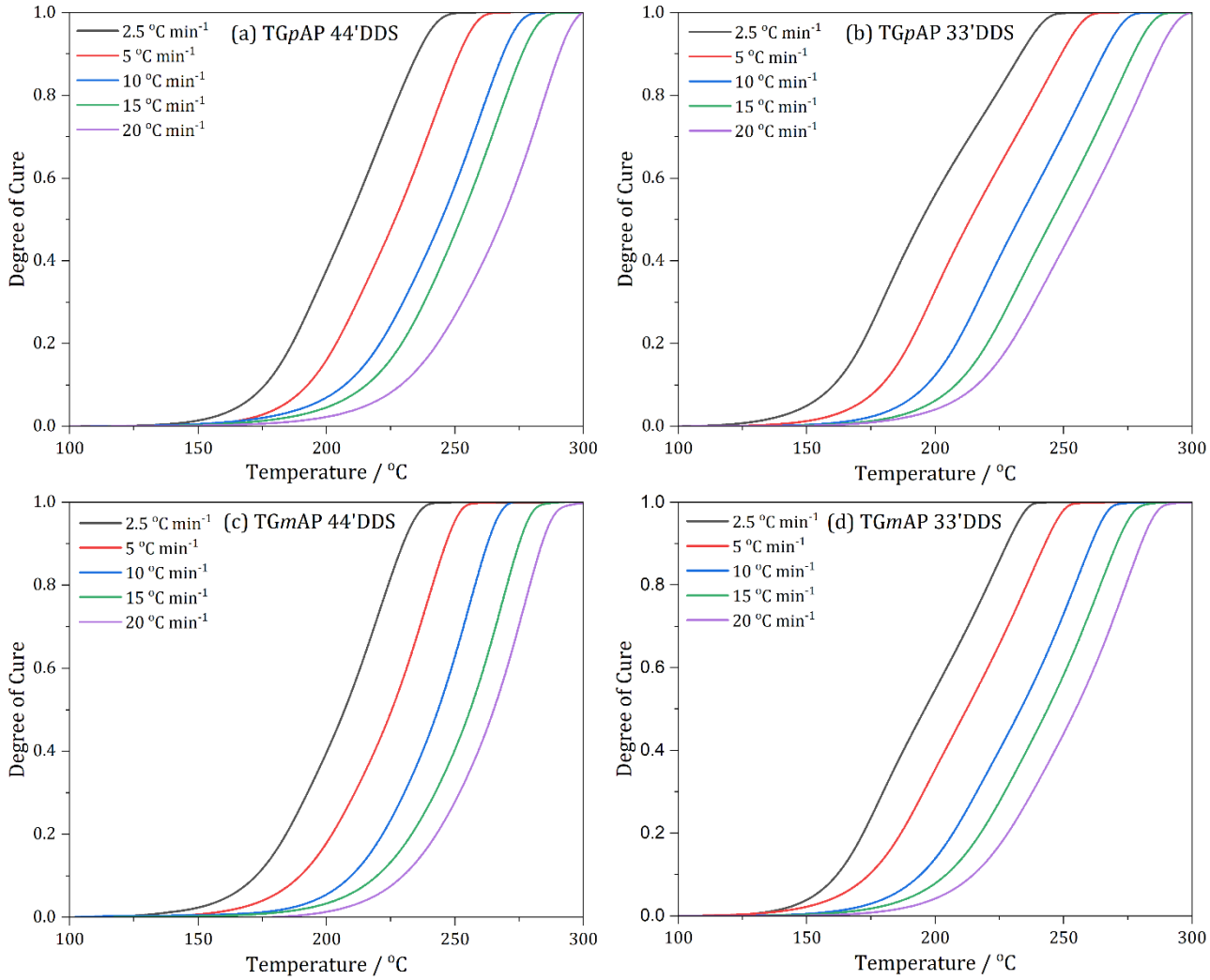

Figure 5.13 – Degree of cure as a function of temperature plots for the four structural isomers of TGAP/DDS under dynamic heating conditions (2.5, 5, 10, 15 and 20 °C min^{-1}): (a) TG*p*AP/44'DDS, (b) TG*p*AP/33'DDS, (c) TG*m*AP/44'DDS and (d) TG*m*AP/33'DDS.

All formulations achieve 100 % cure during the heating regime. Slower heating rates achieve complete cure earlier than faster heating rates. The gradient of each curve is similar. Small differences are seen between the formulations, as shown in Figure 5.14, when comparing the four structural isomers of TGAP/DDS under dynamic heating at 20 °C min^{-1}. Initially, the formulations display similar behaviour according to the hardener, but towards the end of the cure, the formulations pair based on epoxy.

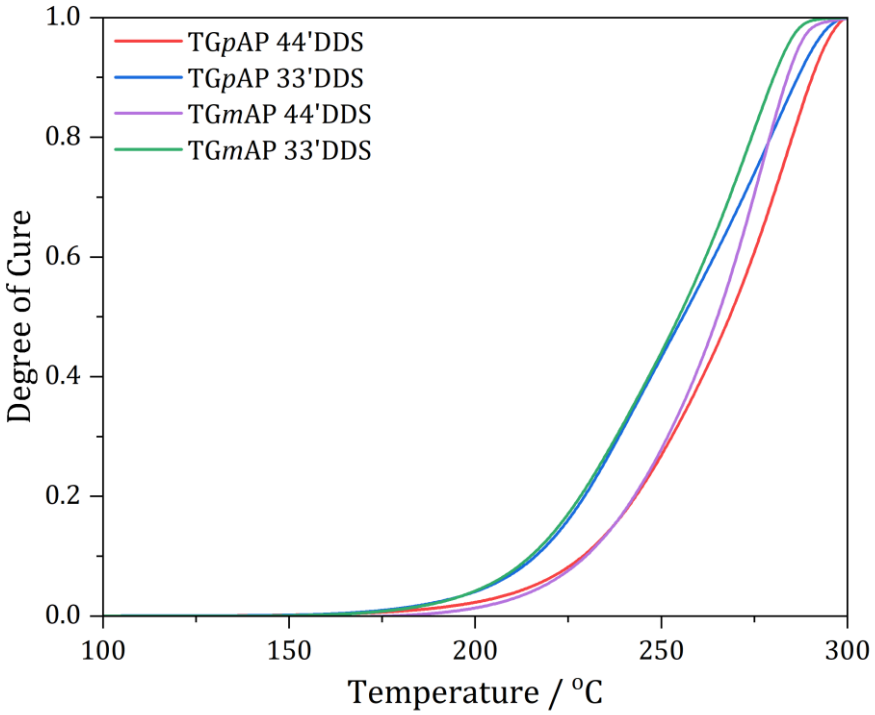

Figure 5.14 – Degree of cure as a function of temperature plots for the four structural isomers of TGAP/DDS under dynamic heating at 20 °C min^{-1}.

The curves can be differentiated to obtain the rate of reaction, which shows, in this case, the change in degree of cure as temperature changes. Where the value is highest is where the rate of reaction is fastest. In the case of dynamic heating, rate of reaction is better interpreted in terms of temperature, not time. Different heating rates cure over different time periods, which results in difficult interpretation if the traditional rate of reaction in terms of time as a function of degree of cure is used. These results are shown in Figure 5.15. Unsurprisingly, these look very similar to the heat flow curves shown in Figure 5.9 and would look the same if the x-axis was temperature rather than the degree of cure.

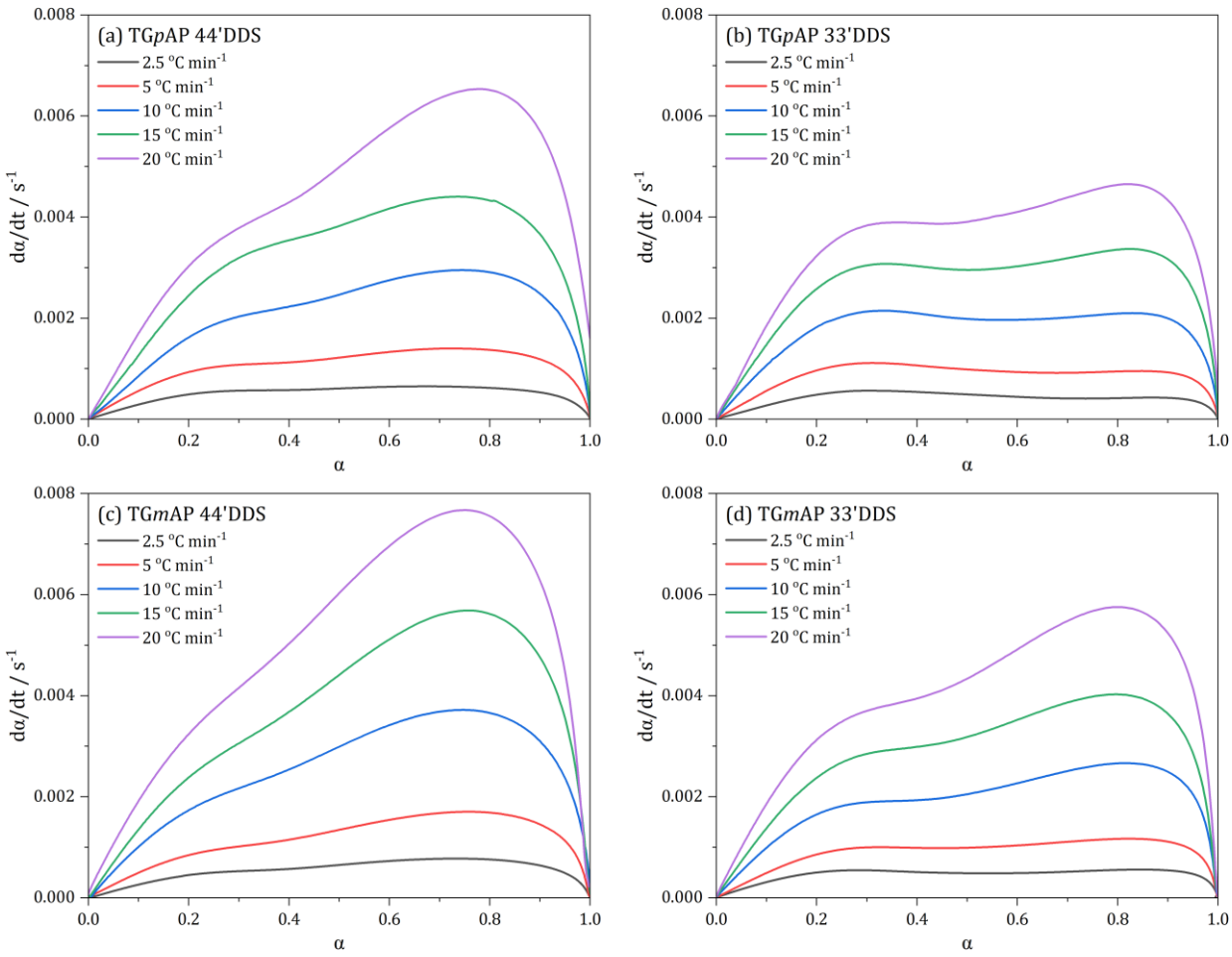

Figure 5.15 – Rate of reaction with respect to time as a function of degree of cure for the four structural isomers of TGAP/DDS under dynamic heating conditions (2.5, 5, 10, 15 and 20 °C min^{-1}): (a) TG*p*AP/44'DDS, (b) TG*p*AP/33'DDS, (c) TG*m*AP/44'DDS and (d) TG*m*AP/33'DDS.

Instead, displaying the rate of reaction with respect to temperature as a function of degree of cure is a better way to show this data as it effectively normalises the data, and a more straightforward comparison of the differences in mechanism can be seen at different heating rates. This is shown in Figure 5.16 for the four structural isomers of TGAP/DDS. The switching of the dominant peaks in TG*p*AP/33'DDS and TG*m*AP/33'DDS and the lack of switching in TG*p*AP/44'DDS and TG*m*AP/44'DDS as heating rate changes are more apparent in this form than in the heat flow plots in Figure 5.9. This indicates that in the 33'DDS formulations, the heating rate impacts the curing mechanism. However, in 44'DDS, there is less of an effect. This is most likely related to the reactivity of the hardener, as discussed earlier.

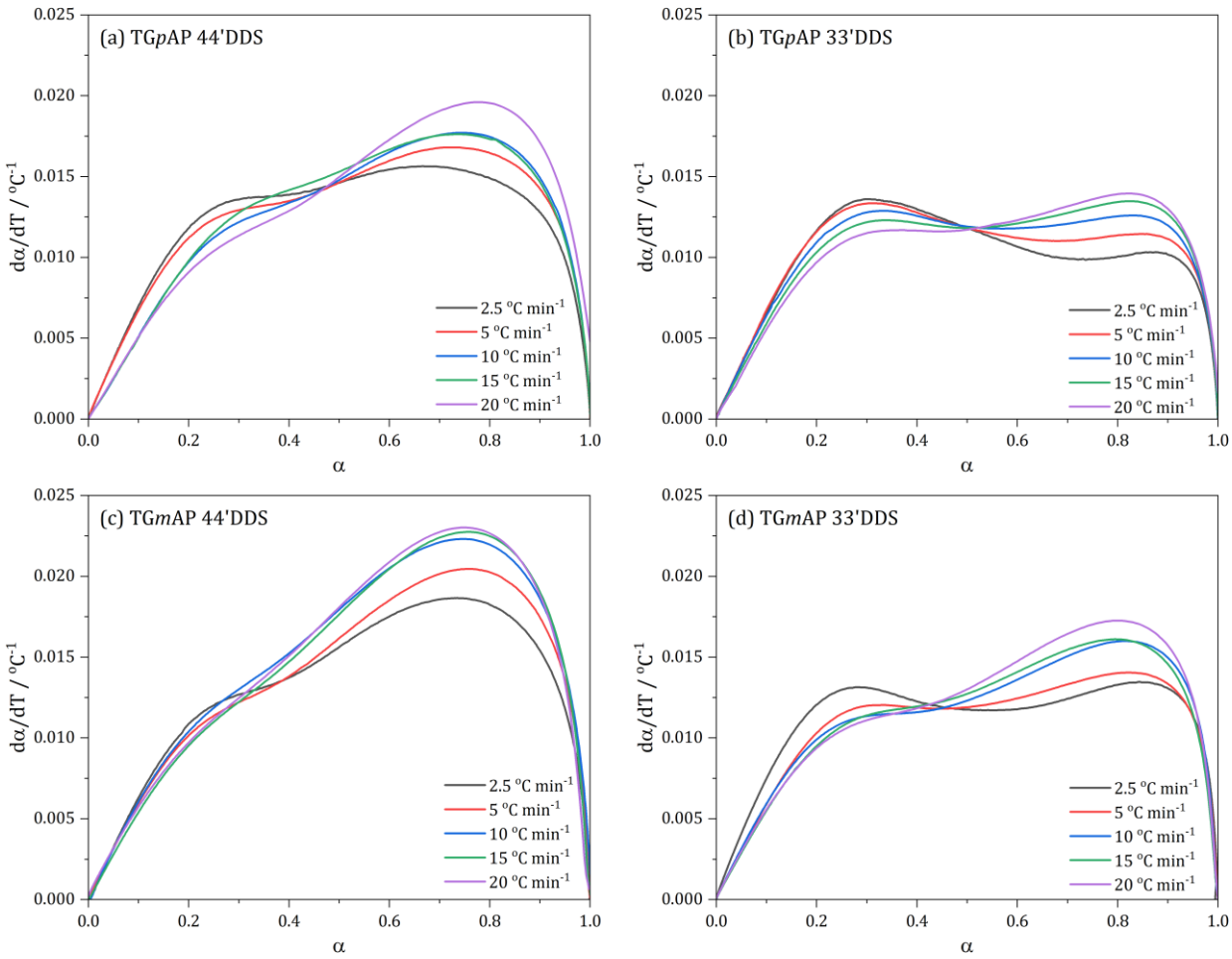

Figure 5.16 – Rate of reaction with respect to temperature as a function of degree of cure for the four structural isomers of TGAP/DDS under dynamic heating conditions (2.5, 5, 10, 15 and 20 °C min^{-1}): (a) TG*p*AP/44'DDS, (b) TG*p*AP/33'DDS, (c) TG*m*AP/44'DDS and (d) TG*m*AP/33'DDS.

The data presented in the above figures can be used to determine the activation energy of the reactions taking place during the cure. The activation energy is the minimum energy required for a reaction to take place. Multiple methods have been determined to do this. The methods are based on the Arrhenius equation, which relates the rate constant, $k(T)$, to activation energy, E_a. In the simplest of forms, the rate constant can be related to the rate of reaction by equation (5-3).

$$\frac{\mathrm{d}\alpha}{\mathrm{dt}} = k(T)f(\alpha) \qquad (5\text{-}3)$$

Where $\frac{\mathrm{d}\alpha}{\mathrm{dt}}$ is rate of reaction, $k(T)$ is the rate constant, and $f(\alpha)$ is a function of fractional conversion. The Arrhenius relationship of the rate constant as a function of temperature is given in equation (5-4).

$$k(T) = A \exp\left(-\frac{E_a}{RT}\right) \tag{5-4}$$

Where A is the pre-exponential factor, which is also known as the frequency factor and considers the number of collisions and orientation of the reactants, E_a is activation energy, R is the molar gas constant, and T is temperature. Combining equations (5-3) and (5-4) gives equation (5-5).

$$\frac{d\alpha}{dt} = A\, f(\alpha) \exp\left(-\frac{E_a}{RT}\right) \tag{5-5}$$

This equation is the basis of the methods that will be used here. These methods are known as model-free methods, where the kinetic behaviour is analysed without the need for exact values of $f(\alpha)$ and A. As a result, each method makes assumptions that may well introduce inaccuracies in the values obtained. It is, therefore, essential to understand the assumptions and how this affects the values obtained.

The first method widely used to calculate activation energy is the Kissinger method [212]. It utilises the relationship between the exothermic peak temperature and heating rate to obtain activation energy. It assumes that the exothermic peak occurs at a fixed stage in the reaction [213]. Single exothermic peak temperatures are commonly observed; this was not the case in TGAP/DDS. A study by Wu *et al.* observed two peaks and applied the Kissinger method to each peak separately [134]. The Kissinger method is shown in equation (5-6). It is derived by differentiating equation (5-5) by parts and under the assumption that the reaction is first order to obtain equation (5-6) [214]. The fact that there are two clear peaks in most of the dynamic measurements suggests that the curing reaction of TGAP/DDS is not first order. Still, Vyazovkin suggested this doesn't give rise to significant error when using linear heating rates [215]. Despite not being a first-order reaction, it is still a worthwhile technique to indicate the

difference in values between the four different formulations, whether they be an exact value of activation energy or not.

$$\ln\left(\frac{\beta}{{T_p}^2}\right) = \ln\left(\frac{AR}{E_a}\right) - \frac{E_a}{RT_p} \qquad (5\text{-}6)$$

Where T_p is the exothermic peak temperature. Activation energy, E_a is determined by plotting $\ln\left(\frac{\beta}{{T_p}^2}\right)$ against $\frac{1}{T_p}$ and multiplying the gradient, $-\frac{E_a}{R}$, by $-R$ (8.314 J K^{-1} mol^{-1}). An example of the plot obtained for TG*m*AP/33'DDS is shown in Figure 5.17.

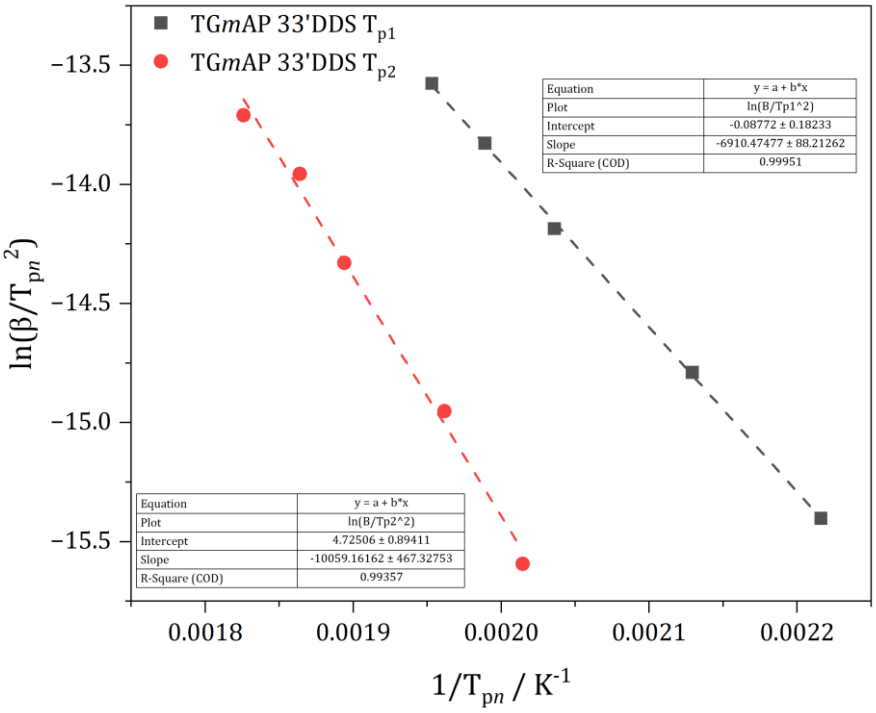

Figure 5.17 – Natural log of heating rate over exothermic peak temperature squared against the reciprocal of exothermic peak temperature for peak 1 (T_{p1}) and peak 2 (T_{p2}) during the dynamic cure of TG*m*AP/33'DDS using five different heating rates (2.5, 5, 10, 15 and 20 °C min^{-1}).

The activation energies for the four structural isomers of TGAP/DDS, as calculated using the Kissinger method when treating the two apparent heat flow peaks separately, are shown in Table 5.3. The R^2 values for each fit are also shown. They indicate how reliable the experimental

data linearly fits the Kissinger method [134,216]. These values should be treated cautiously as they only indicate correlation. Vyazovkin stated that despite perfectly linear plots, the Kissinger method often fails to detect any complexity in the process [215]. Activation energy will change throughout the reaction as the reaction conditions change and the type of reaction changes. Therefore, the value obtained is an average throughout the entire cure.

Table 5.3 – Activation energies for the four structural isomers of TGAP/DDS calculated using the Kissinger method (equation (5-6)) and two exothermic peak temperatures.

	TG*p*AP 44'DDS	R^2	TG*p*AP 33'DDS	R^2	TG*m*AP 44'DDS	R^2	TG*m*AP 33'DDS	R^2
Peak 1 Activation Energy / kJ mol^{-1}	69.08	0.9978	56.28	0.9982	62.01	0.9928	57.45	0.9995
Peak 2 Activation Energy / kJ mol^{-1}	68.66	0.9806	87.38	0.9939	74.68	0.9965	83.63	0.9936

Peak 1 is suggested to consist of mainly epoxy primary amine reactions. The activation energy is, on average, lower for 33'DDS formulations as expected due to its chemical structure. Peak 2 consists of mainly epoxy secondary amine and etherification reactions. However, it is best to say that it consists of the reactions that didn't occur in peak 1. As the activation energy of peak 1 for the 44'DDS formulations is higher, the activation energy for peak 2 would be expected to be lower than the 33'DDS formulations, as is the case. There are more reactants remaining in the second peak for the 44'DDS formulations. Therefore, the possibility of reactions is greater, resulting in a lower activation energy. The R^2 values for all formulations and peaks are around 0.99, apart from peak 2 for TG*p*AP/44'DDS. Despite peak 1 showing a good linear relationship, peak 2 is less well-behaved. The reason behind this is either related to thermal degradation as TG*p*AP/44'DDS is less thermally stable at the temperatures at which peak 2 occurs when heated using the faster heating rates or simply that T_p does not follow that relationship when increasing the heating rate for TG*p*AP/44'DDS. It is not possible to tell using the Kissinger method.

Even by separating the heat flow plots into two different peaks, these peaks are still not single steps. The separately treated peaks still consist of multiple reactions, and the Kissinger method cannot accurately model this. An improved method of analysing the curing process is needed.

Isoconversional methods improve the determination of activation energies by calculating the activation energy at different degrees of conversion or temperature using a model-free method [217]. There is no need to assume a kinetic model such as the rate equation or the reaction order, as the rate of reaction is assumed to be related to temperature and degree of conversion [218]. Multiple examples of model-free isoconversional methods exist: Kissinger-Akahira-Sunrose (KAS), Flynn-Wall-Ozawa (FWO), Starink and Friedman. All four will be applied to the dynamic measurements.

Let's start with the first three methods: KAS, FWO and Straink. These three methods allow for calculating activation energy as a function of degree of cure. Instead of analysing the dependence on the exothermic peak temperature, these methods analyse the dependence of the temperature at specific values of degree of cure when using different heating rates. This study will analyse the dependence at 5 % degree of cure intervals.

These methods are based on the general kinetic equation shown in equation (5-5) and are integrated by parts, and different approximations are used based on the method. As a result, the activation energies have different values and, therefore, different accuracies that depend on the method. An in-depth study by Starink clearly outlines all the assumptions and methods used here; therefore, they will not be repeated in detail [213].

Firstly, equation (5-5) is written in the form of equation (5-7) as heating rate, $\beta = \frac{dT}{dt}$.

$$\beta \frac{d\alpha}{dT} = A\, f(\alpha) \exp\left(-\frac{E_a}{RT}\right) \tag{5-7}$$

Rearranging to give equation (5-8).

$$\frac{d\alpha}{f(\alpha)} = \frac{A}{\beta} \exp\left(-\frac{E_a}{RT}\right)\, dT \tag{5-8}$$

Applying integrals to this gives equation (5-9).

$$f'(\alpha) = \int_0^{\alpha} \frac{d\alpha}{f(\alpha)} = \frac{A}{\beta}\int_0^{T} \exp\left(-\frac{E_a}{RT}\right)\, dT = \frac{AE_a}{\beta R}\int_y^{\infty} \frac{\exp(-y)}{y^2}\, dy \qquad (5\text{-}9)$$

Where $y = \frac{E_a}{RT}$. This is where the methods differ according to the approximation applied. The approximation is known as the temperature integral. Depending on the reactions taking place, therefore, the value of y, determines the suitability of the approximation of the temperature integral. The temperature integral is given by equation (5-10).

$$p(y) = \int_y^{\infty} \frac{\exp(-y)}{y^2}\, dy \qquad (5\text{-}10)$$

Applying this gives equation (5-11).

$$f'(\alpha) = \frac{AE_a}{\beta R} p(y) \qquad (5\text{-}11)$$

Rearranging equation (5-11) and applying natural logs gives equation (5-12).

$$\ln(\beta) = \ln\left(\frac{AE_a}{R}\right) - \ln\big(f'(\alpha)\big) + \ln\big(p(y)\big) \qquad (5\text{-}12)$$

For KAS, when the Coats-Redfern approximation is the case (equation (5-10)), the method is given as equation (5-13).

$$\ln\left(\frac{\beta}{T_\alpha^2}\right) = \ln\left(\frac{AE_a}{Rf'(\alpha)}\right) - \frac{E_a}{RT_\alpha} \qquad (5\text{-}13)$$

Where T_α is the temperature at a given degree of cure. KAS is unsurprisingly very similar to the Kissinger method shown in equation (5-6), just with an additional function of $f'(\alpha)$ as this method is model-free and does not need to assume that the reaction obeys a specific model, such as first-order kinetics. This function remains unsolved and needn't be as to calculate the dependence of activation energy with temperature a plot of $\ln\left(\frac{\beta}{T_\alpha^2}\right)$ against $\frac{1}{T_\alpha}$ is needed where the gradient is equal to $-\frac{E_a}{R}$.

The FWO uses a different approximation for the temperature integral as determined by Doyle [141,219] given in equation (5-14) and equation (5-15). Using the correct form, whether using logarithm or natural logarithm, is important as it will affect the activation energy values.

$$\log\big(p(y)\big) = -2.135 - 0.4567y \tag{5-14}$$

$$\ln\big(p(y)\big) = -5.3305 - 1.052y \tag{5-15}$$

Applying Doyle's approximation to equation (5-12) gives the FWO method in equation (5-16).

$$\ln(\beta) = \ln\left(\frac{AE_a}{R}\right) - \ln\big(f'(\alpha)\big) - 5.3305 - 1.052\frac{E_a}{RT_\alpha} \tag{5-16}$$

Activation energy is determined by plotting $\ln(\beta)$ against $\frac{1}{T_\alpha}$ and the gradient is equal to $-1.052\frac{E_a}{R}$.

The final degree of cure-related method that uses the temperature integral approximation is the Starink method. Starink identified that the temperature integral approximation was derived from equation (5-17) [213].

$$p(y) = \frac{\exp\left(-Ay + B\right)}{y^\kappa} \tag{5-17}$$

Where A, B and κ are optimising exponents. In the previous approximations, A has been assumed to be one, but in their analysis, A was not required to be one, which led to the following temperature integral approximation shown in equation (5-18), which they stated to be a highly accurate approximation compared to the previous two [213].

$$p(y) = \frac{\exp\left(-1.0008y - 0.312\right)}{y^{1.92}} \tag{5-18}$$

Applying this approximation to equation (5-12) gives the Starink method shown in equation (5-19).

$$\ln\left(\frac{\beta}{{T_\alpha}^{1.92}}\right) = \ln\left(\frac{AE_a}{R}\right) - \ln\big(f'(\alpha)\big) - 0.312 - 1.0008\frac{E_a}{RT_\alpha} \tag{5-19}$$

Activation energy is determined by plotting $\ln\left(\frac{\beta}{{T_\alpha}^{1.92}}\right)$ against $\frac{1}{T_\alpha}$ and the gradient is equal to $-1.0008\frac{E_a}{R}$.

The final method is the Friedman method, which differs from KAS, FWO, and Starink as this does not determine activation energy based on an integral. Friedman instead uses the rate of reaction at fixed degree of cure values. Like with the other methods, it is based on the general kinetic equation in (5-5). Instead, natural logs are applied, and the method is given in equation (5-20).

$$\ln\left(\frac{d\alpha}{dt}\right) = \ln(A) + \ln\big(f(\alpha)\big) - \frac{E_a}{RT_\alpha} \tag{5-20}$$

Activation energy is determined by plotting $\ln\left(\frac{d\alpha}{dt}\right)$ against $\frac{1}{T_\alpha}$ and the gradient is equal to $-\frac{E_a}{R}$.

These methods are applied to dynamic DSC measurements of the four structural isomers of TGAP/DDS under five different heating rates (2.5, 5, 10, 15 and 20 °C min^{-1}) to determine the activation energies as the resin cures. Activation energy values are given at 5 % intervals

between 5 % and 95 % degree of cure. The values for 0 % and 100 % degree of cure cannot be obtained as the rate of reaction is 0 s^{-1} at these points.

Figure 5.18 shows the activation energies calculated by the four different methods (KAS, FWO, Starink and Friedman) for the four structural isomers of TGAP/DDS dynamically cured using five different heating rates (2.5, 5, 10, 15, 20 °C min^{-1}). This highlights the similarities and differences between the methods. As would be expected, the trends observed in the $p(y)$ isoconversional methods (KAS, FWO and Starink) are the same, only offset by a factor, whereas the Friedman method, a rate of reaction isoconversional method, is very different. Starink stated that the accuracies of the methods were dependent on six factors [213], as follows:

1. Mathematical approximations, approximating the $p(y)$ temperature integral.
2. Thermal lag: most DSC equipment will output the program temperature rather than the sample temperature. If there is thermal lag, these temperatures will not be the same.
3. Baseline determination of the heat flow data and, in the case of the Friedman method, the determination of the rate of reaction.
4. Inaccuracies in heating rate applied by the DSC.
5. In the case of the exothermic peak temperature method (Kissinger), the degree of cure may not be the same at each heating rate.
6. The assumption that the equilibrium state is constant is not always the case as, towards higher temperatures, thermal degradation occurs.

Due to these factors, the different methods have different levels of accuracy.

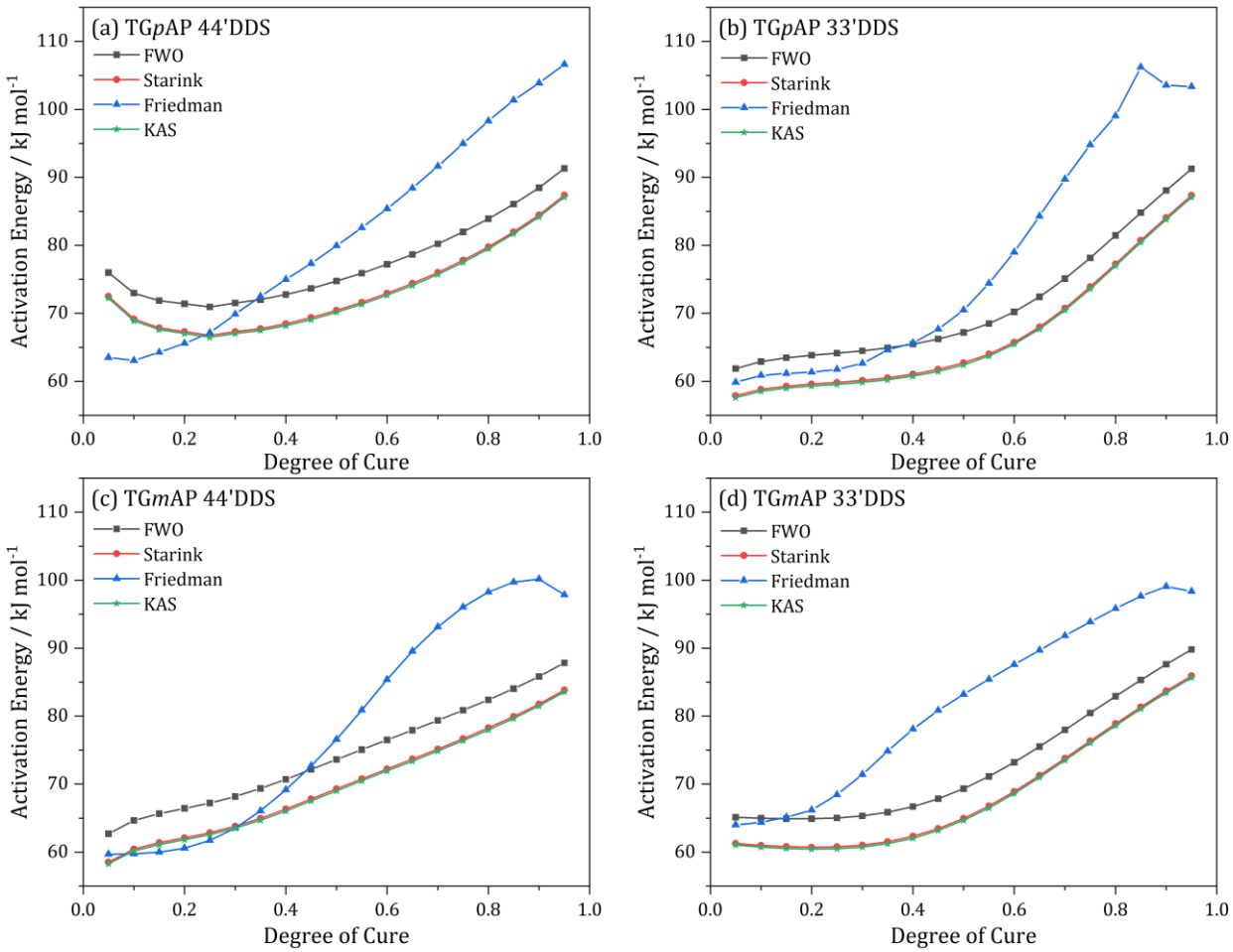

Figure 5.18 – Activation energies as a function of degree of cure for the four structural isomers of TGAP/DDS under dynamic heating conditions (2.5, 5, 10, 15 and 20 °C min^{-1}) calculated using the methods in equations (5-13) (KAS), (5-16) (FWO), (5-19) (Starink) and (5-20) (Friedman): (a) TG*p*AP/44'DDS, (b) TG*p*AP/33'DDS, (c) TG*m*AP/44'DDS and (d) TG*m*AP/33'DDS.

The Friedman method makes no mathematical assumptions, but when the rate of reaction with respect to time changes significantly over a short period of time, as is seen in Figure 5.15, the method is inaccurate, explaining the discrepancy from the $p(y)$ isoconversional methods. Significant differences between the Friedman method and KAS and FWO have been seen in previous studies, most notably in Zhang and Yan *et al.* [216,220].

The $p(y)$ isoconversional methods use a similar method but differing approximations. The accuracies of the approximations vary, with the FWO method thought to be the least accurate as it does not support high values of y in its approximation. FWO activation energies are roughly 5 kJ mol^{-1} higher than KAS and Starink, but the trend is similar. In Starink's study, they suggested

that the Starink method (their method!) was the most accurate. The agreement between the KAS and Starink methods was excellent. However, in this study the exact values are not of particular interest. The trend of how the activation energies change is. So, for this, either technique can be analysed. It is important to remember that even though these methods are model-free, a complex curing mechanism will struggle to be supported by an empirical method. The following will analyse the Friedman method and the Starink method.

The activation energies as a function of cure for the four structural isomers of TGAP/DDS during a dynamic cure as calculated using the Starink method outlined in equation (5-19) are shown in Figure 5.19. The values here are an average of every reaction occurring. From Chapter 4. NIR, it is known that none of the curing reactions occur independently.

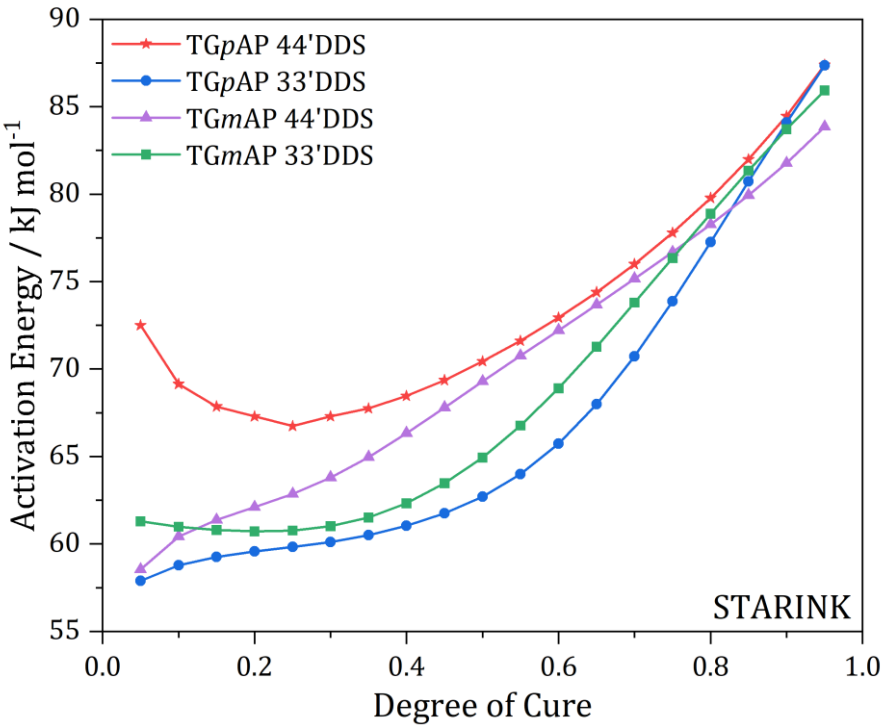

Figure 5.19 – Activation energies as a function of degree of cure for the four structural isomers of TGAP/DDS under dynamic heating conditions (2.5, 5, 10, 15 and 20 °C min^{-1}) calculated using the Starink method outlined in equation (5-19).

The results shown are not what would be initially expected. As seen earlier in the chapter, a pairing up based upon the hardener has been observed for the exothermic behaviour. This does not occur here. Instead, TG*p*AP/44'DDS initially has higher activation energy than the other three formulations. 44'DDS is less reactive; therefore, the barrier for reactions to occur is higher

than that of the 33'DDS counterparts. TG*m*AP/44'DDS does not show this. The explanation behind this is known. It could be related to the method, especially as Starink, FWO and KAS don't consider the rate of reaction, only temperature. Another feature that is not expected is the lack of a decrease in activation energy during the initial stages of the cure. It is observed dramatically in TG*p*AP/44'DDS and, to a small extent, in TG*m*AP/33'DDS, suggesting that the reaction is autocatalytic [102,134,208]. Products of the initial reactions catalyse further reactions, thus lowering the activation energy. This isn't suggesting that this doesn't happen in TG*p*AP/33'DDS and TG*m*AP/44'DDS, but the data doesn't show it, perhaps due to the complexity of the other reactions occurring.

There is a significant increase in activation energy in all formulations after 40 % degree of cure, which, according to the Flory equation, is roughly the point at which gelation occurs. Significant reactions have occurred, and the reactants' mobility is starting to be restricted, resulting in higher activation energy. The rate at which the activation energies increase is similar depending on the hardener. The 33'DDS formulations have a lower activation energy at 40 % due to the increased reactivity of 33'DDS, but once significant crosslinking occurs, the rate at which the activation energy increases is higher than 44'DDS. Towards the end of the cure, TG*p*AP/44'DDS and TG*p*AP/33'DDS have nearly the same value, whereas the TG*m*AP/44'DDS and TG*m*AP/33'DDS are lower. This can be related to the chemical structure of TG*p*AP. It is linear compared to the non-linear structure of TG*m*AP. The configurational entropy is higher for TG*m*AP. Therefore, the possibility of reactions is greater, resulting in a lower activation energy value.

The activation energies as a function of cure for the four structural isomers of TGAP/DDS during a dynamic cure as calculated using the Friedman method outlined in equation (5-20) are shown in Figure 5.20. Despite what was said regarding the inaccuracy of the Friedman method, the results presented show the expected behaviour that isn't seen in the Starink method. The pairing up based on the hardener occurs. However, this is only because this method calculates activation energy based on the relationship between rate of reaction and temperature. The rate of reaction is initially higher for the 33'DDS formulations than the 44'DDS formulations. Therefore, the activation energy is higher in the 44'DDS formulations.

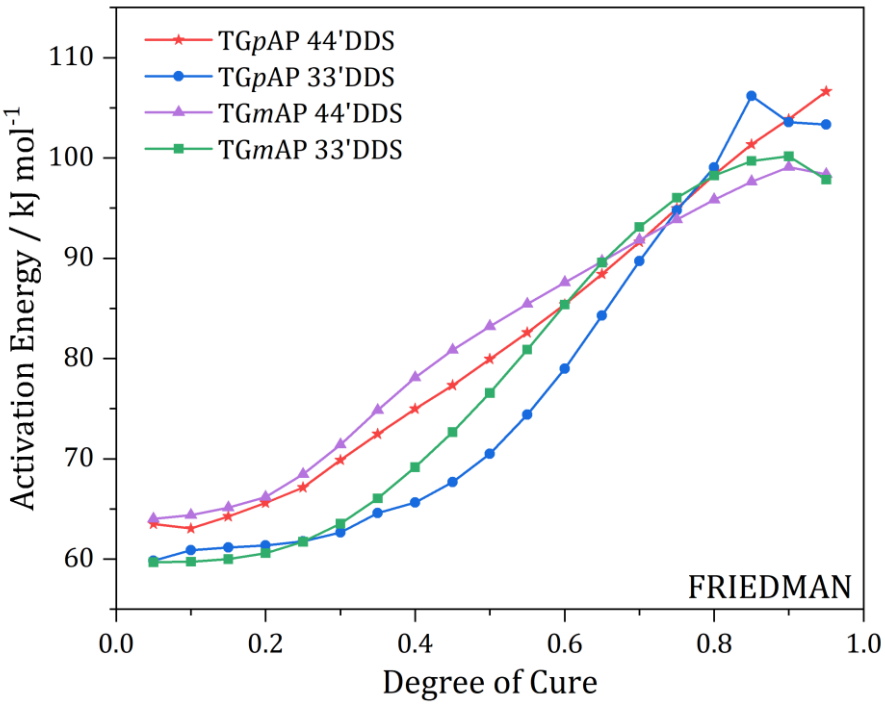

Figure 5.20 – Activation energies as a function of degree of cure for the four structural isomers of TGAP/DDS under dynamic heating conditions (2.5, 5, 10, 15 and 20 °C min^{-1}) calculated using the Friedman method outlined in equation (5-20).

A more autocatalytic behaviour is also observed in all the formulations, although there isn't a decrease in activation energy but rather constant values for the first 20 % of the cure. This is expected as the autocatalytic reactions are not the only reactions taking place. Activation energy then significantly increases as the mobility decreases and steric effects increase. Towards the end of the cure, activation energy stabilises and slightly decreases for TG*p*AP/33'DDS, TG*m*AP/44'DDS and TG*m*AP/33'DDS. This is related to the non-linear structures. At higher degrees of cure, the temperature will be high, and this may result in a decrease in activation energy due to increased effective free volume space and mobility. Due to its linear starting reagents, this doesn't occur in TGpAP/44'DDS. The final activation energies also pair up based on the epoxy structure. Linear TG*p*AP values are roughly 7 kJ mol^{-1} higher than the non-linear TG*m*AP final activation energy values.

The trends observed using the Friedman method are more logical than those seen using the Starink method. The methods use different calculations and assumptions. The behaviour seen in Friedman relates directly to the rate of reaction results. In contrast, Starink uses the relationship between temperatures at specific degrees of cure and heating rate. Which method

is more correct is challenging to say without significant further study. Whether it is needed to be known is perhaps the more critical point. Dynamic heating is only used for ramping up to isotherm temperature. The relevance of this information is, therefore, limited. It is important to understand at what temperatures the resins are more reactive, but in practice, TGAP/DDS is rarely cured using dynamic heating alone. Analysing the isothermal behaviour may give more insight into the curing mechanism.

5.4.2. ISOTHERMAL MEASUREMENTS

Isothermal measurements refer to testing samples using DSC at a single temperature until no more curing reactions occur. It would be expected that the isomers of TGAP/DDS should behave differently from one another, as was the case with dynamic measurements. There are drawbacks to isothermal measurements, just like with dynamic measurements, but significantly more studies have been undertaken focusing on isothermal measurements. The difficulty of a non-constant temperature is removed, allowing for a more accurate kinetic analysis of epoxy resins.

The cure of the four formulations of TGAP/DDS has been investigated using isothermal heating at five different temperatures (130, 160, 200, 210 and 220 °C) and are shown in Figure 5.21. The resins are ramped up to the specific temperature at a heating rate that is fast enough to ensure that minimal amounts of curing occur, in this case, 50 °C min^{-1}. Each isotherm occurs until no more curing occurs, and the rate of heat flow change is zero, resulting in different periods of time for each. Figure 5.21 is separated by isotherm temperature rather than formulation. An example of TG*p*AP/33'DDS is shown in Figure 5.22. The heat flow values differ significantly between 130 °C and 220 °C, meaning the details are unclear for the lower temperature isotherms. The heat flow plots in Figure 5.21 appear more straightforward than the dynamic heat flow plots shown in Figure 5.9 for all isotherms and formulations, as one peak occurs very shortly after the start of the cure. It is worth noting that none of the plots start at 0 W g^{-1} as a small amount of curing occurs in the ramp. The reaction is already underway at 0 minutes.

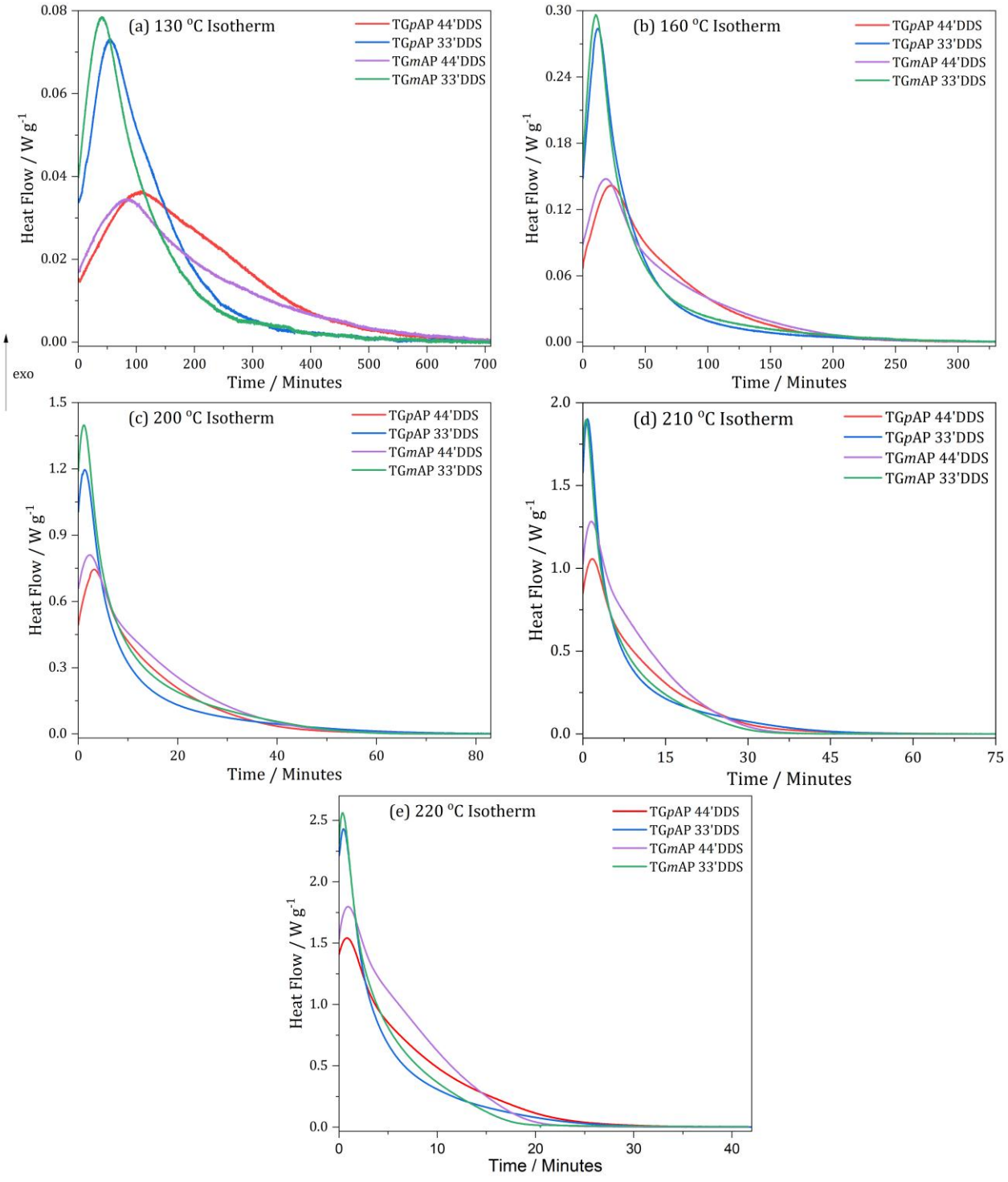

Figure 5.21 – DSC heat flow plots for the four structural isomers of TGAP/DDS under five different isothermal heating conditions: (a) 130 °C, (b) 160 °C, (c) 200 °C, (d) 210 °C and (e) 220 °C. Exothermic is up.

At all isotherm temperatures, the 33'DDS formulations achieve higher heat flow peaks earlier than the 44'DDS formulations. Once again, indicating that the 33'DDS formulations are initially more reactive than the 44'DDS formulations. After the peak, the decrease in heat flow is steeper for the 33'DDS formulations, indicating that most of the curing takes place quicker than 44'DDS formulations. Without further analysis, little more can be said about the difference in cure of the four different TGAP/DDS formulations. It is worth noting that in Figure 5.21, the y and x-axis scales differ between (a), (b), (c), (d) and (e). Despite the peaks appearing to be the same height, they are not. In the 130 °C isotherm data, the y-axis maximum is 0.08 W $g^{-1,}$ whereas the 220 °C isotherm maximum y-axis value is 2.7 W g^{-1}, over 30 times larger. Figure 5.22 highlights this issue for isothermal heat flow plots of TG*p*AP/33'DDS. The apparent differences are not visible due to differences in heat flow and time periods.

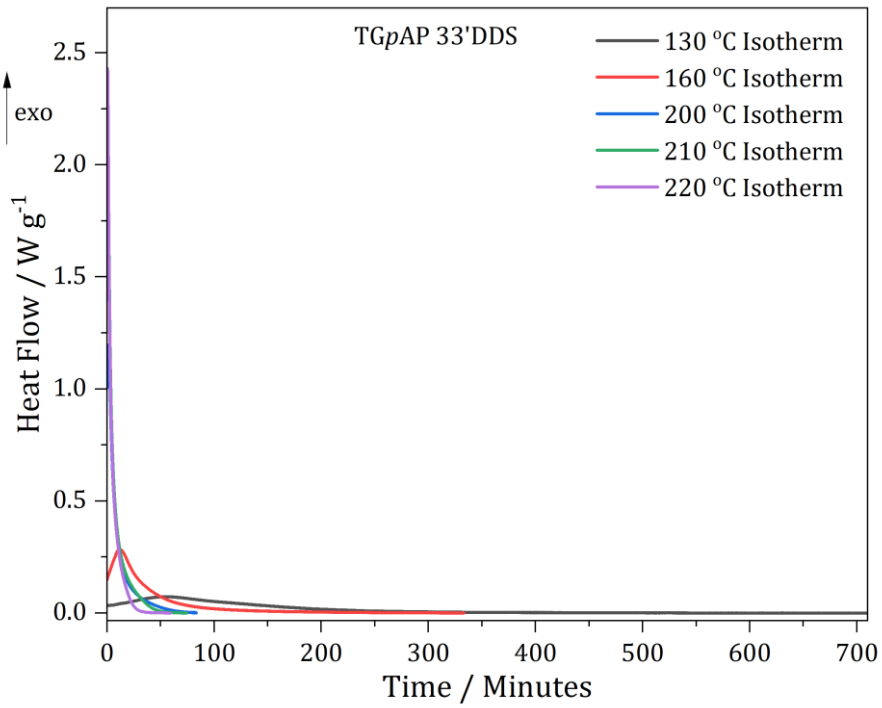

Figure 5.22 – DSC heat flow plot for TG*p*AP/33'DDS under five different isothermal heating conditions (130, 160, 200, 210 and 220 °C). Exothermic is up.

The heat flow plots can be integrated as shown in equation (5-21) to obtain the enthalpy of reaction, $\Delta H(t)$ at time, t.

$$\Delta H(t) = \int_0^t \frac{dq}{dt} dt \quad (5\text{-}21)$$

Where $\frac{dq}{dt}$ is heat flow. This can then by divided by the total enthalpy of cure to obtain the degree of cure as function of time, $\alpha(t)$, as shown in equation (5-22).

$$\alpha(t) = \frac{\Delta H(t)}{\Delta H_0} \quad (5\text{-}22)$$

Where ΔH_0 is the total enthalpy of cure. Studies have used different approaches to obtain the values of ΔH_0. The total enthalpy of cure is often calculated by calculating the enthalpy of reaction and then running a dynamic scan from 30 to 300 ^{o}C to calculate the residual enthalpy and adding the two values. Many studies have done it this way, but the resins used have often been DGEBA. As this is a bifunctional resin, the crosslink density is lower. When using a higher functionality resin, the crosslink density is higher, and when exposed to a higher temperature, reactions occur in proximity. The risk here is that unreacted groups get trapped between the crosslinks, and because there isn't enough time for reactive groups to move and react, a lower enthalpy of cure is often observed. Resulting in falsely high values of the degree of cure. Barton studied TGDDM/44'DDS and used the enthalpy of cure values obtained from dynamic scans of uncured resin rather than residual enthalpy scans [127]. This study will follow the same method, using the total enthalpy of cure values obtained from dynamic scans in Table 5.2. Neither method is perfect; the most suitable method to validate the total enthalpy of cure is using infrared spectroscopy to find the concentration of remaining epoxide groups, but this was not done.

The degree of cure values should be very similar when using either method at low isotherm temperatures. Figure 5.23 shows the residual exotherm peak in the DSC heat flow plot of TG*p*AP/33'DDS heated dynamically at 10 °C min^{-1} after an isothermal cure at 130 °C for 710 minutes. Integrating the exothermic peak and dividing it by the heating rate, 10 °C min$^{-1,}$ will give the residual enthalpy of cure. This plot also gives an endothermic peak where the glass transition temperature (T_g) is. This relates to enthalpy lost when the sample undergoes ageing during the isothermal cure, something seen and commented on by Hutchinson *et al*. when

studying TG*p*AP/44'DDS using modulated DSC to identify the vitrification point [221]. The longer the samples are cured and at higher temperatures, the bigger the endothermic relaxation recovery peak is.

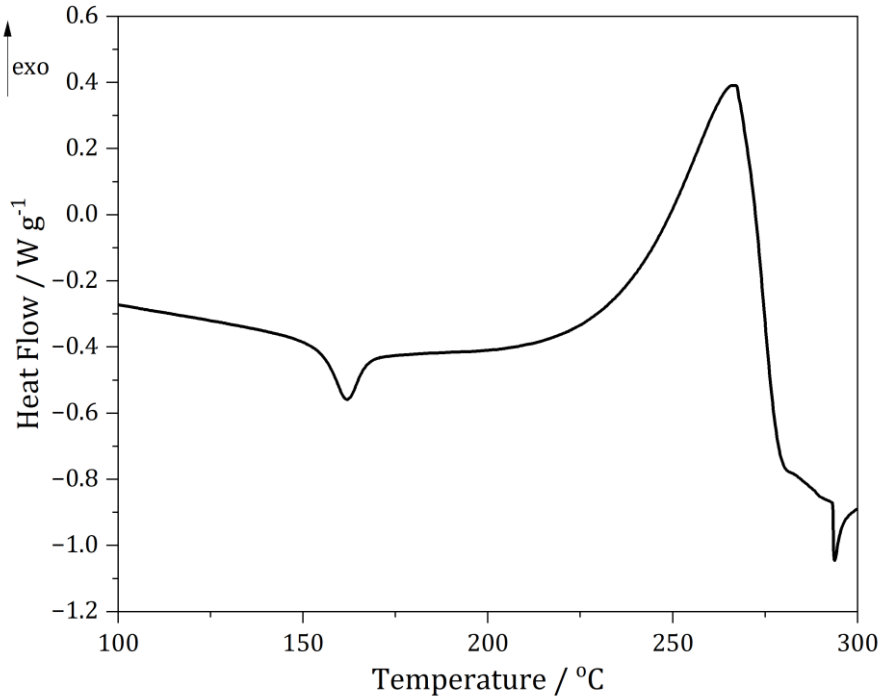

Figure 5.23 – DSC heat flow plot of TG*p*AP/33'DDS when dynamically heated at 10 °C min^{-1} to determine residual after an isothermal cure at 130 °C for 710 minutes (not normalised). Exothermic is up.

Table 5.4 shows good agreement between residual enthalpy and using average total enthalpy of cure from dynamic scans for TG*p*AP/33'DDS at 130 °C isotherm, within 2 kJ mol^{-1}. There is similar agreement for all four TGAP/DDS formulations at both 130 and 160 °C isotherms. However, in the high-temperature isotherms, the total enthalpy of cure is lower than that determined by dynamic scans. This shouldn't be the case as the total enthalpy of cure should be similar irrespective of the heating method. The fast curing in isothermal measurements affects this. It is worth being aware of this as some degree of cure values may be surprising later in the chapter.

Table 5.4 – A comparison of the total enthalpy of cure values obtained for the cure of TG*p*AP/33'DDS using the residual enthalpy method vs an average of five dynamic scans.

	TG*p*AP 33'DDS 130 °C Isotherm	TG*p*AP 33'DDS Dynamic Average
Isotherm ΔH_r / J g^{-1}	645.22	-
Residual ΔH_r / J g^{-1}	194.58	-
ΔH_0 / J g^{-1}	839.80	829.68
ΔH_0 / kJ mol^{-1}	114.21	112.84

It is possible to use equation (5-22) to compare how the degree of cure progresses during the reaction when using different isotherm temperatures. Figure 5.24 shows the degree of cure values as a function of time for the four structural isomers of TGAP/DDS at each different isotherm (130, 160, 200, 210 and 220 °C). The isotherm temperatures have been chosen based on the standard multi-dwell cure cycle used for curing TGAP/DDS. There are dwells at 130, 160 and 200 °C. Those are the main temperatures of focus. 210 and 220 °C have been chosen to allow for enough overlap to undertake activation energy calculations accurately.

For the 130, 160 and 200 °C isotherms, the final degree of cure value increases as temperature increases for all formulations. However, none reach 100 % degree of cure. Figure 5.24 shows that in the TG*m*AP/33'DDS formulations, isotherm 210 and 220 °C go to lower degrees of cure than the 200 °C. This is slightly counterintuitive and hasn't been commented on in the literature, as it may not be seen when calculating degree of cure using residual enthalpy. It is related to the speed at which the resin cures. As the curing is so fast, crosslinks trap in unreacted groups, which are so sterically hindered that they will not react even with a post-cure. The resins would never be cured at these temperatures at low degrees of cure, maybe only as a post-cure once the resin is mostly cured and has higher thermal resistance. The high temperatures and the small molecules present could have resulted in evaporation, resulting in a lower concentration of reactive groups than the initial concentration. In hindsight, good

practice would have been to measure the mass of the final cured sample to see if this had an effect.

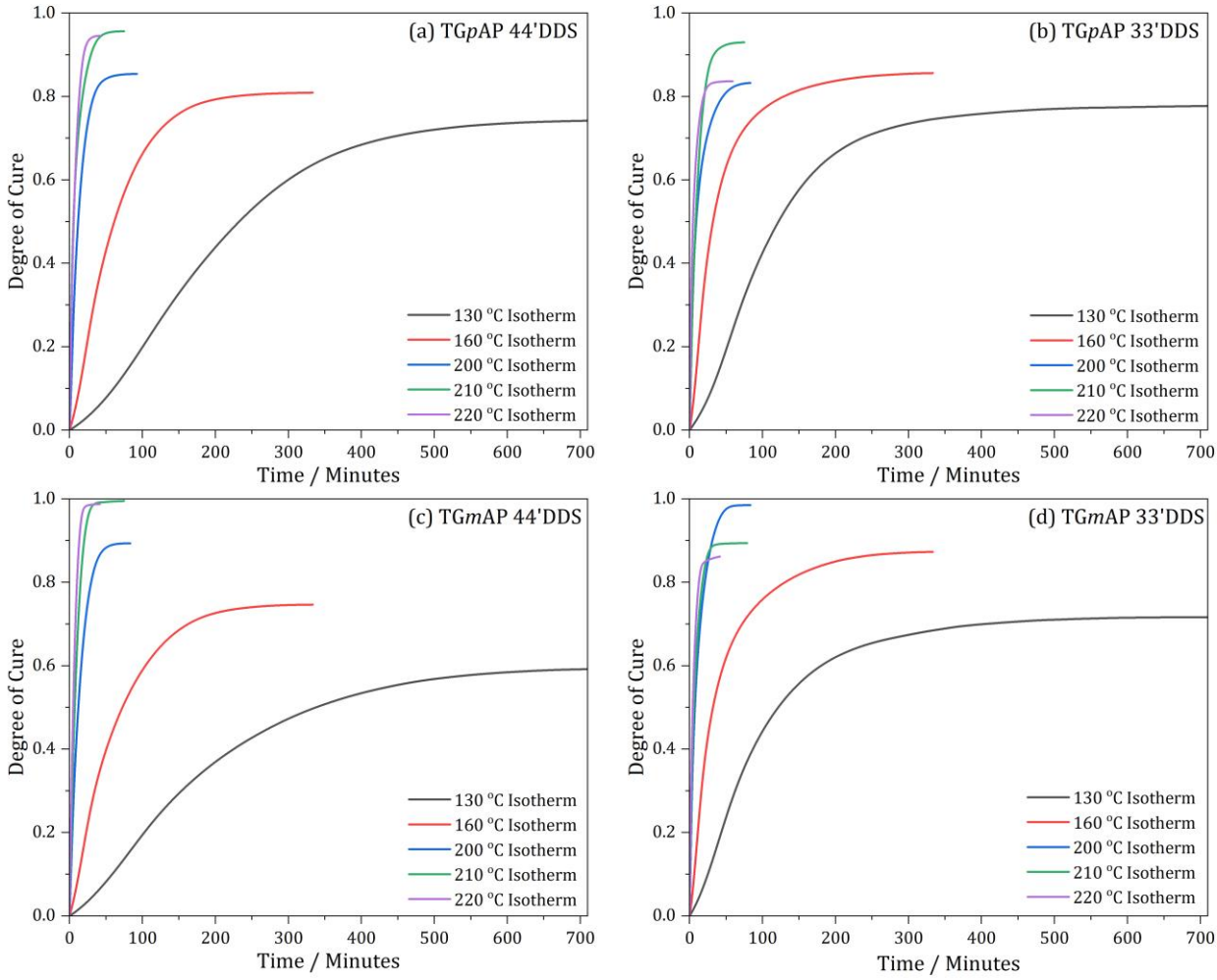

Figure 5.24 – Degree of cure as a function of time for the four structural isomers of TGAP/DDS under isothermal heating conditions (130, 160, 200, 210 and 220 °C): (a) TG*p*AP/44'DDS, (b) TG*p*AP/33'DDS, (c) TG*m*AP/44'DDS and (d) TG*m*AP/33'DDS.

Another source of error that might cause the degree of cure values to be lower in higher temperature isotherms may have been related to curing during the ramp-up to temperature. This would be expected as from the dynamic scans heating at 20 ^{o}C min^{-1}, the reaction kick-off temperature was between 130 and 150 ^{o}C for the TGAP/DDS formulations. When ramping at 50 ^{o}C min^{-1}, the onset will be slightly higher but still have an impact. Due to the increased reactivity of the 33'DDS hardener, the effect will be more prominent. The ramp-up to the 210

and 220 °C isotherms in TG*m*AP/33'DDS was analysed to see the impact. Figure 5.25 shows the ramp up to 220 °C, where the exothermic 'peak' can be integrated and the enthalpy found. One of the issues with doing this is having to guess the baseline because, unlike in dynamic measurements, where the sample is heated until curing has stopped, there is no end here, so the accuracy cannot be guaranteed.

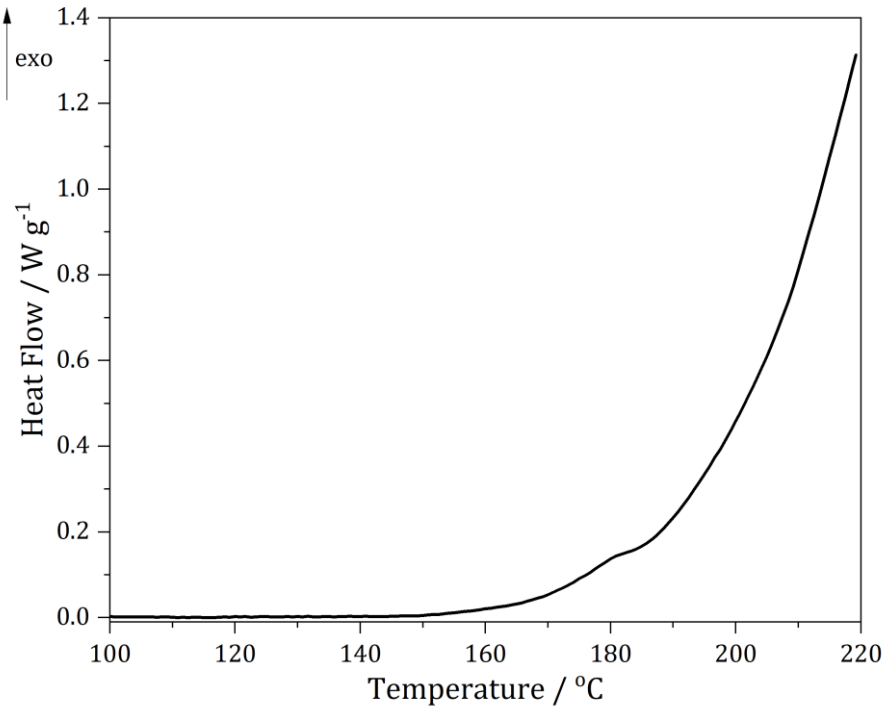

Figure 5.25 – Dynamic DSC heat flow of TG*m*AP/33'DDS during the ramp up to 220 °C isotherm using a 50 °C min^{-1} heating rate. Exothermic is up.

Using Figure 5.25, the enthalpy of reaction was found to be 26.86 J g^{-1} for the ramp up to 220 °C and doing the same analysis for the ramp up to 210 °C, the enthalpy of reaction was found to be 11.54 J g^{-1}. This accounted for 3.20 % and 1.38 % degree of cure, respectively, during the ramp. This is not a large amount, especially when compared to a study by Anagwu and Skordos, who investigated DGEBA cured with 4-aminophenyl disulphide, and when ramping to 200 °C, they found the resin cured 65 % [111]. As TG*m*AP/33'DDS is thought to be the most reactive, 3.20 % is the most amount of curing during the ramp for all the formulations. It was decided that this would not be added to the final values as the accuracy of the baseline determination during the ramp cannot be guaranteed. All the heat flow plots shown in Figure 5.21 show a maximum heat

flow peak after the start of the measurements. Therefore, the effect on the further analysis will be limited.

The degree of cure as a function of time plots for the 130, 160 and 200 °C isotherms for the four structural isomers of TGAP/DDS are shown in Figure 5.26. For all isotherms, the 33'DDS formulations cure quicker than the 44'DDS formulations. At 130 and 160 °C, TG*m*AP/44'DDS cures significantly slower than TG*p*AP/44'DDS at around 20 and 40 % cured, respectively. The reason behind this is potentially related to the ability of TG*p*AP to undergo etherification reactions at lower temperatures, whereas, in the 200 °C isotherm, the curing is very similar until the end, where TG*m*AP/44'DDS goes to a slightly higher final degree of cure. This is related to the non-linear shape of TG*m*AP. The ability of TG*p*AP to etherify at lower temperatures, as discussed in Chapter 4. NIR, allows for a slightly higher final degree of cure in TG*p*AP/33'DDS compared to TG*m*AP/33'DDS in the 130 °C isotherm. At 160 °C, the evolution of cure is very similar for the 33'DDS formulations, suggesting that that temperature is sufficient for a similar curing mechanism. However, in the 200 °C isotherm, TG*m*AP/33'DDS goes to a significantly higher degree of cure than TG*p*AP/33'DDS, suggesting that the epoxy primary amine reactions dominate initially. Then, due to the non-linear shape of TG*m*AP, it can undergo greater amounts of etherification later, whereas TG*p*AP/33'DDS linear epoxy shape limits this. It must be remembered that DSC cannot give information about specific reactions. These are only assumptions based on the behaviour displayed in Chapter 4. NIR. Additionally, TG*m*AP/33'DDS achieves a higher final degree of cure value at 200 °C due to its T_g. From DMA (see Table 4.3 for DMA data), TG*m*AP/33'DDS was the only resin with a T_g under 200 °C. This would suggest TG*m*AP/33'DDS is in a less glassy state that the other formulations with a T_g higher than the cure temperature. TG*p*AP/44'DDS, TG*p*AP/33'DDS and TG*m*AP/44'DDS will be vitrified and completely diffusion controlled once its T_g reaches 200 °C or higher whereas TG*m*AP/33'DDS will still have some flexibility in the crosslinked network allowing it to go to a higher degree of cure.

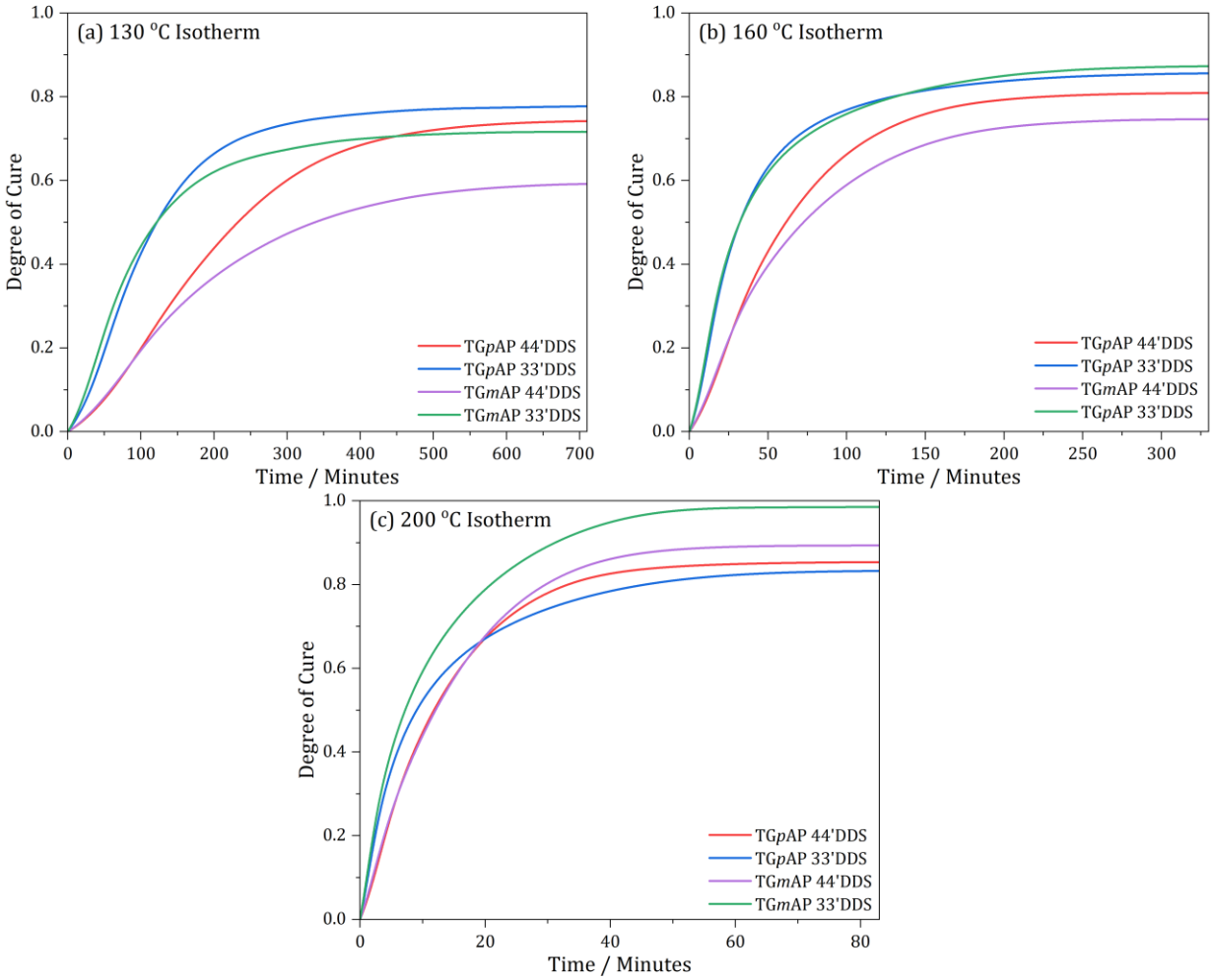

Figure 5.26 – Degree of cure as a function of time for the four structural isomers of TGAP/DDS under isothermal heating conditions: (a) 130 °C isotherm, (b) 160 °C isotherm and (c) 200 °C isotherm.

Like in dynamic DSC, the next step in the analysis is looking at the rate of reaction. The rate of reaction can be determined using equation (5-23).

$$\frac{\mathrm{d}\alpha}{\mathrm{dt}} = \frac{\frac{dq}{dt}}{\Delta H_0} \qquad (5\text{-}23)$$

Where $\frac{\mathrm{d}\alpha}{\mathrm{dt}}$ is rate of reaction with respect to time. Figure 5.27 shows the rate of reaction as a function of degree of cure for the four structural isomers of TGAP/DDS, comparing the five different isotherm temperatures (130, 160, 200, 210 and 220 °C). As isotherm temperature increases, the maximum rate of reaction value increases for all formulations. The behaviour

observed in Figure 5.24, where degree of cure goes to lower values at the higher isotherm temperatures for the 33'DDS formulations, is seen in the rate of reaction going to zero before the lower isotherm. For TG*p*AP/33'DDS, the isotherm 220 °C rate of reaction goes to zero before isotherm 210 °C as is the same for TG*m*AP/33'DDS, and also isotherm 210 °C with respect to isotherm 200 °C. The shape of the rate of reaction curves is similar for the higher temperature isotherms (200, 210 and 220 °C) for each formulation. The shape is difficult to see for the lower temperature isotherms due to the y-axis scale. It is better displayed in Figure 5.28.

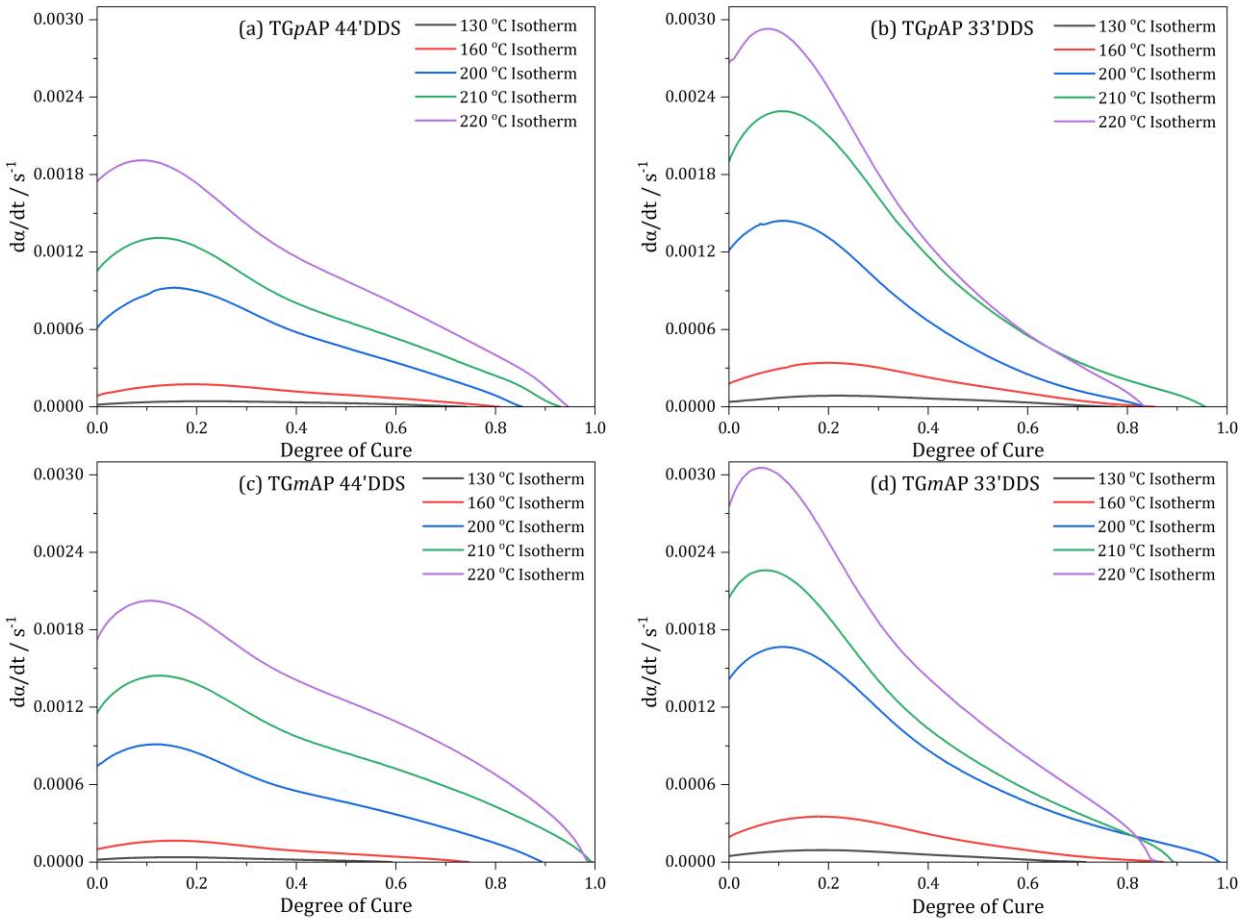

Figure 5.27 – Rate of reaction as a function of degree of cure for the four structural isomers of TGAP/DDS comparing the five different isothermal conditions (130, 160, 200, 210 and 220 °C): (a) TG*p*AP/44'DDS, (b) TG*p*AP/33'DDS, (c) TG*m*AP/44'DDS and (d) TG*m*AP/33'DDS.

Figure 5.28 compares the rate of reaction as a function of degree of cure for the four structural isomers of TGAP/DDS under the five different isotherm temperatures.

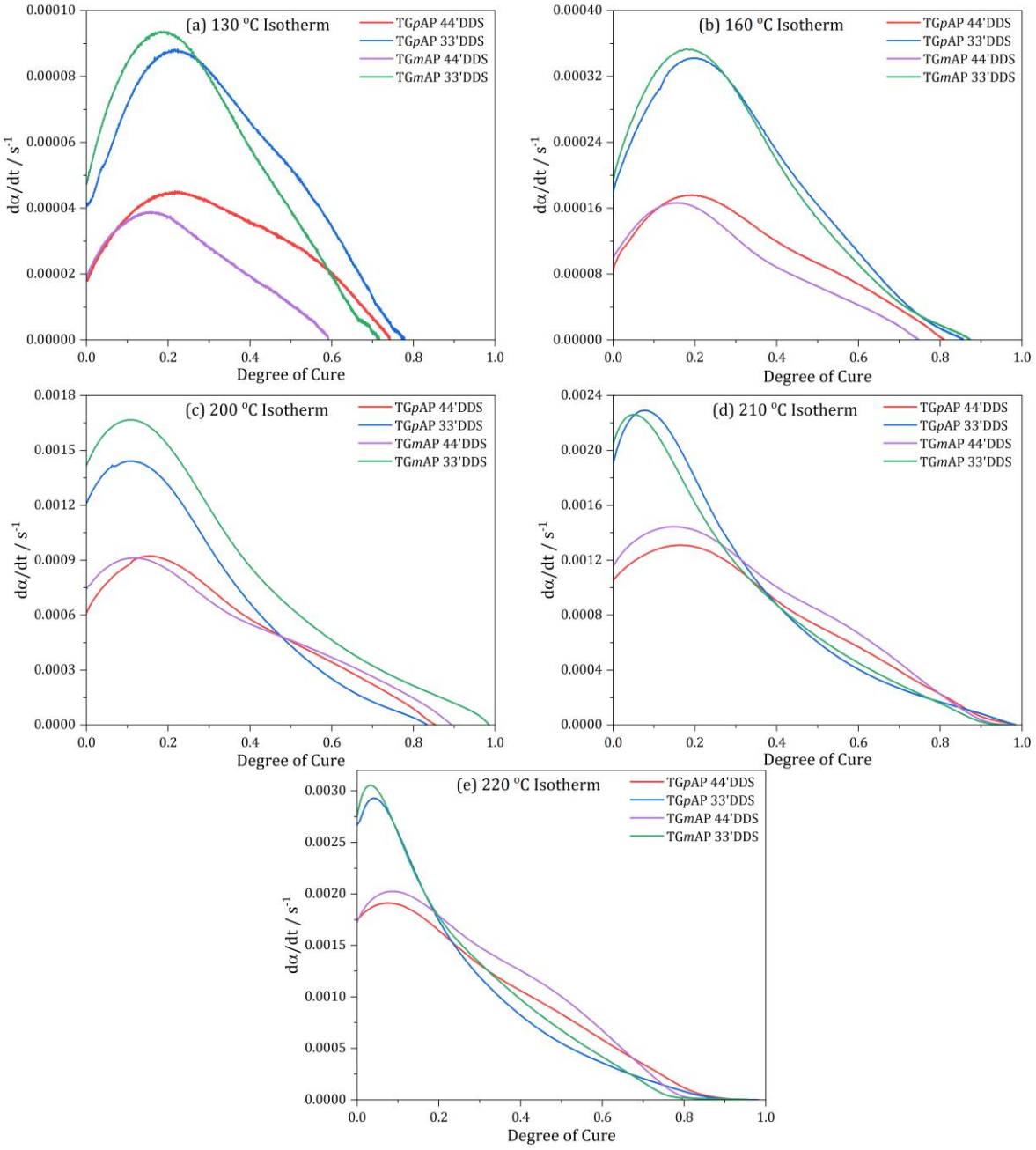

Figure 5.28 – Rate of reaction as a function of degree of cure comparing the four structural isomers of TGAP/DDS under five different isothermal conditions: (a) 130 °C isotherm, (b) 160 °C isotherm, (c) 200 °C isotherm, (d) 210 °C isotherm and (e) 220 °C isotherm. Note the y-axis scales are different for each isotherm.

For all isotherm temperatures, the rate of reaction peak is higher for the 33'DDS formulations than for the 44'DDS formulations. TG*m*AP/33'DDS consistently has a higher rate of reaction than TG*p*AP/33'DDS for all temperatures apart from isotherm 210 °C. TG*p*AP/44'DDS has a higher rate of reaction than TG*m*AP/44'DDS for the first two isotherms (130 and 160 °C),

whereas TG*m*AP/44'DDS has a higher rate of reaction in the higher temperature isotherm (200, 210 and 220 °C).

The shape of the curves is slightly different depending on the formulation. In 130 °C isotherm, the shape of the curve for all formulations is 'quadratic', but the TG*p*AP formulations have a slight hump towards the end of the curve. The shape of the curves for the other isotherms is based on the hardener. The 44'DDS formulations have a slight hump after the peak, whereas the 33'DDS formulations peak then continually decreases. The hump form at a consistently similar degree of cure values for both TG*p*AP/44'DDS and TG*m*AP/44'DDS, suggesting it is something related to the chemical structure of the remaining reactive groups, which allows the reaction to progress at a slightly increased reaction rate.

The hump is related to etherification. As discussed in Chapter 4. NIR, TG*p*AP can undergo etherification reactions at lower temperatures due to its behaviour as a tertiary amine catalyst. At 130 °C, the temperature is not high enough for significant etherification to occur without a tertiary amine catalyst. TG*p*AP sees a hump in the rate of reaction plot indicating potential etherification. The TG*m*AP formulations do not show an obvious deviation at 130 °C indicating little, if any etherification.

In the higher temperature isotherms, the 44'DDS formulations undergo more etherification reactions as the 44'DDS itself is not as reactive as 33'DDS, so reactions do not occur as quickly, and reactive groups are less restricted than in the 33'DDS formulations. In Chapter 4. NIR, comments were made on the fact that areas of localised areas of crosslinking form when reactions occur simultaneously and quickly. In the case of isotherms, this occurs more readily in the 33'DDS formulations. This better mobility means that any tertiary amines formed from the reaction of epoxide groups and secondary amines can catalyse etherification reactions more readily than those formed in the 33'DDS formulations. This was not seen in isothermal DSC analysis of TG*p*AP/44'DDS in studies by Varley *et al.* and Hutchinson *et al.* [102,221]. The case is that the epoxy:amine ratio used in their studies was 1.1:1, whereas in this study, the ratio was extremely epoxy rich, 1.72:1. The use of epoxy rich mixture allowed for etherification to have a greater influence on the rate of reaction as the reactions took place *via* a different mechanism to the mechanism in the not as epoxy rich formulations in the aforementioned studies. Although an interesting finding, it can be undesirable, especially when undertaking kinetic analysis.

5.4.2.1. ISOTHERMAL KINETIC ANALYSIS

Like with dynamic measurements in 5.4.1, the activation energy of the cure can be calculated. Numerous methods can be used, but firstly, the general rate equation outlined in equation (5-5) can be utilised by applying natural logs to give equation (5-24), the same equation as that of the Friedman method used for dynamic measurements.

$$\ln\left(\frac{d\alpha}{dt}\right) = \ln(A) + \ln\big(f(\alpha)\big) - \frac{E_a}{RT} \qquad (5\text{-}24)$$

By plotting $\ln\left(\frac{d\alpha}{dt}\right)$ against $\frac{1}{T}$ at every 5 % degree of cure, the activation energy, E_a, is determined by multiplying the gradient by R. An example of the analysis for TG*p*AP/44'DDS is given in Figure 5.29. Five isotherms were used to allow for accurate linear regression to be undertaken. The linear relationship is generally good at low degrees of cure as the isotherms 'overlap' at these points. However, when higher degrees of cure are obtained, not every isotherm achieves that level of curing, reducing the number of points used for linear regression. Once the number of data points reaches two, activation energy cannot be calculated.

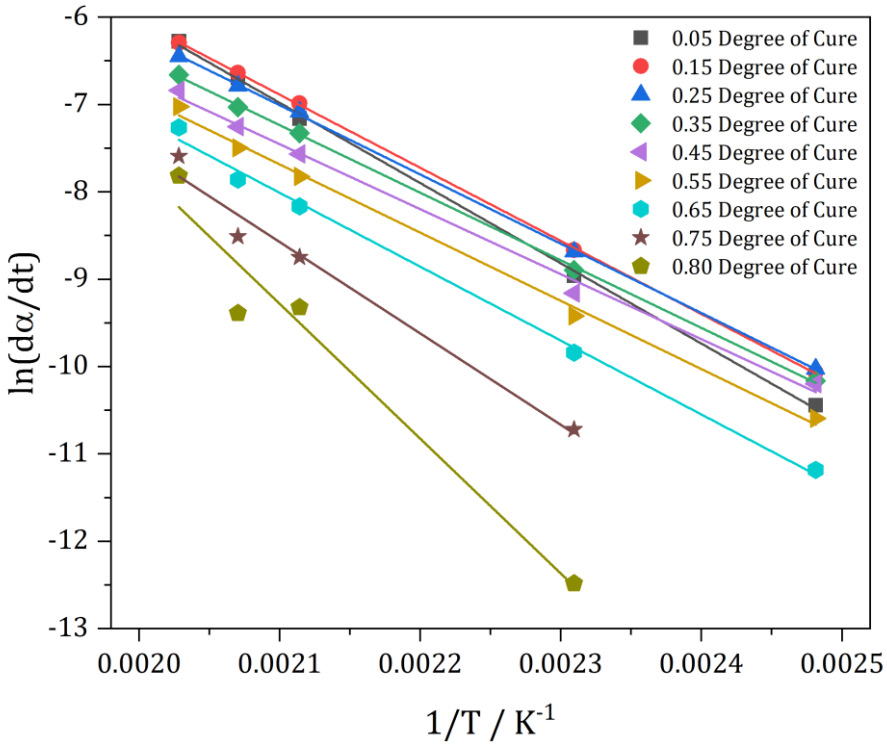

Figure 5.29 – Natural log of rate of reaction against the reciprocal of isotherm temperature at varying degrees of cure for the cure of TG*p*AP/44'DDS.

Applying this analysis to all four structural isomers of TGAP/DDS results in the activation energies shown in Figure 5.30. The activation energies are given between different degrees of cures for each formulation due to different extents to which the isotherms overlap. The TG*m*AP/44'DDS point at 75 % is marked with an asterisk as this is incorrect because this is the point at which the linear relationship transitions from being calculated by four isotherms to three isotherms. TG*m*AP/33'DDS activation energies only go up to 70 %, as after this point, there is an inverse relationship between isotherm temperature and rate of reaction, which would result in negative activation energies. This is known not to be the case. It can be assumed that it will continue to increase activation energy to a similar point as TG*m*AP/44'DDS.

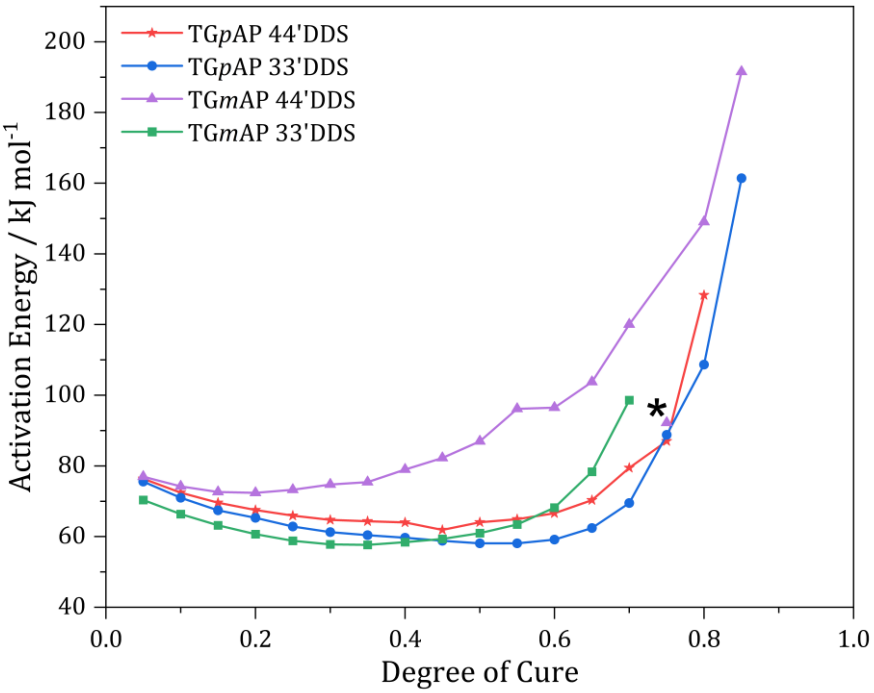

Figure 5.30 – Activation energies as a function of degree of cure for the four structural isomers of TGAP/DDS as calculated using equation (5-24). The asterisk noted values are anomalous data due to the analysis method.

At 10 % cured, all formulations show decreased activation energy, indicating that they are all autocatalytic reactions. The products of one reaction further catalyse the later reactions, resulting in a lower activation energy. All formulations start at nearly the same value, approximately 76 kJ mol^{-1}, apart from TG*m*AP/33'DDS, where the first activation energy value is 70 kJ mol^{-1}. All formulations then decrease until the trend separates based on the epoxy. The activation energies increased in the TG*m*AP formulations earlier at around 30 % degree of cure compared to that of TG*p*AP at 55 %. This could be related to the ease of etherification reactions compared to those in TG*m*AP. Varley *et al.* commented that the final activation energy of TGDDM was higher than the final activation energy of TG*p*AP because it only contained glycidyl amines [102]. If the result were extrapolated, the final values of TG*p*AP would be higher than TG*m*AP, which could be related to the behaviour of the glycidyl amine nitrogen as a tertiary amine catalyst in the initial portion of the reaction, which directs reactions to take place on glycidyl amine portion of the epoxy towards the end of the cure. Stutz and Mertes found that glycidyl amine-containing epoxies had a higher activation energy than glycidyl ether-containing epoxies [201].

The activation energies significantly increase towards higher degrees of cure as the epoxide group becomes more restricted in the crosslinked network, decreasing the possibility of reaction. The final trend is not as clear as the activation energies calculated when using the Friedman method under dynamic DSC measurements, as the overlap between the isotherm scans is smaller than the overlap between the dynamic scans, as commented on by Mittemeijer [222].

These values are useful but only model the cure as one reaction. The values are effectively an average of all reactions during the cure [208]. A more detailed kinetic analysis method is needed where the different reactions in the cure can be accounted for, and a better description of the cure mechanism is possible.

The general kinetic equation in (5-5) can be improved upon by assigning the function of conversion, $f(\alpha)$, a value shown in equation (5-25).

$$f(\alpha) = (1-\alpha)^n \tag{5-25}$$

Where n is the order of reaction and α is conversion or degree of cure. This refers to the concentration of the reactant, epoxide group, at any point during the cure and is shown in equation (5-26).

$$\alpha = \frac{[EP]_{initial} - [EP]_t}{[EP]_{initial}} \tag{5-26}$$

Where $[EP]_{initial}$ is the initial epoxide concentration, and $[EP]_t$ is the epoxide concentration at time t. At early points during the cure $1-\alpha$ will be large as the concentration of epoxide groups is large, resulting in a high probability of reactions, therefore a fast rate of reaction and low activation energy and *vice versa* towards the end of the cure. Applying equation (5-25) to the general kinetic equation gives equation (5-27) known as *n*th-order kinetics.

$$\frac{d\alpha}{dt} = k(1-\alpha)^n \tag{5-27}$$

Applying natural logs gives equation (5-28).

$$\ln\left(\frac{d\alpha}{dt}\right) = \ln(k) + n\ln(1-\alpha) \qquad (5\text{-}28)$$

If the reaction obeys *n*th-order kinetics, then the maximum rate of reaction should occur at $t = 0$. The rate of reaction plots for the five isotherms of the structural isomers of TGAP/DDS in Figure 5.27 shows this is not the case. It can also be shown by plotting $\ln\left(\frac{d\alpha}{dt}\right)$ against $\ln(1-\alpha)$ and as equation (5-28) takes the form of $y = mx + c$, the plot should be linear with the gradient being the order of reaction, n. This is shown in Figure 5.31 where the rate of reaction has been analysed for the four structural isomers of TGAP/DDS at a 160 °C isotherm. These are clearly not linear plots, indicating that the formulations do not obey nth-order kinetics. This is true for all isotherms, but it is not shown here; see Appendix 2 and Appendix 3. The results agree with the findings of Varley *et al.,* who studied the isothermal cure of TG*p*AP/44'DDS [102].

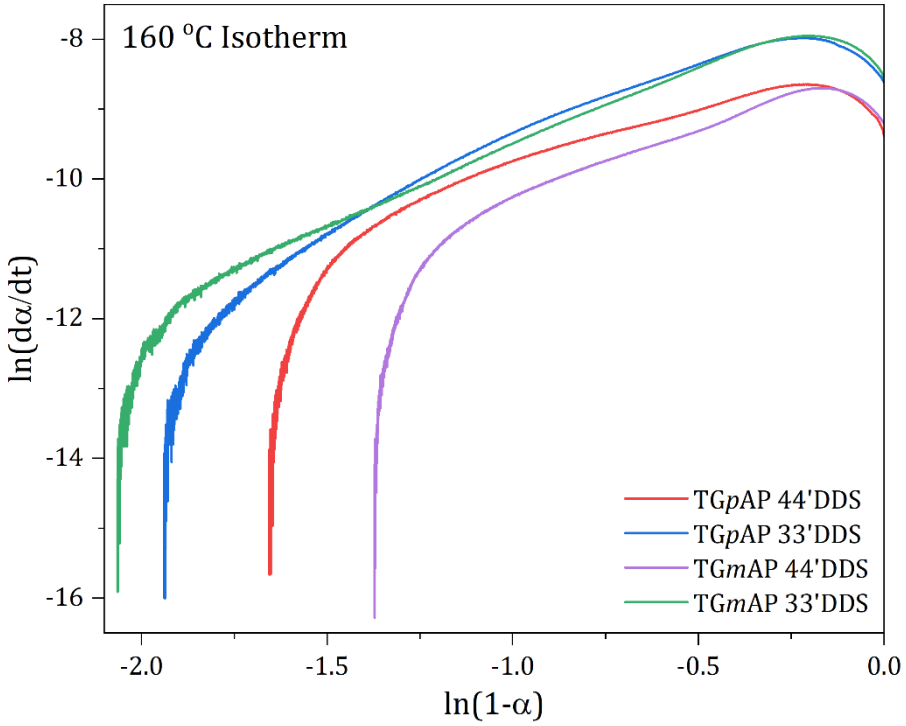

Figure 5.31 – Natural log of rate of reaction against natural log of $(1-\alpha)$ for the four structural isomers of TGAP/DDS under 160 °C isothermal heating.

Smith *et al.* proposed that any hydrogen bond-containing species could catalyse reactions in the epoxy amine cure by forming a termolecular transition state [223]. The reaction scheme for this catalysis is shown in Figure 5.32. Any hydrogen-containing species in the system can do this, whether they are impurities or products of the epoxy amine reaction.

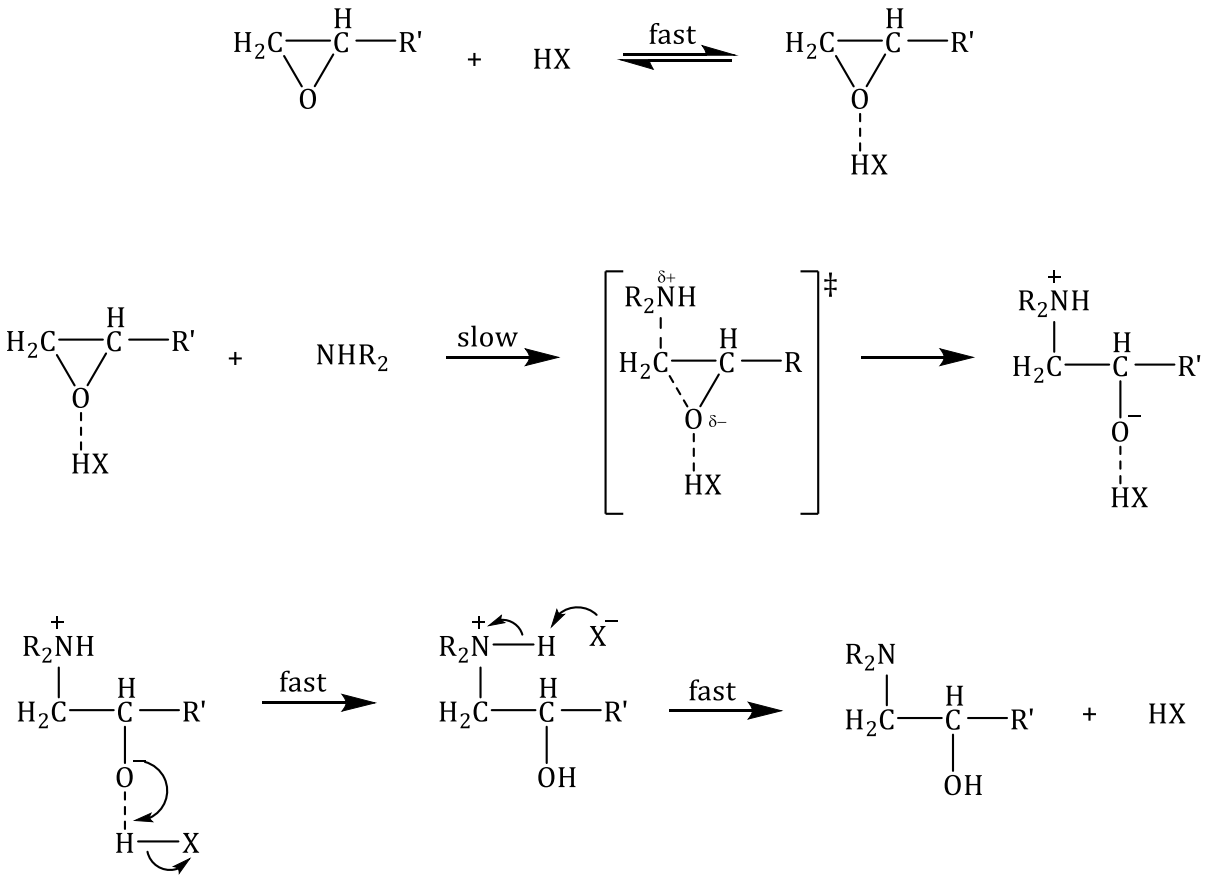

Figure 5.32 – Reaction scheme for the HX catalysed epoxy secondary amine reaction

The slow step is the rate-determining step, and due to the possibility of catalysis by the products of the epoxy amine reaction, an additional rate constant for this autocatalytic process results. From this interaction, Horie *et al.* derived the equation shown in equation (5-29) [105].

$$\frac{d\alpha}{dt} = (k_1 + k_2\alpha)(1-\alpha)(B-\alpha) \qquad (5\text{-}29)$$

Where k_1 is the un-catalysed (or non-autocatalysed) rate constant, k_2 is the autocatalysed (catalysed by the hydroxyls formed in the epoxy amine reaction) rate constant, and B is the ratio

of amine hydrogens to epoxy groups in the initial starting reagents. This model assumes that only epoxy amine reactions occur and that the reactivity of primary and secondary are the same [224]. This model has been simplified using a semi-empirical approach by Kamal and workers to give equation (5-30) [142,143,225].

$$\frac{d\alpha}{dt} = (k_1 + k_2\alpha^m)(1-\alpha)^n \qquad (5\text{-}30)$$

Where Kamal and Sourour have stated that m and n are temperature-independent constants [142]. $m + n$ are equal to the reaction the order, if $m + n = 2$, the reaction is said to bimolecular [102,224]. As with the Horie model, the Kamal and Sourour model also assumes that only epoxy amine reactions occur although the m and n values often allow for a better fit.

Literature often assumes that $m = 1$, such as the techniques used in both the TG*p*AP/44'DDS DSC study by Varley *et al.* and the TGDDM/44'DDS DSC study by Barton [102–104,127]. Applying $m = 1$ to equation (5-30) results in equation (5-31) when rearranged and should result a straight-line plot when the value of n is varied.

$$\frac{\frac{d\alpha}{dt}}{(1-\alpha)^n} = k_1 + k_2\alpha \qquad (5\text{-}31)$$

Equation (5-31) has been applied to all formulations at all isotherm temperatures. Figure 5.33 shows the resultant plots for the 160 °C isotherm for all formulations. Given the availability and ease of polynomial fitting tools using software such as OriginPro [178], this technique is not required. However, to highlight the quality of the fitting parameters, $m + n$ it is useful as the results do not agree with the values found in the literature. When Barton used this technique for TGDDM/44'DDS there was only deviation at high degrees of cure when the reaction became diffusion controlled [127]. Looking at the fits with a bit of forgiveness, some n values fit better than others. For TG*p*AP/44'DDS, it is approximately $n = 2.5$, TG*p*AP/33'DDS approximately $n = 3$, TG*m*AP/44'DDS approximately $n = 3$ and TG*m*AP/33'DDS approximately $n = 3$. The reason behind this poor fitting is that the autocatalytic model does not account for any other reaction other than epoxy amine reactions. The ratio used in this study has a significant epoxy excess, a

1.72:1 epoxy to amine ratio. When this is the case, a larger proportion of the reactions will be etherification. These unaccounted etherification reactions cause the plot to kink meaning a good linear fit will unlikely be achieved. Corezzi *et al*. suggests that the m and n are included in the model to account for non-stoichiometry and simplify the calculation but this doesn't seem to be the case here [224]. When stoichiometric ratios are used, the agreement is good, such as in Barton, and the same in near stoichiometric ratios, such as Varley *et al.,* who used a 1.1:1 epoxy to amine ratio and achieved sensible data [102,127].

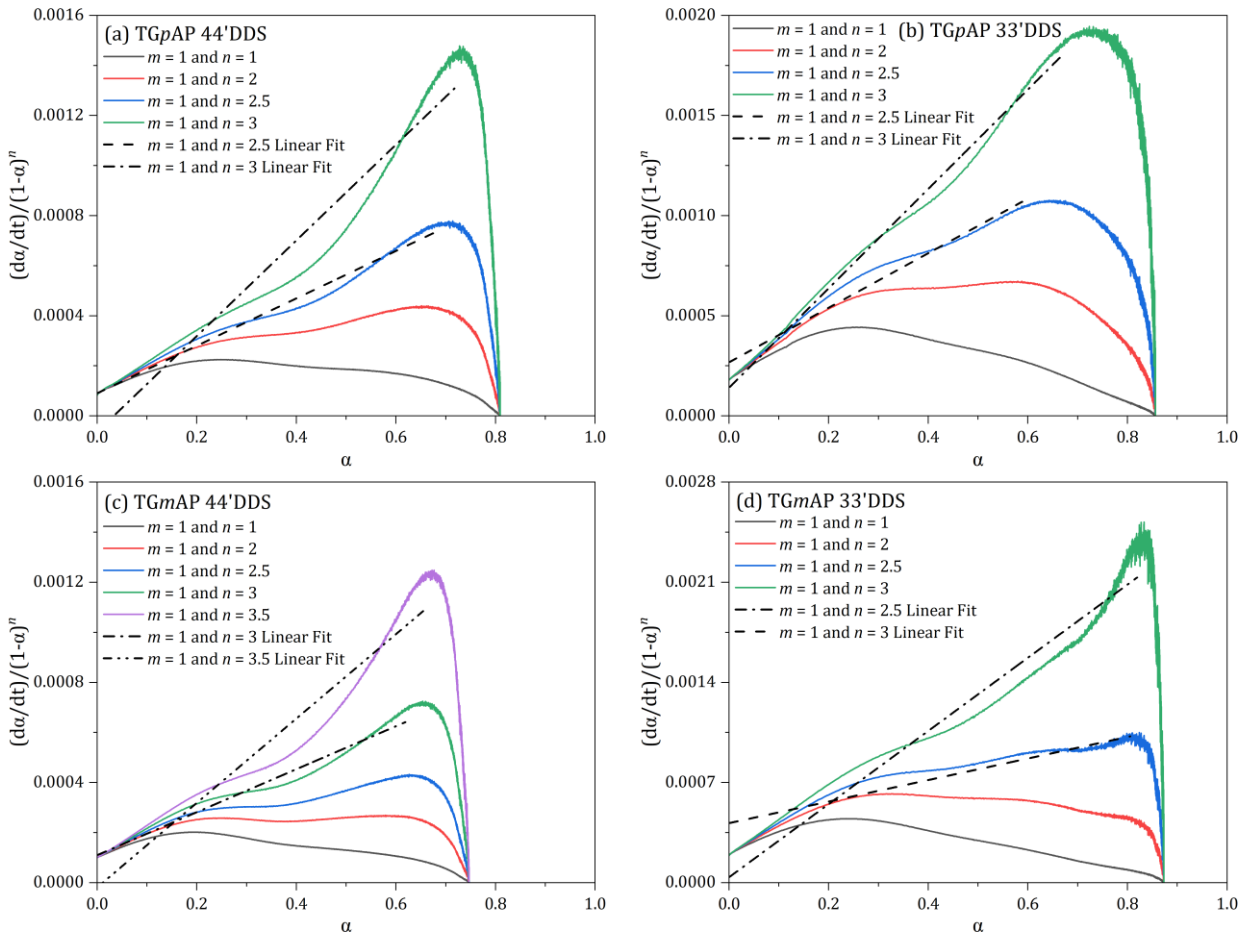

Figure 5.33 – Determination of n when $m = 1$ using equation (5-31) for the four structural isomers of TGAP/DDS under 160 °C isothermal heating conditions: : (a) TG*p*AP/44'DDS, (b) TG*p*AP/33'DDS, (c) TG*m*AP/44'DDS and (d) TG*m*AP/44'DDS.

The values of m and n indicate the order of reaction for the rate-determining step. Varley *et al.* found that $m + n = 3$, suggesting the reaction order was three, which agrees with the rate-

determining step being termolecular as suggested by Smith *et al.* [102,223]. This is not the case here, $m + n > 3$. This is not suggesting that the rate determining step is not termolecular, just that due to the excess epoxy in the system, the values of m and n must be higher to account for the additional etherification reactions that take place during the reaction that are not accounted for by the autocatalytic model.

Taking these m and n into account, it is possible to fit the data to equation (5-30) using a polynomial fitting tool. It is possible to assign the values of m and n with the tool and fit the data, and obtain values for the rate constants, k_1 and k_2 or the tool can be allowed to guess the values of m and n, therefore removing the need to set $m = 1$ and obtain possibly more accurate values.

The rate of reaction against degree of cure plot for TG*p*AP/44'DDS in Figure 5.34 shows that if either $m = 1$ and $n = 1$ or $m = 1$ and $n = 2$ is used the fit is extremely poor. This is the case for all formulations at all isotherm temperatures; therefore, further analysis will not show these values.

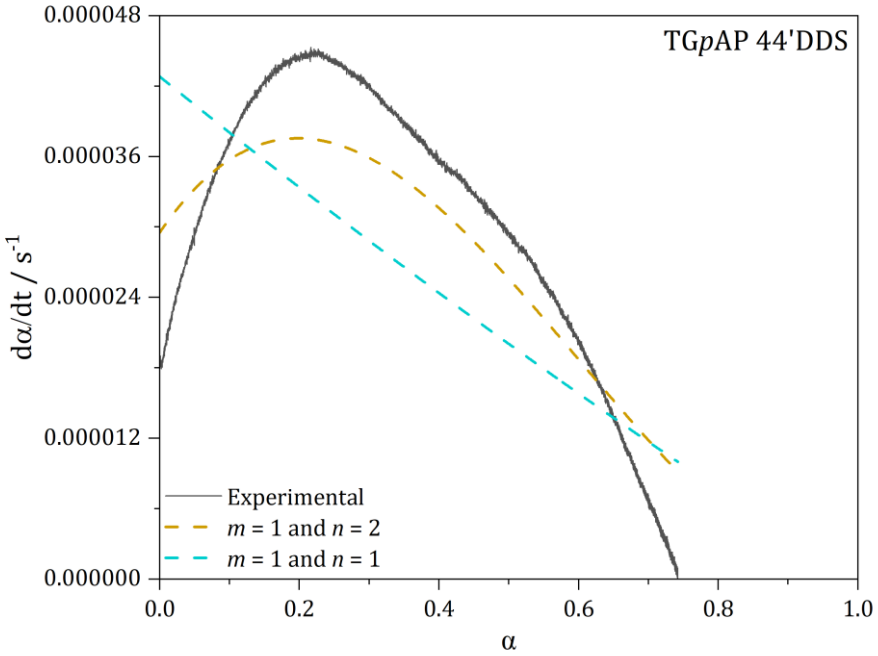

Figure 5.34 – Rate of reaction against degree of cure for the TG*p*AP/44'DDS under 130 °C isothermal heating conditions fitted to the autocatalytic model in equation (5-30) with m and n set to $m = 1$ and $n = 1$ and $m = 1$ and $n = 2$.

The same method is applied to all formulations at all isotherm temperatures. Determining the goodness of fit is difficult, but generally, where the fit is good at low degrees of cure will determine the suitability. At higher degrees of cure, the reaction becomes diffusion-controlled, and this model does not account for this. Vyazovkin and Sbirrazzuoli suggested that diffusion control can impact the cure as early as 30 % cured [208]. Given the model's assumptions, the fit towards the end should be higher than the experimental data if diffusion control dominates.

Figure 5.35 shows the difference in fitting when using different m and n values for the 130 °C isotherm for the structural isomers of TGAP/DDS where the underlined legend is the parameters with the best fit. $m = 1$ results in best fit for all formulations, but the n values differ based on epoxy. For the TG*p*AP formulations, n is approximately 3 and for the TG*m*AP, it is 4.0 for 33'DDS and 4.7 for 44'DDS.

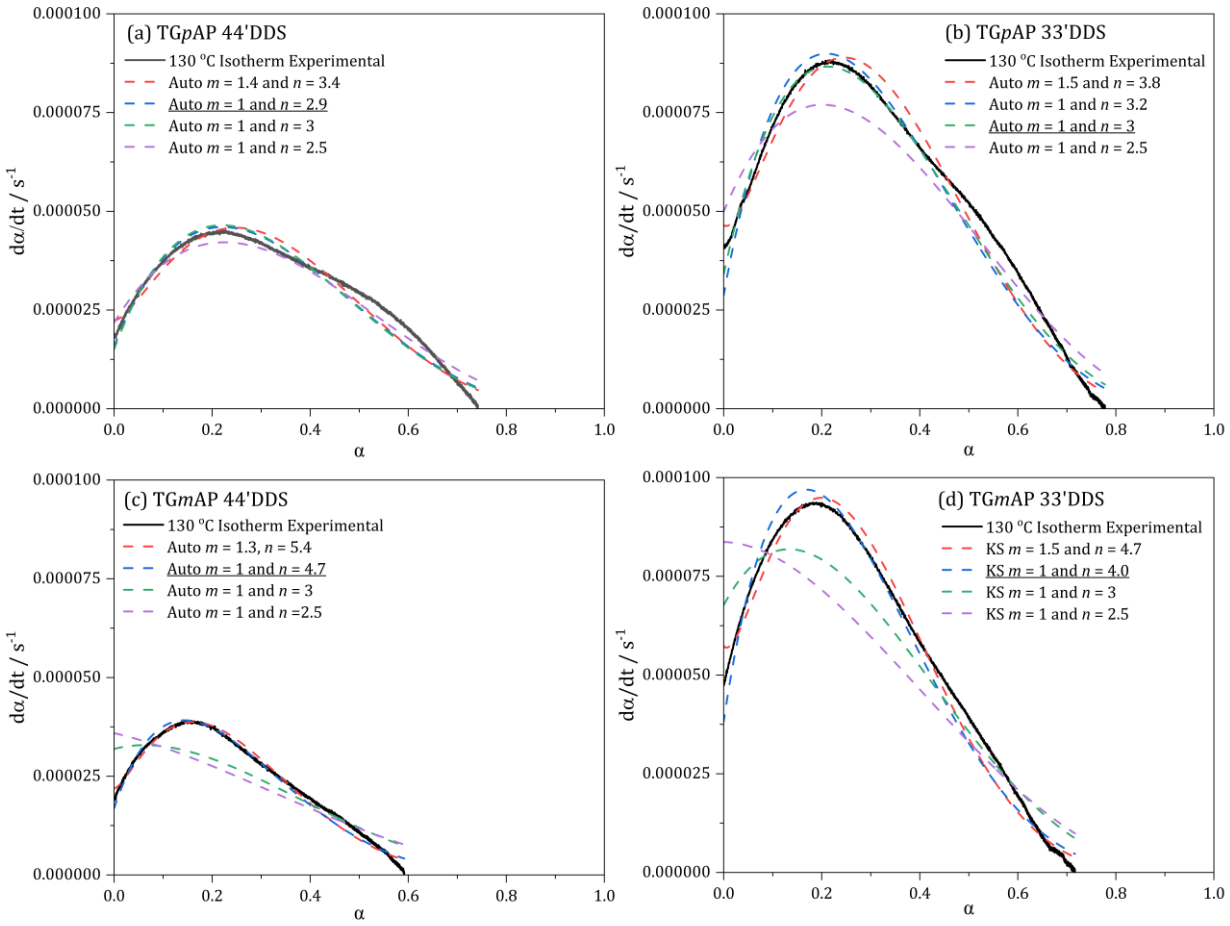

Figure 5.35 – Rate of reaction against degree of cure for the structural isomers of TGAP/DDS under 130 °C isothermal heating conditions fitted to the autocatalytic model in equation (5-30) where m and n vary: (a) TG*p*AP/44'DDS, (b) TG*p*AP/33'DDS, (c) TG*m*AP/44'DDS and (d) TG*m*AP/44'DDS.

Between 50 and 60 % degree of cure, the autocatalytic model underpredicts the rate of reaction for the TG*p*AP formulations. This suggests that a reaction that isn't taken into account by the model is occurring. Potentially indicating, etherification reactions.

When degree of cure exceeds 60 % and rate of reaction decreases towards 0 s^{-1}, the autocatalytic model over predicts the rate of reaction. This relates to vitrification of the material and the limit of the autocatalytic mode [104]. Initially, the cure is chemically controlled as the reactants are yet to be crosslinked. However, upon crosslinking, the reaction becomes diffusion controlled, as the mobility of the reactive groups are restricted. Diffusion control is more apparent in isothermal measurements, as the temperature remains constant, as T_g increases, whereas in dynamic measurements, temperature constantly increases to a temperature that usually exceeds the maximum T_g of the cure network, so there is still flexibility in the network allowing reactive groups to further react although much slower than when the reactive groups are not crosslinked. A similar trend of diffusion control is also seen when the autocatalytic model is applied to the 160 °C isotherm for the four formulations of TGAP/DDS.

Figure 5.36 shows the difference in fitting when using different m and n values for the 160 °C isotherm for the structural isomers of TGAP/DDS where the underlined legend is the parameters with best fit. In this case, m is roughly 1 for all formulations. The n values are not exactly 3 for all formulations: TG*p*AP/44'DDS $n = 2.9$, TG*p*AP/33'DDS $n = 3.1$, TG*m*AP/44'DDS $n = 3.5$ and TG*m*AP/33'DDS $n = 3.2$.

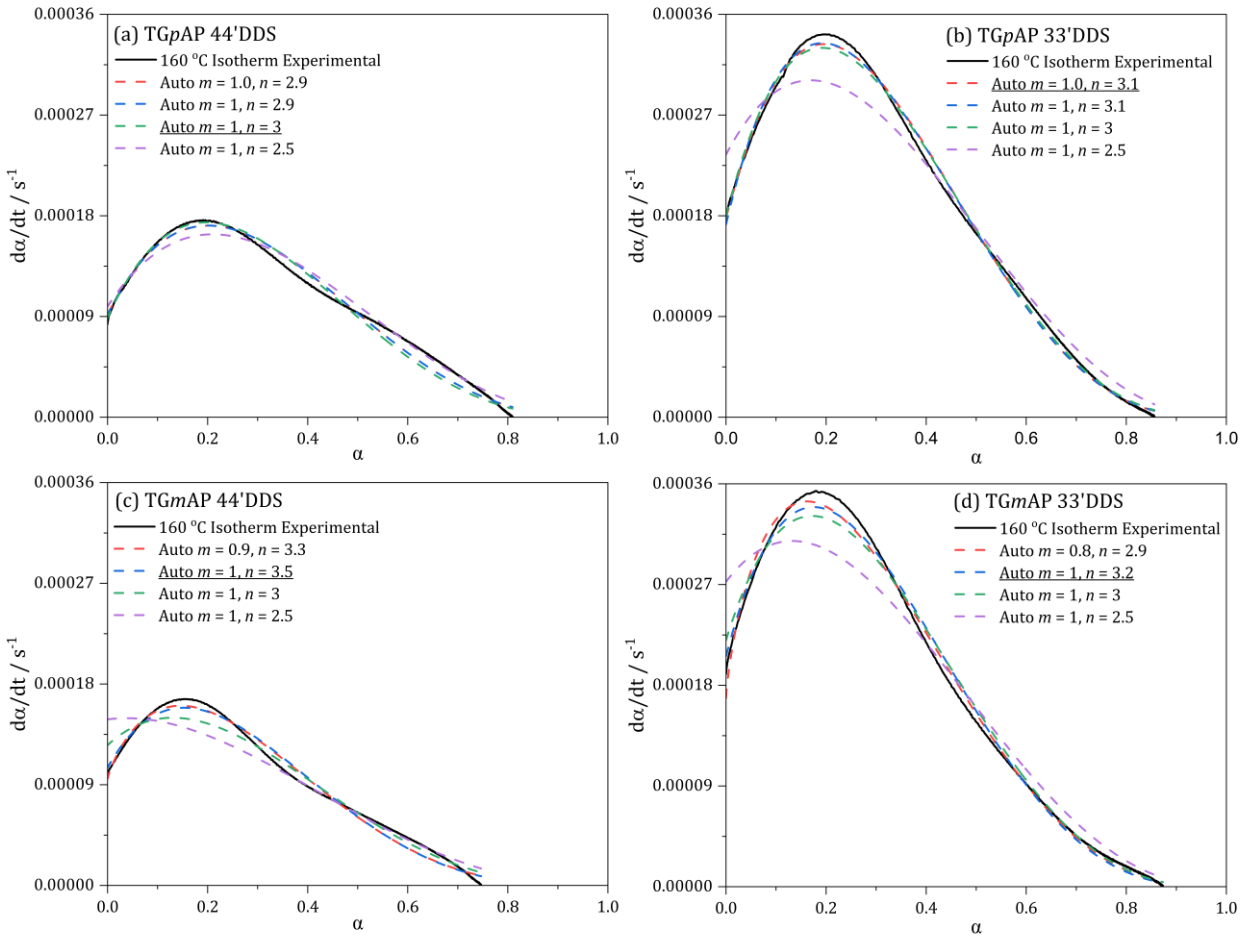

Figure 5.36 – Rate of reaction against degree of cure for the structural isomers of TGAP/DDS under 160 °C isothermal heating conditions fitted to the autocatalytic model in equation (5-30) where m and n vary: (a) TG*p*AP/44'DDS, (b) TG*p*AP/33'DDS, (c) TG*m*AP/44'DDS and (d) TG*m*AP/44'DDS.

Figure 5.37 shows the difference in fitting when using different m and n values for the 160 °C isotherm for the structural isomers of TGAP/DDS where the underlined legend is the parameters with the best fit, as with the previous isotherm temperatures, $m = 1$. At 200 °C there is better agreement between the formulations as $n = 3$ for TG*p*AP/44'DDS, TG*m*AP/44'DDS and TG*m*AP/33'DDS, whereas for TG*p*AP/33'DDS $n = 3.2$. It must be noted that the fit with experimental data at this temperature is considerably worse than both 130 and 160 °C. This is related to etherification, as it can readily occur at this temperature. For TG*p*AP/44'DDS, TG*m*AP/44'DDS and TG*m*AP/33'DDS at 30 to 50 % degree of cure, the model overpredicts the rate of reaction, suggesting that diffusion control occurs here. However, after

this point, the epoxy rate of reaction is higher than the model, suggesting that significant etherification occurs at this point.

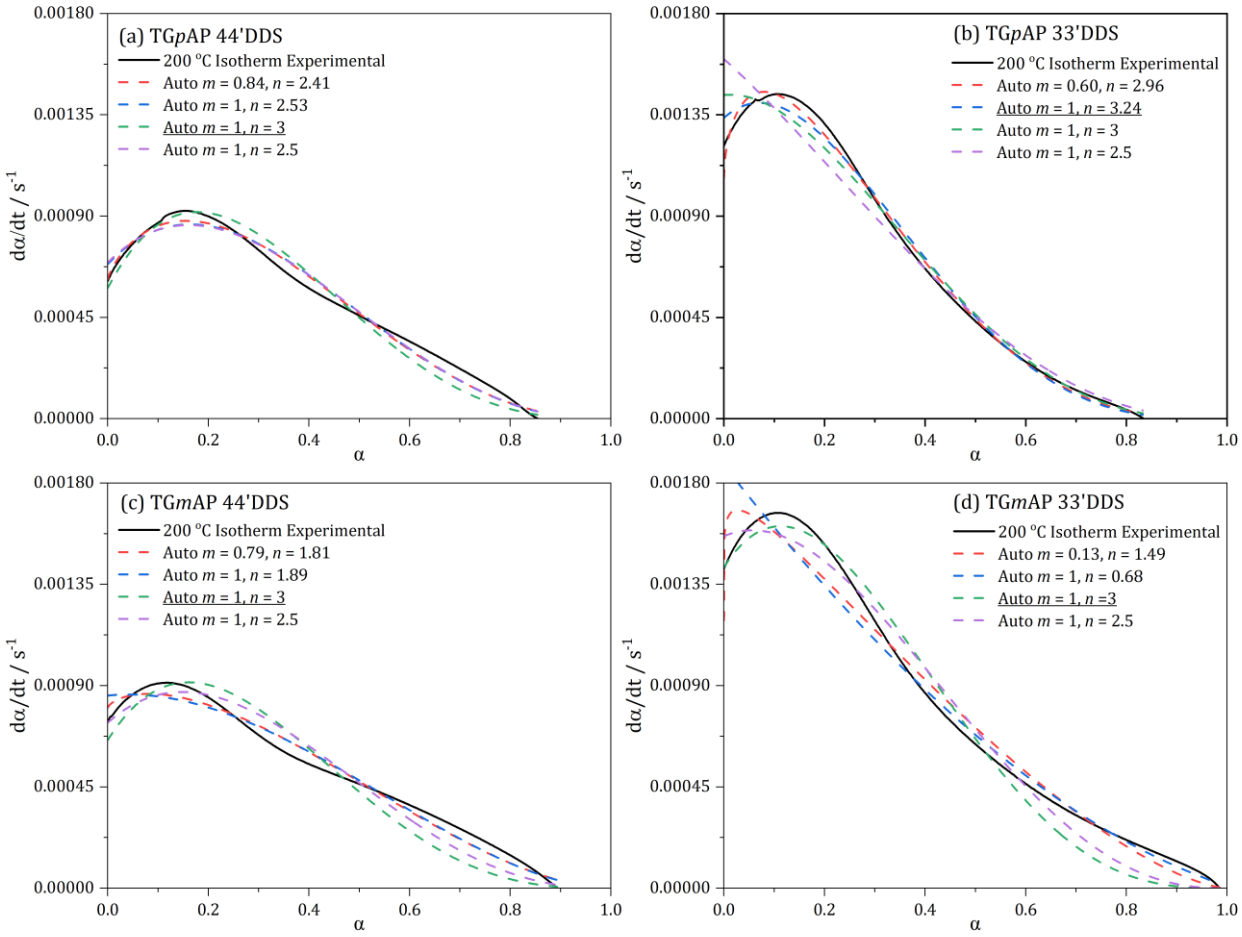

Figure 5.37 – Rate of reaction against degree of cure for the structural isomers of TGAP/DDS under 200 °C isothermal heating conditions fitted to the autocatalytic model in equation (5-30) where *m* and *n* vary: (a) TG*p*AP/44'DDS, (b) TG*p*AP/33'DDS, (c) TG*m*AP/44'DDS and (d) TG*m*AP/44'DDS.

As seen above, the values of *m* and *n* do vary according to temperature, especially in the TG*m*AP formulations. The values are summarised in Table 5.5. Cole *et al.* commented on this in their study of TGDDM/44'DDS. They found that as temperature increased, both the values of *m* and *n* decreased, with *m* decreasing from 1.07 to 0.77 and *n* decreased from 3.13 to 1.96 in a 40 °C temperature range [104]. Going off the general assumption that *m* and *n* indicate reaction order this would indicate that the rate determining step was changing depending on temperature.

Table 5.5 - m and n values for the four structural isomers of TGAP/DDS when fitting experimental data to the autocatalytic equation (5-30).

		TG*p*AP 44'DDS	TG*p*AP 33'DDS	TG*m*AP 44'DDS	TG*m*AP 33'DDS
130 °C Isotherm	m	1	1	1	1
	n	2.9	3	4.7	4.0
160 °C Isotherm	m	1	1.0	1	1
	n	3	3.1	3.5	3.2
200 °C Isotherm	m	1	1	1	1
	n	3	3.2	3	3

It is easy to get bogged down in the m and n values and their significance, but in the case of this model, they are effectively fitting factors. Treating them as this, as it is known that the model does not fully support these epoxy systems, helpful information can still be obtained. The rate constants, k_1 and k_2 are obtained from the fitting using the m and n values shown above and are shown in Table 5.6 The rate constant is one order of magnitude higher for the autocatalysed rate constant, suggesting that this reaction occurs at a much higher rate than the non-autocatalysed reaction. The rate constants for the 33'DDS formulations are approximately double that of the 44'DDS formulations in the 130 and 160 °C isotherm. In contrast, in the 200 °C isotherm, the 33'DDS autocatalysed rate constants are similar to the 44'DDS formulations, although still slightly higher, suggesting the reaction occurs faster for reasons discussed throughout.

Table 5.6 – Kinetic parameters for the four formulations of TGAP/DDS using the autocatalytic model in equation (5-30) at three different isotherm temperatures (130, 160 and 200 °C).

	TG*p*AP 44'DDS		TG*p*AP 33'DDS		TG*m*AP 44'DDS		TG*m*AP 33'DDS	
Temperature / °C	k_1 / x 10^{-4} s^{-1}	k_2 / x 10^{-4} s^{-1}	k_1 / x 10^{-4} s^{-1}	k_2 / x 10^{-4} s^{-1}	k_1 / x 10^{-4} s^{-1}	k_2 / x 10^{-4} s^{-1}	k_1 / x 10^{-4} s^{-1}	k_2 / x 10^{-4} s^{-1}
130	0.158	3.63	0.341	6.74	0.169	4.48	0.382	9.79
160	0.890	12.6	1.79	26.1	1.05	11.6	2.06	23.8
200	5.80	60.3	13.4	64.3	6.57	55.4	14.3	77.8

The respective rate constants' activation energy and pre-exponential factors can be obtained using the Arrhenius relationship shown in equation (5-32).

$$\ln(k_n) = \ln(A_n) - \frac{E_{a_n}}{RT} \qquad (5\text{-}32)$$

The linear relationship between the two rate constants and isotherm temperature is shown in Figure 5.38. Without analysing the activation values, there are apparent similarities based on the hardener.

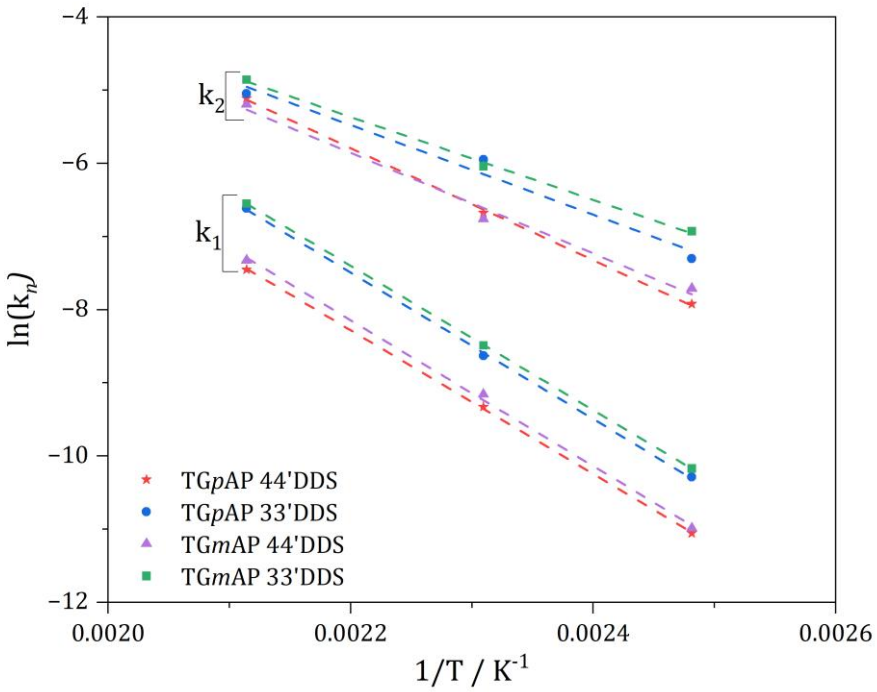

Figure 5.38 – Natural log of rate constant against the reciprocal of isotherm temperature for the four structural isomers of TGAP/DDS after fitting the autocatalytic model in equation (5-30) at three different isotherm temperatures (130, 160 and 200 °C). Where the non-autocatalysed rate constant is k_1 and the autocatalysed rate constant is k_2.

Activation energies and pre-exponential factors are given in Table 5.7 for the four structural isomers of TGAP/DDS from the kinetic parameters obtained from fitting the autocatalytic model in equation (5-30) using the Arrhenius relationship in equation (5-32). It is important to remember that the activation energies are not of specific reactions. Instead, the general reactions catalysed by either impurities (non-autocatalysed) or by catalysis from reaction products (autocatalysis).

Table 5.7 – Activation energies and pre-exponential factors for the four structural isomers of TGAP/DDS using kinetic rate constants obtained from the autocatalytic model in equation (5-30) as calculated using the Arrhenius relationship in equation (5-32).

		TG*p*AP 44'DDS	TG*p*AP 33'DDS	TG*m*AP 44'DDS	TG*m*AP 33'DDS
E_a / kJ mol^{-1}	k_1	81.5	83.2	82.8	82.0
	k_2	63.7	50.8	57.1	47.0
A / s^{-1}	k_1	595,000	202,0000	946,000	162,0000
	k_2	64100	2850	10600	1180

The activation energy for k_1, the non-autocatalysed reaction is similar between formulations, whereas the activation energy for the autocatalysed reaction is lower in the 33'DDS formulations. The pre-exponential factor is a magnitude higher in the 33'DDS formulations, suggesting that the number of collisions that occur with the required activation energy is much higher. Therefore, the number of species capable of catalysing the epoxide group is higher. However, this number of successful collisions is lower for the autocatalysed reaction, as shown by the much lower pre-exponential factor in the 33'DDS formulations. TG*m*AP/44'DDS has slightly lower autocatalysed activation energy than TG*p*AP/44'DDS, owing to its non-linear epoxy structure. Still, the frequency factor shows the number of collisions with the required activation energy is lower.

The activation energies for TG*p*AP/44'DDS are similar to that obtained by Varley *et al.* despite the difference in the m and n values, they obtained 79.6 kJ mol^{-1} for the non-autocatalysed reaction and 62 kJ mol^{-1} for the autocatalysed reaction [102].

This analysis has shown that the autocatalytic model can easily describe the kinetics of the cure of the four structural isomers of TGAP/DDS while obtaining activation energies comparable to those in the literature. It is possible to use more accurate models such as ones that account for diffusion control when epoxy vitrifies, such as those by Barton or Chern and Poehlein [126,127,147]. However, in this case, these models only slightly improve the fit, most probably due to the excess of epoxy used in the formulations; therefore, they will not be analysed here. An example of the Barton diffusion control model fitted to experimental data is shown in Appendix 4. Cole *et al.* also developed a model for accounting for etherification during the cure by analysing the seven different etherification reactions possible, but this didn't

improve the fit as well as expected because it still had to make assumptions about the relative reactivities of the primary and secondary amines which incorporated significant error [104,224,226]. Kinetic modelling would only be improved by moving to a mechanistic model rather than an empirical one, which essentially defeats the point that an empirical model should be able to be implemented with minimal data and be easy.

5.4.3. CURE CYCLE MEASUREMENTS

The previous sections have highlighted how dynamic and isothermal measurements can be used to investigate the cure mechanism of epoxy resins by making predictions about the kinetic parameters and being able to calculate the activation energies. While this is very useful as it can allow predictions about the cure of epoxy resins, it doesn't give information about the multi-dwell cure cycles commonly used in curing composite parts. In the isothermal DSC measurements section 5.4.2, the isotherm temperatures used are also included in the standard cure cycle, but what happens in the ramp is not predicted, and when each isotherm starts, the resin is at different degrees of cure. The following section will analyse the thermal events of the four structural isomers of TGAP/DDS during the standard multi-dwell cure cycle.

It is possible to program the multi-dwell cure cycle into the DSC and measure the heat flow as if the resin were in the oven. The heat flow plot looks odd, but if the dwells and ramps are treated separately as isotherms and dynamic measurements, sense can be made of it.

One of the difficulties with this measurement is calculating the baseline to analyse the data. For dynamic measurements, the baseline was calculated as sigmoid from the start to the end of the cure. In contrast, for isothermal measurements, the baseline is taken as a straight line from the horizontal section where no more curing occurs. For a multi-dwell cure cycle, the baseline is calculated by curing the sample following the cure cycle and then repeating the procedure on the cured sample. It was determined that the samples are effectively 100 % cured after the cure cycle (no discernible residual exotherm peak in the dynamic scan); therefore, the baseline should be that of the cured sample. This method was taken from "Differential Scanning Calorimetry" by Höhne *et al.. W*hile not perfect, as the heat capacity of the cured sample and sample during cure differs significantly, it is the most accurate way possible with the equipment available [227]. An example of the baseline determination is shown in for the cure of TG*m*AP/33'DDS is shown in Figure 5.39.

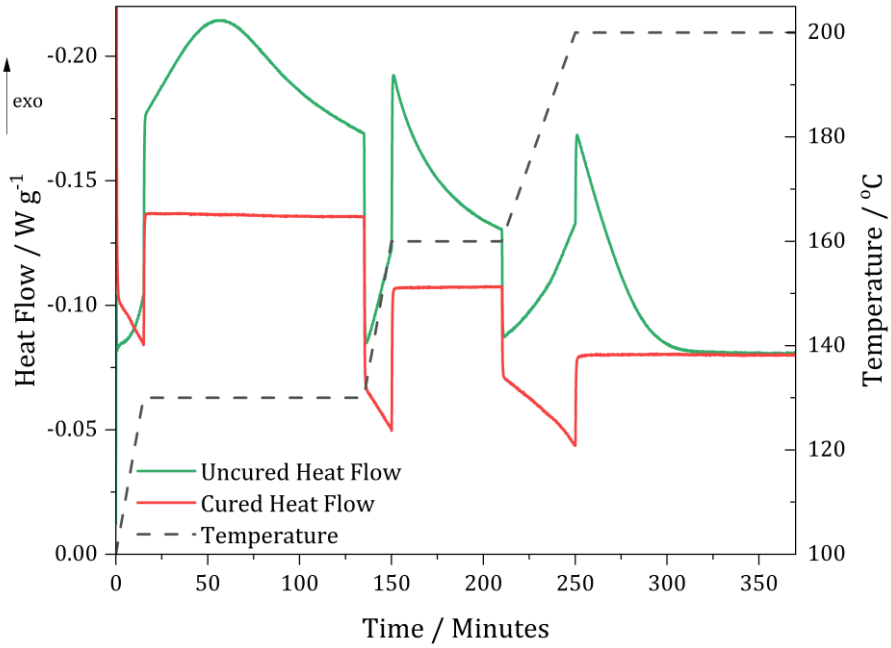

Figure 5.39 – An example of DSC heat flow baseline determination when taking a combination of dynamic and isothermal DSC measurements for TG*m*AP/33'DDS using the standard cure cycle. Red line indicates baseline determined from cured TG*m*AP/33'DDS DSC measurements.

The DSC heat flow plot for the four structural isomers of TGAP/DDS using the standard cure cycle is shown in Figure 5.40. As seen in section 5.3.1, when temperature measurements of the resin are taken during the cure, the same behaviour is seen. In the first dwell, the 33'DDS formulations are more exothermic. In the second dwell, the 44'DDS formulations are more exothermic, and finally, in the third dwell, the TG*m*AP formulations are more exothermic, but this final trend is not as clear cut as it was when directly measuring the temperature of the resins.

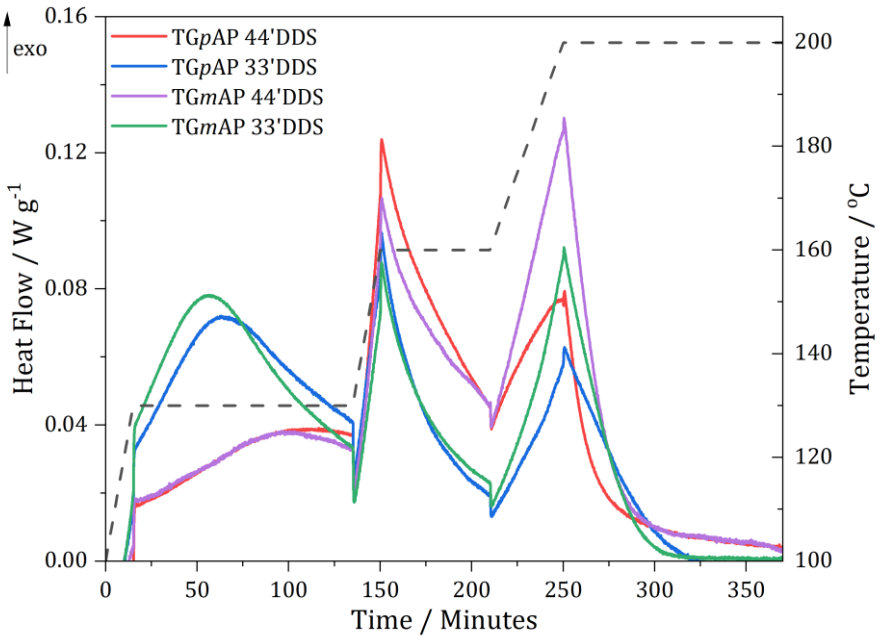

Figure 5.40 – DSC heat flow plot as a function of time for the four structural isomers of TGAP/DDS using the standard cure cycle. Exothermic is up.

Figure 5.40 will be separated into ramps and dwell to make analysing the different stages easier. Two plots will be shown, one to show the dwell and one to show the ramp up to the dwell where the x-axis is different, time and temperature, respectively.

For parts A and B of the cure (as defined in Figure 5.3), the heat plots are shown in Figure 5.41. (a) shows the temperature ramp up to 130 °C at 2 °C min^{-1}. Due to the significant difference in heat capacity between the uncured and cured samples, the baseline is not properly normalised compared to a standard dynamic plot. As it is over such a small temperature range, it would be foolish to do it by eye as well; therefore, rather than calculate enthalpy from this section, it is better qualitatively analysed. The gradient of the heat flow plots is similar based on the hardener initially. However, the 33'DDS formulations deviate from linearity in the exothermic direction at approximately 120 °C, whereas the 44'DDS formulations do not, suggesting a small amount of curing occurs during the ramp. Figure 5.41 (b) shows the 130 °C dwell where the plots are similar to the 130 °C isotherm measurements. The 33'DDS formulations peak earlier and to a higher heat flow value than the 44'DDS formulations and the TG*p*AP formulations peak slightly later than TG*m*AP formulations. The reason behind the delayed response of TG*p*AP is related to its linear structure, where the number of geometrical

configurations is lower; therefore, TG*m*AP has a higher probability of reacting, thus, a greater rate of reaction.

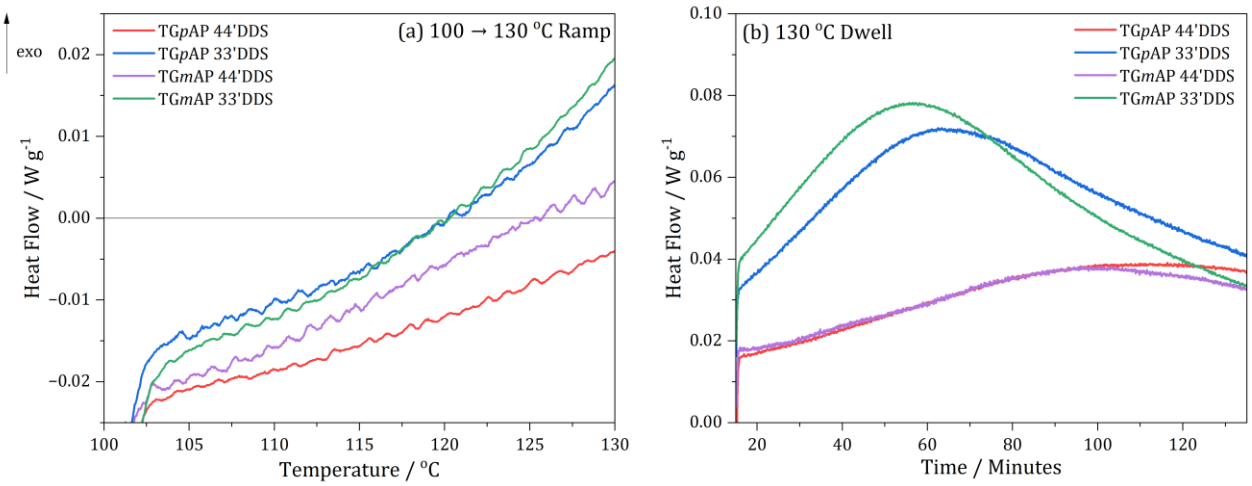

Figure 5.41 – DSC heat flow plots for the four structural isomers of TGAP/DDS: (a) as a function of temperature for the 100 to 130 °C temperature ramp (2 °C min^{-1}) and (b) as a function of time for the 130 °C dwell. Exothermic is up.

The heat flow plots in Figure 5.41 are for parts C and D of the cure. (a) shows the temperature ramp from 130 to 160 °C at 2 °C min^{-1}. The opposite is seen when compared to the 100 to 130 °C temperature ramp. The 44'DDS formulations are more exothermic during this ramp. This was seen when temperature measurements were taken for TGpAP/44'DDS but not for TGmAP/44'DDS, which behaved similarly to the 33'DDS formulations. TG*m*AP/44'DDS does show less exothermic behaviour but still more than the 33'DDS formulations. In the 44'DDS formulations, fewer reactions have occurred at this point, as shown in comparing the size of the 130 °C dwell peaks; therefore, there is a greater possibility of reactions occurring when the temperature increases. This follows on to the 160 °C dwell. The area of the exotherm is greater in the 44'DDS formulations than in the 33'DDS. The peak overall heat flow value is reached in the 160 °C dwell for the TG*p*AP formulations, suggesting the reaction rate is the greatest in the 160 °C dwell. However, the rate of reaction immediately starts to decrease after the peak value at 150 minutes.

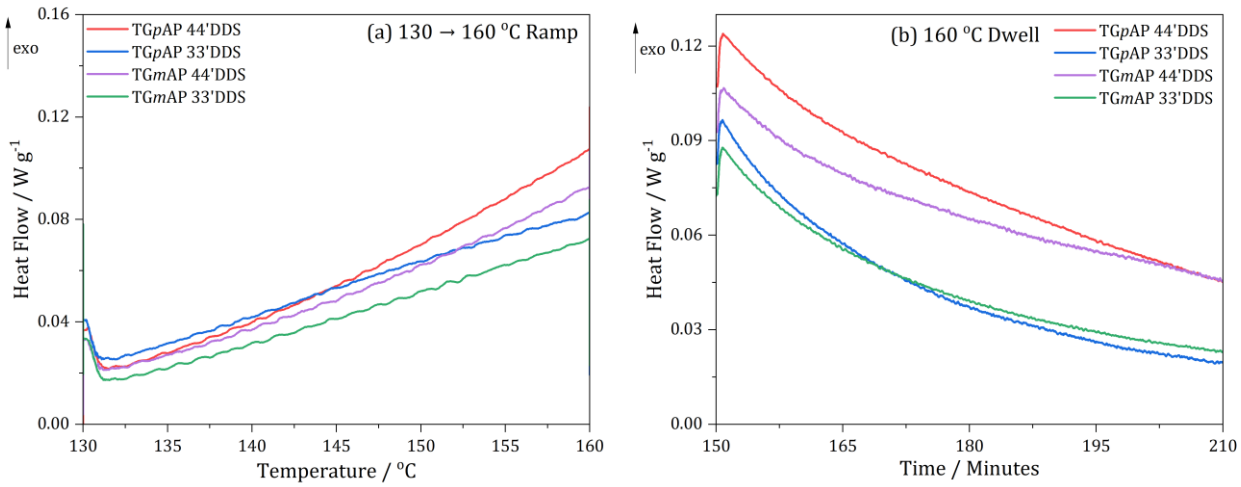

Figure 5.42 – DSC heat flow plots for the four structural isomers of TGAP/DDS: (a) as a function of temperature for the 130 to 160 °C temperature ramp (2 °C min^{-1}) and (b) as a function of time for the 160 °C dwell. Exothermic is up.

For parts E and F, the heat flow plots are shown in Figure 5.43. (a) shows the temperature ramp from 160 to 200 °C at 1 °C min^{-1}. The hardener formulations are paired initially, and then at higher temperatures, the TGmAP formulations show more exothermic behaviour in the ramp than the TG*p*AP formulations. Towards the end of the ramp, the rate of reaction in TG*p*AP/33'DDS increases, whereas in TG*p*AP/44'DDS, the rate of reaction decreases. The ramp provides additional energy and results in an increase in the rate of reaction as the effective free volume space increases, resulting in more space for diffusion, and as TG*m*AP and 33'DDS have non-linear components, this results in increased levels of curing, this doesn't seem to have the same effect on TG*p*AP/44'DDS due to its linear components. The 200 °C dwell sees the TG*m*AP formulations reach their highest rate of reaction point. The rate at which the heat flow decreases is greater in the 44'DDS formulations than the 33'DDS formulations, which is most likely related to diffusion control at this point; therefore, the probability of reactions is based on proximity and as 33'DDS has more possible geometrical configurations the probability of reacting should be higher. The 33'DDS formulations are fully cured by approximately 320 minutes, whereas the 44'DDS formulations don't show that they are fully cured. Towards the end, the heat flow plot is not entirely horizontal, suggesting some residual enthalpy, but this was not the case. This is, therefore, most likely related to baseline calculation.

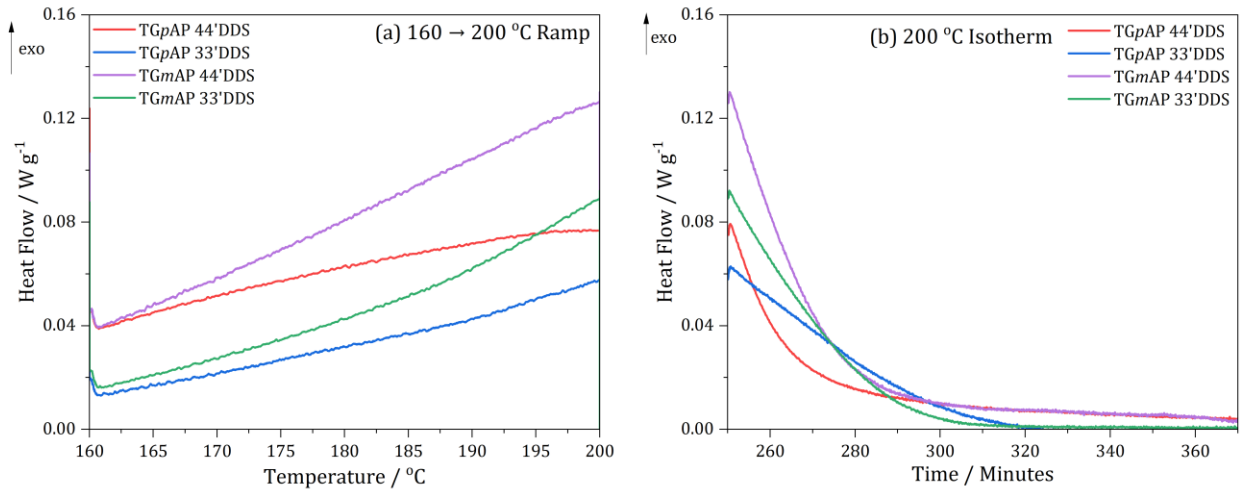

Figure 5.43 – DSC heat flow plots for the four structural isomers of TGAP/DDS: (a) as a function of temperature for the 160 to 200 °C temperature ramp (1 °C min^{-1}) and (b) as a function of time for the 200 °C dwell. Exothermic is up.

The degree of cure can be calculated using the equations in (5-2) for temperature ramps and (5-22) for dwells. Using the same method as above, the average enthalpy of cure obtained from dynamic scans will be used rather than assuming that the formulations are fully cured as no residual exotherm was shown. The enthalpy of reaction for the first temperature ramp from 100 to 130 °C will be assumed to be zero as the baseline calculation is not accurate at the very start of the reaction. The total enthalpy of reaction values are shown in Table 5.8 for each formulation compared to the average enthalpy of cure. TG*p*AP/44'DDS and TG*m*AP/33'DDS are effectively 100 % cured, with TG*m*AP/44'DDS slightly less cured, and then TG*p*AP/33'DDS is significantly less cured. This is unexpected as there was no exothermic peak in the residual dynamic scan, but this could be related to inaccuracies in the baseline determination. Accounting for this error, the values agree with the average values obtained from dynamic scans and confirm that the odd trends observed when undertaking isothermal measurements on TG*m*AP/33'DDS where the degree of cure decreased with isotherm temperature past 200 °C are correct.

Table 5.8 – Enthalpy of reaction and degree of cure values for the four structural isomers of TGAP/DDS cured using the standard cure cycles compared to the enthalpy of cure values obtained from five dynamic scans.

	TG*p*AP 44'DDS	TG*p*AP 33'DDS	TG*m*AP 44'DDS	TG*m*AP 33'DDS
ΔH_r / J g^{-1}	804.37	789.52	873.93	837.07
ΔH_0 / J g^{-1}	806.78	829.68	887.74	838.44
α / %	99.70	95.16	98.44	99.84

The evolution of degree of cure for the four structural isomers of TGAP/DDS is shown as a function of time in Figure 5.44. As seen throughout, the degree of cure behaviour initially pairs up according to the hardener. During the 160 °C dwell, TG*p*AP/44'DDS increases greater than TG*m*AP/44'DDS, where it then slows in the 160 to 200 °C temperature ramp and TG*m*AP/44'DDS significantly increases. Degree of cure stabilises early in the 200 °C dwell for the 33'DDS formulations, whereas the 44'DDS continue to cure until the cure cycle finishes. In all formulations, the rate at which the degree of cure increases, the rate of reaction, slows towards the end of each dwell and then increases at the start of a new dwell at a higher temperature. Through a temperature increase, the input of additional energy promotes reactions that may not have been possible at lower temperatures due to steric hindrance.

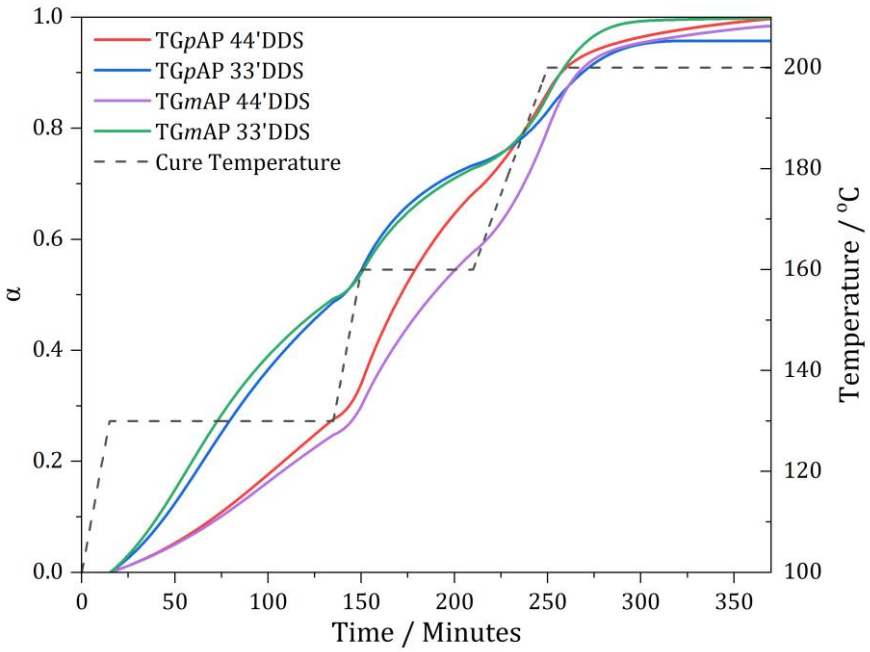

Figure 5.44 – Degree of cure for the four structural isomers of TGAP/DDS determined from DSC measurements of the standard multi-dwell cure cycle.

Having obtained the degree of cure, it is possible to obtain the rate of reaction and compare it to the rate of reaction values obtained in the earlier sections. It will not be done for the whole cure cycle as the ramps use a heating rate that was not tested in the dynamic measurements, and due to the baseline determination difficulties, they would not show good agreement. A comparison between the rate of reaction obtained for isothermal and cure cycle measurements at the same degree of cure values are made for the four structural isomers of TGAP/DDS in Figure 5.45. Note that the isothermal data overlaps with the cure cycle data, where the degree of cure values are at the same level. For some isothermal data, such as the 200 °C isotherm for TG*p*AP/44'DDS and TG*p*AP/33'DDS, the reaction did not cure to as high an extent as the cure cycle did; therefore, there is no or very little data to compare.

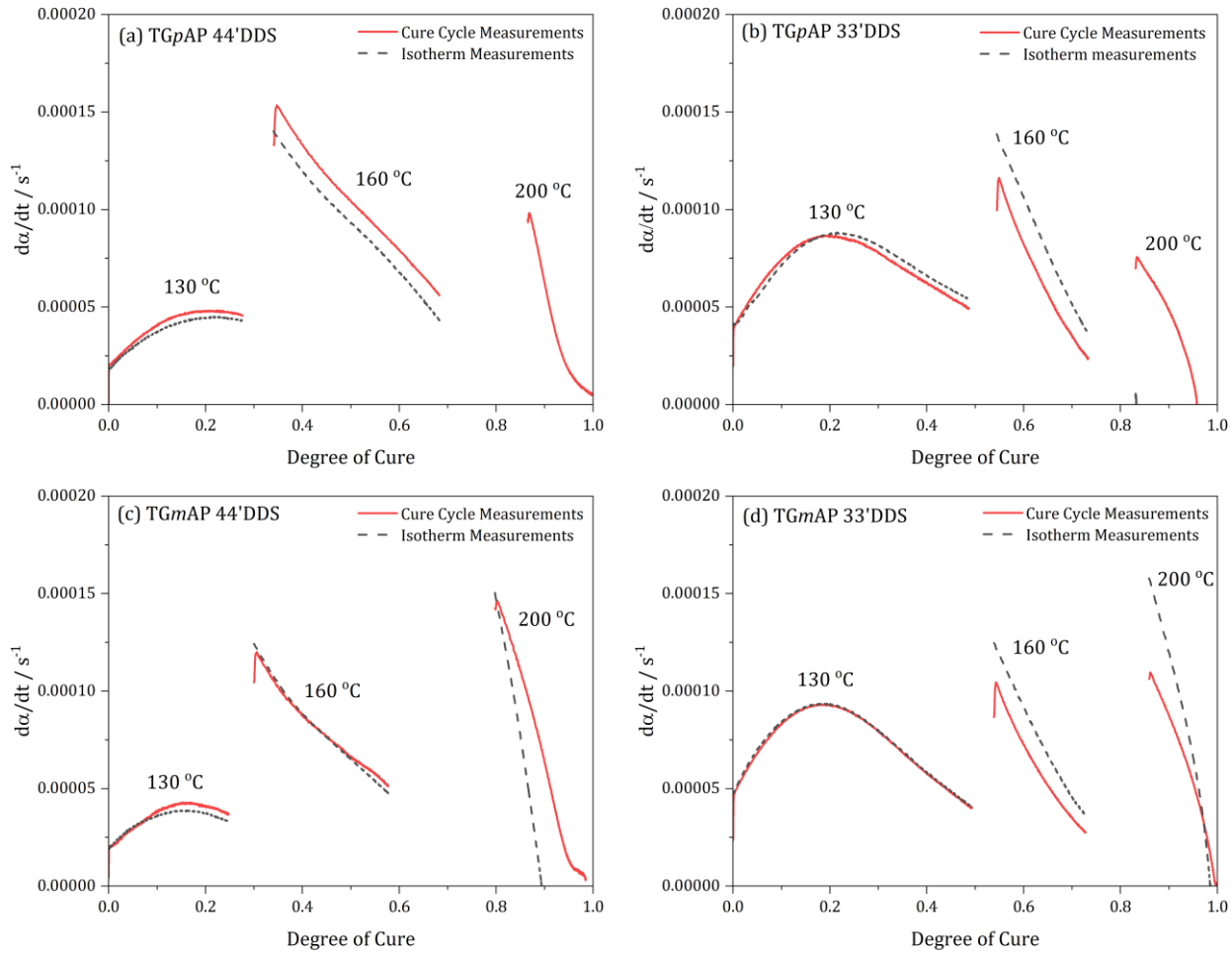

Figure 5.45 – Rate of reaction comparison between the measurements taken from the standard cure cycle and isothermal heating regimes for the four structural isomers of TGAP/DDS: (a) TG*p*AP/44'DDS, (b) TG*p*AP/33'DDS, (c) TG*m*AP/44'DDS and (d) TG*m*AP/33'DDS.

Generally, good agreement is seen at lower temperatures. The 130 °C agreement is excellent, mainly because this is at the start of the reaction. The curing mechanism will proceed similarly, which essentially shows good repeatability. The agreement for the 160 °C isotherm is also good but with some explainable disagreements. The TG*p*AP/44'DDS isotherm data shows lower rate of reaction values compared to the cure cycle data because the resin has undergone reactions at 130 °C, which are mainly epoxy primary amine reactions forming a linear structure. In contrast, in the isotherm measurements, the initial temperature is higher, 160 °C, the reactions are a combination of epoxy primary amine and epoxy secondary amine, the resin is more crosslinked. Therefore, in the cure cycle, when the temperature is increased to 160 °C, the rate of reaction is slightly higher as the network is less crosslinked and more mobile. The opposite

trend is seen for the 33'DDS formulations. The rate of reaction is shifted to lower values in the cure cycle measurements. As seen in the Chapter 4. NIR, epoxy primary amine and epoxy secondary amine reactions can occur at 130 °C; therefore, it could be expected that at those levels of cure, the amount of crosslinking is similar. When the temperature is constant in the isotherm, the reaction effectively self-heats, allowing further reactions to occur consistently. However, in the cure cycle, the 130 °C dwell causes the rate of reaction to drop and as the ramp is short and only goes up to 160 °C, there isn't sufficient enough energy in the system to react as fast as the 160 °C isotherm as the crosslinked network has slowed down and to get started again requires more energy than what the 130 to 160 °C ramp provides.

The comparison with the 200 °C isotherm and cure data is poor mainly due to the isotherms not achieving that level of cure as the reaction becomes diffusion controlled once the resin has vitrified. As the temperature is constant in an isotherm when curing reactions occur, the effective free volume decreases and the mobility of reactive species is hindered, reducing the ability of the network to achieve 100 % cure. In the case of the cure cycle, when the temperature ramp occurs, the effective free volume increases [17]. This allows for increased mobility and the reaction to go to higher levels of cure.

The good agreement between the 130 and 160 °C isotherms and cure cycle data suggests that even if the heating regime is different, similar reactions will occur at the same cure and temperature levels. The curing of epoxy resins can be effectively predicted using DSC.

5.5. CONCLUSION

While this has been an extensive chapter with large amounts of data, it has shown that the thermal response of epoxies can be measured and analysed to gain insight into the different network development that occurs. A simple technique such as measuring the resin temperature against oven temperature has shown that despite being rudimentary, the insight gained, while qualitative, gives a good understanding of what differences occur when different isomers of TGAP and DDS are used. It has confirmed the findings from Chapter 4. NIR that the 33'DDS formulations are initially more reactive than the 44'DDS formulations. The additional exothermic behaviour of 33'DDS initially suggests that more reactions occur in the 130 °C dwell than in 44'DDS, leading to the confirmation that not only epoxy primary amine reactions occur in this part of the cure, resulting in areas of localised crosslink density.

DSC, a significantly more sensitive method, has allowed for kinetic calculations of the curing process under isothermal and dynamic heating conditions. Obtaining activation energies and rate constants that agreed with literature for all formulations, the reaction was confirmed to be autocatalytic, with the effect being more significant in the 44'DDS formulations than in the 33'DDS formulations as shown by the high-frequency factor calculated in the isothermal data. Despite DSC not giving information on the types of reactions occurring, the poor agreement with the autocatalytic model at high degrees of cure suggested that etherification plays a prominent role in the cure of the four TGAP/DDS formulations, with the reaction occurring at lower temperatures for TG*p*AP formulations confirming the tertiary amine catalysis behaviour suggested in Chapter 4. NIR.

From this, DSC was applied to the multi-dwell cure cycle, which has not been seen before, and a comparison between the isothermal and cure cycle data resulted in good agreement. This suggests that the same mechanism occurs in the system at the same temperatures and degrees of cure.

This is only a basic application of kinetic analysis to these TGAP/DDS systems. There is considerably more work to be done and more insight that can be gained, ultimately allowing for predictions about structure properties and curing characteristics without lab experiments. However, the downside to DSC, unlike temperature measurements, these cure monitoring measurements cannot be taken while curing in the oven. The application to the manufacturing industry is limited as it would require downtime and lab space. A technique that can be run online, like near-infrared spectroscopy, is needed. This leads to the next chapter, where the findings from this and previous chapters will be applied to dielectric cure monitoring.

6. INVESTIGATING THE NETWORK DEVELOPMENT IN STRUCTURAL ISOMERS OF TGAP/DDS BY THEIR DIELECTRIC BEHAVIOUR

6.1. INTRODUCTION

In previous chapters of this study, epoxy resin's cure was monitored using optical and thermal behaviour. Another property that can be monitored is the electrical behaviour. Cured epoxy resins are poor conductors but can store charge because of their crosslinked structure. As a result, they are known as a dielectric material [150]. However, the starting materials are not due to the lack of crosslinking. They are 'good' conductors or at least better conductors than cured resin. The evolution of how conductivity changes during the cure can be monitored, and if the network formation is different, differences in the conductivity change can be seen. This method is known as dielectric analysis or dielectric cure monitoring.

It is a widely used technique in manufacturing due to its ability to determine whether a part is suitably cured [153]. Generally, industry is not interested in how conductivity changes in the cure, only the final value. The measurements are difficult to analyse, as suggested by Skordos and Partridge [151]. Still, most dielectric electric cure monitoring equipment is provided by a supplier that has developed its own software that can indicate the cure state directly from the obtained measurements, removing the need for expert analysis. In this study, the dielectric measurements will be obtained and then further analysed.

One of the benefits of dielectric analysis is that it can be run online while the resin or composite part is curing, unlike differential scanning calorimetry, where aliquots of the sample are removed to run tests. The sensors used in this study are single-use sensors, but it is possible to use reusable sensors. It is important to note that this study has not tested composites. Still, the results should be very similar as long as precautions are taken to account for the conductivity of the fibres if carbon fibre is used.

Researchers have studied the dielectric relaxations of different cured epoxy resins to investigate the differences in network morphologies. This can be very complicated. However, this will not be done in this chapter. Instead, a dielectric cure monitor manufactured by Lambient Technologies for use in industry will be used to investigate the differences in cure of the structural isomers of TGAP/DDS using a simple metric known as ion viscosity. A lot of the analysis techniques will be derived from a handbook written by Lee on behalf of Lambient

Technologies [153]. The idea is to see if similar behaviours seen in Chapter 4. NIR and Chapter 5. Thermal can be seen using this simple technique and to gain additional insights into the differences in network formation. If so, the technique can be used online to fine-tune the thermomechanical and mechanical properties of the resin while the part is being manufactured.

6.2. CHAPTER OVERVIEW

This chapter of the study will monitor the dielectric behaviour of the structural isomers of TGAP (triglycidyl-*para*-aminophenol and triglycidyl-*para*-aminophenol) and DDS (4,4'-diaminodiphenyl sulphone and 3,3'-diaminodiphenyl sulphone) during network formation using dielectric cure monitoring equipment. The dielectric behaviour will allow the identification of the critical points during the standard multi-dwell cure cycle, something that has not been widely studied in the literature. A comparison of when linear chain and crosslinking reactions occur during the standard cure cycle will be made possible. Following the theme of DSC, an analysis of the dielectric behaviour during isothermal and dynamic heating will also be made. The reliability of calculating cure state from dielectric measurements will also be investigated. Using dielectric analysis will give further information into the differences in network formation in the four structural isomers of TGAP/DDS and allow an understanding of how the curing process can be changed to fine-tune the epoxy resins' resultant properties. The methods used have been outlined in Chapter 3. Materials and Methods. Any changes or additional equations will be provided in this chapter.

6.3. DIELECTRIC CURE MONITORING

6.3.1. ISOTHERMAL MEASUREMENTS

Like with DSC and resin temperature measurements, different heating regimes have been used to understand the differences in the network formation in the four structural isomers of TGAP/DDS. The first type is isothermal heating, holding the samples at a constant temperature. However, unlike DSC isothermal measurements, it is not possible to heat the samples in the oven at a heating rate where no curing occurs, as this results in an exotherm. Two isotherms will be used, 130 °C and 160 °C, where the heating rate is 1 °C min^{-1} and 0.5 °C $min^{-1,}$ respectively, and

each will hold the samples at the respective temperatures for 12 hours. The two heating regimes will be named “130 °C dwell” and “160 °C dwell”.

6.3.1.1. 130 °C DWELL

As outlined in the Chapter 3. Materials and Methods, an alternating voltage is applied to the material, and the response current allows calculation of the relative permittivity and dielectric loss factor. Loss factor is given in the form of equation (6-1).

$$\varepsilon'' = \frac{\sigma}{\omega \varepsilon_0} \tag{6-1}$$

Where ε'' is dielectric loss factor, σ is conductivity, ω is angular frequency, and ε_0 is the permittivity of free space. From this, ion viscosity can be obtained, as shown in equation (6-2).

$$\log(IV) = \log\left(\frac{1}{\sigma}\right) = \log(\rho) \tag{6-2}$$

Where $\log(IV)$ is ion viscosity, and ρ is resistivity. Throughout this study, IV will be referred to as ion viscosity when it is actually $\log(IV)$. However, equation (6-1) only accounts for the component unaffected by frequency. There is a frequency-dependent component that must be considered, despite the assumption that it is negligible and is shown in equation (6-3).

$$\varepsilon'' = \frac{(\varepsilon_r - \varepsilon_u)\omega\tau}{1 + \omega^2\tau^2} + \frac{\sigma}{\omega \varepsilon_0} \tag{6-3}$$

Where ε_r is the relaxed permittivity, ε_u is the unrelaxed permittivity, and τ is the relaxation time. If the frequency-independent component is negligible, the IV data should be the same across all frequencies, which it is often not. Therefore, conductivity has to be considered as having both a frequency-dependent component (σ_{AC}) and frequency-independent component (σ_{DC}). Therefore, true IV is actually equation (6-4).

$$\log(IV) = \log\left(\frac{1}{\sigma_{DC}}\right) = \log(\rho_{DC}) \quad (6\text{-}4)$$

Where DC refers to direct current rather than AC, alternating current. Figure 6.1 shows IV as function of time for the 130 °C dwell cure of the four structural isomers of TGAP/DDS. The different frequencies show different values and also different trends.

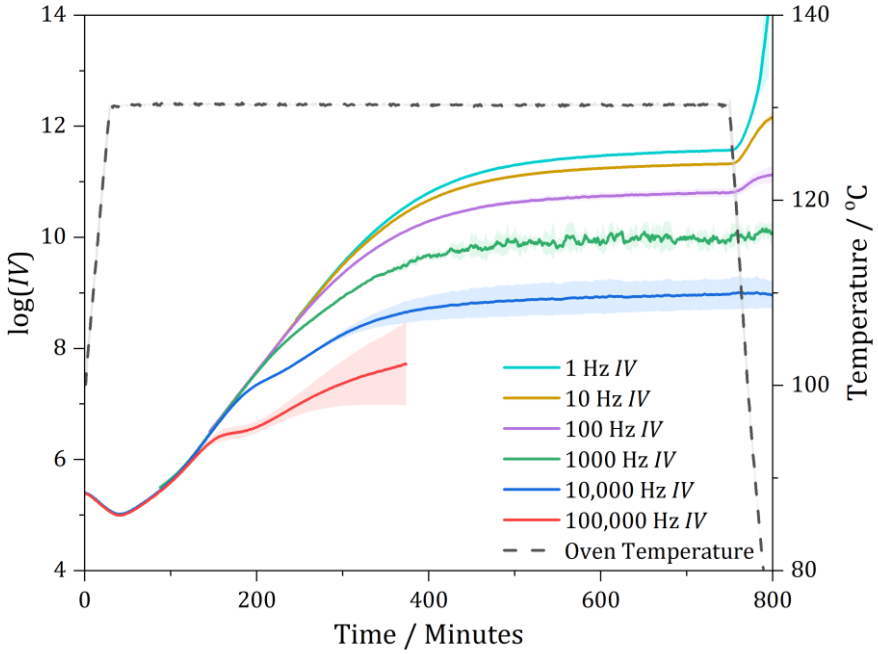

Figure 6.1 – Dielectric analysis of TG*p*AP/44'DDS using the 130 °C dwell cure at six different testing frequencies (1, 10, 100, 1000, 10,000 and 100,000 Hz). IV is given as an average of two separate tests where the shaded region is standard deviation.

The difference in IV between the frequencies is shown as the values consist of two components. One, the dielectric loss from ion flow, the component of interest, and two, the the dielectric loss due to dipole motion. Dipole motion is affected by frequency, whereas ion flow is not. Where there is a disagreement between frequencies, the values are not true IV values. Literature does not often account for this and generally uses a single test frequency [99,138].

If a single-frequency technique is used, incorrect trends would be seen. The expanded view of the 10,000 and 100,000 Hz dielectric measurements and resin temperature measurements are shown in Figure 6.2. A kink in the curve suggests that the rate at which IV is increasing has

slowed but then increases. It is sensible to suggest that the rate at which *IV* increases slows as the number of reactions taking place reduces, as shown by the decrease in the difference between resin temperature and oven temperature. However, there is no explanation why the rate of *IV* change increases as there is no increase in temperature. This kink is not accountable for when considering ion flow alone. It must be related to a change in dipole motion. That change in dipole motion is not confirmed, but it could be potentially related to the point at which the resin gels and dipoles are bonded into a larger network. As these are high frequencies, if the crosslinked structure has started to form, the components of the structures that are most affected by this quick alternating voltage will be dipoles rather than ions or reactive species. Note the significant error for both 10,000 and 100,000 Hz, whereas the error shown in Figure 6.1 is small for the lower frequencies. The error originates in the dipole motion behaviour rather than the ion flow behaviour. True ion flow is more reproducible.

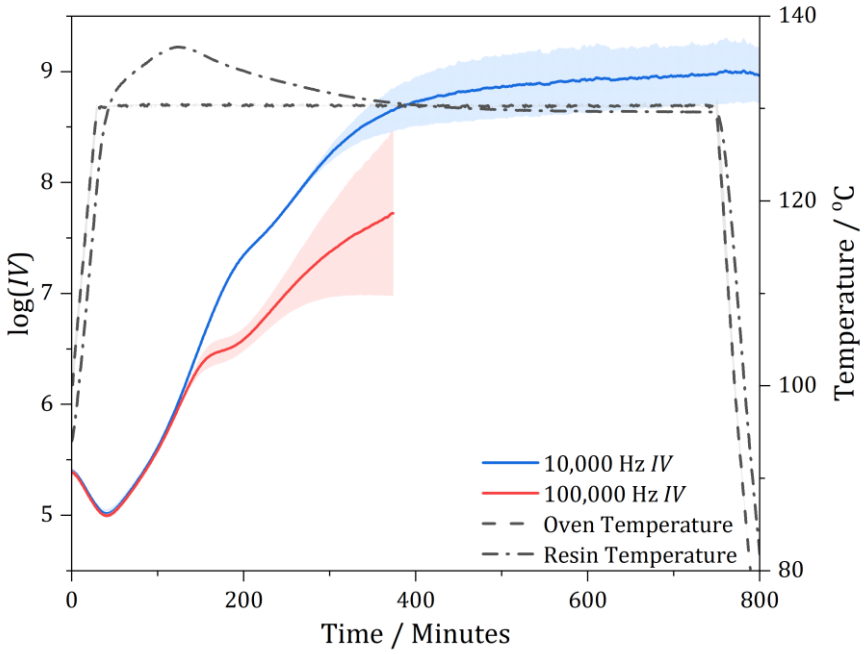

Figure 6.2 – Dielectric analysis of TG*p*AP/44'DDS using the 130 °C dwell cure at two testing frequencies (10,000 and 100,000 Hz) with resin and oven temperature measurements. *IV* is given as an average of two separate tests where the shaded region is standard deviation.

Due to this effect, a multi-frequency technique must be used to observe the 'true' *IV* values. Snippets of each frequency, where there is agreement, are used to obtain the true *IV* plot. The

frequency combined dielectric analysis plot of TG*p*AP/44'DDS when cured using the 130 °C dwell cure cycle is shown in Figure 6.3. This looks very similar to 1 Hz plot in Figure 6.1, however, the 1 Hz data does not start recording till approximately 250 minutes, see Appendix 5. This is related to the Lambient equipment being programmed to remove erroneous data at low frequencies at the start of the cure.

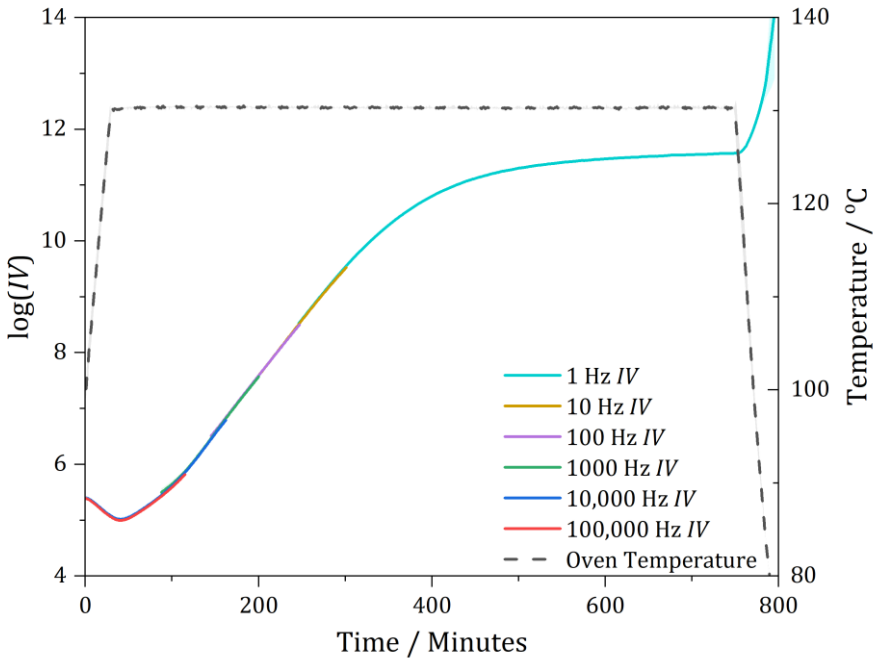

Figure 6.3 – Dielectric analysis of TG*p*AP/44'DDS cured with the 130 °C dwell cure using a combination of six different testing frequencies (1, 10, 100, 1000, 10,000 and 10,000 and 100,000 Hz). *IV* is given as an average of two separate tests where the shaded region is standard deviation.

This technique will be used for all of the following plots. Multiple other influences affect the data; therefore, errors due to the measurement technique must be minimised. This effect is also not only limited to the TGAP/DDS formulations. It is an issue seen in other resins such as DGEBA and TGDDM, as shown in Appendix 6 and Appendix 7 respectively.

The dielectric analysis plots for the four structural isomers of TGAP/DDS cured with the 130 °C dwell cure using the multi-frequency approach are shown in Figure 6.4. There are five critical points to each of these individual plots. Firstly, the initial *IV* value, secondly, the minimum *IV* value, thirdly, the rate at which *IV* increases, fourthly, the trend of *IV* towards the end of the

dwell; and finally, the increase in *IV* during the cool. Figure 6.4 will be split into sections and presented below to aid analysis.

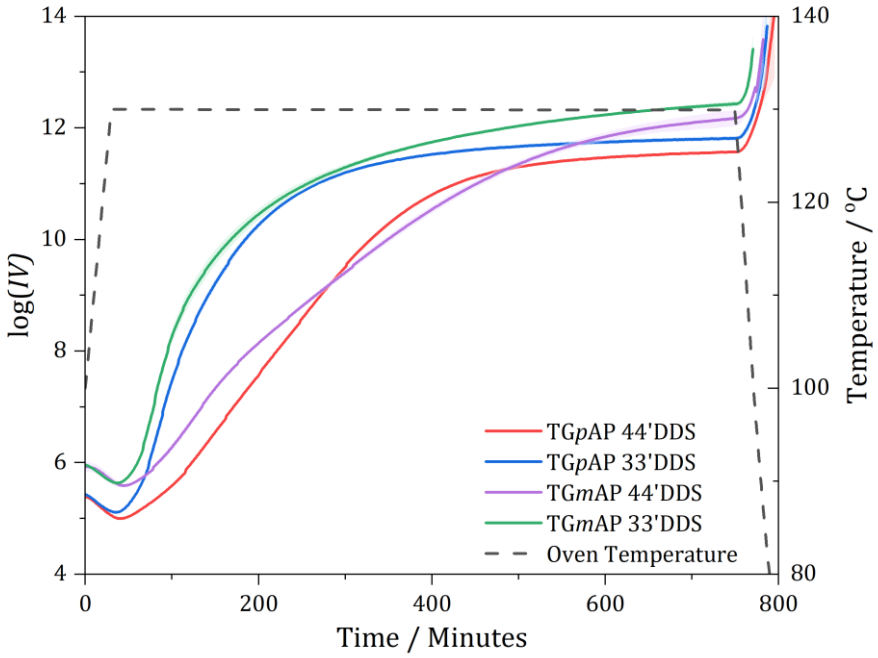

Figure 6.4 – Dielectric analysis of the four structural isomers of TGAP/DDS cured with the 130 °C dwell cure using a combination of six different testing frequencies (1, 10, 100, 1000, 10,000 and 10,000 and 100,000 Hz). *IV* is given as an average of two separate tests where the shaded region is standard deviation.

One of the downsides of dielectric analysis (DEA) is the competing effects that can effect *IV*. Understanding how DEA works is essential, but a general understanding of what happens in the curing reaction is also needed. Having undertaken DSC and temperature measurements in Chapter 5. Thermal is a good starting point. The temperatures at which reactions start, which are most reactive and when reactions end are generally known.

6.3.1.1.1. CRITICAL POINT 1 AND 2

The first two critical points of Figure 6.4 can be visualised on the dielectric analysis plot shown in Figure 6.5. The first critical point (CP1) refers to the initial *IV* value and the second critical point (CP2) refers to the minimum *IV* value. CP1 pair up based upon epoxy with the 33'DDS formulations slightly higher by 0.05 *IV*. CP2 occurs when the cure cycle has reached the 130 °C

dwell temperature, with 33'DDS formulations occurring at approximately 35 minutes, TG*p*AP/44'DDS occurring at 40 minutes and TG*m*AP/44'DDS at 45 minutes.

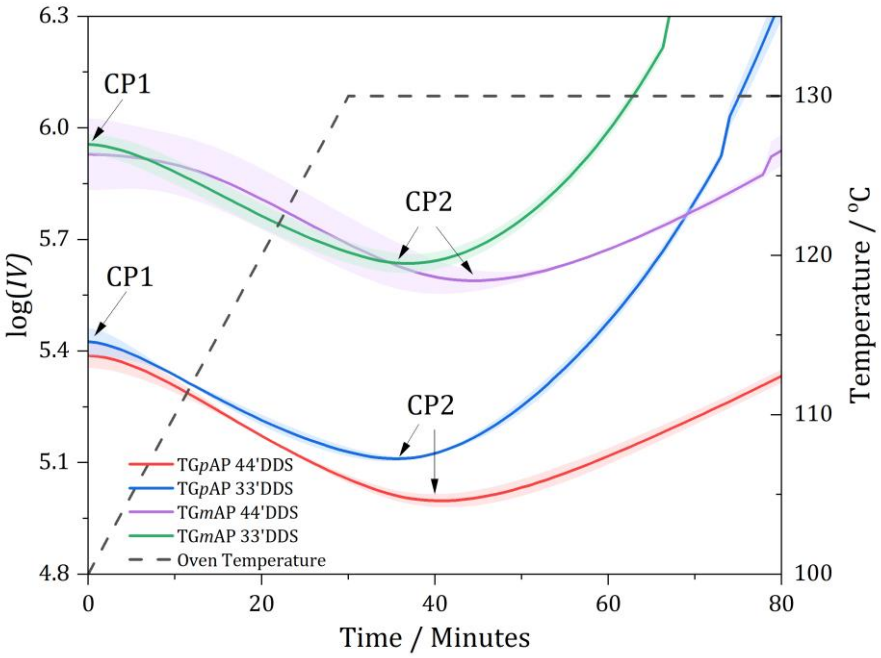

Figure 6.5 – Dielectric analysis of the four structural isomers of TGAP/DDS cured with the 130 °C dwell cure using a combination of six different testing frequencies (1, 10, 100, 1000, 10,000 and 10,000 and 100,000 Hz) highlighting critical points one (CP1) and two (CP2). *IV* is given as an average of two separate tests where the shaded region is standard deviation.

CP1 relates to the initial mechanical viscosity of the epoxy amine mixtures, as minimal curing reactions have occurred. *IV* can be related to mechanical viscosity through the following equations. First, ionic conductivity can be related to *IV* by equation (6-5).

$$IV = \frac{1}{\sigma_{DC}} = \frac{1}{\mu\, q\, n} \qquad (6\text{-}5)$$

Where μ is free ion mobility, q is magnitude of electronic charge, and n is free ion concentration. Free ion mobility is related to diffusion using the Einstein-Smoluchowski equation in equation (6-6).

$$D = \frac{\mu\, k_B\, T}{q} \tag{6-6}$$

Where D is the diffusion coefficient, k_B is the Boltzmann constant, and T is temperature. Then diffusion can be related to mechanical viscosity when the reactants are modelled as spherical particles with low Reynolds numbers using the Stokes-Einstein equation in equation (6-7).

$$D = \frac{k_B\, T}{6\,\pi\,\eta\, r} \tag{6-7}$$

Where η is mechanical viscosity, and r is the radius of the spherical particle. Combining equations (6-5), (6-6) and (6-7) gives equation (6-8). Ultimately showing that the relationship between IV and mechanical viscosity is proportional.

$$IV = \frac{1}{\sigma_{DC}} = \frac{6\,\pi\,\eta\, r}{q^2\, n} \tag{6-8}$$

This highlights a benefit of DEA as when taking mechanical viscosity measurements using a rheometer, mechanical viscosity will tend towards infinity once the material is vitrified. However, DEA will continue to give IV data as it utilises the electrical properties of the material to determine both the mechanical viscosity and ionic viscosity [153].

Referring to Figure 6.5 and considering the proportional relationship between IV and mechanical viscosity. The initial IV values show that initial mechanical viscosity of TG*m*AP formulations is higher than that of the TG*p*AP formulations. This can be explained through chemical structure. TG*m*AP has an epoxide group in the *meta* position, resulting in a bent shape, whereas in TG*p*AP, the epoxide group is in the *para* position; the shape is more linear, resulting in less resistance to flow, resulting in a lower initial mechanical viscosity.

The same logic can be applied to the type of hardener used. However, there is a less significant difference between the 44'DDS and 33'DDS formulations, which could result from error within the testing method. Still, due to the less linear chemical structure in 33'DDS, the resistance to flow is greater, resulting in a higher initial mechanical viscosity. As the molar ratio

of epoxy to amine in the formulations is 1.72:1, the hardener will have a smaller effect on mechanical viscosity than the epoxy component.

The second critical point, CP2, refers to the minimum IV value, the minimum viscosity point. At this point, the oven temperature has increased from 100 to 130 °C, and the dwell has started. Two things will impact this point. One is the start of curing reactions. From Chapter 5. Thermal, it is known that curing reactions begin during the ramp-up to 130 °C. Therefore, the formation of chemical bonds will result in an increase in both ion and mechanical viscosity. This is why the minimum viscosity points for the 44'DDS formulations are lower and occur later than in the 33'DDS formulations. The reactions begin at lower temperatures and earlier for the 33'DDS formulations, indicating that the they are initially more reactive and TG*p*AP/44'DDS is slightly more reactive than TG*m*AP/44'DDS.

Although the mechanical viscosity is expected to drop upon application of heat, it may not drop as dramatically as shown in Figure 6.5. The viscosity of the mobile ions is also influenced by a change in temperature. Referring back to the Einstein-Smoluchowski equation in equation (6-6), the diffusion coefficient is exponentially temperature dependent through the Arrhenius equation as shown in equation (6-9).

$$D = D_0 \exp\left(-\frac{E_a}{RT}\right) \tag{6-9}$$

Where D_0 is the maximum diffusion coefficient, E_a is activation energy, R is the molar gas constant, and T is temperature. Substituting equation (6-9) into equations (6-5) and (6-6) gives equation (6-10).

$$IV = \frac{1}{\sigma_{DC}} = \frac{k_B}{q^2\, n\, D_0} T \exp\left(\frac{E_a}{RT}\right) \tag{6-10}$$

Applying logs to this gives equation (6-11).

$$\log(IV) = \log\left(\frac{k_B}{q^2\, n\, D_0}\right) + \log\,(T) + \frac{E_a}{R\ln(10)} \cdot \frac{1}{T} \qquad (6\text{-}11)$$

When everything else remains the same, IV has an inverse relationship with temperature [153]. There is a $\log(T)$ function but $\frac{1}{T}$ will vary more. Using a cure cycle that uses a single temperature dwell while taking dieletric analysis simplifies the analysis process which explains why this is the main focus of the literature available [138,165,171].

6.3.1.1.2. CRITICAL POINT 3 AND 4

CP3 and CP4 are best described using the derivative of the IV plot, as these two points relate to the rate of reaction. IV is the ion viscosity, and as bonds are formed, the mobility of the ions or mobile species will become restricted. An increase in IV suggests that curing reactions are taking place. The greater the rate of change of IV, the greater the rate of reaction.

The derivative plots of the dielectric analysis plots for the structural isomers of TGAP/DDS cured using the 130 °C dwell cure are shown in Figure 6.6. CP3 is identified as the maximum rate of change in IV. As this is an isothermal cure, there should be one single peak. Referring back to Chapter 5. Thermal, these plots look very similar to heat flow plots for the 130 °C isotherm measurements using DSC. The 33'DDS formulations peak significantly earlier than the 44'DDS formulations, and the rate slows dramatically, whereas in the 44'DS formulations, there is a more gradual decrease.

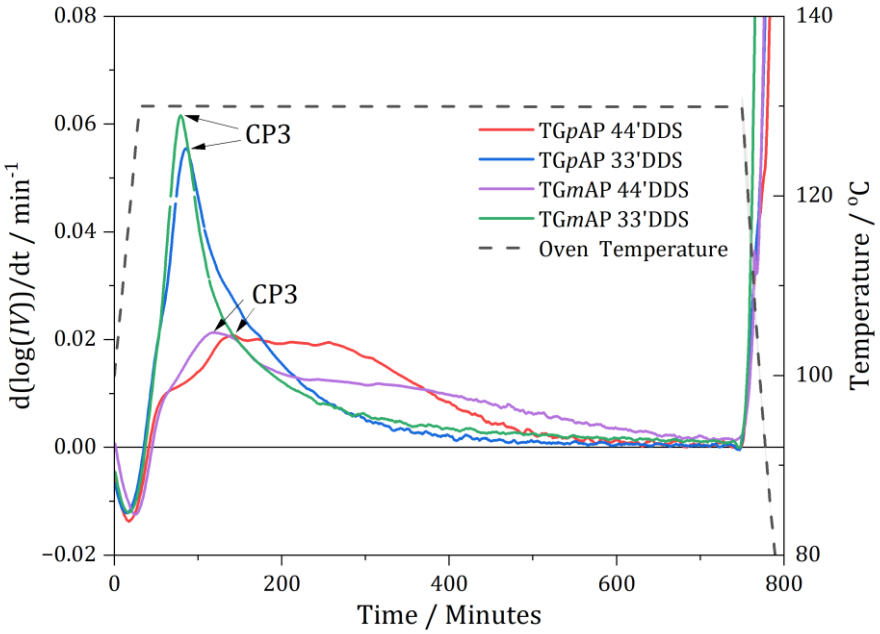

Figure 6.6 – First derivative of the dielectric analysis of the four structural isomers of TGAP/DDS cured with the 130 °C dwell cure using a combination of six different testing frequencies (1, 10, 100, 1000, 10,000 and 10,000 and 100,000 Hz) highlighting critical point three (CP3). Smoothed.

Like with DSC, it is not possible to identify the reactions occurring using DEA. TG*p*AP/33'DDS and TG*m*AP/33'DDS behave very similarly. However, TG*p*AP/44'DDS and TG*m*AP/44'DDS behave differently despite the rate of reaction occurring at similar points in the cure. The rate in TG*p*AP/44'DDS stays constant for approximately 100 minutes and then decreases. This suggests that TG*p*AP/44'DDS can undergo more reactions than TG*m*AP/44'DDS at 130 °C. This is more evidence of TG*p*AP's ability to undergo etherification reactions at low temperatures than TG*m*AP due to its greater ability to behave as a tertiary amine catalyst.

Despite DEA not being able to identify the type of reactions taking place, the greater rate of *IV* change in the 33'DDS formulations suggests that more significant crosslinking reactions are taking place initially, which restrict the flow of mobile ions more than the more linear (epoxy primary amine) reactions that take place in the 44'DDS formulations.

CP4 is the point at which the curing reactions stop; this should be shown by a horizontal line in the *IV* plot, or the derivative value should be zero. However, this doesn't often occur. It is difficult to distinguish. The 33'DDS formulations slow earlier but the 44'DDS formulations do not behave the same. The curing reactions in the 33'DDS formulations and TG*p*AP/44'DDS stop at approximately 600 minutes compared to TG*m*AP/44'DDS, where curing reactions take place

till nearly the end of the cure at approximately 700 minutes. The curing reactions have stopped, but this does not mean the resin is fully cured.

The *IV* values at the end of dwell may indicate the cure state. Qualitatively, only the formulations with similar initial *IV* values can be compared. Referring back to Figure 6.4, the final *IV* values are higher in the 33'DDS formulations than the 44'DDS formulations, suggesting that these have a higher final degree of cure value. However, it is difficult to suggest that TG*m*AP/44'DDS has a higher degree of cure than TG*p*AP/44'DDS as the initial *IV* values are different.

6.3.1.1.3. CRITICAL POINT 5

The final critical point, CP5, is the increase in *IV* upon cooling. As temperature decreases, from the relationship shown in equation (6-11), *IV* increases. This relates to the previously defined theory and also what is happening to the network when cooled. Upon cooling, the specific volume decreases, which restricts the flow of any remaining ions (impurities from synthesis or any remaining mobile species), resulting in an increase in *IV*. The ions also have less kinetic energy as the energy applied to the system is lower, so their ability to move is also restricted. Using the multi-frequency approach gives poor data or no data at this stage as the equipment perceives the high *IV* values as error and cuts out at low frequencies. However, using a single frequency to observe the change in *IV* is also not suitable, as the frequency-dependent data will impact the final results and give misleading trends. If it did work, it could give information about network morphology, but there are perhaps more reliable techniques to do this.

6.3.1.2. 160 °C DWELL

The dielectric analysis plot for the four structural isomers of TGAP/DDS using the 160 °C dwell cure cycle is shown in Figure 6.7. The four different formulations show less separated behaviour as they did when cured using the 130 °C dwell cure cycle. The same similar initial *IV* values based upon epoxy and then the pairing up based on hardener once curing reactions have begun is seen. Final *IV* values indicate the 33'DDS formulations reach a higher degree of cure than the 44'DDS formulations when considering the TG*p*AP and TG*m*AP separately.

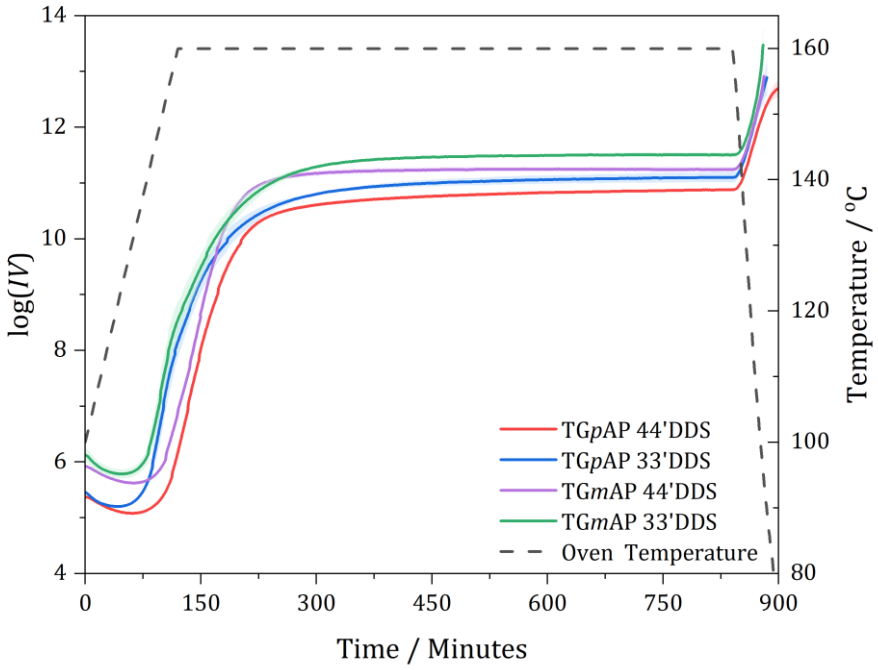

Figure 6.7 – Dielectric analysis of the four structural isomers of TGAP/DDS cured with the 160 °C dwell cure using a combination of six different testing frequencies (1, 10, 100, 1000, 10,000 and 10,000 and 100,000 Hz). *IV* is given as an average of two separate tests where the shaded region is standard deviation.

6.3.1.2.1. CRITICAL POINT 1 AND 2

Highlighting the first 150 minutes in Figure 6.8, where the 160 °C dwell temperature is reached after a 0.5 °C min^{-1} ramp from 100 °C, shows a clearer view of the initial *IV* (CP1) and minimum viscosity point (CP2). Once again, the 33'DDS formulations for the respective epoxies have a slightly higher initial *IV* value in CP1. A slower heating rate is used compared to the 130 °C dwell cure. Therefore, the CP2 occur at lower temperatures as the onset of curing begins at lower temperatures. CP2 occurs at approximately 40 minutes for TG*p*AP/33'DDS, 45 minutes for TG*m*AP/44'DDS, 60 minutes for TG*p*AP/44'DDS and 65 minutes for TG*m*AP/44'DDS.

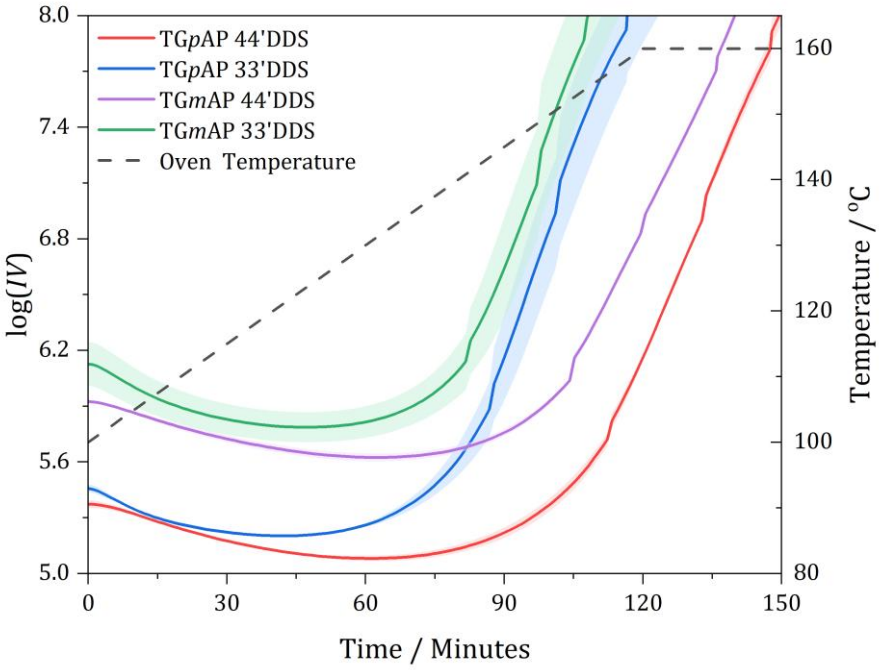

Figure 6.8 – Dielectric analysis of the four structural isomers of TGAP/DDS cured with the 160 °C dwell cure using a combination of six different testing frequencies (1, 10, 100, 1000, 10,000 and 10,000 and 100,000 Hz) highlighting critical points one (CP1) and two (CP2). *IV* is given as an average of two separate tests where the shaded region is standard deviation.

The rate at which the *IV* decreases in the 33'DDS formulations is faster than in the 44'DDS formulations. This can't be fully explained at this point.

6.3.1.2.2. CRITICAL POINT 3 AND 4

All formulations begin curing during the ramp, as shown by the increase in *IV*, and pair up based on hardener. The rate of change of *IV* as a function of time for the four structural isomers of TGAP/DDS cured using the 160 °C dwell cure is shown in Figure 6.9. CP3 occurs earlier for the 33'DDS formulations than the 44'DDS formulations. Approximately 100 minutes for the 33'DDS formulations, 130 minutes for TG*p*AP/44'DDS and 145 minutes for TG*m*AP/44'DDS. For each curve other than TG*p*AP/44'DDS, a shoulder is seen. This is not part of the curing behaviour but rather an artefact of the multi-frequency technique. The 44'DDS formulations behave similarly, unlike in the 130 °C dwell where the rate of *IV* change TG*m*AP/44'DDS was generally slower.

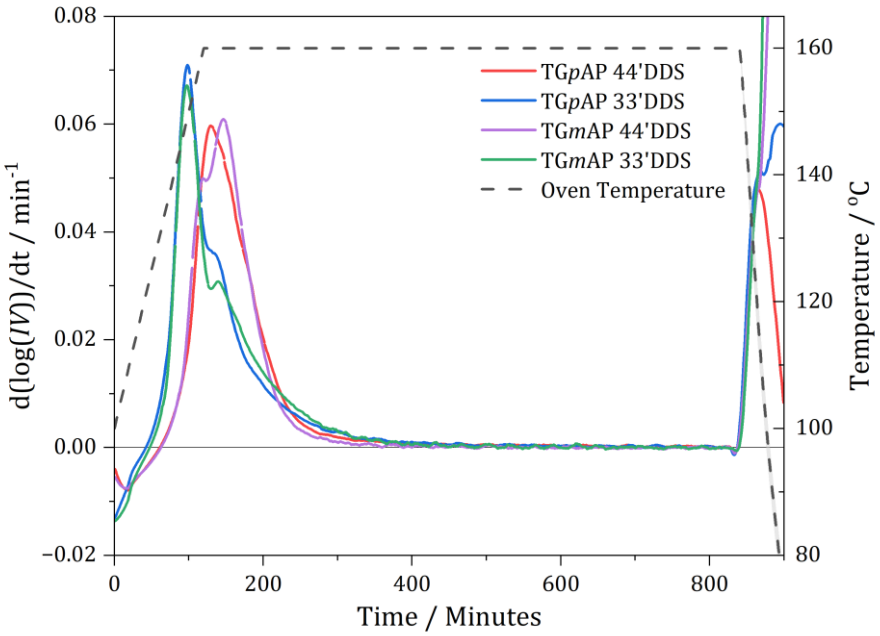

Figure 6.9 – First derivative of the dielectric analysis of the four structural isomers of TGAP/DDS cured with the 160 °C dwell cure using a combination of six different testing frequencies (1, 10, 100, 1000, 10,000 and 10,000 and 100,000 Hz) highlighting critical point three (CP3). Smoothed.

It's important to remember that the rate of *IV* change is not as reliable as heat flow or rate of reaction obtained from DSC as one measures the electrical response and the other the thermal response. However, it is expected that they may be similar and that any differences can be accounted for. Referring back to the Figure 5.21, the difference in the maximum heat flow values of the 33'DDS and 44'DDS is significant, the peak height for the 44'DDS formulations is that of 50 % of 33'DDS indicating that fewer reactions are taking place in 44'DDS formulations. The rate of change of *IV* is similar here and indicates the restriction to flow of mobile species. If it is similar between the formulations, it suggests that crosslinking occurs in all formulations in the 160 °C dwell whereas crosslinking occurs more prominently in the 33'DDS formulations in the 130 °C.

Unlike the 130 °C dwell cure, all formulations have a clear point where curing reactions stop, CP4. This is approximately 500 minutes. A higher temperature requires less time to cure. Once again, there is no guarantee that any of the formulations are 100 % cured, just that no more reactions are occurring that result in an increase in *IV*.

6.3.2. DYNAMIC HEATING

Ideally, a dwell temperature of 200 °C would be used, but no ramp is possible that would not result in a runaway reaction with thermal degradation occurring. Instead, a dynamic cure can be used where the heating rate is slow enough (0.25 °C min^{-1}) that all the curing occurs during the ramp, as seen in Chapter 5. Thermal when taking resin temperature measurements. The dielectric analysis plot for the four structural isomers of TGAP/DDS using the 0.25 °C min^{-1} dynamic cure cycle is shown in Figure 6.10. Pairing up based on hardener is seen, although the behaviour is different.

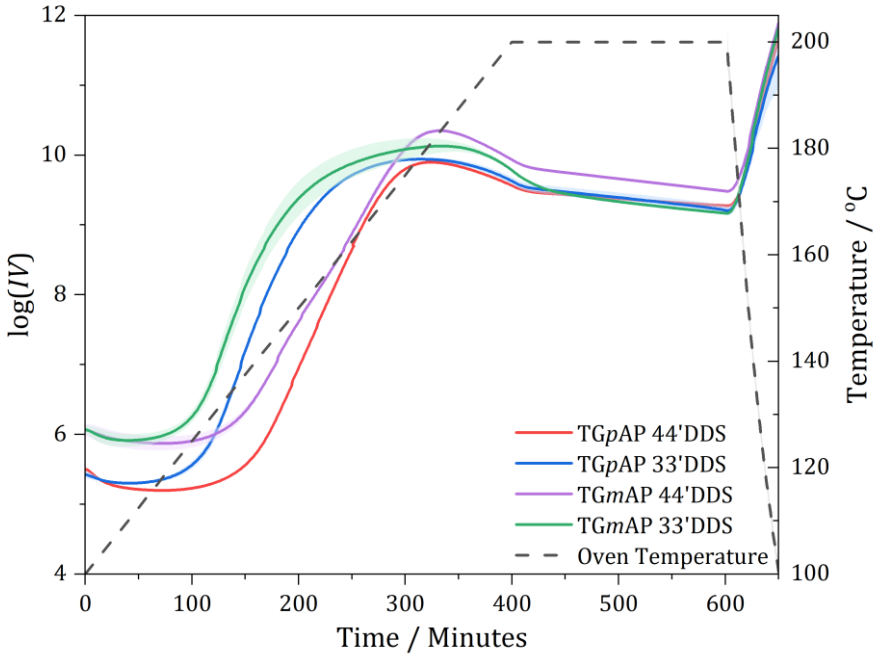

Figure 6.10 – Dielectric analysis of the four structural isomers of TGAP/DDS cured with the 0.25 °C min^{-1} dynamic cure using a combination of six different testing frequencies (1, 10, 100, 1000, 10,000 and 10,000 and 100,000 Hz). *IV* is given as an average of two separate tests where the shaded region is standard deviation.

6.3.2.1. CRITICAL POINT 1 AND 2

The first 200 minutes, where the *IV* drop occurs, is shown in Figure 6.11. The initial *IV* values, CP1, show similar values based on epoxy, but instead of the 33'DDS formulations having a slightly higher value, the TG*m*AP *IV* values are the same and TG*p*AP/44'DDS higher than TG*p*AP/33'DDS. This value depends on the temperature of the resin; the resin temperatures are

never precisely the same due to subtle variances in the mixing process. The differences in *IV* are small, therefore the comment earlier that 33'DDS formulations should be higher than the 44'DDS formulations is a coincidence rather than fact. The possible sources of variance are too great to comment on conclusively.

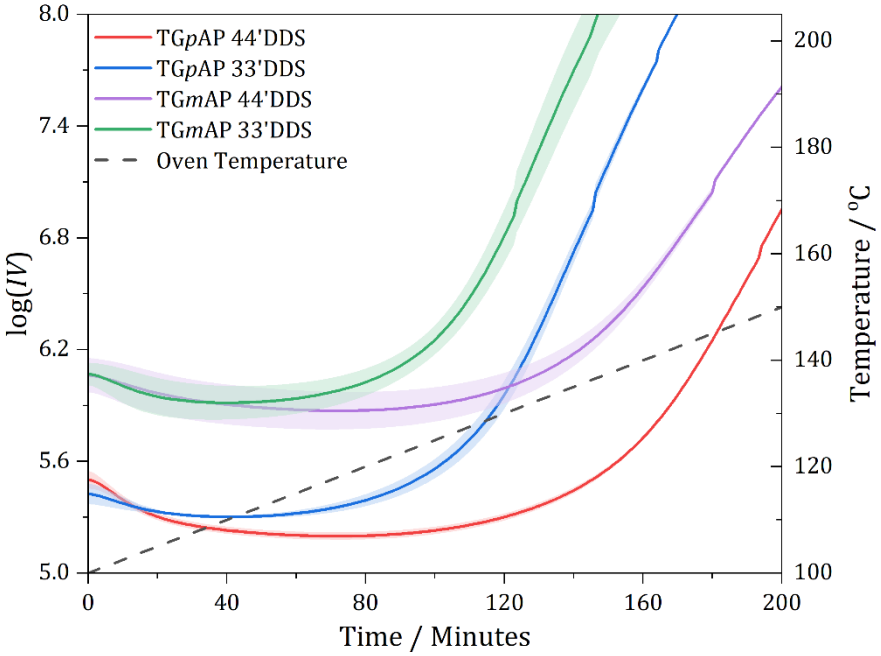

Figure 6.11 – Dielectric analysis of the four structural isomers of TGAP/DDS cured with the 0.25 °C min^{-1} dynamic cure using a combination of six different testing frequencies (1, 10, 100, 1000, 10,000 and 10,000 and 100,000 Hz) highlighting critical points one (CP1) and two (CP2). *IV* is given as an average of two separate tests where the shaded region is standard deviation.

The 33'DDS formulations reach minimum viscosity, CP2, at approximately 40 minutes when the oven temperature is 110 °C, and the 44'DDS formulations at 70 minutes when the oven temperature is 118 °C indicating that curing reactions begin earlier in the 33'DDS formulations than the 44'DDS formulations. The drop in *IV* is smaller than in the previous heating regimes, which could suggest that the extent of curing is higher when mechanical viscosity is dropping. However, it must also be noted that the heating rate is slower, so the inverse relationship with *IV* has less effect.

As this cure cycle uses a constant heating rate, problems arise from the inverse dependence on *IV* with temperature. There will be a constant competing effect between *IV* rising due to

curing reactions and *IV* decreasing due to temperature increase. Curing reactions will dominate when they are significant, but when they start to slow and stop, *IV* will decrease.

6.3.2.2. CRITICAL POINTS 3 AND 4

The rate of change of *IV* as a function of time for the four structural isomers of TGAP/DDS for the 0.25 °C min^{-1} dynamic cure is shown in Figure 6.12. The maximum rate, CP3, occurs at a lower temperature for the 33'DDS formulations than the 44'DDS formulations. A sharp peak is seen, whereas the 44'DDS formulations show a broad peak for TG*p*AP/44'DDS and a double peak for TG*m*AP/44'DDS.

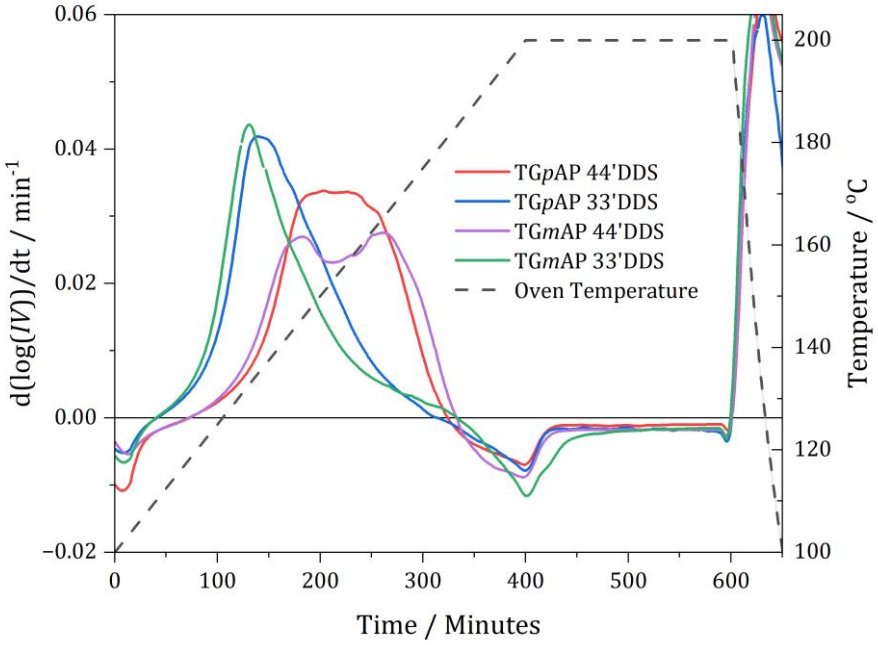

Figure 6.12 – First derivative of the dielectric analysis of the four structural isomers of TGAP/DDS cured with the 0.25 °C min^{-1} dynamic cure using a combination of six different testing frequencies (1, 10, 100, 1000, 10,000 and 10,000 and 100,000 Hz) highlighting critical point three (CP3). Smoothed.

The double peak shown for TG*m*AP is unexpected. However, when the same cure cycle is considered when taking temperature measurements from Chapter 5. Thermal, similar results are shown in Figure 6.13 (a duplication of Figure 5.8). Sharp, distinct peaks are shown for the 33'DDS formulations, whereas broad peaks are shown for the 44'DDS formulations. TG*m*AP/44'DDs shows a shoulder at a similar temperature/time to DEA results. This suggests

it is not an anomaly. Instead, the *IV* decrease due to temperature increase causes the peak rate to drop between the two peaks as the curing reactions slows, just not as significant as the DEA results indicate.

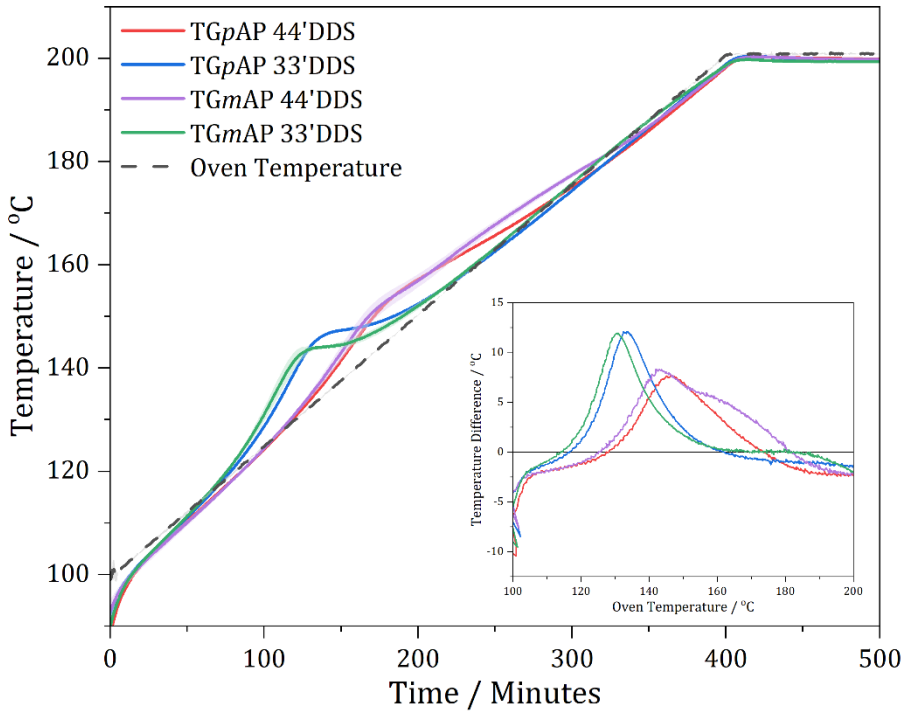

Figure 6.13 – Temperature profiles for the four structural isomers of TGAP/DDS during the 0.25 °C min^{-1} dynamic heat as a function of time measured by thermocouples for resin and oven temperatures, where the shaded region is the standard deviation. The temperature difference between resin and oven temperature is shown on the inset graph as a function of oven temperature. A duplication of Figure 5.8.

Referring back to Figure 6.12, the rate becomes negative during the ramp. This does not suggest that the resin becomes less viscous; it is just that the curing reactions have slowed down or stopped. This results in *IV* dropping as the ions, or remaining mobile species, become less viscous as they have greater energy or free volume space due to the temperature increase. The rate at which *IV* decreases is greater in the TG*m*AP formulations, suggesting that curing reactions are less dominant at higher temperatures.

According to the rate and Figure 6.10, the *IV* plot doesn't show a horizontal trend, CP4, for any formulations once the temperature reaches 200 °C and remains at that for 200 minutes. It suggests that in all of the networks, the formulations' *IV* drops. This was not seen in any of the

lower temperature heating regimes, indicating that the resins are not curing but something else. What this is is not clear. One possible cause is thermal degradation. Breaking chemical bonds in the network allows for increased flow of mobile ions. Another could be network relaxation or annealing, which causes mobile ions to flow.

The final feature is the *IV* value at the end of the dwell. These are less clear than the dwells. These values can only be compared between formulations containing the same epoxy. For both, the 44'DDS formulations have the highest *IV* value. TG*m*AP/44'DDS is significantly higher than TG*m*AP/33'DDS, whereas the TG*p*AP/44'DDS *IV* value is only slightly higher than TG*p*AP/33'DDS. This may show that the 44'DDS formulations are more cured than the 33'DDS counterparts. Or, if not cured, a higher crosslink density, restricting the flow of mobile ions greater.

6.3.3. CURE SCHEDULE

Having introduced all the potential problems faced when taking dielectric measurements of epoxy resins, the standard multi-dwell cure cycle can be analysed. This is shown in the dielectric analysis plots of the four structural isomers of TGAP/DDS in Figure 6.14. This plot is more complex because it contains a mixture of temperature ramps and dwells. However, similar trends are seen to the ones discussed above.

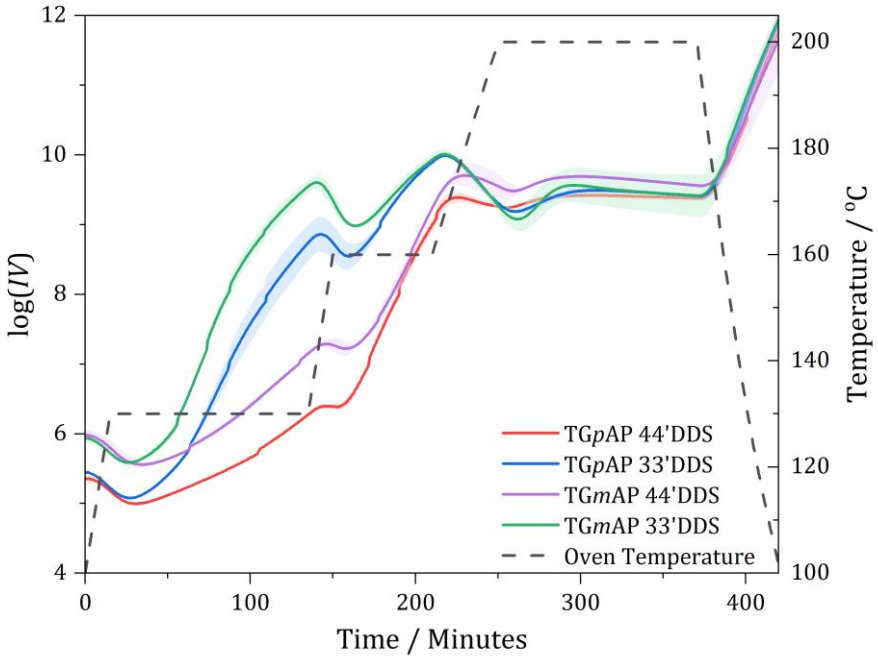

Figure 6.14 – Dielectric analysis of the four structural isomers of TGAP/DDS cured with the standard cure cycle using a combination of six different testing frequencies (1, 10, 100, 1000, 10,000 and 10,000 and 100,000 Hz). *IV* is given as an average of two separate tests where the shaded region is standard deviation.

6.3.3.1. CRITICAL POINT 1 AND 2

Highlighting the first 80 minutes where the first 2 °C min^{-1} ramp up to 130 °C occurs in Figure 6.15. The initial *IV*, CP1, TG*m*AP is higher than TG*p*AP. The minor differences between 44'DDS and 33'DDS differ from what was seen in both the dwells and the dynamic cure cycles. TG*m*AP/44'DDS initial *IV* value is higher than TG*m*AP/33'DDS, and TG*p*AP/33'DDS is higher than TG*p*AP/44'DDS.

All formulations do not begin significant curing reactions until after the 130 °C dwell temperature is reached, 15 minutes. *IV* continues to decrease even after the temperature dwell is reached, suggesting that few curing reactions are occurring, and the resin is undergoing flow as mechanical viscosity is dropping. The minimum viscosity, CP2, occurs at approximately 27 minutes for both TG*p*AP/33'DDS and TG*m*AP/33'DDS. In comparison, CP2 occurs at 30 minutes for TG*p*AP/44'DDS and 35 minutes for TG*m*AP/44'DDS. This indicates that curing reactions occur earliest in the 33'DDS formulations, then TG*p*AP/44'DDS, and then in TG*m*AP/44'DDS.

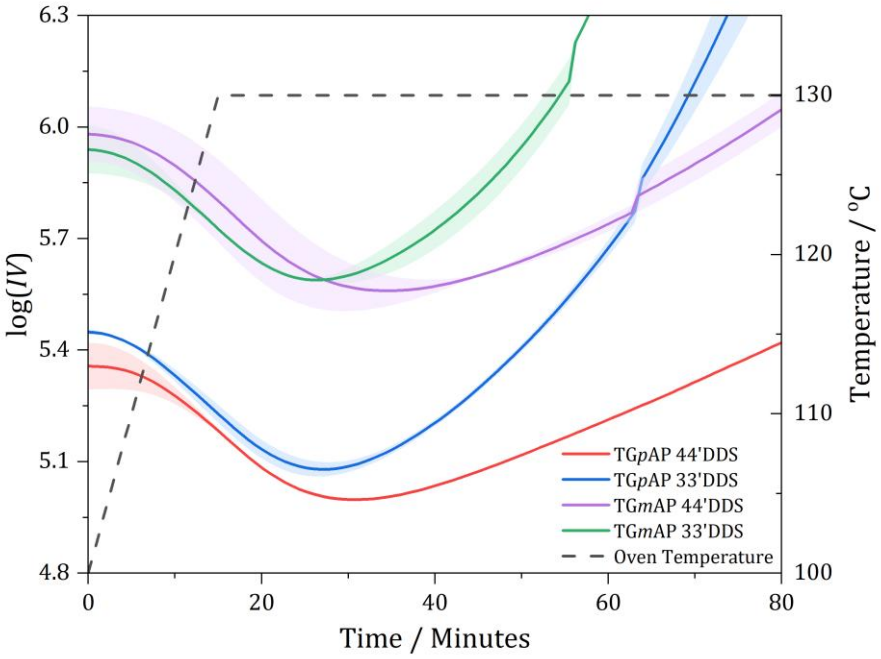

Figure 6.15 – Dielectric analysis of the four structural isomers of TGAP/DDS cured with the standard cure cycle using a combination of six different testing frequencies (1, 10, 100, 1000, 10,000 and 10,000 and 100,000 Hz) highlighting critical points one (CP1) and two (CP2). *IV* is given as an average of two separate tests where the shaded region is standard deviation.

6.3.3.2. CRITICAL POINT 3 AND 4

The rate of change of *IV* as a function of time for the four structural isomers of TGAP/DDS cured using the standard cure cycle is shown in Figure 6.16. Due to the combination of temperature ramps and dwells, the findings are slightly different. The maximum rate of *IV* change, CP3, will occur at different dwells for the different formulations, similar to what was seen in the DSC rate of reaction plots in Chapter 5. Thermal. The highest rate of change in the first dwell is seen for TG*m*AP/33'DDS at 70 minutes, indicating that curing reactions are fastest for this formulation. TG*p*AP/33'DDS occurs at a slightly lower rate and later at 75 minutes. The rate slows towards the end of dwell, indicating curing reactions are still occurring and faster than the 44'DDS. Both 44'DDS formulations show similar behaviour, but TG*m*AP/44'DDS reaches its highest rate in 130 °C dwell before the end of the dwell at 110 minutes, whereas TG*p*AP/44'DDS reaches its highest rate at the end of the dwell.

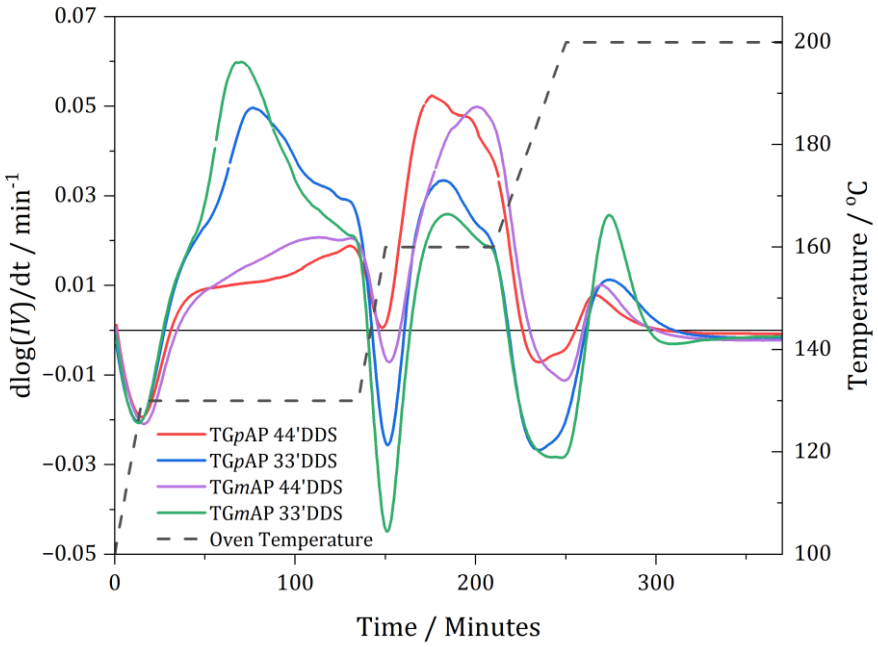

Figure 6.16 – First derivative of the dielectric analysis of the four structural isomers of TGAP/DDS cured with the standard cure cycle using a combination of six different testing frequencies (1, 10, 100, 1000, 10,000 and 10,000 and 100,000 Hz). Smoothed.

Referring back to Figure 6.14, the difference in the absolute *IV* values indicate the amount of reactions that have taken place, which have reduced the mobility of reactive species or ions. The difference between the 33'DDS and 44'DDS indicates that more crosslinks have been formed in the 33'DDS formulations during the first 130 °C dwell.

The next feature is the *IV* drop during the temperature ramp. If no curing reactions occurred during the ramp for each formulation, the rate of *IV* should be similar. This is not the case. TG*p*AP/44'DDS does not achieve a negative rate of *IV* change, suggesting that curing reactions are more significant than the inverse relationship between *IV* and temperature increase. The other formulations show a decrease in *IV*, and a negative rate of *IV* change, suggesting curing reactions are not as significant during the ramp. The 33'DDS formulations show a more significant drop as more reactions have occurred during the 130 °C dwell.

In the 160 °C dwell, the positive rate of *IV* change is more significant in the 44'DDS formulations, with the maximum occurring for TG*p*AP/44'DDS at 175 minutes and 200 minutes for TG*m*AP/44'DDS. The maximum rate change, CP3, occurs at 180 minutes for the 33'DDS formulations. However, a lower value than that of the 44'DDS formulations indicating crosslinking reactions are more dominant in the 44'DDS formulations. The rate slows towards

the end of the 160 °C dwell for all formulations other than TG*m*AP/44'DDS, where the maximum rate occurs towards the end.

In the next temperature ramp up to 200 °C, a similar drop and rate of change occur in the 33'DDS formulations, suggesting that few curing reactions occur here. Whereas, in the 44'DDS formulations, there is a less significant negative rate of *IV* change, suggesting that curing reactions occur in the ramp.

In the final 200 °C dwell, a similar rate of *IV* change is observed in all formulations apart from TG*m*AP/33'DDS, where the rate of change is significantly higher. Suggesting more curing reactions occur than in the other formulations. However, this might not be true. At the end of the cure, it is difficult to say if it is significant curing reactions or just small amounts of crosslinking that cause a significant reduction in the mobility of ions or mobile reactive species. It is known from both DSC and NIR that etherification reactions mainly occur at this point.

TG*m*AP/33'DDS perhaps results in a more significant reduction in ion mobility due to its morphology. It was suggested in Chapter 4. NIR that TG*m*AP/33'DDS forms a less homogeneous network than TG*p*AP/44'DDS due to the increased reactivity of 33'DDS which forms areas of high crosslink density connected by areas of low crosslink density. These areas of low crosslink density will allow for greater ion mobility in the 200 °C dwell. When etherification reactions occur, the 'dangling chains' crosslink and the *IV* values will increase at a greater rate than those formulations with a more homogenous network.

All formulations finish curing reactions, or *IV* stops increasing, CP4, at approximately 300 minutes, 70 minutes before the end of the cure cycle. A constant, small decrease in *IV* is observed. The rate at which *IV* drops is similar for the TG*m*AP/44'DDS, TG*m*AP/33'DDS and TG*p*AP/33'DDS formulations. The rate at which TG*p*AP/44'DDS drops is less. One of the causes of this was speculated to be thermal degradation. Thermogravimetric analysis was run while curing the four different TGAP/DDS formulations to investigate whether there was significant thermal degradation during the final dwell. Table 6.1 shows the % mass change during the 200 °C dwell for the four structural isomers of TGAP/DDS calculated using thermogravimetric analysis. There are small amounts of thermal degradation, less than 0.3 % for all formulations. This is minimal and most probably not the cause of the decreasing *IV* values once significant curing reactions have finished.

Table 6.1 – % mass change during the 200 °C temperature dwell of the standard cure cycle for the four structural isomers of TGAP/DDS found using thermogravimetric analysis.

	TG*p*AP 44'DDS	TG*p*AP 33'DDS	TG*m*AP 44'DDS	TG*m*AP 33'DDS
Starting Mass / mg	20.77	17.52	7.16	6.71
Finishing Mass / mg	20.73	17.49	7.14	6.70
% Mass Change	0.19	0.17	0.28	0.15

The cause of the IV decrease must be something else. The cured properties must be considered, most importantly the glass transition temperature, T_g. This is the temperature at which there is an onset of significant chain mobility, and the network transitions from a glassy state to a rubbery state [17]. The more crosslinked a network is, the higher the T_g is. During the cure, the network forms and the number of crosslinks increase, thus resulting in an increase in IV. However, in the latter part of the cure, fewer reactions occur, the near-maximum T_g will have been reached at 300 minutes when the IV values stop increasing for all formulations. The resin will have vitrified and become glassy, although not determined experimentally, during the ramp from 160 to 200 °C. The network morphology dictates what happens to the IV values in the final dwell. If the T_g is lower than the final dwell temperature, flow can occur due to the increased chain mobility and will result in IV decreasing.

The T_g values of the four cured resins obtained using dynamic mechanical analysis are given in Table 6.2. The values for TG*p*AP/44'DDS, TG*p*AP/33'DDS and TG*m*AP/44'DDS are above the final dwell temperature. TG*m*AP/33'DDS has a T_g below the final dwell temperature. Going off these values, it could be expected that TG*m*AP/33'DDS would show a reduction in IV but the other three formulations would not. This is not the case and is related to how T_g is defined. The values in Table 6.2 are the peak centre of the tan δ peak observed at high temperatures. However, the change from a glassy to a rubbery state does not occur at one set temperature. It is a temperature range. Parts of the network will become rubbery before other parts. However, the peak temperature defines the temperature at which most of the network has transitioned.

Table 6.2 – Glass transition temperatures (T_g) of the four structural isomer formulations of TGAP/DDS obtained using dynamic mechanical analysis in single cantilever configuration at 1 Hz.

	TG*p*AP 44'DDS	TG*p*AP 33'DDS	TG*m*AP 44'DDS	TG*m*AP 33'DDS
T_g / °C	253.7 ± 0.3	216.2 ± 0.8	226.2 ± 0.1	198.6 ± 0.5

The tan δ against temperature plot obtained from DMA for the four structural isomers of TGAP/DDS is shown in Figure 6.17. The dashed line at 200 °C indicates the oven temperature in the final dwell. The temperature occurs when TG*m*AP/33'DDS has reached its peak T_g value and when TG*p*AP/33'DDS and TG*m*AP/44'DDS have started to undergo the transition. However, TG*p*AP/44'DDS does not undergo any transition at this point; the material is glassy, and the chains have restricted mobility.

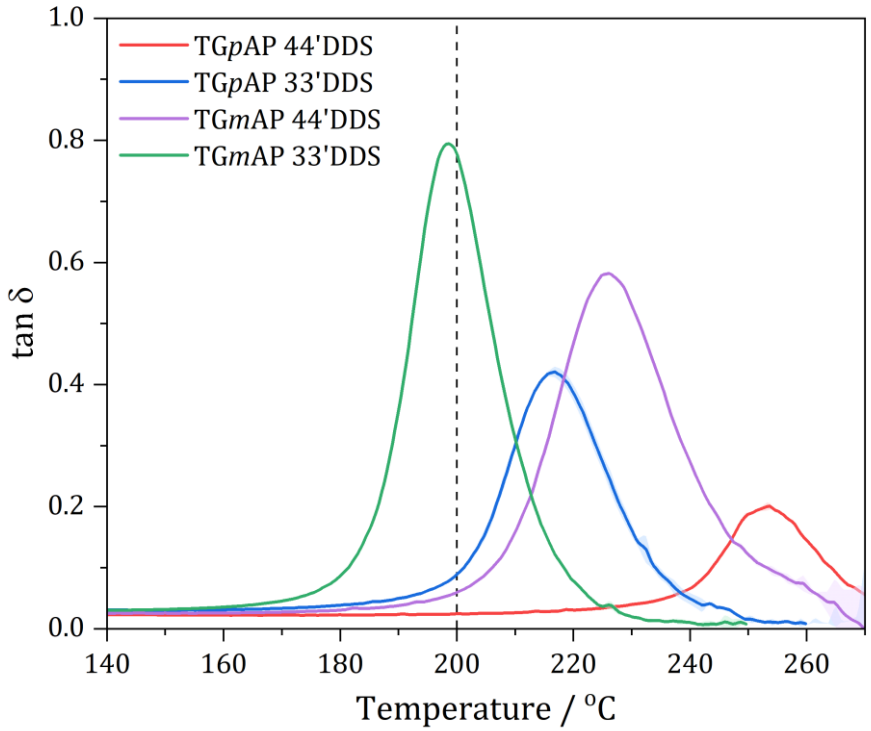

Figure 6.17 – tan δ against temperature plot for the four structural isomers of TGAP/DDS obtained using dynamic mechanical analysis in single cantilever configuration at 1 Hz. Plots are given as an average of two separate tests where the shaded region is standard deviation. The dashed line indicates the oven temperature in the final dwell.

This explains why different rates of change in the *IV* values in the final dwell are seen. The rate is more negative initially for TG*m*AP/33'DDS as a large proportion of the network is rubbery and can flow. The rate of decrease in TG*p*AP/33'DDS and TG*m*AP/44'DDS is similar and less, but the crosslinked networks still undergo flow. TG*p*AP/44'DDS sees very little increased flow as the final dwell temperature is much lower than the onset of T_g, resulting in a much more horizontal *IV* trend.

When flow occurs, the network is essentially annealing or relaxing. The network becomes denser. The different formulations have different configurational entropy. The configurational entropy in TG*m*AP/33'DDS is greater than that of TG*p*AP/44'DDS [47,192,193]. Therefore, density would be expected to be higher for TG*m*AP/33'DDS, but how much of an increase in density the annealing accounts for in the final dwell is difficult to say. Investigation using positron annihilation lifetime spectroscopy (PALS) can help here. This technique can give information regarding the pore size and % free volume space, as shown in Table 6.3.

Table 6.3 – Average pore volume and % free volume space for the four structural isomers of TGAP/DDS determined using positron annihilation lifetime spectroscopy.

	TG*p*AP 44'DDS	TG*p*AP 33'DDS	TG*m*AP 44'DDS	TG*m*AP 33'DDS
Average pore volume / Å^3	60.7 ± 0.5	59.1 ± 0.5	55.3 ± 0.5	55.9 ± 0.5
Fractional free volume / %	10.67 ± 0.09	10.45 ± 0.09	10.30 ± 0.09	9.76 ± 0.09

The first value, average pore volume, appears to depend on the type of epoxy in the formulation. TG*p*AP-containing formulations have a higher value than the TG*m*AP-containing formulations. The second value, % fractional free volume, appears to follow a similar trend; however, instead of the TG*m*AP values being similar, TG*m*AP/33'DDS is lower than TG*m*AP/44'DDS. TG*p*AP/44'DDS has the highest % fractional free volume, followed by TG*p*AP/33'DDS, TGmAP/44'DDS, and TG*m*AP/33'DDS. If the resins can anneal during the final dwell, the cured free volume is lower, but the average pore size is not affected as significantly. This shows further proof that when the final dwell temperature lies in the T_g temperature range, the resins can further anneal and achieve a denser network.

6.3.3.3. CRITICAL POINT 5

The final feature of Figure 6.14 is the increase of IV upon cooling. Dipole motion impacts the results here, and 1 Hz is not a low enough testing frequency to obtain true ion viscosity data. If lower frequencies were used it may be possible to obtain information about how the networks changed during cooling if the resin were at the same cure state. However, this is not the case.

A study by Hussain *et al.* suggested that the T_g could be obtained by identifying the temperature at which IV stabilised during the cooling [163]. If this technique was applied to the results, the T_g values would be over 100 °C lower than those determined by DMA. However, their cure cycle cured at temperatures higher than the resins' final T_g, so it may be possible but still Hussain *et al.* only observed one testing frequency. The higher testing frequency, the lower the T_g will be.

6.3.4. CURE INDEX

In the previous two chapters, Chapter 4. NIRand Chapter 5. Thermal, the degree of cure could be used to describe how cured each resin was as a function of cure. Degree of cure derived by either method has been compared interchangeably by literature, and good agreement has been found despite NIR and DSC measuring different phenomena. The method of calculating degree of cure using NIR is given in equation (6-12).

$$\alpha(t) = \frac{[EP]_0 - [EP]_t}{[EP]_0} \tag{6-12}$$

Where α is degree of cure, $[EP]_0$ is the initial epoxide group concentration, and $[EP]_t$ is the epoxide group concentration at time, t. The method of calculating degree of cure using DSC is given in equation (6-13).

$$\alpha(t) = \frac{\Delta H(t)}{\Delta H_0} \tag{6-13}$$

Where $\Delta H(t)$ is the enthalpy of reaction at time, t, and ΔH_0 is the total enthalpy of cure. The NIR method is based on the concentration of epoxide groups as determined by their optical properties, which decrease as curing reactions occur. Whereas the DSC method is based on the exothermic behaviour curing reactions, the enthalpy of reaction increases as curing reactions take place.

Both these techniques normalise the values to a completely cured resin. Therefore, the final values should be very similar. Still, it could be possible that during the cure, the evolution of degree of cure could be different due to measuring different phenomena. This study has not investigated it, but there is discussion surrounding the difference in exothermic behaviour between epoxy amine and etherification reactions [104,208]. If the epoxy amine reactions are more exothermic than etherification reactions, degree of cure may be higher when using NIR when compared to the DSC method and vice versa. Either technique is not perfect.

While the resin cures, a crosslinked network forms. The increasing crosslink density results in an increase in T_g as discussed by Nielsen [55] and shown by the relationship in equation (6-14).

$$T_g - T_{g_0} = \frac{3.9 \times 10^4}{M_c} \tag{6-14}$$

Where T_{g_0} is the glass transition temperature of the uncured resin and M_c is the molecular weight between crosslinks. This relationship led their group to develop the DiBenedetto equation, first reported as equation (6-15) [137].

$$\frac{T_g - T_{g_0}}{T_{g_0}} = \frac{\left(\frac{\epsilon_X}{\epsilon_M} - \frac{F_X}{F_M}\right)\alpha}{1 - \left(1 - \frac{F_X}{F_M}\right)\alpha} \tag{6-15}$$

Where $\frac{\epsilon_X}{\epsilon_M}$ is the ratio of lattice energies of a crosslinked polymer network, X, and uncrosslinked polymer network, M and $\frac{F_X}{F_M}$ is the ratio of segmental mobilities of the crosslinked network and the uncrosslinked network. Studies found that $\frac{\epsilon_X}{\epsilon_M} = 1$ whereas $\frac{F_X}{F_M}$ varied between 0 and 1 based

on the polymer network in question. It was found that the ratio of the two parameters is given by equation (6-16) [228].

$$\frac{\frac{\epsilon_X}{\epsilon_M}}{\frac{F_X}{F_M}} = \frac{T_{g_\infty}}{T_{g_0}} \tag{6-16}$$

Where T_{g_∞} is the glass transition of an infinitely crosslinked polymer network. Applying this to epoxy amine systems, Pascault and Williams gave the equation (6-17) [228].

$$\frac{T_g - T_{g_0}}{T_{g_0} - T_{g_\infty}} = \frac{\lambda\alpha}{1-(1-\lambda)\alpha} \tag{6-17}$$

Where λ is an adjustable convexity parameter that is equal to $\frac{F_X}{F_M}$. By considering the entropy, Pascault and Williams found the adjustable convexity parameter is also given by equation (6-18) [228,229].

$$\lambda = \frac{\Delta C_{p_\infty}}{\Delta C_{p_0}} = \frac{T_{g_0}}{T_{g_\infty}} \tag{6-18}$$

Where ΔC_p is heat capacity. Equation (6-17) has been used to predict T_g values of epoxy systems at different degree of cure values [111,154,230]. However, if T_g were obtained, the degree of cure could also be predicted. T_g indicates the cure state of the resin, the closer the value to T_{g_∞}, the more cured the resin is.

IV also indicates the cure state. The uncured and infinitely cured IV values can be obtained, allowing for a calculation of the cure state using equation (6-19).

$$\frac{T_g - T_{g_0}}{T_{g_0} - T_{g_\infty}} = \frac{\log(IV)_t - \log(IV)_0}{\log(IV)_0 - \log(IV)_\infty} = \frac{\lambda\alpha}{1-(1-\lambda)\alpha} = cure\ index \tag{6-19}$$

This equation is not perfect as it cannot give degree of cure values without a value of λ, which cannot be obtained without data from a direct technique such as NIR or DSC to either fit the data or experimentally determine the heat capacity ratios. Therefore, instead of using the term 'degree of cure' to indicate the cure state, it is indicated using the term 'cure index' [153]. The downside to this is that it assumes a linear dependence between the cure index, T_g and IV but it can be a good indicator which can be obtained directly from IV measurements in manufacturing conditions without the need for additional DSC measurements.

Using this technique in a multi-dwell cure cycle adds complexity as assumptions must be made. Firstly, in the ramp, as temperature increases, the cure index cannot be calculated as the temperature increase results in a drop in IV, so a gap is shown instead. The second is that the maximum IV before the horizontal trend is $\log(IV)_\infty$ and the minimum viscosity IV value is $\log(IV)_0$. It should also be stated that when the temperature changes, normalising values should be collected at those temperatures. However, this method only supports simple epoxy amine networks, not complex network formation like in TGAP/DDS. This makes it challenging to collect values where the value is true IV for two reasons. One due to the dipole motion effect and secondly due to the uncured state behaving like an ionic liquid. When ionic liquid behaviour occurs IV values at low frequencies cannot be obtained at high temperatures as the change in conductivity is effectively zero [152,231]. Therefore, the IV values will be directly obtained from the dielectric measurements using standard cure cycle.

The cure index as a function of time for the four structural isomers of TGAP/DDS cured using the standard multi-dwell cure cycle is shown in Figure 6.18. As should be expected, the plot looks very similar to the IV plot shown in Figure 6.14, only normalised to one and gaps in the data where IV decreases during the temperature ramps. It is also worth noting that the cure index decreases in the final 200 ^{o}C dwell due to the T_g effect discussed above. This is not seen when calculating degree of cure using either DSC or NIR.

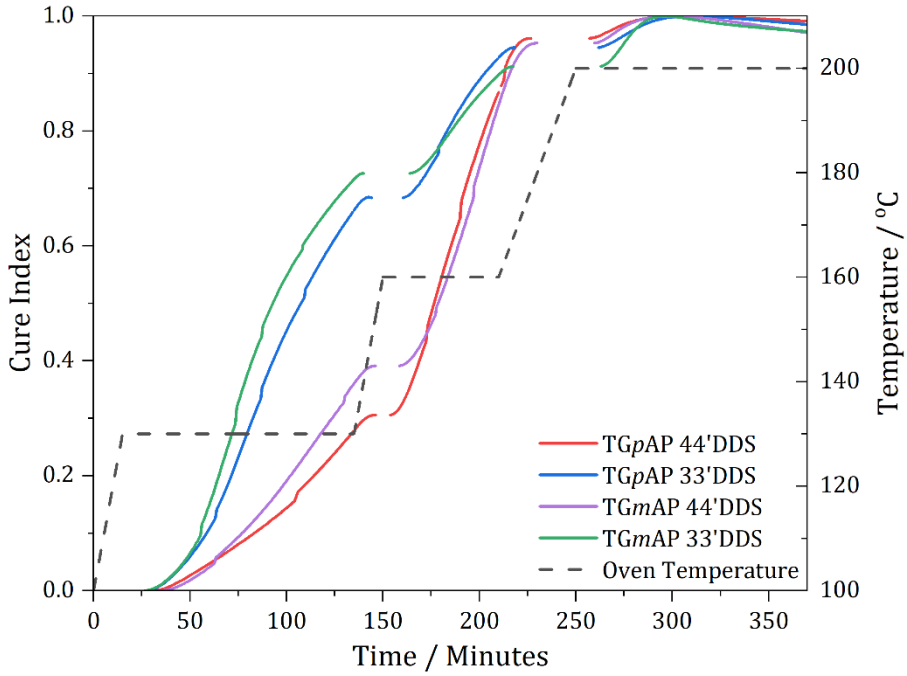

Figure 6.18 – Cure index for the four structural isomers of TGAP/DDS when cured using the standard cure cycle as determined by dielectric analysis and equation (6-19).

Cure index increases dramatically in the first dwell for the 33'DDS formulations, whereas in the second dwell, the 44'DDS cure index increases dramatically. The cure index is lower at the start of the final dwell for TG*m*AP/33'DDS than the other formulations, which is contrary to what was seen in both NIR and DSC, but this is caused by TG*m*AP/33'DDS's T_g being lower than the oven temperature, resulting in lower than expected cure index values.

These different behaviours indicate the points at which flow is restricted. Where flow is restricted, the cure index will be higher. Different types of reactions will restrict flow differently. Epoxy primary amine reactions form linear sections of the network and small amounts of crosslinking in TGAP as it is trifunctional. In contrast, epoxy secondary amine and etherification reactions will form crosslinks between the linear sections. This will restrict flow greater. Therefore, when the cure index increases dramatically, it can be assumed that this is where significant crosslinking occurs. For the 33'DDS formulations, this begins in the 130 °C dwell as found by NIR. For the 44'DDS formulations, significant crosslinking occurs in the 160 °C dwell, also found by NIR.

The dielectric analysis presented for the other heating regimes could be analysed using the same technique, but the downside is that DSC data would also have to be used. The maximum *IV* value for the different TGAP/DDS formulations in the standard cure cycle cannot be used as

the $\log(IV)_\infty$ value as the heating regime is different. The change in temperature in the standard cure cycle lowers the final IV, and it effectively remains in its 'history', so calculating the cure index of the 130 and 160 °C dwell would result in a value of over 1, which is impossible. The degree of cure obtained from DSC would have to be used to normalise the values, which means that the reliability of the technique for calculating undercured samples is not good, and DEA cannot be used as a standalone technique. However, a valid comparison can be obtained for nearly 100 % cured samples using the same heating regimes.

Only one study has been found to have done a similar technique for calculating the cure index for multi-dwell cure cycles [99]. However, DSC was used to aid the results, and unsurprisingly, a good agreement was found between the cure index obtained by DEA and the degree of cure obtained by DSC. Raponi *et al.* and Hardis *et al.* also used equation (6-19) to calculate cure index. However, isothermal heating regimes were used; therefore, the complexity was reduced, and excellent agreement was seen with DSC and IR methods [138,171].

6.4. CONCLUSION

The dielectric analysis presented in this chapter has shown that the different structural isomers of TGAP/DDS form their crosslinked network differently, as shown by the difference in their IV values. Previously, dielectric measurements on cured samples could describe the relaxations that the networks undergo, but this technique analyses the mobility of ions, or reactive species, during the cure. Commercially available equipment has been used as a minimal sample prep and online technique widely used in industry.

Dielectric analysis has shown that the initial mechanical viscosity of TG*m*AP is higher than that of TGpAP due to the bent structure, which restricts flow more than the more linear structure of TG*p*AP. However, whether the 33'DDS or 44'DDS formulations have greater viscosity has not been confirmed, as the results have varied between the different heating regimes.

Understanding the principles behind dielectric analysis has been key to understanding what happens in the cure due to the competing effects between curing and change in temperature. Temperature ramps have been challenging to understand independently, but comparisons between the formulations have allowed for excellent insight. In all heating regimes, the 33'DDS formulations are initially more reactive than the 44'DDS formulations, as found in Chapter 4.

Thermal and Chapter 5. Thermal. The greater the restriction in ion flow, suggests that more reactions occur.

Like DSC, DEA cannot identify the reactions occurring during the cure, but subtle differences can give an idea of the type of reactions. Where there is a significant increase in IV, linear and crosslinking reactions are taking place, and where there is a controlled increase in IV it can be thought that linear (epoxy primary amine) reactions are taking place.

When there is little change, a horizontal trend, in IV, curing reactions have finished. A clear horizontal line was obtained in both the 130 and 160 °C dwells after the curing reactions had finished. However, in the dynamic heat to 200 °C and the standard multi-dwell cure cycle, all formulations, but less so in TG*p*AP/44'DDS, showed a small decrease in IV. This was attributed to the cure temperature being in the glass transition temperature range where the flow of the polymer chains could occur, indicating network relaxation was occurring.

DEA can be used to indicate the cure state using the DiBenedetto equation to obtain the cure index. Despite the need to make some assumptions, good comparison could be made between the different TGAP/DDS formulations. The cure index values' reliability has not been assessed in this chapter as this will be done in Chapter 7. Cured Properties, but as discussed, it is not expected to be perfect. This is not necessarily needed for DEA as its benefits of running alongside manufacturing processes with minimal sample preparation and impact vastly outweigh this.

7. INVESTIGATION OF THE CURED PROPERTIES OF THE STRUCTURAL ISOMERS OF TGAP/DDS AS A RESULT OF VARYING NETWORK DEVELOPMENT

7.1. INTRODUCTION

In the previous three chapters, Chapter 4. NIR, Chapter 5. DSC and Chapter 6. DEA, the cure of the four structural isomers of TGAP/DDS has been monitored. Differences in network formation have been identified. Each technique has identified subtle variances between the different isomers due to reactivity and molecular shape. Variation in network formation should affect the morphology of the cured resins, as will be discussed here using results from various techniques.

7.2. CHAPTER OVERVIEW

This chapter will first compare the evolution of cure with the three different techniques: near-infrared spectroscopy (NIR), differential scanning calorimetry (DSC), and dielectric analysis (DEA). The cured properties of the structural isomers of TGAP (triglycidyl-*para*-aminophenol and triglycidyl-*meta*-aminophenol) and DDS (4,4'-diaminodiphenyl sulphone and 3,3'-diaminodiphenyl sulphone) will then be discussed. The techniques used to characterise the resins will be dynamic mechanical analysis, gas pycnometry, positron annihilation lifetime spectroscopy, flexural mechanical testing and thermogravimetric analysis. A good understanding of how using different structural isomers of TGAP/DDS affects the resultant resin properties can be gained by characterising the resins, allowing the further tailoring of high-performance multifunctional epoxy resins.

7.3. EVOLUTION OF CURE

Each cure monitoring technique has given information regarding the cure state of the four different structural isomers of TGAP/DDS. In theory, there should be very little difference between the techniques. However, there may be differences as the techniques calculate the cure state using different properties. The calculation methods for NIR, DSC and DEA are summarised in Table 7.1. NIR monitors the concentration of epoxide groups, DSC calculates the enthalpy of reaction, and DEA monitors the evolution of ion viscosity throughout the cure.

Table 7.1 – Cure state calculation methods for different cure monitoring techniques.

Technique	Cure state nomenclature	Method
Near-infrared spectroscopy	Degree of cure	$\alpha(t) = \frac{[EP]_0 - [EP]_t}{[EP]_0}$
Differential scanning calorimetry	Degree of cure	$\alpha(t) = \frac{\Delta H(t)}{\Delta H_0}$
Dielectric analysis	Cure index	$cure\ index = \frac{\log(IV)_t - \log(IV)_0}{\log(IV)_0 - \log(IV)_\infty}$

As discussed in the DEA chapter, the degree of cure is not calculated. Instead, the cure index is calculated and is related to the degree of cure by equation (7-1).

$$cure\ index = \frac{\lambda\alpha}{1-(1-\lambda)\alpha} \tag{7-1}$$

Where λ is an adjustable convexity parameter related to the difference in heat capacity between the uncured and fully cured resin. This can be determined using fitting tools with DSC data or can be calculated experimentally but has not been done here and has is assumed to be equal to 1 as done so by Lee [153]. Complexity is added to the calculation as a mix of isothermal and non-isothermal heating regimes are used. Calculating λ would improve the results if only one method of heating is used. Day investigated this for non-isothermal cures when calculating cure state determined by DEA and comparing to DSC degree of cure values and found very limited improvement [232]. This has also been the case when $\lambda = \frac{T_{g_0}}{T_{g_\infty}}$.

The comparison of the evolution of cure state as calculated by NIR, DSC and DEA for the four structural isomers of TGAP/DDS is shown in Figure 7.1. Good agreement can be seen for most parts. The degree of cure, as calculated by NIR, initially varies more with DEA and DSC for the 44'DDS formulations. NIR indicates the resin is more cured than in DSC and DEA. However, for the 33'DDS formulations, NIR and DSC show slightly better agreement. The difference in

agreement could possibly relate to the type of reactions taking place. When the resins are more reactive initially (33'DDS formulations), the exothermic response is similar to epoxide concentration change, as when epoxy secondary amine reactions occur directly after epoxy primary amines, the enthalpy is higher, which is more comparable to the change in concentration. However, when only epoxy primary amine reactions occur, the enthalpy of reaction is not as high, resulting in DSC giving lower degree of cure values. Later in the cure, when primary amines have all been consumed, the agreement between DSC and NIR is much better for all formulations.

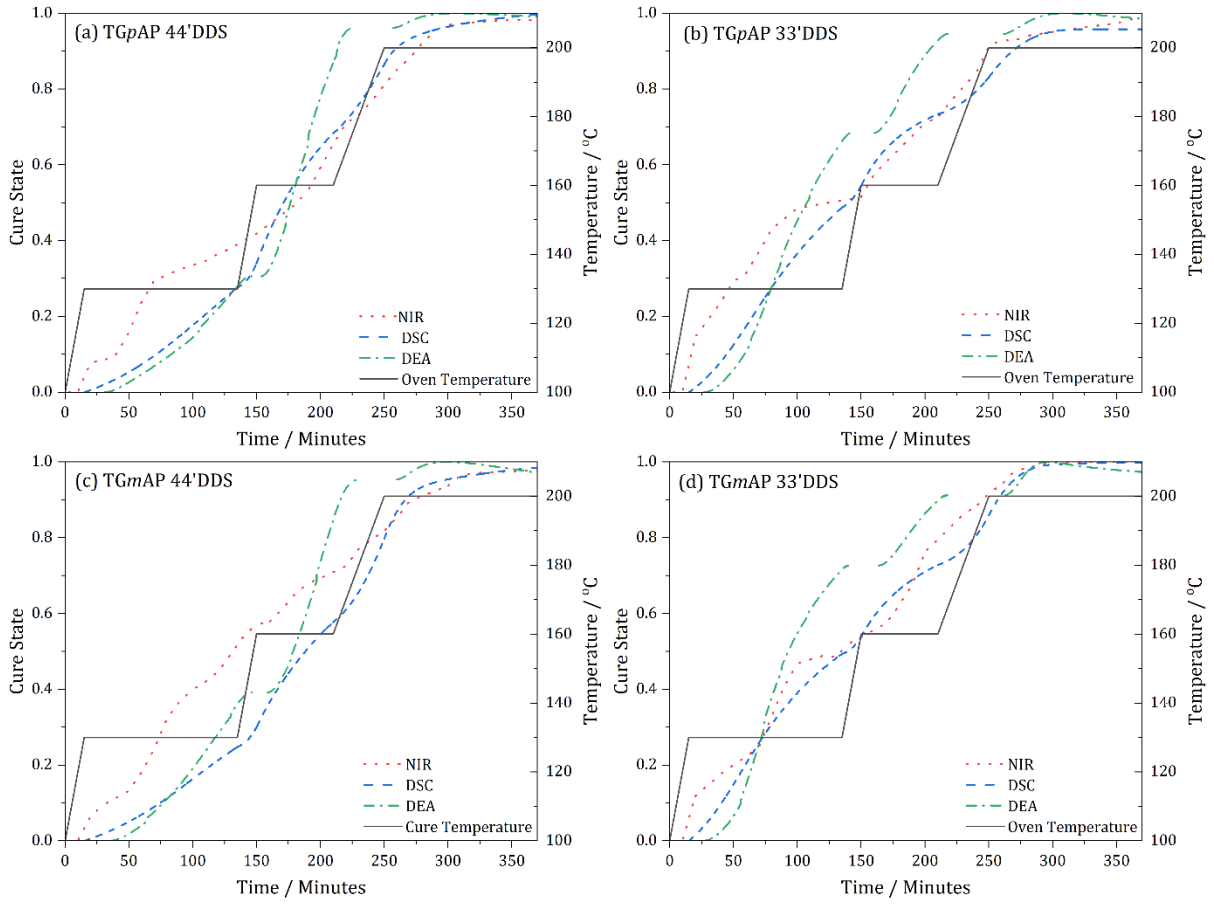

Figure 7.1 – Comparison of the evolution of cure state for the four structural isomer formulations of TGAP/DDS cured using the standard cure cycle as calculated by near-infrared spectroscopy (NIR), differential scanning calorimetry (DSC) and dielectric analysis (DEA): (a) TG*p*AP/44'DDS, (b) TG*p*AP/33'DDS, (c) TG*m*AP/44'DDS and (d) TG*m*AP/33'DDS.

Calculating degree of cure from NIR only considers the epoxide concentration change, not the amine concentration change. In contrast, DSC considers the total enthalpy of reaction. Suppose

different epoxide reactions (primary, secondary amine and etherification) occur, the enthalpy of reaction for each reaction could be different. However, literature and the dynamic DSC measurements undertaken in Chapter 5. Thermal would disagree with this. Total enthalpy of reaction values were found to be very similar to the literature value assigned to the epoxide ring opening reaction. Cole *et al.* investigated using different ratios of TGDDM:DDS and obtained similar total enthalpy of reaction values between ratios, suggesting that irrespective of the functional group reacting with an epoxide ring, the total enthalpy of reaction will be the same [226]. The difference between NIR and DSC could therefore be related to error in the analysis method. NIR is not a perfect technique, there are many opportunities to incorporate error, such as interpretation of the baseline and band overlap.

DEA shows good agreement with DSC data initially in the early stages of the cure for the 44'DDS formulations, as at this point, mainly epoxy primary amine reactions are taking place. TG*m*AP/44'DDS deviates slightly towards the end of 130 °C dwell. From NIR, it is known that a small amount of crosslinking does occur, which could be the reason, but it could also be related to which part of the TGAP molecule reacts. In Chapter 4. NIR, it was suggested that in TG*p*AP, the glycidyl amine portion behaves as a tertiary amine catalyst when reactions are initially 'slow' (44'DDS formulations). Therefore, in TG*p*AP, the reactions initially occur on both ends of the molecule as the glycidyl amine is sterically hindered by the catalysis interaction, whereas in TG*m*AP, the reactions can occur on the both epoxide groups in the glycidyl amine and potentially result in internal cyclisation [45,190]. If the reactions occur on the glycidyl amine, as shown in Figure 7.2 (b), rather than on both the glycidyl amine and glycidyl ether of the TGAP molecule, as shown in Figure 7.2 (a), the ion restriction may be greater as an aromatic branch structure is formed rather than a free epoxide branch.

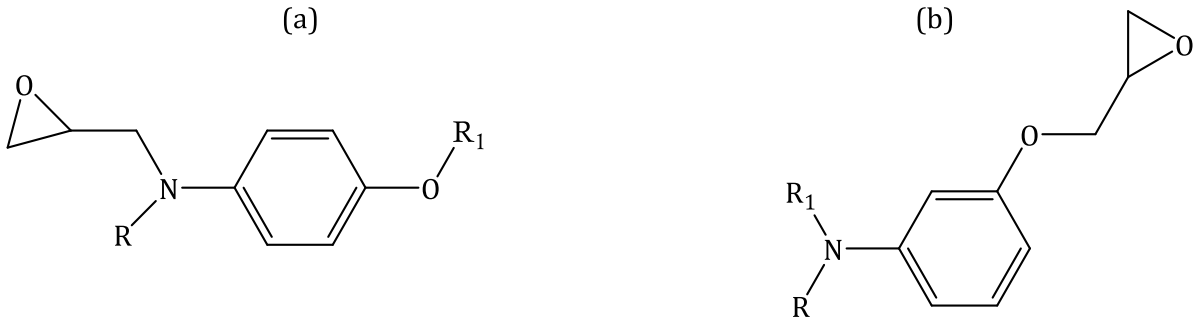

Figure 7.2 – Initial path of reaction in the structural isomers of TGAP molecules: (a) TG*p*AP reacts on both the glycidyl amine and glycidyl ether, and (b) TG*m*AP reacts in the glycidyl amine portion. R and R_1 indicate epoxy amine chain.

These are effectively dangling chains and will restrict the flow of any mobile reactants or unbonded linear chains. The extent to which either dangling chain will restrict flow depends on the chemical structure and molecular weight. A glycidyl amine ether branch, can be considered flexible due to its single carbon-carbon bonds which allow for rotation and movement. Whereas, the aromatic branch structure in shown in Figure 7.2 (b), has a stiff, planar aromatic ring and also higher molecular weight. Ion flow restriction will be more apparent when epoxide ring opening occurs predominantly on the glycidyl amine portion of TG*m*AP compared that of a mixture of both glycidyl amine and glycidyl ether in TG*p*AP. However, this is only a hypothesis, there has been no additional testing to investigate whether this is actually the case.

Poor agreement is shown with the 33'DDS formulations halfway through the 130 °C temperature dwell, as this is when significant crosslinking reactions occur. TG*m*AP/33'DDS cure index deviates more due to slightly more crosslinking than in TG*p*AP/33'DDS but also perhaps due to the positions of the reactions shown in Figure 7.2.

When crosslinking reactions dominate in the 44'DDS formulations in the 160 °C dwell, poor agreement is also seen as the crosslinking reactions restrict ion mobility greater than linear reactions, resulting in a higher cure state than calculated by NIR and DSC. This hasn't been seen in previous literature as DGEBA resins have been used generally [138,154,163]. DGEBA has an epoxy functionality of two compared to TGAP's three, meaning that the rate at which ion mobility is restricted is much lower in DGEBA.

In the final 200 °C dwell of the cure, good agreement is seen between DSC and NIR, with DEA being slightly higher due to DEA not being able to detect the subtle etherification reactions

occurring in the final stages. These reactions crosslink already highly restricted chains, and the annealing effect occurs here, as discussed in the Chapter 6. DEA.

It must also be considered that these formulations use a significant epoxy excess. This will play a major role in the differences as etherification reactions affect the techniques differently. Previous literature has not used as significant an excess epoxy in TGAP studies where these techniques have been compared before. Nor have they used multi-dwell cure cycles. Temperature changes can heavily influence the results.

7.4. DYNAMIC MECHANICAL ANALYSIS

Dynamic mechanical analysis of the cured four structural isomer formulations of TGAP/DDS has been extensively investigated in a previous publication by Ramsdale-Capper and Foreman [32]. The analysis presented here will, therefore, be brief but will link their findings with the differences in network development. The tan δ plots for the four structural isomer formulations of TGAP/DDS are shown in Figure 7.3. Three secondary phase transitions can be identified by these plots. The glass transition temperature, T_g, at temperatures above 150 °C, the omega transition, T_ω, at approximately 50 °C and the beta transition, T_β, at approximately -50 °C.

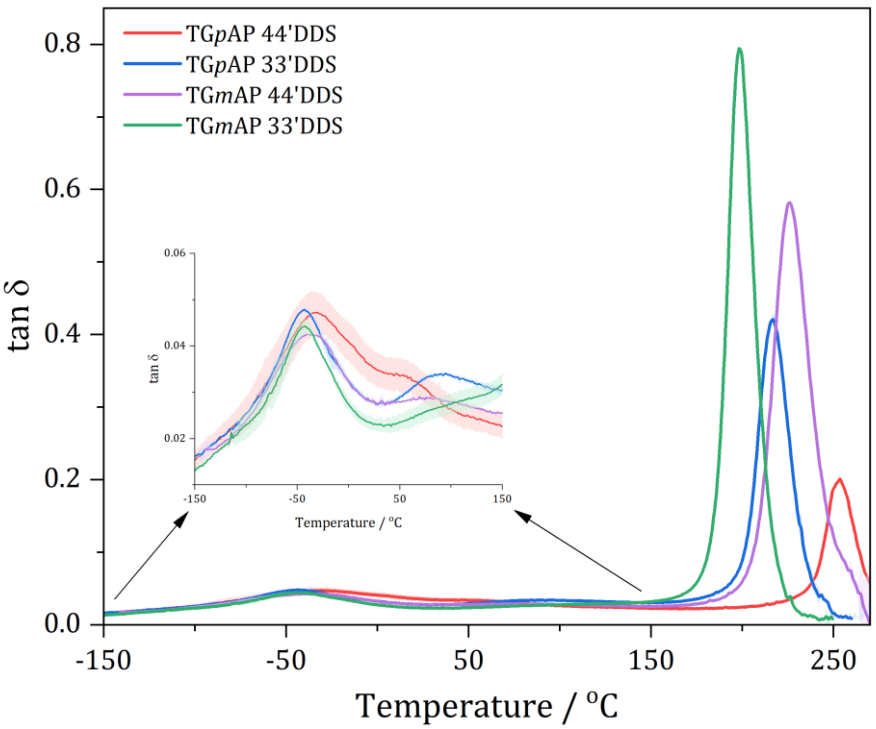

Figure 7.3 – tan δ as a function of temperature for the four structural isomer formulations of TGAP/DDS cured using the standard cure cycle as obtained by dynamic mechanical analysis in single cantilever mode at 1 Hz. The plots are an average of two tests where the shaded area is standard deviation.

7.4.1. GLASS TRANSITION

T_g is shown by a large peak at high temperature in the tan δ plot. As discussed in Chapter 4. NIR and Chapter 6. DEA, this transition is related to crosslink density and chain stiffness. Polymers with a higher crosslink density and chain stiffness should have a higher T_g. The T_g peak centres are summarised in Table 7.2. The values here are slightly lower than those given in Ramsdale-Capper and Foreman, as the temperature calibration of the equipment has recently been improved [32,233].

Lower T_g indicates that the crosslinking density is lower; therefore, TG*p*AP/44'DDS can be said to have the highest crosslink density and TG*m*AP/33'DDS the lowest. However, NIR has determined that TG*m*AP/33'DDS goes to complete consumption of epoxide groups. Therefore, it would be thought that the T_g of TG*m*AP/33'DDS would be the highest, but this is not the case. The chain stiffness must also be considered. More linear molecules, the *para* isomers (TG*p*AP and 44'DDS) are effectively stiffer as the force transmits through the 1,4 position rather than in the *meta* where the force is transmitted through the 1,3 position. Considering the chain stiffness

alone, the trend shown in Table 7.2 is logical, the more linear starting reagents result in a higher T_g. How the crosslinks form in the network also plays a role in determining the T_g [23,197].

Table 7.2 – Glass transition temperatures for the four structural isomer formulations of TGAP/DDS as determined by dynamic mechanical analysis at a testing frequency of 1 Hz.

	TG*p*AP/44'DDS	TG*p*AP/33'DDS	TG*m*AP/44'DDS	TG*m*AP/33'DDS
T_g / °C	253.7 ± 0.3	216.2 ± 0.8	226.2 ± 0.1	198.6 ± 0.5

Due to the increased reactivity of 33'DDS, crosslinking reactions occur earlier in the curing reaction. This results in areas of localised crosslinking connected by areas of low crosslinks. A less homogenous network forms compared to the 44'DDS counterparts, resulting in a difference of 20 – 30 °C in T_g values. This increased reactivity also potentially increased a side reaction known as internal cyclisation, as discussed in Chapter 4. NIR, where cyclic structures are formed on the glycidyl amine due to the proximity of two epoxide groups [45,190]. When analysing the functional group concentrations through NIR, this may appear as a crosslinking reaction, but they do not behave like a crosslink [52]. They effectively behave as linear portions of the network and increase the molecular weight between crosslinks, therefore reducing the T_g. These can form through either epoxy secondary amine or etherification reactions and as suggested in Chapter 4. NIR, occur less so in the TG*p*AP/44'DDS formulation.

The T_g peak identifies the temperature range at which this transition occurs but can also give more information regarding the structure of the polymer network. tan δ is given by equation (7-2).

$$\tan\delta = \frac{E''}{E'} \qquad (7\text{-}2)$$

Where E'' is loss modulus and E' is storage modulus. Storage modulus refers to the amount of energy stored in the material upon deformation, whereas loss modulus refers to the amount of energy lost upon deformation due to friction and internal motions in the network [187]. tan δ is also to referred to as the damping effect and measures how much energy is lost in the material

due to differences in network structure. If the tan δ value is smaller the energy dissipation that occurs when the T_g is reached is lower. A small tan δ indicates a stiffer network where the cooperative motions of the network are less. The peak tan δ values are given in Table 7.3, with TG*p*AP/44'DDS being the lowest and TG*m*AP/33'DDS being the highest. The area of the T_g peak is also given in Table 7.3, which refers to the amount of energy required for this transition to take place [234]. A larger area accounts for the peak's height and width. Despite TG*m*AP/44'DDS having a lower maximum tan δ value, the area is similar to TG*m*AP/33'DDS, indicating the temperature range over which the transition occurs is greater.

Table 7.3 – T_g tan δ values and areas for the four structural isomer formulations of TGAP/DDS obtained from dynamic mechanical analysis in single cantilever mode using a testing frequency of 1 Hz.

	TG*p*AP/44'DDS	TG*p*AP/33'DDS	TG*m*AP/44'DDS	TG*m*AP/33'DDS
T_g tan δ peak value	0.20 ± 0.02	0.42 ± 0.01	0.58 ± 0.00	0.79 ± 0.00
T_g tan δ area	3.31 ± 0.34	9.04 ± 0.06	14.64 ± 0.28	15.15 ± 0.01
T_g range / ^{o}C	24	22	38	27

If the number of cooperative motions that occur in TG*p*AP/44'DDS is less than in TG*m*AP/33'DDS, it could suggest that TG*p*AP/44'DDS is a more homogenous network. However, it could also relate to the chemical structure of starting materials. *meta* starting reagents have a more significant number of energy dissipation mechanisms. This was discussed in-depth in a thesis written by Heinz [235]. An adapted figure from their work is shown in Figure 7.4. TG*m*AP/33'DDS can undergo the greatest number of energy dissipation mechanisms, followed by TG*m*AP/44'DDS and TG*p*AP/44'DDS; however, TG*p*AP/44'DDS cannot.

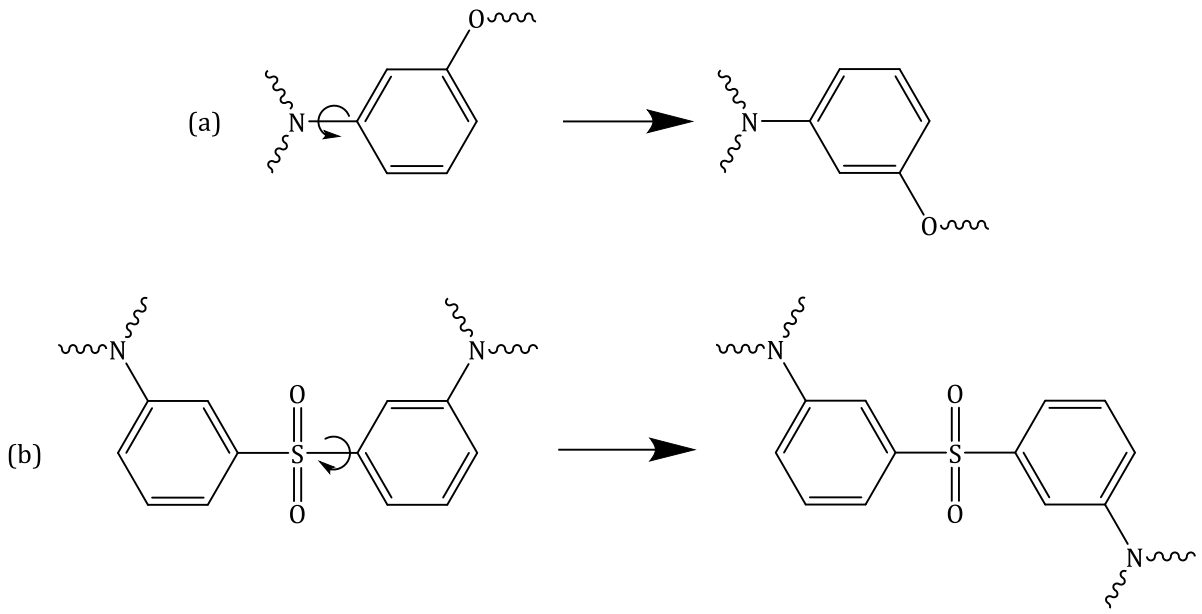

Figure 7.4 – Energy dissipation motions in (a) triglycidyl-*meta*-aminophenol (TG*m*AP) and (b) 3,3'-diaminodiphenyl sulphone (33'DDS). Adapted from Heinz [235].

Consequently, it is hard to say how much the original starting materials affect the damping of the cured material and thus relate to its network development. However, DMA does not just identify the T_g.

7.4.2. BETA TRANSITION

The glass transition region refers to the mobility of the overall network structure. At lower temperatures, the beta transition refers to local cooperative motions within the network [32]. Different parts of the network can undergo different motions. Tu *et al.* found that the lower temperature region of the transition is attributed to the cooperative ring-flipping motion of the two phenylene rings in DGEBA [35]. Shi *et al.* found that the middle region was attributed to the motion of the ether-containing units and the high-temperature region to the ring flipping (phenylene rotation) in the aromatic hardener [236]. Both these studies used DGEBA/DDS systems. These differ from the resins used in this study, where some are *meta*-substituted (TG*m*AP and 33'DDS), and some do not consist of only glycidyl ether groups. However, Ramsdale-Capper and Foreman were able to apply the findings to the isomers of TGAP/DDS and make similar conclusions [32].

The tan δ plot for the four structural isomer formulations of TGAP/DDS highlighting the beta transition region between -100 °C and 30 °C is shown in Figure 7.5. Depending on the structural isomer formulation, the shape of the transition is different. Firstly, the 33'DDS formulations show a sharper peak at lower temperatures, the middle region attributed to the motion of the hydroxy propyl groups. The second is that the TG*p*AP formulations have higher tan δ values at lower temperatures in the region, which is attributed to the aromatic ring flipping in the epoxy units. Thirdly, the shape of the higher temperature region. This region is attributed to the phenylene ring flipping in the hardener units. However, there is less of a noticeable trend.

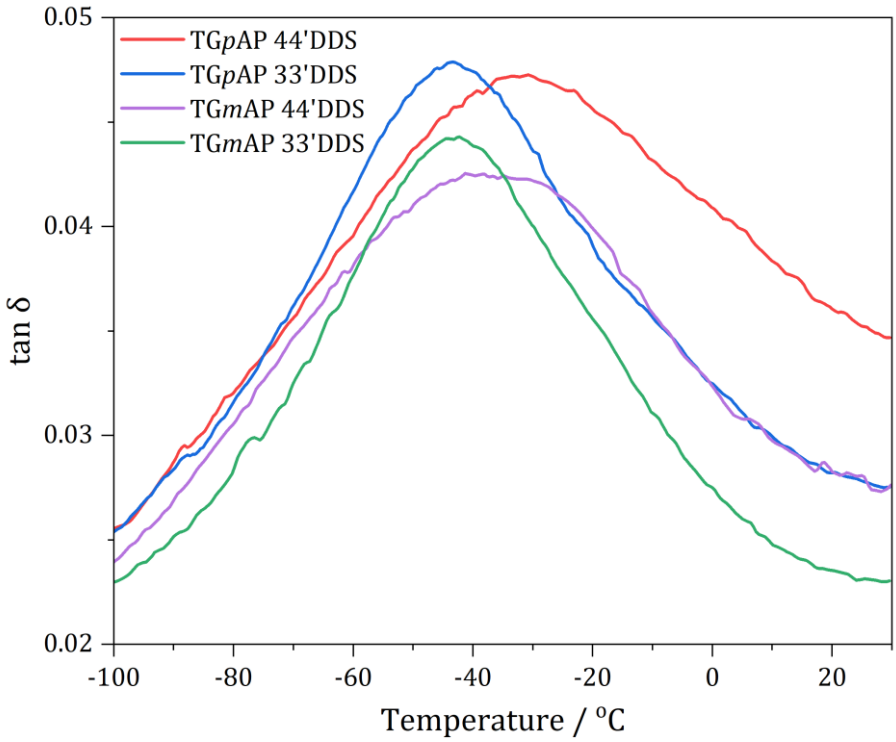

Figure 7.5 - tan δ as a function of temperature between -100 °C and 30 °C showing the beta transition region for the four structural isomer formulations of TGAP/DDS cured using the standard cure cycle as obtained by dynamic mechanical analysis in single cantilever mode at 1 Hz. The plots are an average of two tests where the shaded area is standard deviation.

Like the energy dissipation motions in Figure 7.4, the *para* or *meta* positioning determines how the molecular units can move. Ring flipping, or π flipping, is more prevalent in molecules where the phenylene ring can flip on its axis, the *para* isomers, as shown in Figure 7.6 [28]. Compared to DGEBA, where there is the possibility of two aromatic rings flipping, TG*p*AP only has one;

therefore, the intensity of the lower temperature region is lower if compared to DGEBA systems. However, due to the lack of rotational axis in TG*m*AP, no ring flipping can occur, resulting in lower initial tan δ values than in TG*p*AP. Differences in network formation will have minimal effect on this region as this only relates to the structure of the starting epoxy molecules as far as the current literature is concerned [32,35,236]. The high-temperature region of the peak refers to the phenylene ring flipping in the hardener. The 44'DDS formulations can undergo ring flipping, whereas the 33'DDS formulations cannot. However, TG*p*AP/33'DDS and TG*m*AP/44'DDS display similar high-temperature region trends. This could suggest that this region is the cooperative motion of all phenylene rings.

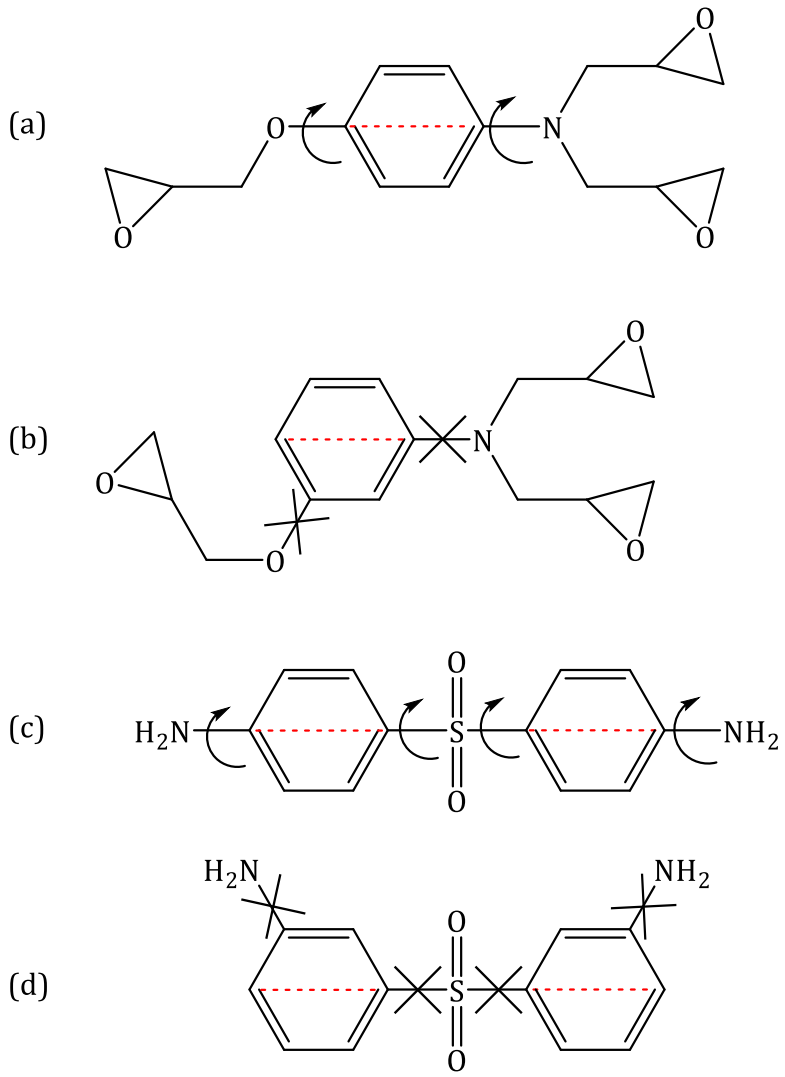

Figure 7.6 – Ring flipping in the structural isomers TGAP: (a) triglycidyl-*para*-aminophenol, (b) triglycidyl-*meta*-aminophenol, (c) 4,4'diaminodiphenyl sulphone and (d) 3,3'diaminodiphenyl sulphone.

The mid-temperature region, the peak, is concerned with the local motion of the epoxy branches, known as the hydroxy propyl groups. Three different types of behaviour can be seen here. Firstly, the peak temperature, secondly, the intensity, and thirdly, the area. These different trends are summarised in Table 7.4.

The peak temperature indicates the energy required for these motions to take place. The 33'DDS formulations peak at a lower temperature than the 44'DDS formulations, suggesting that hydroxyl propyl groups in the 33'DDS networks are less restricted than the 44'DDS networks.

The intensity relates to the number of motions taking place. In this case, the epoxies pair up. It appears that the number of hydroxy propyl motions is greater in the TG*p*AP formulations compared to the TG*m*AP formulations. This could relate to the position of the TGAP molecule, where the network is initially formed on the epoxy molecule. However, these values do not consider the baseline; therefore, like with NIR analysis, the area of the peak is best used. This shows a slightly different trend. TG*p*AP/44'DDS gives the largest area, TG*p*AP/33'DDS and TG*m*AP/44'DDS have similar areas, and TG*m*AP/33'DDS has the smallest area. This trend aligns with the fact that the amount of potential ring flipping results in higher energy dissipation. TG*m*AP/33'DDS can undergo the smallest amount of ring flipping and TG*p*AP/44'DDS the most. Whether this gives information into the result of different network formation paths is difficult to say as there are different influences due to starting molecules. In this case, the peak temperature gives the best information about how the network differs.

Table 7.4 - β transition peak temperature values and areas for the four structural isomer formulations of TGAP/DDS obtained from dynamic mechanical analysis in single cantilever mode using a testing frequency of 1 Hz.

	TG*p*AP/44'DDS	TG*p*AP/33'DDS	TG*m*AP/44'DDS	TG*m*AP/33'DDS
beta peak temperature / °C	-30.7 ± 0.7	-43.4 ± 0.4	-36.8 ± 4.7	-42.2 ± 2.2
tan δ area	1.75 ± 0.13	1.37 ± 0.10	1.35 ± 0.10	1.24 ± 0.01
tan δ peak value	0.047	0.048	0.043	0.044

If the hydroxy propyl groups in the 33'DDS formulations undergo motions at lower temperatures, they are less restricted. TG*m*AP/33'DDS is the densest network, so the fact that it undergoes motions at lower temperatures and requires lower energy suggests that density isn't playing a huge role here. How the hydroxy propyl group is bonded dominates its ability to undergo motions. One reason is the increased reactivity of the 33'DDS hardener, which encouraged the secondary amine reactions to occur quickly after the primary amine reactions, resulting in localised regions of high crosslink density and low crosslink density and potentially the formation of internally cyclised structures. Because of this, the hydroxyl propyl motions can occur at lower temperatures than the more homogenous networks and less internally cyclised structures.

TG*p*AP/44'DDS is considerably higher than the other three formulations. It is expected to be the highest due to the greatest number of aromatic rings that can undergo ring flipping, but the existence of another sub-T_g transition that occurs very soon after the beta transition affects this value, potentially making it falsely high.

7.4.3. OMEGA TRANSITION

The origin of the omega transition is unclear, perhaps even more unclear than the beta transition, partly because it does not always present itself in all resin formulations. The transition is not commonly observed in the DGEBA/44'DDS formulations. Ochi *et al.* observed the omega transition (calling it the β' transition) in 3,9-bis[(3-methoxy-4-glycidyl~phenyl]-2,4,8,l0-tetroxaspiro(5,5)undecane (BMPTU) and 3,9-bis[(4-glycidyl)phenyl]-2,4,8,1O-tetroxaspiro(5,5)undecane (BGPTU) resins cured with 4,4'-diaminodiphenyl methane (DDM) [237,238]. The structure of these two resins is shown in Figure 7.7. These are bifunctional and differ from DGEBA by the oxygen-containing spiro ring between the two aromatic rings instead of two methyl groups.

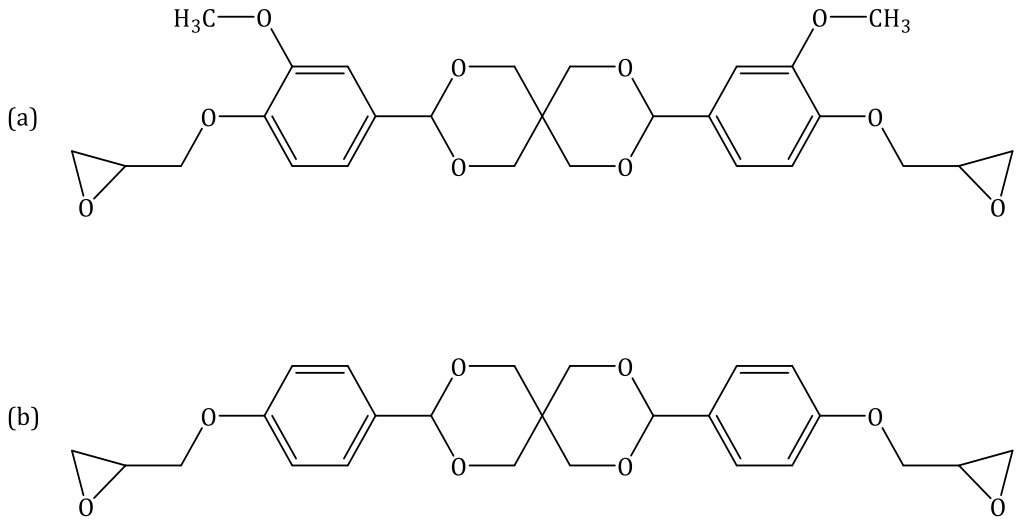

Figure 7.7 – Chemical structures of 3,9-bis[(3-methoxy-4-glycidyl~phenyl]-2,4,8,l0-tetroxaspiro(5,5)undecane (BMPTU) and 3,9-bis[(4-glycidyl)phenyl]-2,4,8,1O-tetroxaspiro(5,5)undecane (BGPTU) from Ochi *et al.* where the omega transition was observed when cured with DDM [238].

Interestingly, the omega transition was not observed in the ortho isomer of BGPTU cured with DDM. Ochi *et al.* concluded that the omega transition originated from the phenylene ring adjacent to the centre spiro structure [237,238]. However, Sasuaga and Udagawa observed the omega transition in DGEBA when cured with DDM along with TGDDM and DGEBF formulations [239]. They attributed the omega transition to "internal stress caused by non-uniformity in the crosslinking structure." They were also able to reduce the size of or shift the omega transition peak by irradiating the samples. Brahatheeswaran and Gupta also came to similar conclusions regarding the omega transition [240]. Rather than irradiating the samples to reduce the omega transition, they aged the samples at temperatures just below the T_g, essentially annealing the sample.

Ramsdale-Capper and Foreman observed the omega transition in the four structural isomers of TGAP/DDS and suggested that more effective hydrogen bonding prevented the cooperative motion of the hydroxyl propyl and phenylene ring groups more so in TG*m*AP/33'DDS than in TG*p*AP/44'DDS [32]. This hypothesis makes sense, and the antiplasticised behaviour of TG*m*AP/33'DDS would support it [241], but why TG*m*AP/33'DDS hydrogen bonds more effectively than TG*p*AP/44'DDS is challenging to understand.

Figure 7.8 shows the DMA plot highlighting the omega transition for the four structural isomers of TGAP/DDS between -50 °C and 150 °C. The omega transition peak is far less prominent than the beta transition, suggesting that it isn't a dominant transition but is still an

important feature of the cured networks. The omega transition occurs at a lower temperature compared to the other formulations, followed by TG*p*AP/33'DDS and TG*m*AP/44'DDS; however, TG*m*AP/44'DDS is less prominent than TG*p*AP/44'DDS and finally, TG*m*AP/33'DDS where the peak isn't as clear as it is less prominent and also overlapping the T_g peak. The peak temperatures are summarised in Table 7.5. Unlike the T_g and beta transition, the peak areas have not been analysed due to overlapping.

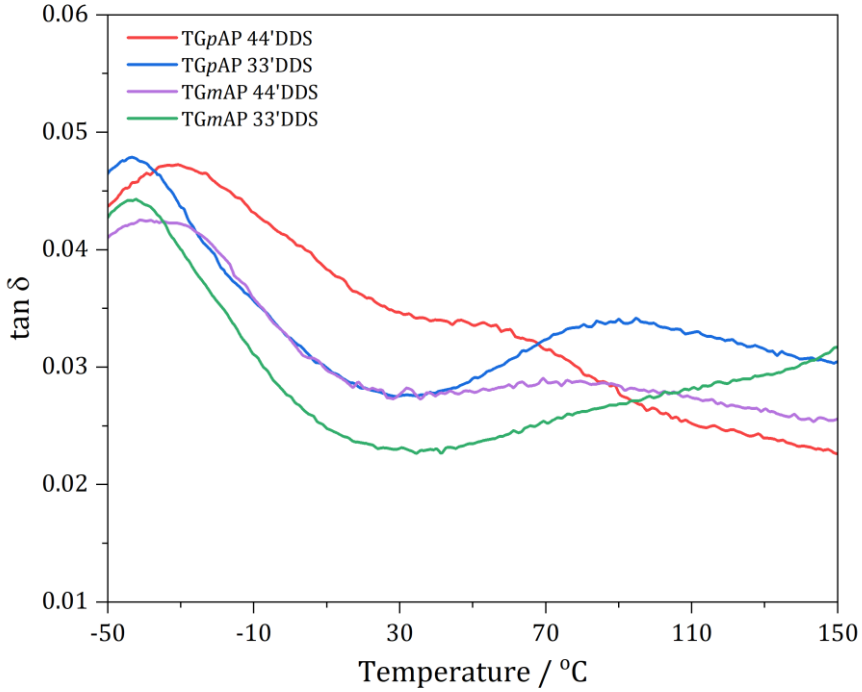

Figure 7.8 - tan δ as a function of temperature between -50 °C and 150 °C showing the omega transition region for the four structural isomer formulations of TGAP/DDS cured using the standard cure cycle as obtained by dynamic mechanical analysis in single cantilever mode at 1 Hz. The plots are an average of two tests.

The fact that the TG*p*AP formulations have a more prominent peak suggests that this transition is related to the cooperative motions of the phenylene ring and hydroxyl propyl groups on the epoxy molecule rather than the motion of the DDS molecule.

Table 7.5 - ω transition peak temperature values for the four structural isomer formulations of TGAP/DDS obtained from dynamic mechanical analysis in single cantilever mode using a testing frequency of 1 Hz. * denotes an approximate value as this peak was significantly overlapped.

	TG*p*AP/44'DDS	TG*p*AP/33'DDS	TG*m*AP/44'DDS	TG*m*AP/33'DDS
omega peak temperature / ^{o}C	53.1 ± 0.3	90.0 ± 1.6	78.4 ± 1.7	*101.9 ± 1.5

The peak temperature would have been initially thought to be related to the energy required for these motions. This is partly true, but the cure conditions must also be considered. A similar study by Heinz into the structural isomers of TGAP/DDS also observed the omega transitions. A slightly different trend in the omega transition was observed [235]. An obvious peak for the omega transition was observed at approximately 90 °C for the 44'DDS formulations, 100 °C for TG*p*AP/33'DDS and a broad shoulder at 125 °C for TG*m*AP/33'DDS. The intensities of the peaks were similar based on the epoxy molecule. TG*p*AP formulations showed a higher peak than the TG*m*AP formulations. They suggested that peak temperature corresponded to the packing efficiency. A higher packing efficiency in the 33'DDS formulations resulted in an omega transition peak at a higher temperature.

A stoichiometric ratio of epoxy:amine was used in this study. This may have an impact as extra crosslinking occurs when an excess epoxy formulation is utilised, but another difference is the cure schedule. The cure was as follows: 115 °C for 3 hours, 150 °C for 3 hours, 180 °C for 3 hours and 200 °C for 1 hour. This cure was longer than the one used in this study apart from the final step, which was held for 1 hour at 200 °C compared to the two hours used. From this, it is apparent that the omega transition is related to internal stress. The extra dwell times at different parts in the cure allow for relaxation resulting in the TG*p*AP/44'DDS omega transition occurring at higher temperatures than the peak in this study (53 °C compared to 90 °C). This is similar to what was observed in TG*m*AP/33'DDS in Chapter 6. DEA. Holding at temperatures just below the T_g resulted in observable relaxation in the dielectric results.

This correlates with what Sasuaga and Udagawa concluded about the transition. By holding the resin at a temperature just below its T_g it allows for annealing in its crosslinked structure and reduces the internal stress buildup during the cooling stage, resulting in a shifted omega

transition peak [239]. The more homogenously crosslinked networks cannot anneal at the cure temperatures as effectively, resulting in a lower-temperature omega transition.

Some additional work has been done to investigate whether it is possible to remove or shift the omega transition peak by post-curing or annealing the resins at temperatures below their T_g. Figure 7.9 shows the shifting of the omega transition after aging at 210 °C for varying periods for TG*p*AP/33'DDS.

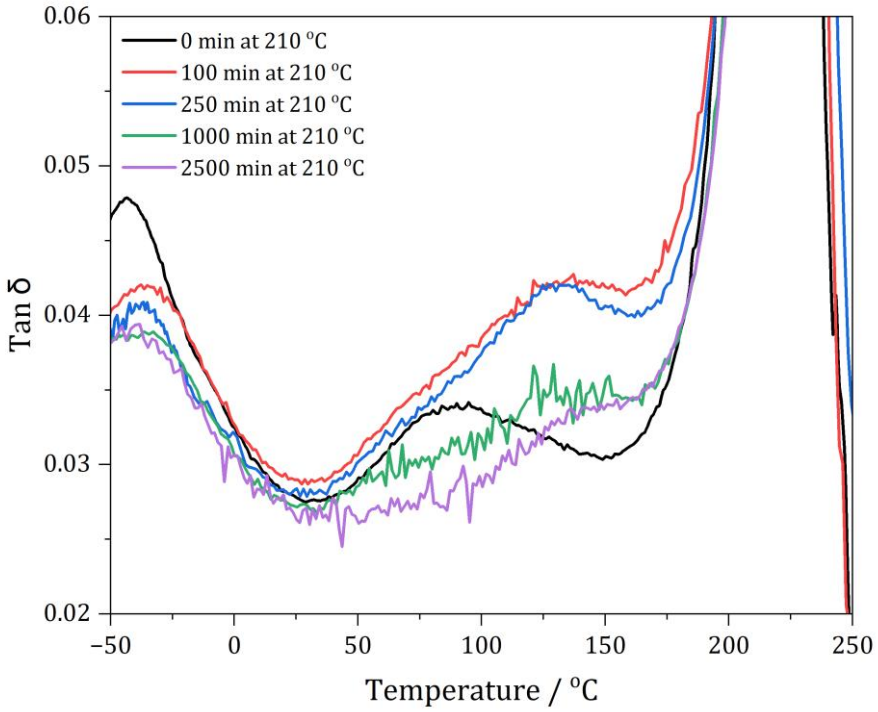

Figure 7.9 – tan δ as a function of temperature between -50 °C and 250 °C showing the omega transition region for TG*p*AP/33'DDS cured using the standard cure cycle and ageing at 210 °C for various time intervals as obtained by dynamic mechanical analysis in single cantilever mode at 1 Hz.

7.5. FREE VOLUME SPACE

7.5.1. GAS PYCNOMETRY

The density of the networks was determined using gas pycnometry to measure the volume of the samples relative to their mass, shown in Table 7.6. The lowest density is TG*p*AP/44'DDS, followed by TG*p*AP/33'DDS and then TG*m*AP/44'DDS and TG*m*AP/33'DDS, which are both very similar, within 0.0001 g cm^{-3} of each other. Considering the beta transition area values as

determined by DMA in Table 7.4, it would be expected that the largest value would have the lowest density and vice versa. This is the case apart from the TG*p*AP/33'DDS and TG*m*AP/44'DDS, where the densities are not as similar as the areas are. If it were just based on the ability of the local motions of the molecules, then it would be the same trend. However, it is not. The packing efficiency of the *meta* TGAP is better than that of the *meta*-DDS with its *para* counterpart.

Table 7.6 – Densities of the four structural isomers of TGAP/DDS determined using gas pycnometry.

	TG*p*AP/44'DDS	TG*p*AP/33'DDS	TG*m*AP/44'DDS	TG*m*AP/33'DDS
Density / g cm^{-3}	1.3112 ± 0.0007	1.3164 ± 0.0014	1.3211 ± 0.0005	1.3212 ± 0.0024

The *meta* isomers have more conformation states, possibly resulting in denser networks. It was suggested in Chapter 4. NIR that TG*p*AP/44'DDS was the most homogenous network due to the non-simultaneous reactions of the primary amines and then secondary amine compared to the 33'DDS formulations. This results in higher crosslink density and lower density as upon cooling, the crosslinks prevent efficient packing and leaves unoccupied free volume space [242]. This may be the case in the TG*m*AP/44'DDS formulations, but as it contains TG*m*AP, the number of conformational states is greater, resulting in more efficient packing. It could be expected that TG*m*AP/33'DDS has a significantly higher density than TG*m*AP/44'DDS like TG*p*AP/33'DDS compared to TG*p*AP/44'DDS, but the potential side reactions, such as internal cyclisation, leave unoccupied free volume space in the network.

7.5.2. POSITRON ANNIHILATION LIFETIME SPECTROSCOPY

Another technique that can indicate the free volume space in the crosslinked networks of cured epoxy resin is positron annihilation lifetime spectroscopy (PALS). It can identify the fractional free volume and average pore volume. Table 7.7 shows both these values for the four structural isomers of TGAP/DDS. Here, the fractional free volume space follows a similar trend to the beta transition area values, with TG*p*AP/44'DDS being the greatest and TG*m*AP/33'DDS being the smallest. Unlike the density values, TG*m*AP/33'DDS has significantly less free volume space than TG*m*AP/44'DDS. This is the trend that, based on results from previous chapters, would be

expected. Gas pycnometry is perhaps not sensitive enough to identify these subtle changes, whereas PALS is an incredibly sensitive technique that penetrates the network.

The average pore volume pairs based on epoxy with the pore volume being greater for the TG*p*AP formulations. This is related to the lack of conformational states in the TG*p*AP epoxies, potentially leading to larger voids between the different molecular chains. In contrast, TG*m*AP can more efficiently fill these gaps, resulting in smaller pores.

Table 7.7 - Average pore volume and % free volume space for the four structural isomers of TGAP/DDS determined using positron annihilation lifetime spectroscopy.

	TG*p*AP 44'DDS	TG*p*AP 33'DDS	TG*m*AP 44'DDS	TG*m*AP 33'DDS
Average pore volume / Å^3	60.7 ± 0.5	59.1 ± 0.5	55.3 ± 0.5	55.9 ± 0.5
Fractional free volume / %	10.67 ± 0.09	10.45 ± 0.09	10.30 ± 0.09	9.76 ± 0.09

7.6. FLEXURAL MECHANICAL TESTING

The flexural moduli of the four structural isomers have been investigated. Both Ramsdale-Capper and Foreman and Heinz have investigated the compressive properties of TGAP/DDS therefore, it will not be done here [32,233,235]. Flexural modulus, strength and strain at break values for the four structural isomers of TGAP/DDS are shown in Figure 7.10.

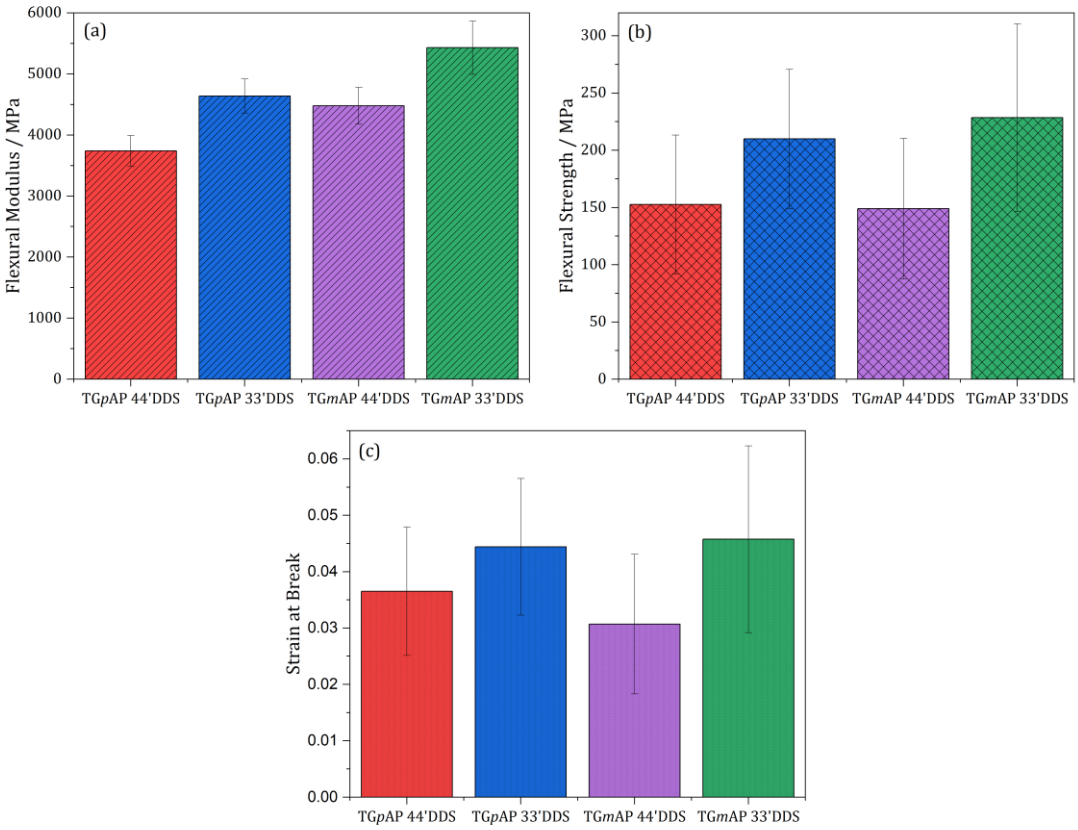

Figure 7.10 – Flexural properties of the four structural isomers of TGAP/DDS cured using the standard cure: (a) flexural modulus, (b) flexural strength and (c) strain at break. Each data set was 17 samples and the error shown is standard deviation.

The flexural modulus was greatest in TG*m*AP/33'DDS, TG*p*AP/33'DDS, and TG*m*AP/44'DDS were similar, and TG*p*AP/44'DDS had the lowest flexural modulus. This was similar behaviour to that observed by Heinz when undertaking compression tests of TGAP/DDS [235]. The trend relates to the fractional free volume space as determined by PALS. TG*m*AP/33'DDS has the lowest free volume space, the most efficient chain packing and, thus, the highest flexural modulus.

Flexural strength pairs based on the hardener, the 33'DDS formulations achieve a higher flexural strength compared to their 44'DDS counterparts. This relates to the beta transition in the 44'DDS case. The ability to undergo ring flipping on the *para*-substituted DDS provides an energy dissipation mechanism that reduces the yield stress, as discussed in another publication by Heinz et al. and Varley *et al.* [28,243]. Because of this, strain softening did not occur as prevalently in the 44'DDS formulations as it did in 33'DDS. In the 33'DDS formulations, this

energy dissipation mechanism was not available, and instead, high energy motions occurred, as shown in Figure 7.4, resulting in higher flexural strength values.

The strain at break values also paired by hardener with the 33'DDS formulations showing the greatest strain at break values. The reasons above can be attributed to this trend, but the network's homogeneity could also influence the strain values. Areas of high crosslink density connected by areas of low crosslink density will result in greater strain at break values as they possess greater molecular mobility compared to the more homogeneous TG*p*AP/44'DDS network.

NIR determined that residual epoxide groups were present in the final cured specimens of TG*p*AP/44'DDS and TG*m*AP/44'DDS. This will result in reduced modulus and strength as additional energy dissipation mechanisms exist. However, this should result in greater strain at break values. The data doesn't show this, indicating it has no significant effect.

It is important to note that flexural testing is not a true deformation mode but a combination of both tensile and compressive modes along with internal shear. It is difficult to determine how each formulation failed, and this will incorporate some uncertainty into the results, as shown by the sometimes-significant error.

7.7. THERMOGRAVIMETRIC ANALYSIS

7.7.1. THERMOGRAVIMETRIC CURE MONITORING

The thermal stability of the four structural isomers has been investigated while curing. Figure 7.11 shows the % weight of the uncured structural isomers of TGAP/DDS as a function of the standard cure schedule. The y-axis only shows a maximum 2 % change, indicating that very little mass change occurs during the cure. This is highly desirable and expected. However, the small changes can be attributed to minor differences in network formation. From the safety data sheets, TG*p*AP (MY0510) is thermally stable in its pure form over 200 ^{o}C, whereas TG*m*AP (MY0610) is thermally stable up to 140 ^{o}C. That could explain the greater mass loss in the TG*m*AP/44'DDS formulation in the first dwell, as the network hasn't formed large chains at this point, whereas TG*m*AP/33'DDS shows very little loss because larger chains or molecules form quicker in the initial dwell. The TG*p*AP formulations show similar behaviour as TG*p*AP is more thermally stable in its neat form and, therefore, less resistant to degradation at the initial dwell.

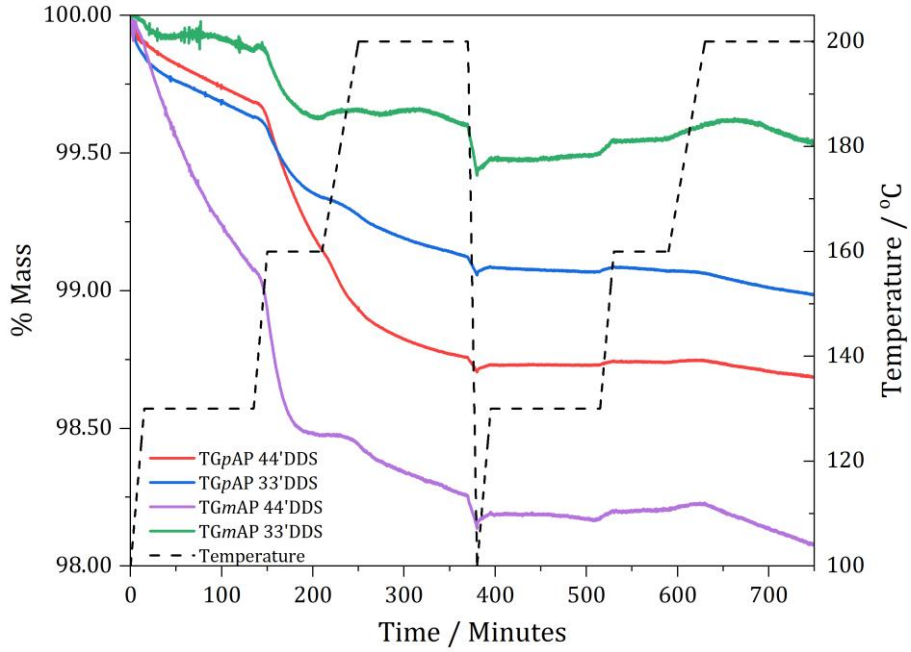

Figure 7.11 – Uncured thermogravimetric analysis of the four structural isomers of TGAP/DDS during the standard cure.

Once the second dwell is reached, the 44'DDS formulations show greater mass loss than the 33'DDS formulations due to a less developed crosslinked network as indicated by cure extent. Upon the temperature increase to the third dwell, TG*m*AP/33'DDS displays a mass increase. This is the result of the sample pan becoming more buoyant due to the change in the density of gas in the chamber.

Mass loss is also seen in the final dwell in TG*p*AP/44'DDS, TG*p*AP/33'DDS and TG*m*AP/44'DDS, all of which are small. The network is still curing at this point; therefore, the rate of mass loss slows towards the end of the dwell. Interestingly, TG*m*AP/33'DDS sees a minimal mass increase in the final dwell. This could be accounted for by oxidation. Morgan and Mones reported that internally cyclised glycidyl amine portions can be degraded by oxidation [44]. This could be evidence of the existence of internally cyclised structures, but without mass spectrometry, it is not possible to confirm, and the mass change is nearly insignificant.

The cure cycle was rerun on the cured resins to observe thermal degradation within the cure cycle dwell temperatures. Small amounts are seen in all formulations. Caution must be advised when analysing this figure as the % mass change is so small.

7.7.2. THERMOGRAVIMETRIC ANALYSIS OF CURED RESIN

The thermal stability of the cured structural isomers of TGAP/DDS have been analysed using TGA, as shown in Figure 7.12, between 30 °C and 800 °C at a heating rate of 10 °C min^{-1}. It can be seen that the onset of degradation occurs at lower temperatures for TG*p*AP formulations. The final mass is lowest in TG*p*AP/33'DDS, then TG*p*AP/44'DDS, followed by TG*m*AP/33'DDS and the highest final mass is TG*m*AP/44'DDS.

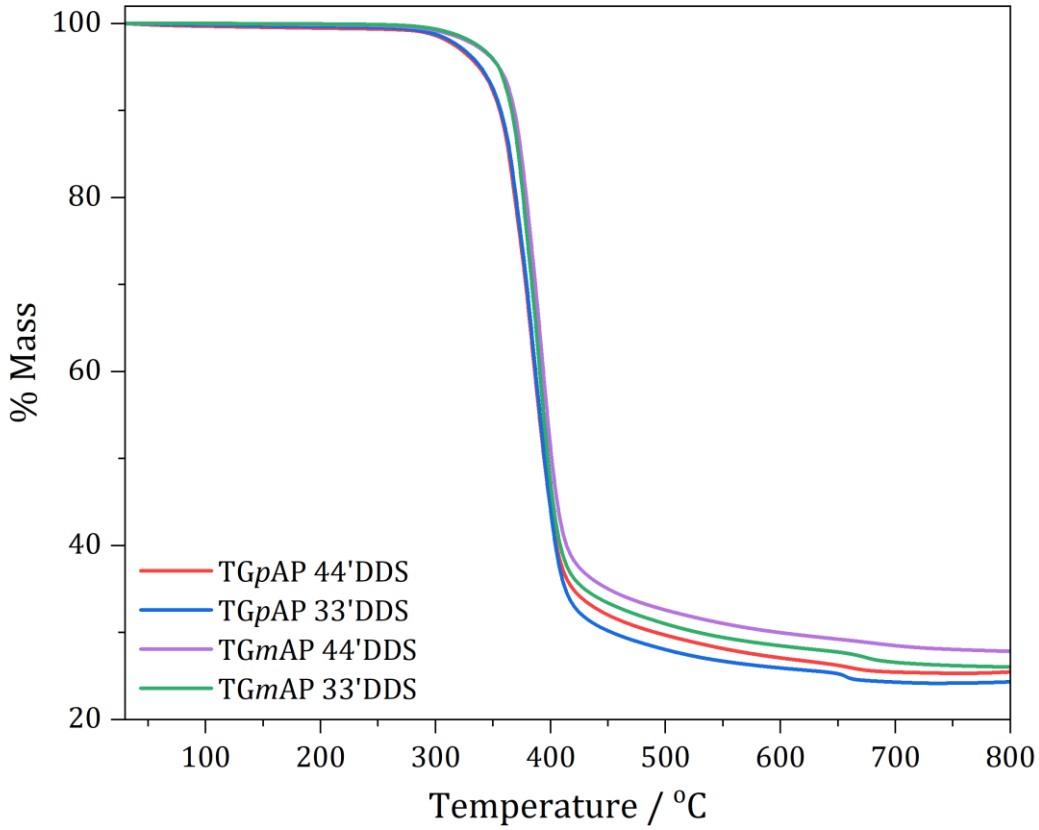

Figure 7.12 – Thermogravimetric analysis of the four structural isomers of TGAP/DDS between 30 °C and 800 °C using a heating rate of 10 °C min^{-1}.

Multiple critical points can be identified during degradation, T_0 is the onset of degradation, T_{10} is the temperature where 10 % mass is lost, T_{max} is the temperature at the maximum rate of degradation, and finally, the % char yield. These values are summarised in Table 7.8 for the four structural isomers of TGAP/DDS. Note the onset temperatures are approximate as it was difficult to accurately determine the point as small amounts of degradation do occur before this

temperature; therefore T_{10} is a more accurate indicator of thermal degradation onset, much like the reaction onset and kick-off method used in Chapter 5. DSC.

Table 7.8 – Thermal degradation characteristic critical points for the four structural isomers of TGAP/DDS obtained by thermogravimetric analysis between 30 °C and 800 °C using a heating rate of 10 °C min^{-1}.

	TG*p*AP 44'DDS	TG*p*AP 33'DDS	TG*m*AP 44'DDS	TG*m*AP 33'DDS
T_0 / °C	~ 265	~ 265	~275	~275
T_{10} / °C	355.9	356.8	368.6	366.3
T_{max} / °C	394.4	394.8	401.0	397.7
% char yield	25.50	24.34	27.85	26.05

The values of T_{10} indicate that the TG*m*AP formulations are more thermally stable. The maximum rate of thermal degradation occurred within 7 °C for all formulations. The thermal stability appears to be unrelated to the isomer of DDS used. The chemical group that provides stability is the sulphur group, which, when cured in the network, is not different between the formulations [244]. Whereas the difference between the isomers of TGAP is apparent. The mechanism through which TG*p*AP degrades has a lower activation energy than the mechanism in TG*m*AP. It is presently unclear, and future work analysing the degradation products using mass spectrometry may provide a clear explanation.

It could be expected that the network with the most crosslinking or homogeneously crosslinked network would have the highest thermal stability; however, it is the reverse in practice.

% char yield is lower in the TG*p*AP formulations compared to the TG*m*AP formulations. It may be related the type of bonds present in the backbone. It was suggested that TG*p*AP formulations could undergo etherification more readily at lower temperatures therefore the C-O-C bonds could potentially thermally degrade at lower temperatures than C-N-C bonds leading to a lower final % mass [245]. In the epoxy pairs, the 33'DDS formulations have a lower char yield, suggesting that their network allows for more significant thermal degradation. This could potentially relate to the homogeneity of the networks. The 33'DDS were more reactive and resulted in areas of low and high crosslinking density. The reactions which connect these areas

of crosslinking may well be etherification reactions. This may result in poorer thermal stability at high temperatures compared to the more homogenous networks of the 44'DDS formulations.

8. CONCLUSIONS AND FUTURE WORKS

The work presented in this thesis has investigated the differences in network development in the four structural isomers of TGAP/DDS using different cure monitoring techniques. Using starting reagents with the same chemical make-up but different positions has had an impact on when reactions occur and the resultant properties.

The cure of the four different isomer combinations was monitored using near-infrared spectroscopy (NIR). This technique was able to determine the concentration of the epoxide, primary amine, and secondary amine functional groups throughout the cure, and from there, conclusions about the reactions could be made. Firstly, the *meta* hardener, 3,3'-diaminodiphenyl sulphone (33'DDS), was found to be initially more reactive than the *para* hardener 4,4'-diaminodiphenyl sulphone. 44'DDS could undergo delocalisation of the lone pair of electrons on the amine through the aromatic structure onto the electron-withdrawing sulphone group, which resulted in 44'DDS being a less effective nucleophile than 33'DDS. As a result, crosslinking could occur quickly in the 33'DDS formulations, leading to areas of high and low crosslink density, whereas the slower reactions in 44'DDS resulted in a more homogeneous network. Secondly, it was found that etherification occurred at lower temperatures in the TG*p*AP formulations due to increased catalytic behaviour of the glycidyl amine in the *para* position. The maximum concentration of secondary amines in TG*m*AP formulations was also found to be lower suggesting tertiary amines formed earlier than in TG*p*AP. This led to the suggestion that internal cyclic structures were able to form more readily in TG*m*AP than in TG*p*AP.

The reactions characterised by NIR have an exothermic response, which was monitored using two different thermal techniques. Firstly, by using thermocouples to make resin temperature measurements and secondly by differential scanning calorimetry (DSC). Resin temperature measurements confirmed that 33'DDS formulations were more reactive initially, shown by a greater temperature overshoot in the first dwell, whereas 44'DDS were more reactive in the second dwell. However, this technique was not sensitive enough to show what was happening in the remainder of the dwell, where reactions were still occurring, just not as high a rate of reaction. DSC was able to monitor the entirety of the cure, even when the rate of reaction was slow or when curing reactions had finished. DSC also allowed for kinetic calculations to be made, calculating rate constants and activation energies using both

isothermal and dynamic heating methods. The cure of TGAP/DDS was confirmed to be autocatalytic, with the effect being more significant in 44'DDS than in 33'DDS. Although autocatalytic, poor agreement was seen, which gave evidence for etherification playing a role in the network development, as the model could not account for this reaction. Comparing the isothermal and dynamic heating measurements to the multi-dwell cure measurements confirmed that when the degree of cure is the same and temperature is the same, the mechanism occurring in the network is similar and is independent of the 'reaction history.'

Dielectric cure monitoring was used to monitor the mobility of reactive species throughout the cure in the different structural isomers. This was completed using equipment that is commercially available and widely used in industry. This technique gave information regarding the initial mechanical viscosity, showing that TG*m*AP had a higher initial mechanical viscosity than TG*p*AP. It also confirmed the recurring theme that 33'DDS was initially more reactive than 44'DDS. The change in ion viscosity (*IV*) was related to rate of reaction in DSC; however, when a large increase in *IV* was observed, this indicated that crosslinking was taking place. As the change in *IV* was related to rate of reaction, DEA could also be used to give an indication of cure state, as done so using the DiBenedetto equation. However, the comparison of the values obtained to the degree of cure obtained using DSC was not perfect. DEA was able to indicate that network relaxation was occurring in the TG*m*AP/33'DDS formulation in the final dwell as the cure temperature was in the glass transition temperature, as shown by a slight decrease in *IV* when a horizontal trend would be seen. Something that was not possible in both DSC and DEA. This highlighted the level of detail this technique could provide, despite being marketed as a simple cure monitoring technique for use in industry.

Finally, comparisons of the cure state as calculated by all three methods were made. Generally, good agreement was seen despite the three techniques measuring different phenomena. There were points where the techniques disagreed, but these were accounted for by reasons such as significant crosslinking and etherification reactions taking place.

The cured properties have been characterised, and the differences accounted for by the difference in starting reagent chemical structure and differences in network development. Most notably, the glass transition temperatures were found to be higher for TG*p*AP/44'DDS due to its *para* structures, resulting in greater chain stiffness and also its more homogenous network. The opposite was seen for TG*m*AP/33'DDS, despite it having the lowest remaining concentration of reactive groups remaining, indicating the highest crosslink density. An inhomogeneous network

and potential internally cyclic structures, resulted in a glass transition temperature approximately 50 °C lower than that of TG*p*AP/44'DDS. Etherification reactions occurring early in the cure were identified by the char yield of the TG*p*AP being lower than TG*m*AP, as more C-O-C bonds were present in the backbone, but also the inhomogeneity in the 33'DDS formulations, as they had lower char yields than the 44'DDS counterparts.

8.1. FUTURE WORKS

This thesis identifies the differences and the reasons behind these differences in network development of the four structural isomers of TGAP/DDS. However, the work is by no means finished; there is a significant amount of future work that can be done:

- Further DSC analysis using a model that accounts for diffusion control in the network, and also one that accounts for the etherification reactions that occur during network development.
- Mid-infrared spectroscopy to directly monitor the evolution of the ether functional group during the network formation of the four formulations of TGAP/DDS.
- Investigation of the effect of varying stoichiometry on the reactions to confirm whether the epoxy excess used in this thesis has had as significant effect as suggested.
- Exploration of different resin systems which do not contain a glycidyl amine group, such as tris(4-hydroxyphenyl)methane triglycidyl ether, to confirm if the tertiary amine catalyst behaviour is as significant as suggested.
- Applying the formulations discussed to composite applications and determining whether the resultant cured properties have the same effect in composite structures.
- Further DMA and PALS to investigate the origin of the omega transition and whether the 'annealing' technique works for all formulations.
- Using the DSC and NIR results to further modify the cure cycle to tailor the temperatures to specific reactions in the different TGAP/DDS isomers and to ultimately create a chart identifying the different factors which affect different properties, allowing for fine tuning of the material properties specific to the intended uses.
- Investigate other applications of the epoxies such as uses in adhesives in pure or blend form.

REFERENCES

[1] J.E. Mark, B. Erman, C.M. Roland, The Science and Technology of Rubber, Fourth, Academic Press, Oxford, England, 2013.

[2] R.J. Young, P.A. Lovell, Introduction to Polymers, Third, CRC Press, Boca Raton, FL, 2011.

[3] D. Feldman, Polymer History, Des. Monomers Polym. 11 (2008) 1–15. https://doi.org/10.1163/156855508X292383.

[4] International Agency for Research on Cancer, International Agency for Research on Cancer, eds., Some industrial chemicals, IARC, Lyon, 1994.

[5] A.S. Fallah, K. Micallef, G.S. Langdon, W.C. Lee, P.T. Curtis, L.A. Louca, Dynamic response of Dyneema® HB26 plates to localised blast loading, Int. J. Impact Eng. 73 (2014) 91–100. https://doi.org/10.1016/j.ijimpeng.2014.06.014.

[6] A. Kumal, A. Gupta, Fundamentals of Polymer Engineering, Revised and Expanded, Second, CRC Press, Boca Raton, FL, 2003.

[7] J. Monni, P. Niemelä, L. Alvila, T.T. Pakkanen, Online monitoring of synthesis and curing of phenol–formaldehyde resol resins by Raman spectroscopy, Polymer 49 (2008) 3865–3874. https://doi.org/10.1016/j.polymer.2008.06.050.

[8] C. He, G. Liu, H. Nie, J. Ni, Synthesis and characterization of polyurethane, J. Wuhan Univ. Technol.-Mater Sci Ed 25 (2010) 984–986. https://doi.org/10.1007/s11595-010-0134-8.

[9] B. Ellis, ed., Chemistry and Technology of Epoxy Resins, Springer Netherlands, Dordrecht, 1993. https://doi.org/10.1007/978-94-011-2932-9.

[10] N. Karak, Overview of Epoxies and Their Thermosets, in: N. Karak (Ed.), ACS Symp. Ser., American Chemical Society, Washington, DC, 2021: pp. 1–36. https://doi.org/10.1021/bk-2021-1385.ch001.

[11] F.-L. Jin, X. Li, S.-J. Park, Synthesis and application of epoxy resins: A review, J. Ind. Eng. Chem. 29 (2015) 1–11. https://doi.org/10.1016/j.jiec.2015.03.026.

[12] S.T. Knox, A. Wright, C. Cameron, J.P.A. Fairclough, Structural Variation and Chemical Performance—A Study of the Effects of Chemical Structure upon Epoxy Network Chemical Performance, ACS Appl. Polym. Mater. 3 (2021) 3438–3445. https://doi.org/10.1021/acsapm.1c00378.

[13] L.Q. Reyes, J. Zhang, B. Dao, D.L. Nguyen, R.J. Varley, Subtle variations in the structure of crosslinked epoxy networks and the impact upon mechanical and thermal properties, J. Appl. Polym. Sci. 137 (2020) 48874. https://doi.org/10.1002/app.48874.

[14] N.A. St John, G.A. George, P.A. Cole-Clarke, M.E. Mackay, P.J. Halley, The effect of impurities on gel times for TGDDM epoxy resins cured with DDS, High Perform. Polym. 5 (1993) 21–36. https://doi.org/10.1088/0954-0083/5/1/003.

[15] Y.-C. Chiu, C.-C. Huang, H.-C. Tsai, A. Prasannan, I. Toyoko, Effect of aromatic and aliphatic amines as curing agents in sulfone epoxy monomer curing process, Polym. Bull. 70 (2013) 1367–1382. https://doi.org/10.1007/s00289-013-0942-z.

[16] G. Lv, E. Jensen, N. Shan, C.M. Evans, D.G. Cahill, Effect of Aromatic/Aliphatic Structure and Cross-Linking Density on the Thermal Conductivity of Epoxy Resins, ACS Appl. Polym. Mater. 3 (2021) 1555–1562. https://doi.org/10.1021/acsapm.0c01395.

[17] U.W. Gedde, Polymer Physics, Springer Netherlands, Dordrecht, 1999. https://doi.org/10.1007/978-94-011-0543-9.

[18] A.J. Lesser, E. Crawford, The role of network architecture on the glass transition temperature of epoxy resins, J. Appl. Polym. Sci. 66 (1997) 387–395. https://doi.org/10.1002/(SICI)1097-4628(19971010)66:2<387::AID-APP19>3.0.CO;2-V.

[19] J. Mijovic, J. Wijaya, Etherification reaction in epoxy-amine systems at high temperature, Polymer 35 (1994) 2683–2686. https://doi.org/10.1016/0032-3861(94)90400-6.

[20] L. Xu, J.R. Schlup, Etherification versus amine addition during epoxy resin/amine cure: Anin situ study using near-infrared spectroscopy, J. Appl. Polym. Sci. 67 (1998) 895–901. https://doi.org/10.1002/(SICI)1097-4628(19980131)67:5<895::AID-APP15>3.0.CO;2-N.

[21] C.L. Sherman, R.C. Zeigler, N.E. Verghese, M.J. Marks, Structure–property relationships of controlled epoxy networks with quantified levels of excess epoxy etherification, Polymer 49 (2008) 1164–1172. https://doi.org/10.1016/j.polymer.2008.01.037.

[22] H. Yamasaki, S. Morita, Two-Step Curing Reaction of Epoxy Resin Studied by Thermal Analysis and Infrared Spectroscopy, Appl. Spectrosc. 66 (2012) 926–933. https://doi.org/10.1366/11-06437.

[23] C.M. Sahagun, S.E. Morgan, Thermal Control of Nanostructure and Molecular Network Development in Epoxy-Amine Thermosets, ACS Appl. Mater. Interfaces 4 (2012) 564–572. https://doi.org/10.1021/am201515y.

[24] A.P. Janisse, J.S. Wiggins, Real-time quantification of network growth of epoxy/diamine thermosets as a function of cure protocol, Adv. Manuf. Polym. Compos. Sci. 5 (2019) 1–5. https://doi.org/10.1080/20550340.2018.1557383.

[25] PubChem, Pentane, (n.d.). https://pubchem.ncbi.nlm.nih.gov/compound/8003 (accessed September 17, 2024).

[26] PubChem, Isopentane, (n.d.). https://pubchem.ncbi.nlm.nih.gov/compound/6556 (accessed September 17, 2024).

[27] PubChem, Neopentane, (n.d.). https://pubchem.ncbi.nlm.nih.gov/compound/10041 (accessed September 17, 2024).

[28] R.J. Varley, B. Dao, S. Tucker, S. Christensen, J. Wiggins, T. Dingemans, W. Vogel, M. Marchetti, Z. Madzarevic, Effect of aromatic substitution on the kinetics and properties of epoxy cured tri-phenylether amines, J. Appl. Polym. Sci. 136 (2019) 47383. https://doi.org/10.1002/app.47383.

[29] K.B. Riad, R. Schmidt, A.A. Arnold, R. Wuthrich, P.M. Wood-Adams, Characterizing the structural formation of epoxy-amine networks: The effect of monomer geometry, Polymer 104 (2016) 83–90. https://doi.org/10.1016/j.polymer.2016.09.077.

[30] M. Jackson, M. Kaushik, S. Nazarenko, S. Ward, R. Maskell, J. Wiggins, Effect of free volume hole-size on fluid ingress of glassy epoxy networks, Polymer 52 (2011) 4528–4535. https://doi.org/10.1016/j.polymer.2011.07.042.

[31] D. Kwon, M. Lee, W. Kwon, E. Lee, E. Jeong, Influence of stereoisomerism of epoxy hardeners on fracture toughness of carbon fiber/epoxy composites, Carbon Lett. 29 (2019) 449–453. https://doi.org/10.1007/s42823-019-00060-w.

[32] R. Ramsdale-Capper, J.P. Foreman, Internal antiplasticisation in highly crosslinked amine cured multifunctional epoxy resins, Polymer 146 (2018) 321–330. https://doi.org/10.1016/j.polymer.2018.05.048.

[33] L. Núñez, S. Gómez-Barreiro, C.A. Gracia-Fernández, Study of the influence of isomerism on the curing properties of the epoxy system DGEBA(n=0)/1,2-DCH by rheology, Rheol. Acta 45 (2005) 184–191. https://doi.org/10.1007/s00397-005-0008-8.

[34] D. Kim, S.R. Nutt, Processability of DDS isomers-cured epoxy resin: Effects of amine/epoxy ratio, humidity, and out-time: Processability of DDs Isomers-Cured Epoxy Resin: Effects of Amine/Epoxy Ratio, Humidity, and Out-Time, Polym. Eng. Sci. 58 (2018) 1530–1538. https://doi.org/10.1002/pen.24738.

[35] J. Tu, S.J. Tucker, S. Christensen, A.R. Sayed, W.L. Jarrett, Phenylene Ring Motions in Isomeric Glassy Epoxy Networks and Their Contributions to Thermal and Mechanical Properties, (2015).

[36] I.K. Varma, P.V.S. Bhama, Epoxy Resins: Effect of Amines on Curing Characteristics and Properties, J. Compos. Mater. 20 (1986) 410–422.

[37] K. Frank, J. Wiggins, Effect of stoichiometry and cure prescription on fluid ingress in epoxy networks, J. Appl. Polym. Sci. 130 (2013) 264–276. https://doi.org/10.1002/app.39140.

[38] R.D. Patel, R.G. Patel, V.S. Patel, Investigation of kinetics of curing of triglycidyl-p-aminophenol with aromatic diamines by differential scanning calorimetry, J. Therm. Anal. 34 (1988) 1283–1293. https://doi.org/10.1007/BF01914352.

[39] M.L. Costa, L.C. Pardini, M.C. Rezende, Influence of aromatic amine hardeners in the cure kinetics of an epoxy resin used in advanced composites, Mater. Res. 8 (2005) 65–70. https://doi.org/10.1590/S1516-14392005000100012.

[40] M.F. Mustafa, W.D. Cook, T.L. Schiller, H.M. Siddiqi, Curing behavior and thermal properties of TGDDM copolymerized with a new pyridine-containing diamine and with DDM or DDS, Thermochim. Acta 575 (2014) 21–28. https://doi.org/10.1016/j.tca.2013.09.018.

[41] Siddaramaiah, K.S. Jagadeesh, Properties of Multifunctional Epoxy Resins Cured with Different Amines, J. Polym. Mater. 13 (1996) 223–231.

[42] C.B. Thompson, Analysis of the Mechanical Properties of DGEBF/4,4'-DDS Thermoset Systems as a Function of Cure Rate, (n.d.).

[43] T. Liu, L. Zhang, R. Chen, L. Wang, B. Han, Y. Meng, X. Li, Nitrogen-Free Tetrafunctional Epoxy and Its DDS-Cured High-Performance Matrix for Aerospace Applications, Ind. Eng. Chem. Res. 56 (2017) 7708–7719. https://doi.org/10.1021/acs.iecr.7b00096.

[44] R.J. Morgan, E.T. Mones, The cure reactions, network structure, and mechanical response of diaminodiphenyl sulfone-cured tetraglycidyl 4,4′diaminodiphenyl methane epoxies, J. Appl. Polym. Sci. 33 (1987) 999–1020. https://doi.org/10.1002/app.1987.070330401.

[45] L. Matějka, M. Tkaczyk, S. Pokorný, K. Dušek, Cyclization in the reaction between diglycidylaniline and amine, Polym. Bull. 15 (1986) 389–396. https://doi.org/10.1007/BF00265719.

[46] A.J. Attias, J. Ancelle, B. Bloch, F. Laupretre, Chemical structure of networks resulting from curing of N,N-diglycidylaniline-type resins with aromatic amines. II. Detection and characterization of intermolecular etherification on model compounds, J. Polym. Sci. Part Polym. Chem. 28 (1990) 1661–1679. https://doi.org/10.1002/pola.1990.080280702.

[47] L. Bonnaud, J.P. Pascault, H. Sautereau, Kinetic of a thermoplastic-modified epoxy-aromatic diamine formulation: modeling and influence of a trifunctional epoxy prepolymer, Eur. Polym. J. 36 (2000) 1313–1321.

[48] R.J. Varley, G.R. Heath, D.G. Hawthorne, J.H. Hodgkin, G.P. Simon, Toughening of a trifunctional epoxy system: 1. Near infra-red spectroscopy study of homopolymer cure, Polymer 36 (1995) 1347–1355. https://doi.org/10.1016/0032-3861(95)95911-J.

[49] N.A. St John, G.A. George, Cure kinetics and mechanisms of a tetraglycidyl-4,4′-diaminodiphenylmethane/diaminodiphenylsulphone epoxy resin using near i.r. spectroscopy, Polymer 33 (1992) 2679–2688. https://doi.org/10.1016/0032-3861(92)90438-3.

[50] B.A. Rozenberg, Kinetics, thermodynamics and mechanism of reactions of epoxy oligomers with amines, Adv. Polym. Sci. 75 (1986). https://doi.org/10.1007/BFb0017916.

[51] Š. Podzimek, I. Dobáš, Š. Švestka, M. Tkaczyk, M. Kubín, V. Štěrba, Epoxy resins based on aromatic glycidylamines. IV. Preparation of *N* , *N* , *N* ′, *N* ′-tetraglycidyl-4,4′-diaminodiphenylmethane from aniline and analysis of the product by GPC and HPLC, J. Appl. Polym. Sci. 42 (1991) 795–800. https://doi.org/10.1002/app.1991.070420323.

[52] S.R. Swan, C. Creighton, J.M. Griffin, B.V. Gashi, R.J. Varley, Aromatic tetra-glycidyl ether versus tetra-glycidyl amine epoxy networks: Influence of monomer structure and epoxide conversion, Polymer 239 (2022) 124401. https://doi.org/10.1016/j.polymer.2021.124401.

[53] P.J. Flory, Molecular Size Distribution in Three Dimensional Polymers. I. Gelation [1], J. Am. Chem. Soc. 63 (1941) 3083–3090. https://doi.org/10.1021/ja01856a061.

[54] N.A.S. John, G.A. George, Diglycidyl amine — epoxy resin networks: Kinetics and mechanisms of cure, Prog. Polym. Sci. 19 (1994) 755–795. https://doi.org/10.1016/0079-6700(94)90032-9.

[55] L.E. Nielsen, Cross-Linking–Effect on Physical Properties of Polymers, J. Macromol. Sci. Part C 3 (1969) 69–103. https://doi.org/10.1080/15583726908545897.

[56] J.C. Capricho, B. Fox, N. Hameed, Multifunctionality in Epoxy Resins, Polym. Rev. 60 (2020) 1–41. https://doi.org/10.1080/15583724.2019.1650063.

[57] L. Wang, J. Wang, F. Zhang, Y. Qi, Z. Weng, X. Jian, PPESK-Modified Multi-Functional Epoxy Resin and Its Application to the Pultrusion of Carbon Fiber, Polymers 10 (2018) 1067. https://doi.org/10.3390/polym10101067.

[58] Z. Man, J.L. Stanford, B.K. Dutta, Reaction kinetics of epoxy resin modified with reactive and nonreactive thermoplastic copolymers, J. Appl. Polym. Sci. 112 (2009) 2391–2400. https://doi.org/10.1002/app.29305.

[59] G. Cicala, S. Mannino, A. Latteri, G. Ognibene, G. Saccullo, Effects of mixing di- and tri-functional epoxy monomers on epoxy/thermoplastic blends, Adv. Polym. Technol. 37 (2018) 1868–1877. https://doi.org/10.1002/adv.21845.

[60] R.J. Varley, J.H. Hodgkin, D.G. Hawthorne, G.P. Simon, D. McCulloch, Toughening of a trifunctional epoxy system Part III. Kinetic and morphological study of the thermoplastic modified cure process, Polymer 41 (2000) 3425–3436. https://doi.org/10.1016/S0032-3861(99)00503-0.

[61] B.-G. Min, Z.H. Stachurski, J.H. Hodgkin, G.R. Heath, Quantitative analysis of the cure reaction of DGEBA/DDS epoxy resins without and with thermoplastic polysulfone modifier using near infra-red spectroscopy, Polymer 34 (1993) 3620–3627. https://doi.org/10.1016/0032-3861(93)90046-D.

[62] C. Shang, X. Zhao, B. Sun, X. Yang, Y. Zhang, W. Huang, Synthesis and properties of novel trifunctional epoxy triglycidyl of 4-(4-aminophenoxy)phenol with high toughness, J. Appl. Polym. Sci. 132 (2015) n/a-n/a. https://doi.org/10.1002/app.41878.

[63] M.J. Lodeiro, D.R. Mulligan, CURE MONITORING TECHNIQUES FOR POLYMER COMPOSITES, ADHESIVES AND COATINGS, Good Pract. Guide - Natl. Phys. Lab. 75 (2005).

[64] Y. Ozaki, C. Huck, S. Tsuchikawa, S.B. Engelsen, eds., Near-Infrared Spectroscopy: Theory, Spectral Analysis, Instrumentation, and Applications, Springer Singapore, Singapore, 2021. https://doi.org/10.1007/978-981-15-8648-4.

[65] P.R. Griffiths, C.C. Homes, Instrumentation for Far-Infrared Spectroscopy, in: J.M. Chalmers, P.R. Griffiths (Eds.), Handb. Vib. Spectrosc., 1st ed., Wiley, 2001. https://doi.org/10.1002/0470027320.s0207.

[66] M.G. González, J.C. Cabanelas, J. Baselga, Applications of FTIR on Epoxy Resins - Identification, Monitoring the Curing Process, Phase Separation and Water Uptake, in: T. Theophanides (Ed.), Infrared Spectrosc. - Mater. Sci. Eng. Technol., InTech, 2012. https://doi.org/10.5772/36323.

[67] B.H. Stuart, Infrared Spectroscopy: Fundamentals and Applications, John Wiley & Sons, Incorporated, Newark, UNITED KINGDOM, 2004. http://ebookcentral.proquest.com/lib/sheffield/detail.action?docID=194354 (accessed October 15, 2024).

[68] X. Fernàndez-Francos, S.G. Kazarian, X. Ramis, À. Serra, Simultaneous Monitoring of Curing Shrinkage and Degree of Cure of Thermosets by Attenuated Total Reflection Fourier Transform Infrared (ATR FT-IR) Spectroscopy, Appl. Spectrosc. 67 (2013) 1427–1436. https://doi.org/10.1366/13-07169.

[69] Hans. Dannenberg, W.R. Harp, Determination of Cure and Analysis of Cured Epoxy Resins, Anal. Chem. 28 (1956) 86–90. https://doi.org/10.1021/ac60109a028.

[70] L. Li, Q. Wu, S. Li, P. Wu, Study of the Infrared Spectral Features of an Epoxy Curing Mechanism, Appl. Spectrosc. 62 (2008) 1129–1136. https://doi.org/10.1366/000370208786049204.

[71] H. Yamasaki, S. Morita, Temperature dependence of isothermal curing reaction of epoxy resin studied by modulated differential scanning calorimetry and infrared spectroscopy, J. Mol. Struct. 1124 (2016) 249–255. https://doi.org/10.1016/j.molstruc.2015.11.071.

[72] N. Poisson, G. Lachenal, H. Sautereau, Near- and mid-infrared spectroscopy studies of an epoxy reactive system, Vib. Spectrosc. 12 (1996) 237–247. https://doi.org/10.1016/0924-2031(96)00027-6.

[73] J. Mijović, S. Andjelić, In situ real-time monitoring of reactive systems by remote fibre-optic near-infra-red spectroscopy, Polymer 36 (1995) 3783–3786. https://doi.org/10.1016/0032-3861(95)93785-K.

[74] S. Cholake, M. Mada, R. Raman, Y. Bai, X. Zhao, S. Rizkalla, S. Bandyopadhyay, Quantitative Analysis of Curing Mechanisms of Epoxy Resin by Mid- and Near- Fourier Transform Infra Red Spectroscopy, Def. Sci. J. 64 (2014) 314–321. https://doi.org/10.14429/dsj.64.7326.

[75] V. Strehmel, T. Scherzer, Structural investigation of epoxy amine networks by mid- and near-infrared spectroscopy, Eur. Polym. J. 30 (1994) 361–368. https://doi.org/10.1016/0014-3057(94)90300-X.

[76] A. Rigail-Cedeño, C.S.P. Sung, Fluorescence and IR characterization of epoxy cured with aliphatic amines, Polymer 46 (2005) 9378–9384. https://doi.org/10.1016/j.polymer.2005.04.063.

[77] S.D. Pandita, L. Wang, R.S. Mahendran, V.R. Machavaram, M.S. Irfan, D. Harris, G.F. Fernando, Simultaneous DSC-FTIR spectroscopy: Comparison of cross-linking kinetics of an epoxy/amine resin system, Thermochim. Acta 543 (2012) 9–17. https://doi.org/10.1016/j.tca.2012.04.024.

[78] D.V. Vashurkin, G.V. Malkov, S.V. Karpov, N.O. Garifullin, A.T. Kapasharov, The Method of the Extent of Epoxy-Amine Cure Reaction Determination by near Infra-Red Spectroscopy, Key Eng. Mater. 816 (2019) 180–186. https://doi.org/10.4028/www.scientific.net/KEM.816.180.

[79] C.J. de Bakker, N.A. St John, G.A. George, Simultaneous differential scanning calorimetry and near-infra-red analysis of the curing of tetraglycidyldiaminodiphenylmethane with diaminodiphenylsulphone, Polymer 34 (1993) 716–725. https://doi.org/10.1016/0032-3861(93)90353-C.

[80] A. Beer, Grundriß des photometrischen Calcüles. - Braunschweig, Friedrich Vieweg u. Sohn 1854, Vieweg, 1854.

[81] R. Luther, A. Nikolopulos, Über die Beziehungen zwischen den Absorptionsspektren und der Konstitution der komplexen Kobaltamminsalze, Z. Für Phys. Chem. 82U (1913) 361–384. https://doi.org/10.1515/zpch-1913-8229.

[82] T.G. Mayerhöfer, S. Pahlow, J. Popp, The Bouguer-Beer-Lambert Law: Shining Light on the Obscure, ChemPhysChem 21 (2020) 2029–2046. https://doi.org/10.1002/cphc.202000464.

[83] E. Duemichen, M. Javdanitehran, M. Erdmann, V. Trappe, H. Sturm, U. Braun, G. Ziegmann, Analyzing the network formation and curing kinetics of epoxy resins by in situ near-infrared measurements with variable heating rates, Thermochim. Acta 616 (2015) 49–60. https://doi.org/10.1016/j.tca.2015.08.008.

[84] C. Billaud, M. Vandeuren, R. Legras, V. Carlier, Quantitative Analysis of Epoxy Resin Cure Reaction: A Study by Near-Infrared Spectroscopy, Appl. Spectrosc. 56 (2002) 1413–1421. https://doi.org/10.1366/00037020260377706.

[85] J. Mijovic, S. Andjelic, A Study of Reaction Kinetics by Near-Infrared Spectroscopy. 1. Comprehensive Analysis of a Model Epoxy/Amine System, Macromolecules 28 (1995) 2787–2796. https://doi.org/10.1021/ma00112a026.

[86] G. Lachenal, A. Pierre, N. Poisson, FT-NIR spectroscopy: Trends and application to the kinetic study of epoxy/triamine system (comparison with DSC and SEC results), Micron 27 (1996) 329–334. https://doi.org/10.1016/S0968-4328(96)00022-4.

[87] S.T. Knox, A. Wright, C. Cameron, J.P.A. Fairclough, Well-Defined Networks from DGEBF—The Importance of Regioisomerism in Epoxy Resin Networks, Macromolecules 52 (2019) 6861–6867. https://doi.org/10.1021/acs.macromol.9b01441.

[88] M. Erdmann, V. Trappe, H. Sturm, U. Braun, E. Duemichen, Cure conversion of structural epoxies by cure state analysis and in situ cure kinetics using nondestructive NIR spectroscopy, Thermochim. Acta 650 (2017) 8–17. https://doi.org/10.1016/j.tca.2017.01.010.

[89] A. Durand, L. Hassi, G. Lachenal, I. Stevenson, G. Seytre, G. Boiteux, Simultaneous Dielectric and Fourier Transform near Infrared Spectroscopy to Monitor a Polyepoxy Curing Process, J. Infrared Spectrosc. 14 (2006) 161–166. https://doi.org/10.1255/jnirs.611.

[90] L. Xu, J.H. Fu, J.R. Schlup, In situ Near-Infrared Spectroscopic Investigation of Epoxy Resin-Aromatic Amine Cure Mechanisms, J. Am. Chem. Soc. 116 (1994) 2821–2826. https://doi.org/10.1021/ja00086a015.

[91] B. Jiang, S. He, Y.D. Huang, H.T. Pan, Investigation of the Kinetics of Curing Reaction for the Resin Matrix Polymer Composite Based on Near-Infrared Spectroscopy, Appl. Spectrosc. Rev. 50 (2015) 627–640. https://doi.org/10.1080/05704928.2015.1049702.

[92] B. Jiang, Y.D. Huang, W. Li, L. Liu, Non-Contact Quality Monitoring of Laid Fabric Carbon/Epoxy Resin Prepreg Using near Infrared Spectroscopy, J. Infrared Spectrosc. 15 (2007) 299–305. https://doi.org/10.1255/jnirs.744.

[93] M. Salzmann, Y. Blößl, A. Todorovic, R. Schledjewski, Usage of Near-Infrared Spectroscopy for Inline Monitoring the Degree of Curing in RTM Processes, Polymers 13 (2021) 3145. https://doi.org/10.3390/polym13183145.

[94] D.M. Harrison, 4 - Epoxy Grout, in: D.M. Harrison (Ed.), Grouting Handb. Second Ed., Elsevier, Oxford, 2013: pp. 69–84. https://doi.org/10.1016/B978-0-12-416585-4.00004-3.

[95] American Society for Testing and Materials, ASTM Committee E20 on Temperature Measurement, eds., Manual on the use of thermocouples in temperature measurement, 4th ed (Online-Ausg.), American Society for Testing and Materials, Philadelphia, Pa, 1993. https://doi.org/10.1520/MNL12-4TH-EB.

[96] P.B. Jacovelli, O.H. Zinke, The Thermocouple Revisited: The Benedicks and Seebeck Effects, J. Non-Equilib. Thermodyn. 44 (2019) 373–383. https://doi.org/10.1515/jnet-2018-0063.

[97] Type K Thermocouple, (n.d.). https://www.tc.co.uk/thermocouples/type-k-thermocouple.html (accessed November 4, 2024).

[98] C.Y. Shigue, R.G.S. dosSantos, C.A. Baldan, E. Ruppert-Filho, Monitoring the Epoxy Curing by the Dielectric Thermal Analysis Method, IEEE Trans. Appl. Supercond. 14 (2004) 1173–1176. https://doi.org/10.1109/TASC.2004.830477.

[99] Z. Wu, Q. Chen, D. Liu, J. Fan, Q. Zhang, W. Chen, In situ monitoring of epoxy resin curing process: Using glass transition as a bridge, Polym. Test. 117 (2023) 107871. https://doi.org/10.1016/j.polymertesting.2022.107871.

[100] Z. Ran, X. Liu, X. Jiang, Y. Wu, H. Liao, Study on curing kinetics of epoxy-amine to reduce temperature caused by the exothermic reaction, Thermochim. Acta 692 (2020) 178735. https://doi.org/10.1016/j.tca.2020.178735.

[101] Z. Zhang, Y. Li, Y. Wu, F. Li, Exothermic effect in the process of electron-beam curing of epoxy resins, J. Appl. Polym. Sci. 94 (2004) 2217–2222. https://doi.org/10.1002/app.21173.

[102] R.J. Varley, J.H. Hodgkin, D.G. Hawthorne, G.P. Simon, Toughening of a trifunctional epoxy system. II. Thermal characterization of epoxy/amine cure, J. Appl. Polym. Sci. 60 (1996) 2251–2263.

[103] N. Rabearison, Ch. Jochum, J.C. Grandidier, A cure kinetics, diffusion controlled and temperature dependent, identification of the Araldite LY556 epoxy, J. Mater. Sci. 46 (2011) 787–796. https://doi.org/10.1007/s10853-010-4815-7.

[104] K.C. Cole, J.J. Hechler, D. Noel, A new approach to modeling the cure kinetics of epoxy/amine thermosetting resins. 2. Application to a typical system based on bis[4-(diglycidylamino)phenyl]methane and bis(4-aminophenyl) sulfone, Macromolecules 24 (1991) 3098–3110. https://doi.org/10.1021/ma00011a012.

[105] K. Horie, H. Hiura, M. Sawada, I. Mita, H. Kambe, Calorimetric investigation of polymerization reactions. III. Curing reaction of epoxides with amines, J. Polym. Sci. [A1] 8 (1970) 1357–1372. https://doi.org/10.1002/pol.1970.150080605.

[106] V.L. Zvetkov, Comparative DSC kinetics of the reaction of DGEBA with aromatic diamines. I. Non-isothermal kinetic study of the reaction of DGEBA with m-phenylene diamine, (2001).

[107] V.L. Zvetkov, Comparative DSC kinetics of the reaction of DGEBA with aromatic diamines. II. Isothermal kinetic study of the reaction of DGEBA with m-phenylene diamine, Polymer 43 (2002) 1069–1080. https://doi.org/10.1016/S0032-3861(01)00695-4.

[108] V.L. Zvetkov, R.K. Krastev, V.I. Samichkov, Rate equations in the study of the DSC kinetics of epoxy-amine reactions in an excess of epoxy, Thermochim. Acta 478 (2008) 17–27. https://doi.org/10.1016/j.tca.2008.08.012.

[109] E. Franieck, M. Fleischmann, O. Hölck, L. Kutuzova, A. Kandelbauer, Cure Kinetics Modeling of a High Glass Transition Temperature Epoxy Molding Compound (EMC) Based on Inline Dielectric Analysis, Polymers 13 (2021) 1734. https://doi.org/10.3390/polym13111734.

[110] J. Mijović, J. Kim, J. Slaby, Cure kinetics of epoxy formulations of the type used in advanced composites, J. Appl. Polym. Sci. 29 (1984) 1449–1462. https://doi.org/10.1002/app.1984.070290437.

[111] F.I. Anagwu, A.A. Skordos, Cure kinetics, glass transition advancement and chemo-rheological modelling of an epoxy vitrimer based on disulphide metathesis, Polymer 288 (2023) 126427. https://doi.org/10.1016/j.polymer.2023.126427.

[112] J.M. Kenny, Determination of autocatalytic kinetic model parameters describing thermoset cure, J. Appl. Polym. Sci. 51 (1994) 761–764. https://doi.org/10.1002/app.1994.070510424.

[113] K.S. Jagadeesh, Siddaramaiah, Kinetics of curing epoxy formulations with diaminodiphenyl ether, Polym. Int. 26 (1991) 129–132. https://doi.org/10.1002/pi.4990260212.

[114] K.S. Jagadeesh, J. Gururaja Rao, K. Shashikiran, S. Suvarna, S.Y. Ambekar, M. Saletore, C. Biswas, A.V. Rajanna, Cure kinetics of multifunctional epoxies with 2,2?-dichloro-4,4?-diaminodiphenylmethane as hardener, J. Appl. Polym. Sci. 77 (2000) 2097–2103. https://doi.org/10.1002/1097-4628(20000906)77:10<2097::AID-APP1>3.0.CO;2-4.

[115] K.S. Jagadeesh, Siddaramaiah, V. Kalpagam, Differential scanning calorimetry cure studies on the effect of addition of epoxy diluents of tetrafunctional epoxy resins, J. Appl. Polym. Sci. 40 (1990) 1281–1288. https://doi.org/10.1002/app.1990.070400716.

[116] Woo Il Lee, A.C. Loos, G.S. Springer, Heat of Reaction, Degree of Cure, and Viscosity of Hercules 3501-6 Resin, J. Compos. Mater. 16 (1982) 510–520. https://doi.org/10.1177/002199838201600605.

[117] Q. Tao, G. Pinter, T. Krivec, Influence of cooling rate and annealing on the DSC Tg of an epoxy resin, Microelectron. Reliab. 78 (2017) 396–400. https://doi.org/10.1016/j.microrel.2017.07.088.

[118] G. Gerami, R. Bagheri, R. Darvishi, Investigation of isothermal and dynamic cure kinetics of epoxy resin/nadic methyl anhydride/dicyandiamide by differential scanning calorimetry (DSC), J. Therm. Anal. Calorim. 137 (2019) 575–582. https://doi.org/10.1007/s10973-018-7961-9.

[119] D. Roşu, F. Mustată, C.N. Caşcaval, Investigation of the curing reactions of some multifunctional epoxy resins using differential scanning calorimetry, Thermochim. Acta 370 (2001) 105–110. https://doi.org/10.1016/S0040-6031(00)00787-5.

[120] J. Hu, J. Shan, J. Zhao, Z. Tong, Isothermal curing kinetics of a flame retardant epoxy resin containing DOPO investigated by DSC and rheology, Thermochim. Acta 632 (2016) 56–63. https://doi.org/10.1016/j.tca.2016.02.010.

[121] M. Hayaty, M.H. Beheshty, M. Esfandeh, Isothermal differential scanning calorimetry study of a glass/epoxy prepreg, Polym. Adv. Technol. 22 (2011) 1001–1006. https://doi.org/10.1002/pat.1607.

[122] R.M. Vinnik, V.A. Roznyatovsky, Kinetic method by using calorimetry to mechanism of epoxy-amine cure reaction, J. Therm. Anal. Calorim. 73 (2003) 807–817.

[123] R.M. Vinnik, V.A. Roznyatovsky, Kinetic method by using calorimetry to mechanism of epoxy-amine cure reaction, J. Therm. Anal. Calorim. (2003) 11.

[124] R.M. Vinnik, V.A. Roznyatovsky, Kinetic method by using calorimetry to mechanism of epoxy-amine cure reaction, J. Therm. Anal. Calorim. (2003) 8.

[125] R.M. Vinnik, V.A. Roznyatovsky, Kinetic method by using calorimetry to mechanism of epoxy-amine cure reaction, J. Therm. Anal. Calorim. (2003) 8.

[126] J.M. Barton, Kinetics of cure of epoxy resin system bisphenoI-A diglycidylether- di(4-aminophenyl)sulphone, Polym. Commun. 21 (1980) 603–606. https://doi.org/10.1016/0032-3861(80)90314-6.

[127] J.M. Barton, Differential Scanning Calorimetry Cure Studies of Tetra- *N* -glycidyldiaminodiphenylmethane Epoxy Resins. Part 1 - Reaction with 4,4′-Diaminodiphenylsulphone, Br. Polym. J. 18 (1986) 37–43. https://doi.org/10.1002/pi.4980180110.

[128] J.M. Barton, I. Hamerton, B.J. Howlin, J.R. Jones, S. Liu, Studies of cure schedule and final property relationships of a commercial epoxy resin using modified imidazole curing agents, Polymer 39 (1998) 1929–1937. https://doi.org/10.1016/S0032-3861(97)00372-8.

[129] E. Sacher, Kinetics of epoxy cure: 3. The systems bisphenoI-A epoxides/dicy, Polymer 14 (1973) 91–95. https://doi.org/10.1016/0032-3861(73)90055-4.

[130] M.E. Ryan, A. Dutta, Kinetics of epoxy cure: a rapid technique for kinetic parameter estimation, Polymer 20 (1979) 203–206. https://doi.org/10.1016/0032-3861(79)90222-2.

[131] N. Sbirrazzuoli, S. Vyazovkin, Learning about epoxy cure mechanisms from isoconversional analysis of DSC data, Thermochim. Acta 388 (2002) 289–298. https://doi.org/10.1016/S0040-6031(02)00053-9.

[132] N. Sbirrazzuoli, S. Vyazovkin, A. Mititelu, C. Sladic, L. Vincent, A Study of Epoxy-Amine Cure Kinetics by Combining Isoconversional Analysis with Temperature Modulated DSC and Dynamic Rheometry, Macromol. Chem. Phys. 204 (2003) 1815–1821. https://doi.org/10.1002/macp.200350051.

[133] F. Shiravand, J.M. Hutchinson, Y. Calventus, Non-isothermal cure and exfoliation of tri-functional epoxy-clay nanocomposites, Express Polym. Lett. 9 (2015) 695–708. https://doi.org/10.3144/expresspolymlett.2015.65.

[134] F. Wu, X. Zhou, X. Yu, Reaction mechanism, cure behavior and properties of a multifunctional epoxy resin, TGDDM, with latent curing agent dicyandiamide, RSC Adv. 8 (2018) 8248–8258. https://doi.org/10.1039/C7RA13233F.

[135] J. Gao, L. Li, Y. Deng, Z. Gao, C. Xu, M. Zhang, Study of gelation using differential scanning calorimetry (DSC), J. Therm. Anal. 49 (1997) 303–310. https://doi.org/10.1007/BF01987451.

[136] A. Apicella, L. Nicolais, M. Iannone, P. Passerini, Thermokinetics and chemorheology of the cure reactions of the tetraglycidyl diamino diphenyl methane–diamino diphenyl sulfone epoxy systems, J. Appl. Polym. Sci. 29 (1984) 2083–2096. https://doi.org/10.1002/app.1984.070290616.

[137] A.T. DiBenedetto, Prediction of the glass transition temperature of polymers: A model based on the principle of corresponding states, J. Polym. Sci. Part B Polym. Phys. 25 (1987) 1949–1969. https://doi.org/10.1002/polb.1987.090250914.

[138] R. Hardis, J.L.P. Jessop, F.E. Peters, M.R. Kessler, Cure kinetics characterization and monitoring of an epoxy resin using DSC, Raman spectroscopy, and DEA, Compos. Part Appl. Sci. Manuf. 49 (2013) 100–108. https://doi.org/10.1016/j.compositesa.2013.01.021.

[139] P.I. Karkanas, Cure modelling and monitoring of epoxy/amine resin systems, Cranfield University, 1998. http://hdl.handle.net/1826/3598.

[140] H.L. Friedman, Kinetics of thermal degradation of char-forming plastics from thermogravimetry. Application to a phenolic plastic, J. Polym. Sci. Part C Polym. Symp. 6 (1964) 183–195. https://doi.org/10.1002/polc.5070060121.

[141] J.H. Flynn, The isoconversional method for determination of energy of activation at constant heating rates: Corrections for the Doyle approximation, J. Therm. Anal. 27 (1983) 95–102. https://doi.org/10.1007/BF01907325.

[142] M.R. Kamal, S. Sourour, Kinetics and thermal characterization of thermoset cure, Polym. Eng. Sci. 13 (1973) 59–64. https://doi.org/10.1002/pen.760130110.

[143] S. Sourour, M.R. Kamal, DIFFFERENTIAL SC AN-NING CALORIMETRY OF EPOXY CURE: ISOTHERMAL CURE KINETICS, Thermochim. Acta 14 (1976) 41–59. https://doi.org/10.1016/0040-6031(76)80056-1.

[144] G. Voto, L. Sequeira, A.A. Skordos, Formulation based predictive cure kinetics modelling of epoxy resins, Polymer 236 (2021) 124304. https://doi.org/10.1016/j.polymer.2021.124304.

[145] H.-J. Tai, H.-L. Chou, Chemical shrinkage and diffusion-controlled reaction of an epoxy molding compound, Eur. Polym. J. 36 (2000) 2213–2219. https://doi.org/10.1016/S0014-3057(99)00278-5.

[146] G. Wisanrakkit, J.K. Gillham, The glass transition temperature (Tg) as an index of chemical conversion for a high-Tg amine/epoxy system: Chemical and diffusion-controlled reaction kinetics, J. Appl. Polym. Sci. 41 (1990) 2885–2929. https://doi.org/10.1002/app.1990.070411129.

[147] C. -S. Chern, G.W. Poehlein, A kinetic model for curing reactions of epoxides with amines, Polym. Eng. Sci. 27 (1987) 788–795. https://doi.org/10.1002/pen.760271104.

[148] J. Fournier, G. Williams, C. Duch, G.A. Aldridge, Changes in Molecular Dynamics during Bulk Polymerization of an Epoxide−Amine System As Studied by Dielectric Relaxation Spectroscopy, Macromolecules 29 (1996) 7097–7107. https://doi.org/10.1021/ma9517862.

[149] H. Cai, P. Li, G. Sui, Y. Yu, G. Li, X. Yang, S. Ryu, Curing kinetics study of epoxy resin/flexible amine toughness systems by dynamic and isothermal DSC, Thermochim. Acta 473 (2008) 101–105. https://doi.org/10.1016/j.tca.2008.04.012.

[150] Vera V. Daniel, Dielectric Relaxation, Academic Press, London, 1967.

[151] A.A. Skordos, I.K. Partridge, Determination of the degree of cure under dynamic and isothermal curing conditions with electrical impedance spectroscopy, J. Polym. Sci. Part B Polym. Phys. 42 (2004) 146–154. https://doi.org/10.1002/polb.10676.

[152] J. Mijović, JoséM. Kenny, A. Maffezzoli, A. Trivisano, F. Bellucci, L. Nicolais, The principles of dielectric measurements for in situ monitoring of composite processing, Compos. Sci. Technol. 49 (1993) 277–290. https://doi.org/10.1016/0266-3538(93)90109-T.

[153] H.L. Lee, The Handbook of Dielectric Analysis and Cure Monitoring, Second Edition, Lambient Technologies, Cambridge, MA, USA, n.d.

[154] S.A. Bidstrup, N.F. Sheppard, S.D. Senturia, Dielectric analysis of the cure of thermosetting epoxy/amine systems, Polym. Eng. Sci. 29 (1989) 325–328. https://doi.org/10.1002/pen.760290510.

[155] R. Casalini, S. Corezzi, A. Livi, G. Levita, P.A. Rolla, Dielectric parameters to monitor the crosslink of epoxy resins, J. Appl. Polym. Sci. 65 (1997) 17–25.

[156] J. Chen, M. Hojjati, Microdielectric analysis and curing kinetics of an epoxy resin system, Polym. Eng. Sci. 47 (2007) 150–158. https://doi.org/10.1002/pen.20687.

[157] M. Demleitner, S.A. Sanchez-Vazquez, D. Raps, G. Bakis, T. Pflock, A. Chaloupka, S. Schmölzer, V. Altstädt, Dielectric analysis monitoring of thermoset curing with ionic liquids: From modeling to the prediction in the resin transfer molding process, Polym. Compos. 40 (2019) 4500–4509. https://doi.org/10.1002/pc.25306.

[158] A. Dimopoulos, A.A. Skordos, I.K. Partridge, Cure kinetics, glass transition temperature development, and dielectric spectroscopy of a low temperature cure epoxy/amine system, J. Appl. Polym. Sci. 124 (2012) 1899–1905. https://doi.org/10.1002/app.34605.

[159] C. Ferrari, E. Tombari, G. Salvetti, G.P. Johari, Real time dielectric spectroscopy and bond connectivity during polymerization of stoichiometric and amine-rich, diepoxide–diamine compositions, J. Chem. Soc. Faraday Trans. 94 (1998) 1293–1300. https://doi.org/10.1039/a800277k.

[160] L. Garden, R.A. Pethrick, Critique of dielectric cure monitoring in epoxy resins – Does the method work for commercial formulations?, Int. J. Adhes. Adhes. 74 (2017) 6–14. https://doi.org/10.1016/j.ijadhadh.2016.12.005.

[161] Giuseppe Gallone, Simone Capaccioli, Giovanni Levita, Pier Angelo Rolla, Silvia Corezzi, Dielectric analysis of the linear polymerization of an epoxy resin, Polym. Int. 50 (2001) 545–551. https://doi.org/10.1002/pi.663.

[162] M.K. Hassan, S.J. Tucker, A. Abukmail, J.S. Wiggins, K.A. Mauritz, Polymer chain dynamics in epoxy based composites as investigated by broadband dielectric spectroscopy, Arab. J. Chem. 9 (2016) 305–315. https://doi.org/10.1016/j.arabjc.2015.07.016.

[163] F. Hussain, J. Chen, M. Hojjati, Epoxy-silicate nanocomposites: Cure monitoring and characterization, Mater. Sci. Eng. A 445–446 (2007) 467–476. https://doi.org/10.1016/j.msea.2006.09.071.

[164] H. Jdidi, N. Fourati, C. Zerrouki, L. Ibos, M. Fois, A. Guinault, W. Jilani, S. Guermazi, H. Guermazi, Exploring the optical and dielectric properties of bifunctional and trifunctional epoxy polymers, Polymer 228 (2021) 123882. https://doi.org/10.1016/j.polymer.2021.123882.

[165] H. Kim, K. Char, Dielectric Changes During the Curing of Epoxy Resin Based on the Diglycidyl Ether of Bisphenol A (DGEBA) with Diamine, Bull. Korean Chem. Soc. 20 (1999) 1329–1334.

[166] J.-S. Kim, D.G. Lee, On-line cure monitoring and viscosity measurement of carbon fiber epoxy composite materials, J. Mater. Process. Technol. 37 (1993) 405–416. https://doi.org/10.1016/0924-0136(93)90105-F.

[167] D.E. Kranbuehl, S.E. Delos, P.K. Jue, Dielectric properties of the polymerization of an aromatic polyimide, Polymer 27 (1986) 11–18. https://doi.org/10.1016/0032-3861(86)90350-2.

[168] D. Kranbuehl, S. Delos, E. Yi, J. Mayer, T. Jarvie, W. Winfree, T. Hou, Dynamic dielectric analysis: Nondestructive material evaluation and cure cycle monitoring, Polym. Eng. Sci. 26 (1986) 338–345. https://doi.org/10.1002/pen.760260503.

[169] G.M. Maistros, C.B. Bucknall, Modeling the dielectric behavior of epoxy resin blends during curing, Polym. Eng. Sci. 34 (1994) 1517–1528. https://doi.org/10.1002/pen.760342002.

[170] H. Park, Dielectric cure determination of a thermosetting epoxy composite prepreg: ARTICLE, J. Appl. Polym. Sci. 134 (2017). https://doi.org/10.1002/app.44707.

[171] O. de A. Raponi, R. de A. Raponi, G.B. Barban, R.M.D. Benedetto, A.C. Ancelotti Junior, Development of a Simple Dielectric Analysis Module for Online Cure Monitoring of a Commercial Epoxy Resin Formulation, Mater. Res. 20 (2017) 291–297. https://doi.org/10.1590/1980-5373-mr-2017-0067.

[172] S.D. Senturia, N.F. Sheppard, Dielectric Analysis of Thermoset Cure, Adv. Polym. Sci. 80 (1986) 1–47. https://doi.org/10.1007/3-540-16423-5_11.

[173] N.F. Sheppard, S.D. Senturia, Dielectric properties of bisphenol-a epoxy resins, J. Polym. Sci. Part B Polym. Phys. 27 (1989) 753–762. https://doi.org/10.1002/polb.1989.090270403.

[174] J.O. Simpson, S.A. Bidstrup, Rheological and dielectric changes during isothermal epoxy-amine cure, J. Polym. Sci. Part B Polym. Phys. 33 (1995) 55–62. https://doi.org/10.1002/polb.1995.090330106.

[175] J.O. Simpson, S.A. Bidstrup, Correlation between chain segment and ion mobility in an epoxy resin system. A free volume analysis, J. Polym. Sci. Part B Polym. Phys. 31 (1993) 609–618. https://doi.org/10.1002/polb.1993.090310512.

[176] K. Venkateshan, G.P. Johari, Dielectric Polarization and the Stages of a Macromolecule's Growth, J. Phys. Chem. B 108 (2004) 15049–15056. https://doi.org/10.1021/jp0476951.

[177] S. Yan, H. Zeizinger, C. Merten, S. Schmauder, In-situ investigation of dielectric properties and reaction kinetics of a glass-fiber-reinforced epoxy composite material using dielectric analysis, Polym. Eng. Sci. 61 (2021) 1673–1684. https://doi.org/10.1002/pen.25691.

[178] OriginLab Corporation, Origin(Pro) 2021b, (n.d.).

[179] M. Wojdyr, *Fityk* : a general-purpose peak fitting program, J. Appl. Crystallogr. 43 (2010) 1126–1128. https://doi.org/10.1107/S0021889810030499.

[180] PubChem, Dapsone, (n.d.). https://pubchem.ncbi.nlm.nih.gov/compound/2955 (accessed October 21, 2024).

[181] PubChem, 3,3'-Sulfonyldianiline, (n.d.). https://pubchem.ncbi.nlm.nih.gov/compound/11741 (accessed October 21, 2024).

[182] A. Janisse, Effect of Cure Protocol on Network Formation and Properties of Epoxy-Diamine Thermosets, (n.d.).

[183] Lambient Technologies, Mini-Varicon Dielectric/Conductivity Sensor Specifications, (2022).

[184] Lambient Technologies, CureView Control and Analysis Software, (2017). http://www.lambient.com/.

[185] Y.A. Tajima, Monitoring cure viscosity of epoxy composite, Polym. Compos. 3 (1982) 162–169. https://doi.org/10.1002/pc.750030310.

[186] M. Van Soestbergen, L.J. Ernst, G.Q. Zhang, R.T.H. Rongen, Transport of Corrosive Constituents in Epoxy Moulding Compounds, in: 2007 Int. Conf. Therm. Mech. Multi-Phys. Simul. Exp. Microelectron. Micro-Syst. EuroSime 2007, IEEE, London, 2007: pp. 1–5. https://doi.org/10.1109/ESIME.2007.360019.

[187] K.P. Menard, Dynamic mechanical analysis: a practical introduction, CRC Press, Boca Raton, FL, 2008.

[188] A.S. Shackleford, Using Positron Annihilation as a Method to Characterise Epoxy Networks with Regards to Chemical Resistance, University of Sheffield, 2019.

[189] Eljen Technology, FAST TIMING PLASTIC SCINTILLATOR EJ-232, EJ-232Q, FAST TIMING Plast. Scintill. EJ-232 EJ-232Q (n.d.). https://eljentechnology.com/products/plastic-scintillators/ej-232-ej-232q.

[190] A.J. Attias, J. Ancelle, B. Bloch, F. Lauprêtre, Chemical structure of networks resulting from curing of diglycidylamine-type resins with aromatic amines: 1. Detection and characterization of cyclisation reactions on model compounds, Polym. Bull. 18 (1987) 217–224. https://doi.org/10.1007/BF00255113.

[191] A.J. Attias, B. Bloch, F. Laupretre, Chemical structure of networks resulting from curing of N,N-diglycidylaniline-type resins with aromatic amines. IV. Characterization of TGDDM/DDS and TGDDM/DDM networks by high-resolution solid-state 13C-NMR, J. Polym. Sci. Part Polym. Chem. 28 (1990) 3445–3466. https://doi.org/10.1002/pola.1990.080281221.

[192] S. Corezzi, D. Fioretto, R. Casalini, P.A. Rolla, Glass transition of an epoxy resin induced by temperature, pressure and chemical conversion: a rationale based on configurational entropy, J. Non-Cryst. Solids 307–310 (2002) 281–287. https://doi.org/10.1016/S0022-3093(02)01477-1.

[193] M. Jensen, J. Jakobsen, Configurational Entropy in Thermoset Polymers, J. Phys. Chem. B 119 (2015) 5645–5649. https://doi.org/10.1021/jp510836y.

[194] C.E. Estridge, The effects of competitive primary and secondary amine reactivity on the structural evolution and properties of an epoxy thermoset resin during cure: A molecular dynamics study, Polymer 141 (2018) 12–20. https://doi.org/10.1016/j.polymer.2018.02.062.

[195] M. Jackson, M. Kaushik, S. Nazarenko, S. Ward, R. Maskell, J. Wiggins, Effect of free volume hole-size on fluid ingress of glassy epoxy networks, Polymer 52 (2011) 4528–4535. https://doi.org/10.1016/j.polymer.2011.07.042.

[196] H. Liu, A. Uhlherr, R.J. Varley, M.K. Bannister, Influence of substituents on the kinetics of epoxy/aromatic diamine resin systems, J. Polym. Sci. Part Polym. Chem. 42 (2004) 3143–3156. https://doi.org/10.1002/pola.20169.

[197] A. Schindler, N. Morosoff, Determination of Crosslinking in High Tg Polymers, Research Triangle Institute, 1980.

[198] K. Fryauf, V. Strehmel, M. Fedtke, Curing of glycidyl ethers with aromatic amines: model studies on the effects of tertiary amines as accelerators, Polymer 34 (1993) 323–327. https://doi.org/10.1016/0032-3861(93)90084-N.

[199] J. Rocks, G.A. George, F. Vohwinkel, Curing kinetics and thermomechanical behaviour of co-anhydride cured aminoglycidyl epoxy resins, Polym. Int. 52 (2003) 1758–1766. https://doi.org/10.1002/pi.1286.

[200] R.J. Varley, W. Liu, G.P. Simon, Investigation of the reaction mechanism of different epoxy resins using a phosphorus-based hardener, J. Appl. Polym. Sci. 99 (2006) 3288–3299. https://doi.org/10.1002/app.23016.

[201] H. Stutz, J. Mertes, Influence of the structure on thermoset cure kinetics, J. Polym. Sci. Part Polym. Chem. 31 (1993) 2031–2037. https://doi.org/10.1002/pola.1993.080310810.

[202] K. Tangthana-umrung, Q.A. Poutrel, M. Gresil, Epoxy Homopolymerization as a Tool to Tune the Thermo-Mechanical Properties and Fracture Toughness of Vitrimers, Macromolecules 54 (2021) 8393–8406. https://doi.org/10.1021/acs.macromol.1c00861.

[203] A.J. Lesser, E. Crawford, The role of network architecture on the glass transition temperature of epoxy resins, J. Appl. Polym. Sci. 66 (1997) 387–395. https://doi.org/10.1002/(SICI)1097-4628(19971010)66:2<387::AID-APP19>3.0.CO;2-V.

[204] A. Gupta, M. Cizmecioglu, D. Coulter, R.H. Liang, A. Yavrouian, F.D. Tsay, J. Moacanin, The mechanism of cure of tetraglycidyl diaminodiphenyl methane with diaminodiphenyl sulfone, J. Appl. Polym. Sci. 28 (1983) 1011–1024. https://doi.org/10.1002/app.1983.070280309.

[205] D. Heider, D.A. Eckel Ii, R.C. Don, B.K. Fink, J.W. Gillespie, Jr., Process monitoring during manufacturing of large-scale composite parts, in: M.A. Marcus, A. Wang (Eds.), Boston, MA, United States, 1999: p. 226. https://doi.org/10.1117/12.335753.

[206] G. Tuncol, M. Danisman, A. Kaynar, E.M. Sozer, Constraints on monitoring resin flow in the resin transfer molding (RTM) process by using thermocouple sensors, Compos. Part Appl. Sci. Manuf. 38 (2007) 1363–1386. https://doi.org/10.1016/j.compositesa.2006.10.009.

[207] J. McHugh, P. Fideu, A. Herrmann, W. Stark, Determination and review of specific heat capacity measurements during isothermal cure of an epoxy using TM-DSC and standard DSC techniques, Polym. Test. 29 (2010) 759–765. https://doi.org/10.1016/j.polymertesting.2010.04.004.

[208] S. Vyazovkin, N. Sbirrazzuoli, Mechanism and Kinetics of Epoxy–Amine Cure Studied by Differential Scanning Calorimetry, Macromolecules 29 (1996) 1867–1873. https://doi.org/10.1021/ma951162w.

[209] R.M. Saeed, J.P. Schlegel, C. Castano, R. Sawafta, Uncertainty of Thermal Characterization of Phase Change Material by Differential Scanning Calorimetry Analysis, Int. J. Eng. Res. 5 (2016) 405–412.

[210] A. Padma, R.M.V.G.K. Rao, C. Subramaniam, G. Nagendrappa, Cure characterization of triglycidyl epoxy/aromatic amine systems, J. Appl. Polym. Sci. 57 (1995) 401–411. https://doi.org/10.1002/app.1995.070570402.

[211] L. Xia, L. Zuo, S. Zha, S. Jiang, R. Guan, D. Lu, Kinetic research on low-temperature cure of epoxy adhesive, Int. J. Adhes. Adhes. 50 (2014) 255–264. https://doi.org/10.1016/j.ijadhadh.2014.02.005.

[212] H.E. Kissinger, Variation of peak temperature with heating rate in differential thermal analysis, J. Res. Natl. Bur. Stand. 57 (1956) 217. https://doi.org/10.6028/jres.057.026.

[213] M.J. Starink, The determination of activation energy from linear heating rate experiments: a comparison of the accuracy of isoconversion methods, Thermochim. Acta 404 (2003) 163–176. https://doi.org/10.1016/S0040-6031(03)00144-8.

[214] R.L. Blaine, H.E. Kissinger, Homer Kissinger and the Kissinger equation, Thermochim. Acta 540 (2012) 1–6. https://doi.org/10.1016/j.tca.2012.04.008.

[215] S. Vyazovkin, Kissinger Method in Kinetics of Materials: Things to Beware and Be Aware of, Molecules 25 (2020) 2813. https://doi.org/10.3390/molecules25122813.

[216] J. Yan, Q. Yang, L. Zhang, Z. Lei, Z. Li, Z. Wang, S. Ren, S. Kang, H. Shui, Investigation of kinetic and thermodynamic parameters of coal pyrolysis with model-free fitting methods, Carbon Resour. Convers. 3 (2020) 173–181. https://doi.org/10.1016/j.crcon.2020.11.002.

[217] E. Tarani, K. Chrissafis, Isoconversional methods: A powerful tool for kinetic analysis and the identification of experimental data quality, Thermochim. Acta 733 (2024) 179690. https://doi.org/10.1016/j.tca.2024.179690.

[218] H. Li, S. Niu, C. Lu, Thermal Characteristics and Kinetic Calculation of Castor Oil Pyrolysis, Procedia Eng. 205 (2017) 3711–3716. https://doi.org/10.1016/j.proeng.2017.10.297.

[219] C.D. Doyle, Estimating Thermal Stability of Experimental Polymers by Empirical Thermogravimetric Analysis, Anal. Chem. 33 (1961) 77–79. https://doi.org/10.1021/ac60169a022.

[220] X. Zhang, Applications of Kinetic Methods in Thermal Analysis: A Review, Eng. Sci. (2020). https://doi.org/10.30919/es8d1132.

[221] J.M. Hutchinson, F. Shiravand, Y. Calventus, I. Fraga, Isothermal and non-isothermal cure of a tri-functional epoxy resin (TGAP): A stochastic TMDSC study, Thermochim. Acta 529 (2012) 14–21. https://doi.org/10.1016/j.tca.2011.11.008.

[222] E.J. Mittemeijer, Analysis of the kinetics of phase transformations, J. Mater. Sci. 27 (1992) 3977–3987. https://doi.org/10.1007/BF01105093.

[223] I. Smith, The Mechanism of the Crosslinking of Epoxide Resins by Amines, Polymer 2 (1961) 95–108. https://doi.org/10.1016/0032-3861(61)90010-6.

[224] S. Corezzi, D. Fioretto, G. Santucci, J.M. Kenny, Modeling diffusion-control in the cure kinetics of epoxy-amine thermoset resins: An approach based on configurational entropy, Polymer 51 (2010) 5833–5845. https://doi.org/10.1016/j.polymer.2010.09.073.

[225] M.R. Kamal, Thermoset characterization for moldability analysis, Polym. Eng. Sci. 14 (1974) 231–239. https://doi.org/10.1002/pen.760140312.

[226] K.C. Cole, A new approach to modeling the cure kinetics of epoxy/amine thermosetting resins. 1. Mathematical development, Macromolecules 24 (1991) 3093–3097. https://doi.org/10.1021/ma00011a011.

[227] G.W.H. Höhne, W.F. Hemminger, H.-J. Flammersheim, Differential Scanning Calorimetry, Springer, Berlin, Heidelberg, 2003. https://doi.org/10.1007/978-3-662-06710-9.

[228] J.P. Pascault, R.J.J. Williams, Glass transition temperature versus conversion relationships for thermosetting polymers, J. Polym. Sci. Part B Polym. Phys. 28 (1990) 85–95. https://doi.org/10.1002/polb.1990.090280107.

[229] J.P. Pascault, R.J.J. Williams, Relationships between glass transition temperature and conversion: Analyses of limiting cases, Polym. Bull. 24 (1990) 115–121. https://doi.org/10.1007/BF00298330.

[230] K. Wudy, T. Budde, Reaction kinetics and curing behavior of epoxies for use in a combined selective laser beam melting process of polymers, J. Appl. Polym. Sci. 136 (2019) 46850. https://doi.org/10.1002/app.46850.

[231] J.F. Johnson, R.H. Cole, Dielectric Polarization of Liquid and Solid Formic Acid [1], J. Am. Chem. Soc. 73 (1951) 4536–4540. https://doi.org/10.1021/ja01154a012.

[232] D.R. Day, Dielectric determination of cure state during non-isothermal cure, Polym. Eng. Sci. 29 (1989) 334–338. https://doi.org/10.1002/pen.760290512.

[233] R. Ramsdale-Capper, J.P. Foreman, Data from static and dynamic mechanical tests of different isomers of amine cured multifunctional epoxy resins, Data Brief 19 (2018) 992–996. https://doi.org/10.1016/j.dib.2018.05.125.

[234] X. Wang, H. Liu, S. Ouyang, Damping properties of flexible epoxy resin, J. Wuhan Univ. Technol.-Mater Sci Ed 23 (2008) 411–414. https://doi.org/10.1007/s11595-007-3411-4.

[235] S.R. Heinz, Development and Utilization of Digital Image Correlation Techniques for the Study of Structural Isomerism Effects on Strain Development in Epoxy Network Glasses, (2011).

[236] J.-F. Shi, P.T. Inglefield, A.A. Jones, M.D. Meadows, Sub-Glass Transition Motions in Linear and Cross-Linked Bisphenol-Type Epoxy Resins by Deuterium Line Shape NMR, Macromolecules 29 (1996) 605–609. https://doi.org/10.1021/ma9512418.

[237] M. Ochi, T. Shiba, H. Takeuchi, M. Yoshizumi, M. Shimbo, Effect of the introduction of methoxy branches on low-temperature relaxations and fracture toughness of epoxide resins, Polymer 30 (1989) 1079–1084. https://doi.org/10.1016/0032-3861(89)90084-0.

[238] M. Ochi, M. Shimbo, M. Saga, N. Takashima, Mechanical and dielectric relaxations of epoxide resins containing spiro-ring structure, J. Polym. Sci. Part B Polym. Phys. 24 (1986) 2185–2195. https://doi.org/10.1002/polb.1986.090241003.

[239] T. Sasuga, A. Udagawa, Molecular motion of several epoxy resins and influence of electron irradiation, Polymer 32 (1991) 402–408. https://doi.org/10.1016/0032-3861(91)90442-L.

[240] C. Brahatheeswaran, V.B. Gupta, Internal stress in a cured epoxy resin system, Polymer 34 (1993) 289–294. https://doi.org/10.1016/0032-3861(93)90079-P.

[241] L. Mascia, Y. Kouparitsas, D. Nocita, X. Bao, Antiplasticization of Polymer Materials: Structural Aspects and Effects on Mechanical and Diffusion-Controlled Properties, Polymers 12 (2020) 769. https://doi.org/10.3390/polym12040769.

[242] R.J. Varley, J.H. Hodgkin, G.P. Simon, Toughening of trifunctional epoxy system. V. Structure-property relationships of neat resin, J. Appl. Polym. Sci. 77 (2000) 237–248. https://doi.org/10.1002/(SICI)1097-4628(20000711)77:2<237::AID-APP1>3.0.CO;2-5.

[243] S. Heinz, J. Tu, M. Jackson, J. Wiggins, Digital image correlation analysis of strain recovery in glassy polymer network isomers, Polymer 82 (2016) 87–92. https://doi.org/10.1016/j.polymer.2015.11.026.

[244] R.D. Patel, R.G. Patel, V.S. Patel, Kinetics of thermal degradation of cured epoxy resins based on triglycidyl-p-aminophenol, Thermochim. Acta 128 (1988) 149–156. https://doi.org/10.1016/0040-6031(88)85361-9.

[245] A. Ahrens, A. Bonde, H. Sun, N.K. Wittig, H.C.D. Hammershøj, G.M.F. Batista, A. Sommerfeldt, S. Frølich, H. Birkedal, T. Skrydstrup, Catalytic disconnection of C–O bonds in epoxy resins and composites, Nature 617 (2023) 730–737. https://doi.org/10.1038/s41586-023-05944-6.

APPENDIX

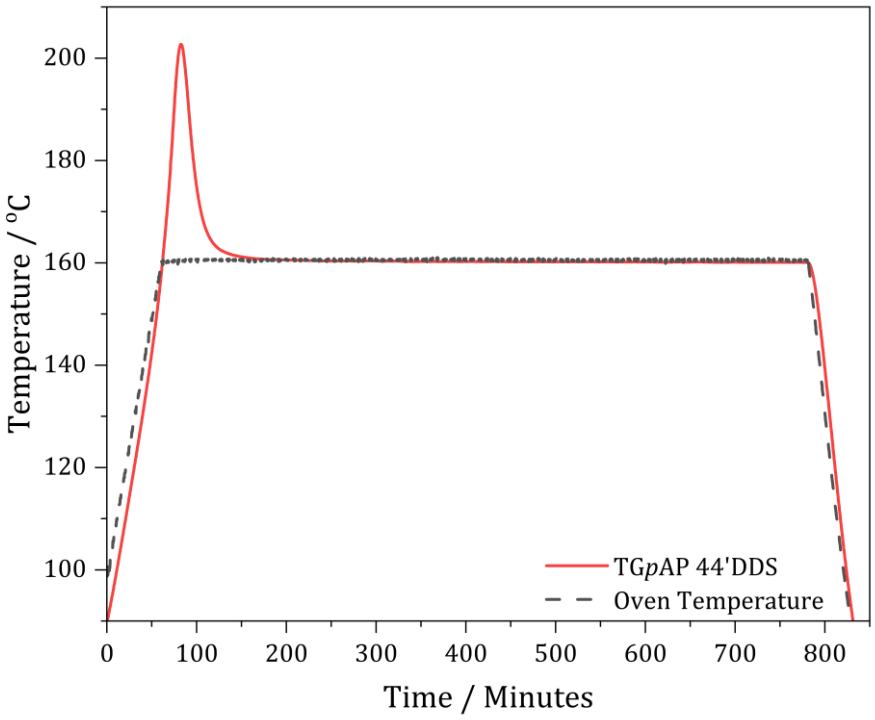

Appendix 1 - Temperature profile for TG*p*AP/44'DDS during a 160 °C dwell where the heating rate was 1 °C min^{-1} as a function of time as measured by thermocouples for resin and oven temperatures. The overshoot was substantial – 40 °C over oven temperature.

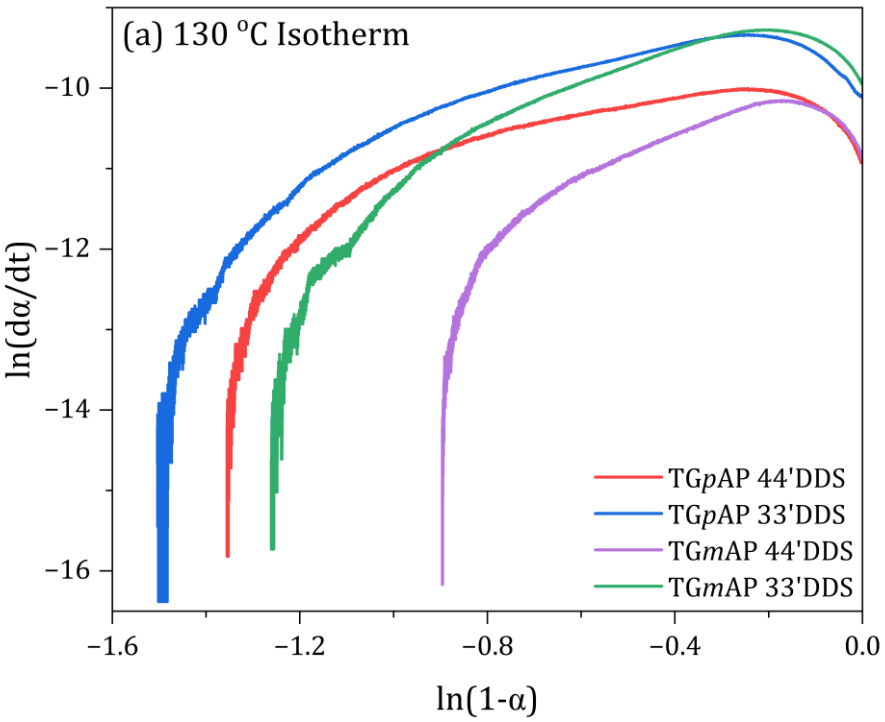

Appendix 2 - Natural log of rate of reaction against natural log of $(1-\alpha)$ for the four structural isomers of TGAP/DDS under 130 °C isothermal heating.

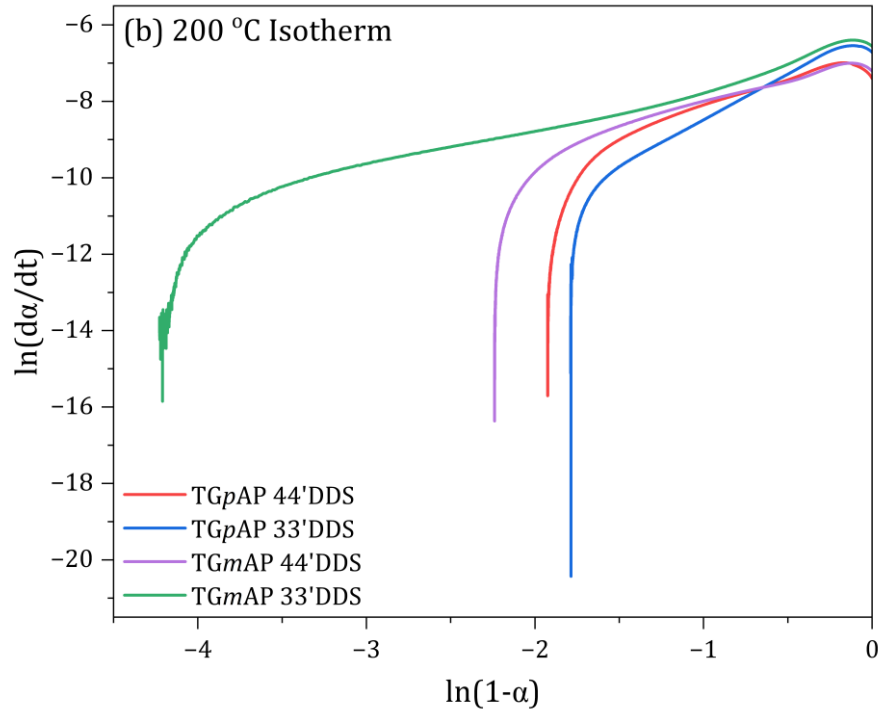

Appendix 3 - Natural log of rate of reaction against natural log of $(1-\alpha)$ for the four structural isomers of TGAP/DDS under 200 °C isothermal heating.

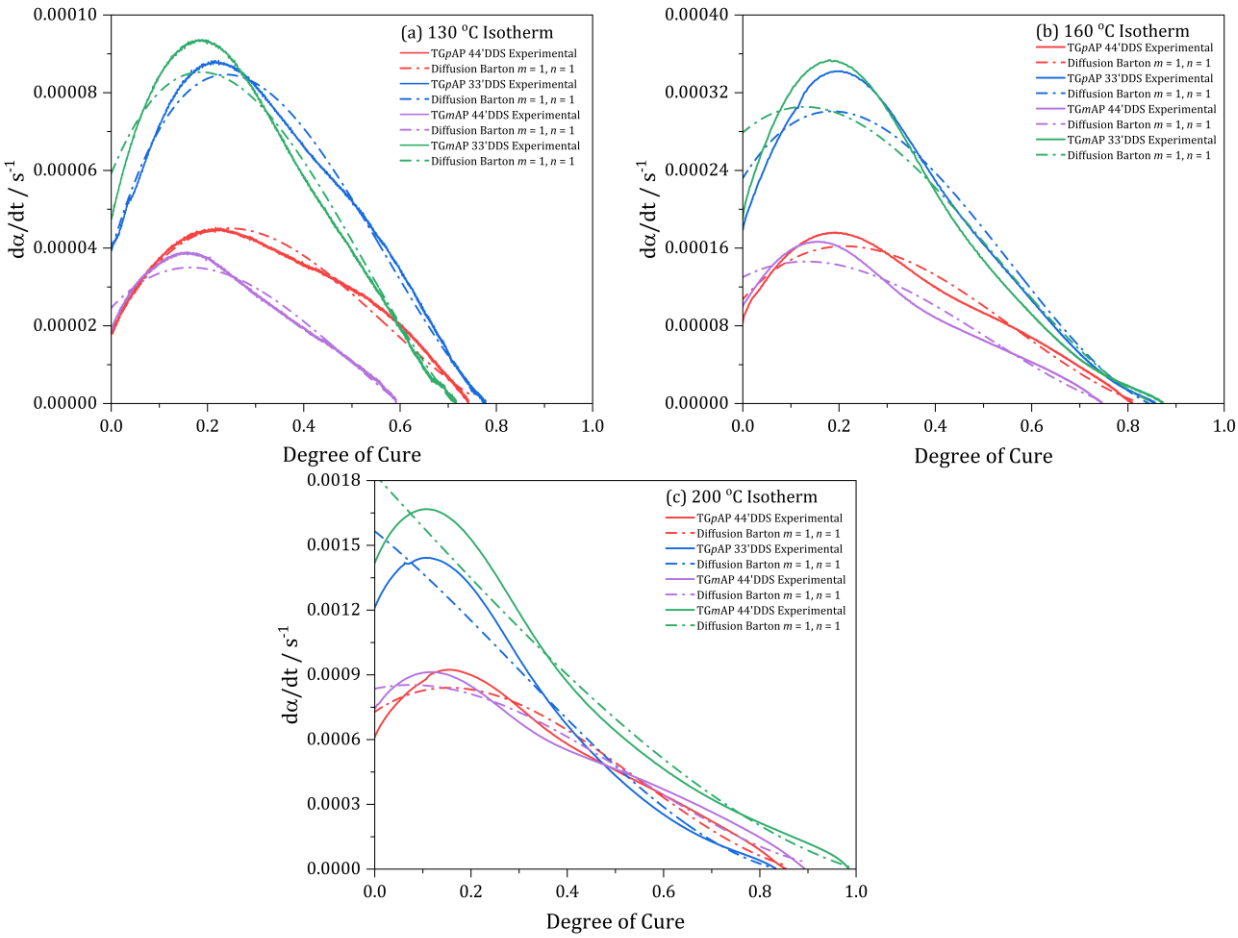

Appendix 4 - Rate of reaction against degree of cure for the structural isomers of TGAP/DDS under varying isothermal heating conditions fitted to the Barton diffusion control model [126] where $m = 1$ and $n = 1$: (a) 130 °C isotherm, (b) 160 °C isotherm and (c) 200 °C isotherm.

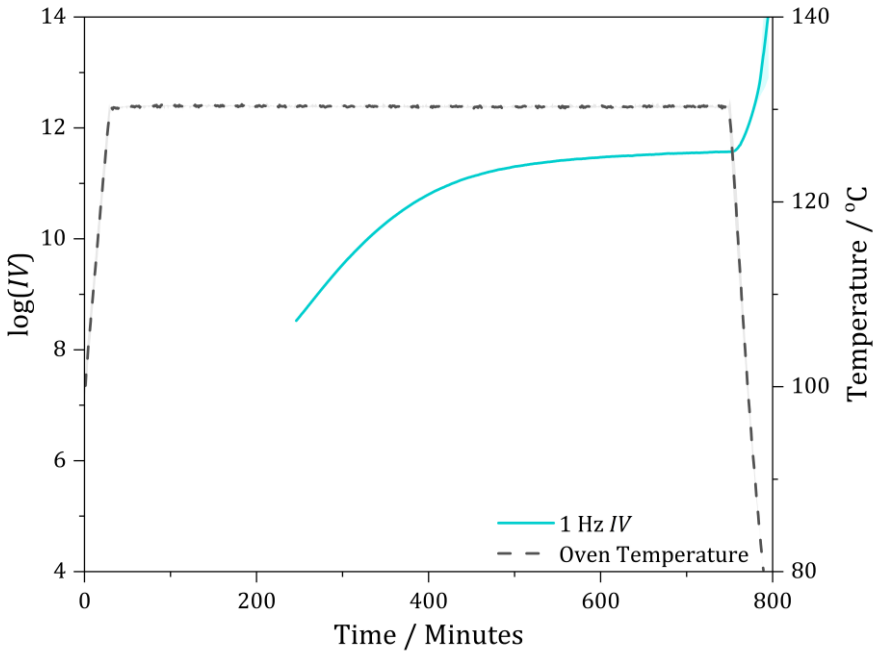

Appendix 5 - Dielectric analysis of TG*p*AP/44'DDS using the 130 °C dwell cure at 1 Hz. *IV* is given as an average of two separate tests where the shaded region is standard deviation.

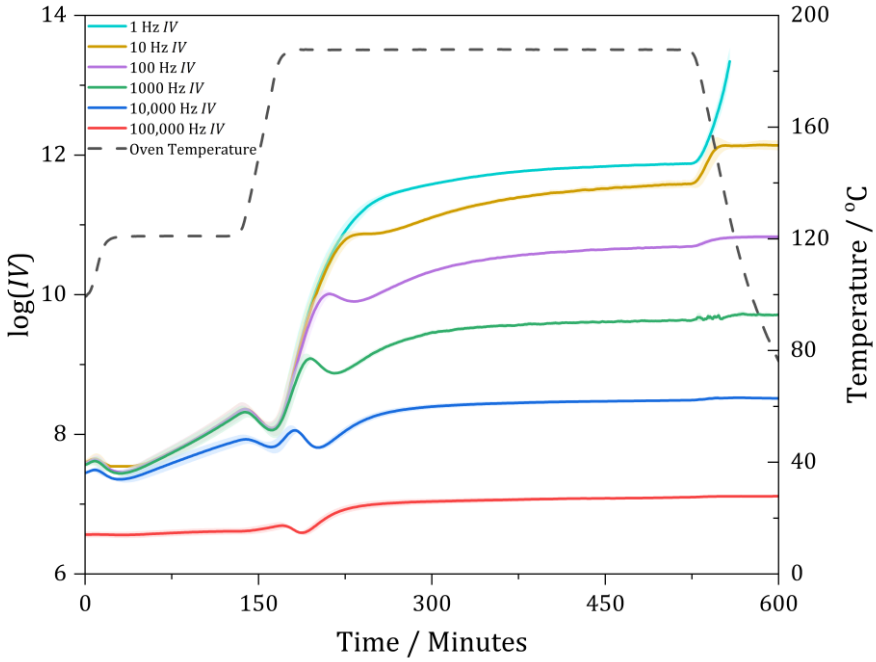

Appendix 6 - Dielectric analysis of DGEBA/44'DDS using the cure shown at six different testing frequencies (1, 10, 100, 1000, 10,000 and 100,000 Hz). *IV* is given as an average of two separate tests where the shaded region is standard deviation.

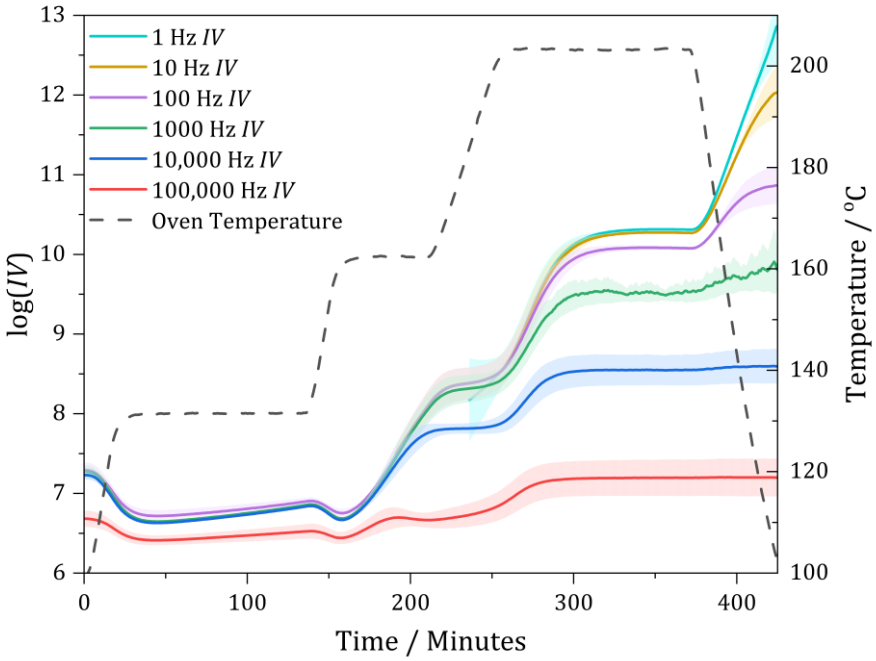

Appendix 7 – Dielectric analysis of TGDDM/44'DDS using the standard cure cycle at six different testing frequencies (1, 10, 100, 1000, 10,000 and 100,000 Hz). *IV* is given as an average of two separate tests where the shaded region is standard deviation.